ANALYSIS OF OPEN CANOPY STRUCTURES WITH PARAPETS UNDER WIND

By

Augusto Poitevin Vera

A thesis submitted in partial fulfillment of the requirements for the degree of

DOCTOR OF PHILOSOPHY

In

CIVIL ENGINEERING

UNIVERSITY OF PUERTO RICO
MAYAGUEZ CAMPUS
2009

Approved by:

Luis A. Godoy, Ph. D. Chairman, Graduate Committee	Date
Ricardo R. López, Ph. D. Member, Graduate Committee	Date
Luis E. Suárez, Ph. D. Member, Graduate Committee	Date
Raúl E. Zapata López, Ph. D. Member, Graduate Committee	Date
Sonia Bartolomei, Ph. D. Representative, Graduate Studies	Date
Ismael Pagán Trinidad, MSCE. Chairman, Civil Engineering & Surveying Department	Date

ABSTRACT

A literature review shows that there is a lack of information on the wind load pressures acting on canopy structures with a parapet on the roof perimeter. On the other hand, a large number of those structures suffered catastrophic damages due to hurricanes, for example during Hurricanes Katrina and Rita in 2005. The latest version of the predominant standard and commentary for wind design in the eastern part of the US, the ASCE 7-05, introduced for the first time the issue of open structures. However, the code recommendations do not address open structures with parapets. In this research, the author addresses the problem using two different (but complementary) approaches: a numerical simulation using Computational Fluid Dynamics (CFD) and wind tunnel testing. Values of pressure coefficients, Cp and Cn, were obtained with the use of both methods, on top and bottom surfaces of the open canopy, and windward and leeward surfaces for parapets, showing that the obtained values had good agreement between both methodologies.

With the use of CFD, parametric studies further explore different plan geometries and incremental parapet heights in order to obtain extreme Cn values. The obtained extreme values were implemented on four case studies of collapsed open canopy structures, due to Hurricanes Rita and Katrina in 2005. With the use of structural analysis software, the structural members suffering extreme stresses, were identified and compared with the actual collapsed structures on the case studies selected. Structural design procedure is suggested for the analysis of open canopy structures with parapets and is implemented on each of the cases studied.

RESUMEN

La revisión de la literatura demuestra la falta de información disponible sobre las presiones de viento actuando sobre estructuras abiertas con parapetos en la periferia del techo de las mismas. Por otra parte, un gran número de este tipo de estructuras sufren daños catastróficos, por ejemplo durante los Huracanes Katrina y Rita que ocurrieron en el año 2005. La más reciente versión del estándar y comentario en la parte Este de los Estados Unidos, el ASCE 7-05, introdujo por vez primera el tema de las estructuras abiertas. Es de notar, que las recomendaciones de este código no incluyen las estructuras abiertas con parapetos. En esta investigación, el autor investiga el problema usando dos enfoques distintos, pero complementarios: Usando Dinámica Computacional de Fluidos (CFD) y pruebas hechas en un túnel de viento, valores de presión, Cp y Cn fueron obtenidos con el uso de ambos métodos, en las superficies superiores e inferiores de la estructura abierta, y sotavento y barlovento en las superficies de los parapetos, siendo los valores obtenidos muy parecidos entre ambas metodologías.

Mediante el uso de CFD, estudios paramétricos exploran más profundamente diferentes geometrías en planta y diferentes alturas para poder obtener valores Cn extremos. Estos valores son entonces implementados en estudio de casos particulares, de estructuras abiertas que colapsaron debido a los efectos de los Huracanes Katrina y Rita en el año 2005. Con el uso de un programa de análisis de estructuras, miembros que sufrieron esfuerzos máximos, pudieron ser identificados y comparados con las estructuras colapsadas en los casos seleccionados. Un

procedimiento de diseño estructural para estructuras abiertas con parapetos es sugerido e implementado para cada uno de los casos estudiados.

DEDICATION

I would like to dedicate this work, to my wife Yvonne and to my daughter Amanda. All the time and effort during all this years, those two beautiful ladies were near me, encouraging me and supporting me. I will be forever grateful for all the help, love and support from them during all this time.

ACKNOWLEDGEMENTS

I would like to thank Dr. Luis A. Godoy. Thank you for your patience and support during all these years. Besides being my mentor, I consider him a very good friend. In addition, I would like to thank Dr. Bruno Natalini, from the Universidad Nacional del Nordeste (UNNE) for the help and support on the experimental part of this research. Thank you for all the help.

TABLE OF CONTENTS

LIST OF FIGURES xi

LIST OF TABLES xxiii

LIST OF APPENDIX xxiv

CHAPTER 1 PROBLEM STATEMENT 1

1.1 General information 1

1.2 Motivation 3

1.3 Importance 8

1.4 Objectives 8

1.5 Proposed Methodology 9

1.6 Original Contributions 12

CHAPTER 2 LITERATURE REVIEW 13

2.1 Introduction 13

2.2 Open Canopies 13

2.3 Computational Fluid Dynamics (CFD) 19

2.4 Wind Tunnel Testing 21

2.5 Parapet Pressures 22

CHAPTER 3 SIMULATION OF WIND FLOW USING COMPUTATIONAL FLUID DYNAMICS (CFD) 24

3.1 Theoretical Background 24

3.2 EFD.Lab program description 32

3.3 CFD model 32

CHAPTER 4 WIND TUNNEL TESTING 46

4.1 General features of wind tunnel studies 46

4.2 Wind tunnel description 48

4.3 Construction of models 53

4.4 Instrumentation 58

4.5 Data processing 62

CHAPTER 5 AVAILABLE DESIGN CODE INFORMATION 66

5.1 General code information 66

5.2 UBC 97 66

5.3 ASCE 7-05 67

5.4 IBC 2006 69

5.5 Additional building codes 69

CHAPTER 6 RESULT OF WIND PRESSURES IN CANOPIES 71

6.1 Comparison between wind tunnel results and previous work 71

6.2 CFD and wind tunnel results for top surface, wind at 0 degrees 74

6.3 CFD and wind tunnel results for bottom surface, wind at 0 degrees 77

6.4 CFD and wind tunnel results for top surface, wind at 30 degrees 78

6.5 CFD and wind tunnel results for bottom surface, wind at 30 degrees 79

6.6 CFD and wind tunnel results for parapets, wind at 0 degrees.....83

6.7 CFD and wind tunnel results for parapets, wind at 30 degrees.....94

CHAPTER 7 PARAMETRIC STUDIES OF PRESSURE COEFFICIENTS IN CANOPIES USING CFD.....106

7.1 Description 106

7.2 Open canopy models, 7.6 m (25 ft) x 7.6 m (25 ft) at 0 degrees.....109

7.3 Open canopy models, 7.6 m (25 ft) x 7.6 m (25 ft) at 30 degrees.....116

7.4 Open canopy models, 7.6 m (25 ft) x 12.2 m (40 ft) at 0 degrees.....123

7.5 Open canopy models, 7.6 m (25 ft) x 12.2 m (40 ft) at 30 degrees.....129

7.6 Open canopy models, 7.6 m (25 ft) x 15.2 m (50 ft) at 0 degrees.....137

7.7 Open canopy models, 7.6 m (25 ft) x 15.2 m (50 ft) at 30 degrees.....144

7.8 Conclusions 150

CHAPTER 8 CASE STUDIES OF CANOPIES AND COMPARISONS WITH FIELD EVIDENCE.....152

8.1 Structural analysis 152

8.2 Case study #1, Shell Gas Station at Pt. Arthur, Texas, Method #1.....154

8.3 Case study #1, Shell Gas Station at Pt. Arthur, Texas, Method #2.....161

8.4 Case study #1, Shell Gas Station at Pt. Arthur, Texas, Method #3 164

8.5 Case study #2, Texaco Gas Station, Port Arthur, Texas 172

8.6 Case study #3, Chevron Gas Station, Vidor, Texas 179

8.7 Case study #4, Exxon Gas Station, Hillerbrandt, Texas 186

8.8 Conclusions drawn from the Case Studies 193

CHAPTER 9 CONCLUSIONS, ORIGINAL RESULTS, FUTURE RESEARCH AND RECOMMENDATIONS 194

9.1 Conclusions 194

9.2 Original results 196

9.3 Future research 198

9.4 Final recommendations 199

REFERENCES 201

APPENDIX 210

LIST OF FIGURES

Figure 1.1. Schematic view of a canopy used in gas stations 2

Figure 1.2. Open canopy of a Gas Station, Quebradillas, PR, (Photograph by the Author)..... 3

Figure 1.3. Failed canopy in Chalmette, New Orleans, during Hurricane Katrina..... 5

Figure 1.4. Canopy structure collapsed at Meraux, New Orleans, Hurricane Katrina, (Photograph by Godoy)..... 5

Figure 1.5. Lateral deflections of open canopy due to wind pressures..... 7

Figure 1.6. Stress ratio of open canopy members using ASCE 7-98 and AISC 89..... 7

Figure 1.7. Flow and wind pressure distribution in the longitudinal direction..... 10

Figure 1.8. Flow and wind pressure distribution in the transversal direction..... 10

Figure 1.9. Wind tunnel at UNNE, photograph by B. Natalini 11

Figure 2.1. Pressure gages used on Gumley's investigation..... 14

Figure 2.2. Model used on Altman study, at Clemson University, USA. (Photograph by the Author)..... 15

Figure 2.3. Wind tunnel model (Uematsu et al. 2008)..... 17

Figure 2.4. Pressure taps arrangement (Uematsu et al. 2008) 18

Figure 3.1. Model of an infinitesimal small element assumed fixed in space..... 26

Figure 3.2. Computational domain for Model #1, with boundary definition and laminar wind profile. The inlet condition is defined in the plane of the left.....34

Figure 3.3. Computational domain for Model #2, without boundary definition and uniform wind profile.....35

Figure 3.4. Computational domain for Model #3, without boundary definition and uniform wind profile.....36

Figure 3.5. Model #1 top surface Cp values.....37

Figure 3.6. Model #2 top surface Cp values.....37

Figure 3.7. Model #3 top surface Cp values.....38

Figure 3.8. Computational domain and meshing used on Model #3.....40

Figure 3.9. Open canopy showing mesh, submeshing and further meshing at Model #3, domain intercept.....41

Figure 3.10. Pressure tap locations on top, bottom and parapet surfaces used for CFD and wind tunnel scale model.....42

Figure 3.11. Location of pressure taps and measured wind pressures on the top surface. Wind direction acting from the right (0 degrees).....43

Figure 3.12. Model pressure taps on the canopy model.....43

Figure 3.13. Wind direction in CFD model at 0 degrees.....44

Figure 3.14. Wind direction in CFD model at 30 degrees.....45

Figure 4.1. View of the UNNE wind tunnel facility. (Photograph by the Author).....49

Figure 4.2. Typical Irwin spires used on the UNNE wind tunnel.....51

Figure 4.3. View the UNNE surface roughness and Irwin spires. (Photograph by the Author)....51

Figure 4.4. Wind tunnel plan at UNNE (reproduced from Wittwer and Moller 2000) 52

Figure 4.5. Mean velocity profiles at the UNNE wind tunnel (Wittwer and Moller 2000).....52

Figure 4.6. Model with parapets with PVC tubes and columns. (Photograph by the Author) 55

Figure 4.7. Top view of the model, showing the distribution of 16 pressure taps on the top surface of the canopy and parapets. (Photograph by the Author).....55

Figure 4.8. Distribution of pressure taps on the model with bundle of tubes and columns. (Photograph by the Author) 56

Figure 4.9. Distribution of pressure taps on the model.....57

Figure 4.10. View of the model with parapets on the turntable (Photograph by the Author) 57

Figure 4.11. View the pressure electronic transducer Honeywell 163PC. (Photograph by the Author).....58

Figure 4.12. View of the Scanivale 48 D9-1/2 w/PVC tubes (Photograph by the Author).....59

Figure 4.13. View of the UNNE Keithley 2000 digital multimeter (Photograph by the Author) .60

Figure 4.14. View of the Van Essen 2500 Betz differential micro manometer (Photograph by the Author).....61

Figure 4.15. View of the Pitot-Prandtl tube (Photograph by the Author).....61

Figure 4.16. View of the UNNE tunnel fan (Photograph by the Author).....62

Figure 4.17. Calibration data on model without parapets.....63

Figure 4.18. Photograph showing the author taking data from the wind tunnel test 63

Figure 4.19. Processed data for the calibration of the transducer 64

Figure 4.20. Processed data for the pressure coefficient Cp 65

Figure 6.1. No parapets, net pressures, wind direction of 0° from Ginger et al. (1994).....72

Figure 6.2. No parapets, wind tunnel net pressures, wind direction of 0°, present research 72

Figure 6.3. No parapets, net pressures, wind direction of 30° (Ginger et al. 1994) 73

Figure 6.4. No parapets, wind tunnel net pressures, wind direction of 30°, present research 73

Figure 6.5. Canopy surface nomenclature 75

Figure 6.6. Cp results from top surface from CFD (a) and wind tunnel (b) model for incident wind at 0 degrees from the structural axis 76

Figure 6.7. Cp results from bottom surface from CFD (a) and wind tunnel (b) model for incident wind at 0 degrees from the structural axis.....77

Figure 6.8. Cp results from top surface from CFD (a) and wind tunnel (b) model for incident wind at 30 degrees from the structural axis 78

Figure 6.9. Cp results from bottom surface from CFD (a) and wind tunnel (b) model for incident wind at 30 degrees from the structural axis.....80

Figure 6.10. Cn results from CFD (a) and wind tunnel (b) model for incident wind at 0 degrees from the structural axis 81

Figure 6.11. Cn results from CFD (a) and wind tunnel (b) model for incident wind at 30 degrees from the structural axis 82

Figure 6.12. Cp and Cn results for CFD model at 0 degrees for (25x25x4 ft) canopy.....83

Figure 6.13. Cp results at parapet surface #1 at 0 degrees from CFD (a) and wind tunnel (b) 84

Figure 6.14. Cp results at parapet surface #2 at 0 degrees from CFD (a) and wind tunnel (b) 85

Figure 6.15. Cp results at parapet surface #3 and #7 at 0 degrees from CFD (a) and wind tunnel (b) 86

Figure 6.16. Cp results at parapet surface #4 and #8 at 0 degrees from . CFD (a) and wind tunnel (b) 87

Figure 6.17. Cp results at parapet surface #5 at 0 degrees from CFD (a) and wind tunnel (b) 88

Figure 6.18. Cp results at parapet surface #6 at 0 degrees from CFD (a) and wind tunnel (b) 89

Figure 6.19. Cn results at parapet surface #1 and #2 at 0 degrees from . CFD (a) and wind tunnel (b) 90

Figure 6.20. Cn results at parapet surface #3 and #4 at 0 degrees for CFD (a) and wind tunnel (b) 91

Figure 6.21. Cn results at parapet surface #5 and #6 at 0 degrees for CFD (a) and wind tunnel (b) 92

Figure 6.22. Cn results at parapet surface #7 and #8 at 0 degrees for CFD (a) and wind tunnel (b) 93

Figure 6.23. Cp results at parapet surface #1 at 30 degrees for CFD (a) and wind tunnel (b) 94

Figure 6.24. Cp results at parapet surface #2 at 30 degrees for CFD (a) and wind tunnel (b) 95

Figure 6.25. Cp results at parapet surface #3 at 30 degrees for CFD (a) and wind tunnel (b) 96

Figure 6.26. Cp results at parapet surface #4 at 30 degrees for CFD (a) and wind tunnel (b) 97

Figure 6.27. Cp results at parapet surface #5 at 30 degrees for CFD (a) and wind tunnel (b) 98

Figure 6.28. Cp results at parapet surface #6 at 30 degrees for CFD (a) and wind tunnel (b) 99

Figure 6.29. Cp results at parapet surface #7 at 30 degrees for CFD (a) and wind tunnel (b) 100

Figure 6.30. Cp results at parapet surface #8 at 30 degrees for CFD (a) and wind tunnel (b) 101

Figure 6.31. Cn results at parapet surface #1 and #2 at 30 degrees for CFD (a) and wind tunnel (b) 102

Figure 6.32. Cn results at parapet surface #3 and #4 at 30 degrees for CFD (a) and wind tunnel (b) 103

Figure 6.33. Cn results at parapet surface #5 and #6 at 30 degrees for CFD (a) and wind tunnel (b) 104

Figure 6.34. Cn results at parapet surface #7 and #8 at 30 degrees for CFD (a) and wind tunnel (b) 105

Figure 7.1. Nomenclature used for description of open canopy investigation 107

Figure 7.2. Model #1, contour plan for Cn values for wind at 0 degrees 110

Figure 7.3. Model #1, 3D contour plot for Cn values for wind at 0 degrees 110

Figure 7.4. Model #3, contour plan for Cn values for wind at 0 degrees 111

Figure 7.5. Model #3, 3D contour plot for Cn values for wind at 0 degrees 112

Figure 7.6. Model #5, contour plan for Cn values for wind at 0 degrees 113

Figure 7.7. Model #5, 3D contour plot for Cn values for wind at 0 degrees 113

Figure 7.8. Model #7, contour plan for Cn values for wind at 0 degrees 114

Figure 7.9. Model #7, 3D contour plot for Cn values for wind at 0 degrees 115

Figure 7.10. Influence of parapet height. 2D graph of Cn values for all 7.6 m (25 ft) x 7.6 m (25 ft) at 0 degrees 116

Figure 7.11. Model #2, contour plan for Cn values for wind at 30 degrees 117

Figure 7.12. Model #2, 3D contour plot for Cn values for wind at 30 degrees 117

Figure 7.13. Model #4, contour plan for Cn values for wind at 30 degrees 118

Figure 7.14. Model #4, 3D contour plot for Cn values for wind at 30 degrees 119

Figure 7.15. Model #6, contour plan for Cn values for wind at 30 degrees 120

Figure 7.16. Model #6, 3D contour plot for Cn values for wind at 30 degrees 120

Figure 7.17. Model #8, contour plan for Cn values for wind at 30 degrees 121

Figure 7.18. Model #8, 3D contour plot for Cn values for wind at 30 degrees 122

Figure 7.19. 2D graph of Cn values for all 7.6 m (25 ft) x 7.6 m (25 ft) at 30 degrees.....123

Figure 7.20. Model #9, contour plan for Cn values for wind at 0 degrees 124

Figure 7.21. Model #9, 3D contour plot for Cn values for wind at 0 degrees 124

Figure 7.22. Model #11, contour plan for Cn values for wind at 0 degrees 125

Figure 7.23. Model #11, 3D contour plot for Cn values for wind at 0 degrees 125

Figure 7.24. Model #13, contour plan for Cn values for wind at 0 degrees 126

Figure 7.25. Model #13, 3D contour plot for Cn values for wind at 0 degrees 127

Figure 7.26. Model #15, contour plan for Cn values for wind at 0 degrees 128

Figure 7.27. Model #15, 3D contour plot for Cn values for wind at 0 degrees 128

Figure 7.28. 2D graph of Cn values for all 7.6 m (25 ft) x 12.2 m (40 ft) at 0 degrees.....129

Figure 7.29. Model #10, contour plan for Cn values for wind at 30 degrees 130

Figure 7.30. Model #10, 3D contour plot for Cn values for wind at 30 degrees.....131

Figure 7.31. Model #12, contour plan for Cn values for wind at 30 degrees 132

Figure 7.32. Model #12, 3D contour plot for Cn values for wind at 30 degrees.....132

Figure 7.33. Model #14, contour plan for Cn values for wind at 30 degrees 133

Figure 7.34. Model #14, 3D contour plot for Cn values for wind at 30 degrees.....134

Figure 7.35. Model #16, contour plan for Cn values for wind at 30 degrees 135

Figure 7.36. Model #16, 3D contour plot for Cn values for wind at 30 degrees.....135

Figure 7.37. Graph of Cn values for all 7.6 m (25 ft) x 12.2 m (40 ft) at 30 degrees.....136

Figure 7.38. Model #17, contour plan for Cn values for wind at 0 degrees 137

Figure 7.39. Model #17, 3D contour plot for Cn values for wind at 0 degrees.....138

Figure 7.40. Model #19, contour plan for Cn values for wind at 0 degrees 139

Figure 7.41. Model #19, 3D contour plot for Cn values for wind at 0 degrees.....139

Figure 7.42. Model #21, contour plan for Cn values for wind at 0 degrees 140

Figure 7.43. Model #21, 3D contour plot for Cn values for wind at 0 degrees.....141

Figure 7.44. Model #23, contour plan for Cn values for wind at 0 degrees 142

Figure 7.45. Model #23, 3D contour plot for Cn values for wind at 0 degrees.....142

Figure 7.46. 2D graph of Cn values for all 7.6 m (25 ft) x 15.2 m (50 ft) at 0 degrees.....143

Figure 7.47. Model #18, contour plan for Cn values for wind at 30 degrees 144

Figure 7.48. Model #18, 3D contour plot for Cn values for wind at 30 degrees.....145

Figure 7.49. Model #20, contour plan for Cn values for wind at 30 degrees 146

Figure 7.50. Model #20, 3D contour plot for Cn values for wind at 30 degrees.....146

Figure 7.51. Model #22, contour plan for Cn values for wind at 30 degrees 147

Figure 7.52. Model #22, 3D contour plot for Cn values for wind at 30 degrees.....148

Figure 7.53. Model #24, contour plan for Cn values for wind at 30 degrees 149

Figure 7.54. Model #24, 3D contour plot for Cn values for wind at 30 degrees.....149

Figure 7.55. Graph of Cn values for all 7.6 m (25 ft) x 15.2 m (50 ft) @ 30 degrees.....150

Figure 8.1. Proposed Cn values to be applied for Method #3 to the structural analysis model.....154

Figure 8.2. Canopy floor plan and elevations for Case study #1.....155

Figure 8.3. Contours for wind pressures for open canopy Case #1 at 0 degrees.....156

Figure 8.4. Contours for wind pressures for open canopy Case #1 at 30 degrees.....156

Figure 8.5. Computer model with wind pressures applied to roof surface at 0 degrees.....157

Figure 8.6. Computer model with wind pressures applied to roof surface at 30 degrees.....157

Figure 8.7. Etabs model for Case #1 showing the refined roof mesh and deflected shape of the wind loading at (a) 0 degrees (b) 30 degrees 158

Figure 8.8. Structural steel results from Etabs for Case #1, showing members stress ratios using Method #1 for (a) wind at 0 degrees (b) wind at 30 degrees.....160

Figure 8.9. Roof canopy wind pressures for case #1, Method #2, wind at 0 degrees,
(+ means downward pressure, - means uplift pressure).....161
Figure 8.10. Roof canopy wind pressures for case #1, Method #2, wind at 30 degrees,
(+ means downward pressure, - means uplift pressure).....162
Figure 8.11. Structural steel results from Etabs showing members stress ratios using
Method #2 for (a) wind at 0 degrees (b) wind at 30 degrees.....163
Figure 8.12. Maple output of Wind pressure calculations using proposed Cn values with
ASCE 7-05 procedure, Case #1.....165
Figure 8.13. Maple output of Wind pressure results on parapets using ASCE 7-05
Cn values.....166
Figure 8.14. Roof canopy pressure Cn and wind pressures for case #1, + means downward
pressure, - means uplift pressure.....166
Figure 8.15. Structural model for Case #1 on Etabs.....167
Figure 8.16. Structural model for Case #1 on Etabs showing deflected shape due to wind
pressures.....168
Figure 8.17. Structural model on Etabs showing overstress ratios on roof steel members.....169
Figure 8.18. Case #1 collapsed roof layout showing some of the roof beam damages.
Permanent deformation is clearly shown on some of the roof members.....170
Figure 8.19. Case #1 partial collapsed roof from below. Bottom of roof cladding has
been taken away due to high wind pressures.....170

Figure 8.20. Case #1 roof cladding and beam structural layout. Photograph showing permanent deformation on roof members 171

Figure 8.21. Case #1, transversal view of the deformed and collapsed roof 171

Figure 8.22. Case #1, close up photograph of roof beams showing buckling and extreme corrosion damage 171

Figure 8.23. Canopy floor plan and elevations for Case study #2 173

Figure 8.24. Maple output of wind pressure calculations using proposed Cn values with ASCE 7-05 procedure, Case #2 175

Figure 8.25. Roof canopy pressure Cn and wind pressures for case #2, + means downward pressure, - means uplift pressure 176

Figure 8.26. Structural model on Etabs showing overstress ratios on steel columns 177

Figure 8.27. Case #2, open canopy structure completely collapsed 177

Figure 8.28. Case #2, photograph showing a buckled round steel column 178

Figure 8.29. Case #2, closer photograph of the round steel column base 178

Figure 8.30. Case #2, photograph showing the open canopy structure on top of the gas pumps 179

Figure 8.31. Case #2, photograph showing the roof beam layout 179

Figure 8.32. Canopy floor plan and elevations for Case study #3 180

Figure 8.33. Maple output of wind procedure calculations using proposed Cn values with ASCE 7-05 procedure, Case #3 182

Figure 8.34. Maple output of Wind pressure results on parapets using ASCE 7-05 Cn values ..183

Figure 8.35. Roof canopy pressure Cn and wind pressures for case #3, + means downward pressure, - means uplift pressure.....183

Figure 8.36. Structural model on Etabs showing overstress ratios of roof steel members for Case #3 184

Figure 8.37. Case #3, open canopy photograph of the inverted steel structure after the steel columns failed due to corrosion and wind pressures 185

Figure 8.38. Case #3, photograph of the existing corrosion condition at the column base 185

Figure 8.39. Case #3, additional photograph of the inverted steel structure 186

Figure 8.40. Canopy floor plan and elevations for Case study #4.....187

Figure 8.41. Maple output of wind pressure calculations using proposed Cn values with ASCE 7-05 procedure, Case #4 189

Figure 8.42. Roof canopy pressure Cn and wind pressures for Case #4, + means downward pressure, - means uplift pressure.....190

Figure 8.43. Structural model on Etabs showing overstress ratios on all steel columns 191

Figure 8.44. Case #4, photograph showing closer detail of the buckled steel columns 191

Figure 8.45. Case #4 photograph showing the collapsed steel columns.....192

Figure 8.46. Case #4, additional photograph of buckled steel columns. The photograph shows the buckling of the internal column flange 192

Figure 8.47. Case #4, upper roof beam layout on the collapsed open canopy roof.....192

LIST OF TABLES

Table 7.1. Model geometry description for the CFD parametric study 108

Table 8.1. Table of wind pressures for case #1 to be used for the structural analysis 167

Table 8.2. Table of wind pressures for case #2 to be used for the structural analysis 176

Table 8.3. Table of wind pressures for case #3 to be used for the structural analysis 184

Table 8.4. Table of wind pressures for case #4 to be used for the structural analysis 190

LIST OF APPENDIX

APPENDIX A. EFD.Lab modeling procedure 210

APPENDIX B. Wind Tunnel Data 217

APPENDIX C. Open canopy without parapets: spreadsheet calculations 234

APPENDIX D. Open canopy with parapets: spreadsheet calculations 238

APPENDIX E. Parapets: spreadsheet calculations 242

APPENDIX F. CFD test of different wind angles 246

APPENDIX G. T-test statistical analysis example 250

CHAPTER 1. PROBLEM STATEMENT

1.1 General Information

Open canopies are frequently used in the construction of civil engineering facilities, either as components of larger structures or as self supported structures. An example of the second type may be found in most gas stations throughout the nation, in which the roof covers the gas pumps and incoming vehicles. There are many other applications, including parts of industrial buildings and processing plants, and sport courts. A large number of such structures suffered catastrophic damages during hurricanes, including Hurricanes Katrina and Rita in 2005, (NIST 2006).

In their typical configurations, open canopies are commonly supported by interior columns in different patterns, without having any perimeter walls. The roof is formed by a system of beams in two directions to support the roof panels. The supporting columns may be aligned in one or more rows, depending on the size of the roof and on the functionality of the facility. In small gas stations, canopies are frequently supported by a single row of columns as illustrated in Figure 1.1. Typical dimensions vary from 6 m (20 ft.) to 15 m (50 ft.) in each horizontal direction and from 3.7 m (12 ft.) to 6 m (20 ft.) in height.

From the structural point of view, it would be desirable to have a frame structure that integrates columns and beams into a single resisting structure. However, the inspection of many structures of this kind in the United States clearly shows that the beam-column connections are not rigid connections, with the consequence that the majority of the connections used between the elements are simple shear and tension connections. The majority of the canopy columns inspected are designed as cantilever elements taking all the lateral forces due to wind pressure

and wind uplift. In addition, maintenance to open canopy structures appears to be a very important factor that may reduce their factor of safety, but maintenance work is often neglected with the consequence that corrosion is present in many canopies.

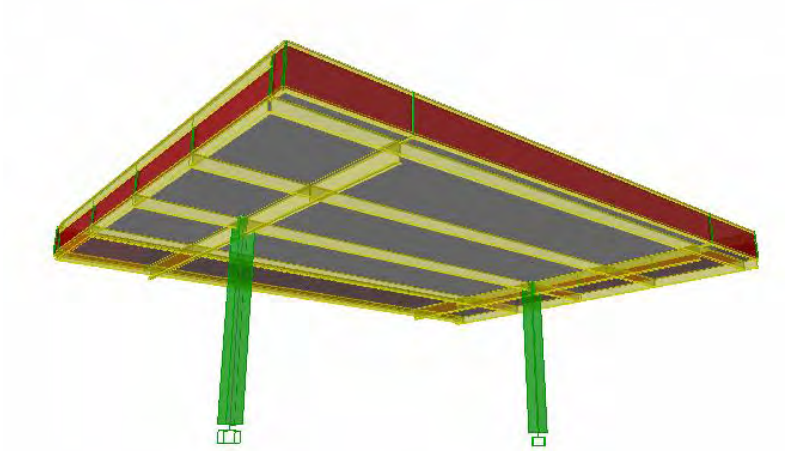

Figure 1.1: Schematic view of a canopy used in gas stations.

In hurricane-prone areas, such as the Caribbean islands and the coastal areas in the US, the most critical structural conditions occur during high winds due to hurricanes. As it is known, several hurricanes in recent years have been of category 3 and 4. This generates sustained wind velocities of above 64.82 m/s (145 mph) in some regions, and those levels of wind velocities and pressures have been incorporated in design codes such as ASCE 7-05, Figure 6-1. With such high wind velocities, a surprise comes associated to the absence of information on the wind load pressures acting on open structures with parapets. This void in our current state of knowledge is also reflected in the design recommendations available to engineers and the catastrophic effects on such structures due to the lack of design data and testing.

The majority of canopy structures have a parapet on the roof perimeter (as schematically illustrated in Figure 1.1). The wind pressures that these types of structures are exposed to are

very complex, because pressures on the top and bottom surfaces of the roof are not uniform and their values are different on each surface. Open canopy structures which include parapets have not been studied in detail in the research literature or in the current codes used for design in the United States.

1.2 Motivation

The predominant building code for wind design in the eastern part of the United States, is the ASCE -7. It did not properly address the issue of open structures for a number of years. The most recent version ASCE-7 05, was the first of various versions of this code that includes open structures. However, it does not address the issue of open structures with parapets, which is perhaps the most common configuration found in real constructions (see, for example Figure 1.2).

Figure 1.2: Open canopy of a Gas Station, Quebradillas, PR. (Photograph by the Author).

The pressure coefficients currently employed for the design of open canopy structures do not include parapets on the structure perimeter. The Uniform Building Code, 1997 Edition, is the

predominant building code in the western part of the United States. This code addresses the issue of open structures but does not provide any recommendations regarding the effects of parapets in open structures.

In the event of a hurricane, the results on such structures have proven to be devastating. Illustrations from some of 2005 hurricanes, Katrina and Rita, are shown in Figure 1.3 and Figure 1.4. The structure shown in Figure 1.3 was a new construction, completed during 2005. However improper knowledge of the pressures acting due to wind effects may have been a major factor contributing to the collapse. It was surprising during the field inspection in Texas and New Orleans after hurricanes Katrina and Rita by Godoy (2006), the close relation of the poor maintenance of open canopies and failure cases. There are several mechanisms leading to a rapid deterioration of the structure: first, environmental action; second poor roof drainage (the drains are located inside the hollow columns); and third, lack of preventive inspection.

Therefore, motivation to carry out this research is the need to establish basic recommendations for the safe design of the main wind force resisting system (MWFRS) for such structures. These recommendations will help in the proper maintenance and even possible retrofit of existing structures and to improve their safety level.

Figure 1.3: Failed canopy in Chalmette, New Orleans, during Hurricane Katrina, (Photograph by L. Godoy).

The case shown in Figure 1.4 is catastrophic in the sense that a total collapse occurred. However, even in this case it is possible to reconstruct the main mechanisms leading to the collapse, provided that rational estimates of wind pressures are taken into consideration. Thus, one motivation for this research is the need to reconstruct failure mechanisms and understand what design considerations need to be improved.

Figure 1.4: Canopy structure collapsed at Meraux, New Orleans, Hurricane Katrina, (Photograph by L. Godoy).

The results of a preliminary study of the causes of open canopy structures during high winds (Godoy and Poitevin, 2006) revealed that the current design code at that time, ASCE-7 98, did not address open structures. For the preliminary study, wind pressures and coefficients of enclosed structures were used. The pressure values for this study were generated using a wind design program named Wind Loads on Structures 2005 by Standard Design Group (SDGS 2005). This computer program generates wind pressures for enclosed and partially enclosed structures, including the MWFRS and the cladding on any structure.

Using the ASCE 7-98, values of the wind pressures were obtained from the basic design wind conditions specified for the location of the stations. Those wind pressures were applied to various three dimensional structural models. The structural analysis software used was ETABS developed by the firm called Computers and Structures, (CSI 2009). One of the computer models used in the study is shown in Figure 1.5. Figure 1.6 shows the results corresponding to the same model. A linear elastic analysis was performed on various model configurations taken from field measurements made during the reconnaissance of the hurricane effects of Rita and Katrina in 2005, to evaluate the stresses throughout the structure. The stress ratio refers to the ratio between the actual stresses and the allowable stresses using the Allowable Stress Design Code, AISC 1989 edition, as illustrated in Figure 1.6.

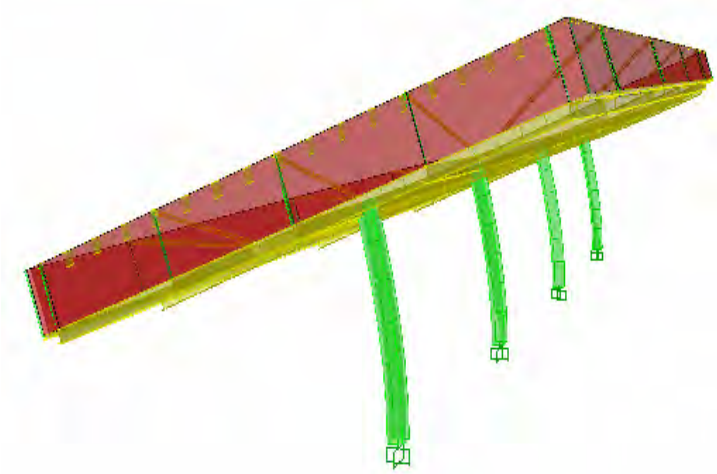

Figure 1.5: Lateral deflections of open canopy due to wind pressures.

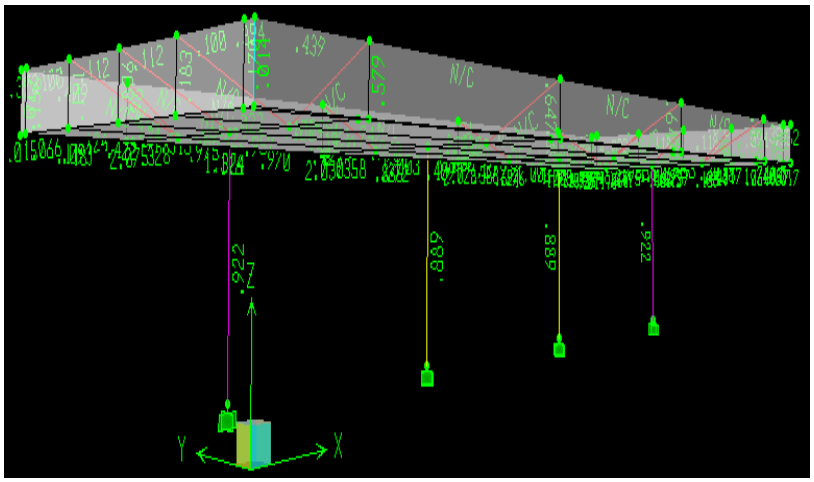

Figure 1.6: Stress ratio of open canopy members using ASCE 7-98 and AISC ASD89.

As said before, the latest version of the ASCE 7, the 2005 edition, addresses open structures for the first time. Figure 6-18 of the ASCE 7-05 provide the design coefficients for such structures. The studies for those coefficients provided by the code were performed on open structures without parapets. This preliminary study opened a number of questions regarding the wind pressures and structural response that motivated further studies to quantify both issues in which the most complex part appeared to be the assessment of wind pressures.

1.3 Importance

Failures of open canopy structures are so common that during the event of a hurricane or high winds, one does not need to specifically search for the collapse of those types of structures, because they are easily found in most towns, as shown by the site reconnaissance made by Godoy (2006). The collapse of an open canopy structure, in a gas station, interrupts the supply of gasoline to the public and government agencies that need continued gas supply specially during an emergency period. Therefore, this type of structures should be designed as a critical and of high importance (essential facilities) in terms of human risks and security in the time of an emergency. Unfortunately, this type of structure has been not been investigated in depth until the current research, as shown by the literature review reported in Chapter 2. Research of open structures without parapets has been conducted in several countries, including Australia, Canada, Japan and in the United States. However, open canopy structures like those of gas stations have a parapet on the perimeter of the roof. As mentioned before, the effects of that parapet and the correlation between the height of the parapet and the geometry of the building are of crucial importance to estimate wind pressures and have not been investigated in detail.

1.4 Objectives

The main objectives of this research may be divided in three major areas:

1. To investigate the characteristics of wind flow through open canopy structures with parapets, in order to evaluate wind coefficients for the main wind force resisting system (MWFRS) due to such conditions.

2. To explain the structural behavior of open canopy structures under wind, leading to the identification of most severely stressed components and possibly of collapse mechanisms and design problems.
3. To propose recommendations for design and future research based on rational basis for open canopy structures with parapets.

1.5 Proposed Methodology

The proposed methodology in this work includes two stages. In a first stage, pressure coefficients will be evaluated under the assumption of a rigid structure. In a second stage, the pressure coefficients will be used as the loads acting on an elastically deformable structure to estimate the response of the structure.

The first stage will be tackled by two different (but complementary) approaches: first, a wind tunnel testing simulation will be carried out. Second, a computational simulation will be performed using Computational Fluid Dynamics (CFD). A commercial CFD software named EFD.Lab (Engineering Fluid Dynamics), developed by a firm called Flomerics (2009), will be used for the computational fluid analysis. Such CFD simulation is able to calculate wind pressures on the top and bottom surfaces of the structure with a wind velocity similar as those specified by design codes such as ASCE 7 (2005). Factors such as turbulence, roughness, humidity, and temperature can also be included in the CFD analysis to emulate real conditions. As an introduction to the type of results expected from a CFD simulation, Figure 1.7 and 1.8 illustrate velocity field vectors as computed using EFD.Lab.

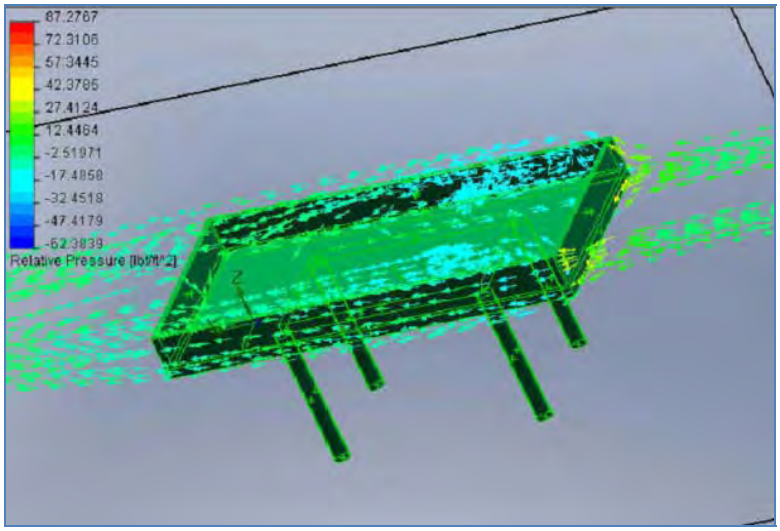

Figure 1.7: Flow and wind pressure distribution in the longitudinal direction.

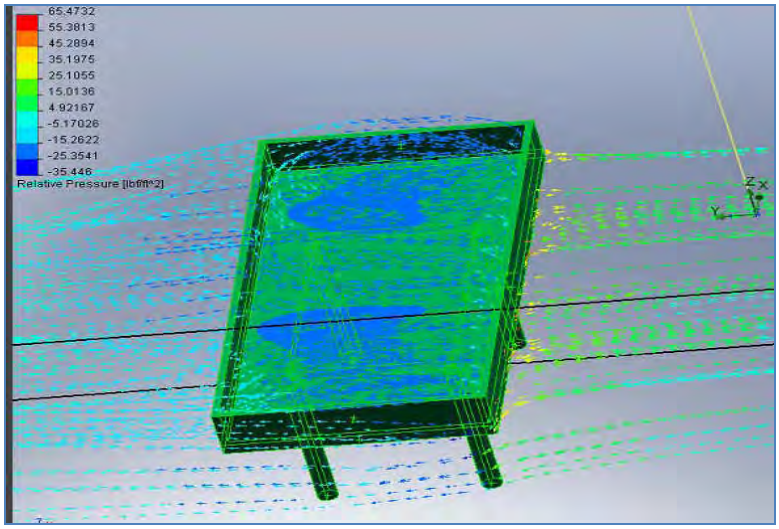

Figure 1.8: Flow and wind pressure distribution in the transversal direction.

With the use of wind tunnel results, a calibrated CFD model can be used to explore various models with different parapet heights. The wind tunnel facility used for this research is located at the Universidad Nacional del Nordeste (UNNE) in Resistencia, Argentina. The UNNE wind tunnel facility is a low velocity atmospheric boundary layer wind tunnel, built with the aim of performing aerodynamic studies of structural models.

The facility is an open circuit tunnel with a length of 22.8 m (74.8 ft), the testing chamber being a square section of 2.4 m (7.87 ft) width and 1.8 m (5.9 ft) in height and uses a 2.25 m (7.38 ft) diameter fan with a 92 kW motor. The maximum wind velocity that may be obtained in this tunnel is 25 m/s (55.9 mph) when the testing section is empty. Further details are given in Chapter 4.

Figure 1.9: Wind tunnel at UNNE, (Photograph by B. Natalini).

The results obtained from the models tested in the wind tunnel will be used to calibrate the computational simulation. This would help to asses if the method of using CFD for analysis can be used with confidence for the parametric analysis instead of only using the wind tunnel method. Pressure coefficients and wind pressures through the selected models will be determined experimentally. Once those results are determined, structural analysis of selected configurations, using commercially available structural software will be investigated. Actual shapes and

geometries of open canopy structures will be analyzed to assess their safety levels to withstand design wind velocities.

1.6 Original Contributions

The proposed research will produce contributions to advance both, academic research and engineering practice. On the academic front, pressure coefficients for the design of open canopy structures with parapets do not exist at present. Open canopy structures without parapets have been recently investigated and wind pressure distributions and design coefficients have been proposed on a small number of previous investigations. However, no previous testing has been reported with open canopy structures that consider the effects of parapets on wind flow. Because this may be a controversial topic (due to its engineering significance), it is desirable to have methodological redundancy to make sure that adequate pressure coefficients are reliable. Correlation between the possible modeling and prediction of open canopy structures with the use of CFD software has not been previously investigated. The possibility of the confirmation of the use of CFD in the analysis of open canopy structures with parapets is another original contribution of this research. Finally, a design procedure is needed to be used for the safe and secure structural design of such structures.

CHAPTER 2. LITERATURE REVIEW

2.1 Introduction

The focus of this investigation is the effect of wind on open canopy structures with parapets. This chapter contains a review of previous work presented by researchers on open canopies and in the area of CFD, which is relevant to the current investigation. The literature review covers the area of wind tunnel testing and parapet pressures.

2.2 Open Canopies

The past half century, has witnessed interesting developments in the understanding of wind loading on structures. During this time, the description of wind load has moved from simple static drag forces to sophisticated models (Davenport, 2002). A review of recent literature on wind pressures in similar structures shows a wide variety of previous investigations. The need for more detailed information on the wind flow and perhaps on open canopies is a consequence of the collapse of a large number of open canopies in gas stations in areas affected by hurricanes Katrina and Rita in 2005 (Godoy 2006).

Several researchers had the opportunity to study wind loads on open canopy structures. Gumley (1984) made a parametric study investigating the effects of the roof shape, roof pitch, roof aspect ratio, eave height, and wind direction and internal stacking arrangements. He measured pressures averaged on roof areas using wind tunnel procedures. The effects of stacking patterns under the roof were also investigated, but only the envelope results were presented. Figure 2.1 shows the location of pressure gages used on Gumley's investigation. The drawing is interesting because it shows the number and location of pressure gauges employed by other

authors in wind tunnel tests. The results were used for updating the Eurocode (2002) and Australian (1989) wind loading codes.

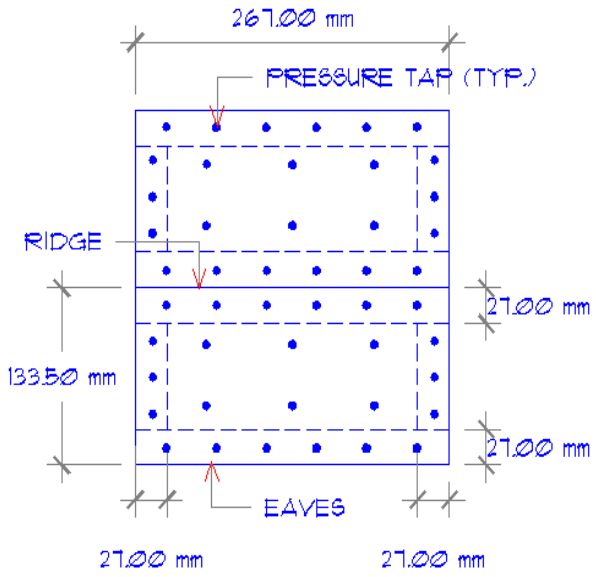

Figure 2.1: Pressure gages used on Gumley's investigation

Full scale measures of agricultural canopy structures were reported by Robertson et al. (1985). These structures had an aspect ratio *l/b* (length/width) of approximately 2. Based on those results they proposed a set of wind force coefficients for designing such structures. Various wind tunnel studies were subsequently carried to validate the conditions obtained from the full-scale measurements by Robertson et al. (1985).

Another set of experiments were performed by Letchford and Ginger (1992) and Ginger and Letchford (1994), who measured the mean and peak point pressures over several roof areas. They compared the obtained results with the Australian wind loading code at the time, to conclude that the code provisions underestimated the wind loads. Altman (2001) made extensive measurements of the forces and moments on mono-sloped and gable roofs at Clemson University, USA. The roof models used in the study were made of high-density foam of 6 mm

thick. Figure 2.2 shows the model used on Altman's study. He compared the obtained results against various codes. In some cases, the code provisions underestimate and in others they overestimated. From the measurements taken by Altman, based on the obtained experimental results, he proposed wind force coefficients to be used for the design of main wind force resisting systems.

Figure 2.2: Model used on Altman study, at Clemson University, USA. (Photograph by the Author).

Letchford et al. (2000) measured mean wind forces on solid and porous canopy models. The mean drag and lift forces on various open canopy roof geometries were investigated. In conclusion, from the obtained result, the lift forces decrease as the pitch decreases and drag forces increases as porosity increases. Lam and Zhao (2002) performed wind tunnel tests on large cantilevered roofs, which are used mostly as grandstand roofs. The objective of the investigation was to identify the generation mechanism of wind pressure and peak lifting action on a large cantilevered roof. It was found that a horizontal roof is under a mean lifting action at

most wind incidence angles. However, at the wind incidence from the front of the roof, very high suction was found on the front edge of the roof.

Natalini et al. (2002) investigated the pressure distribution on curved canopy roofs with the use of wind tunnel testing. Curved canopy roofs are a very common type of structure in South America. Mean pressure coefficient from the wind tunnel tests were presented on the investigation. Paluch et al. (2003) investigated arch roof industrial buildings, adding the effect of attached canopies on the sides. Six scale models with five different canopies were investigated. The results showed that the aerodynamic coefficients for the roof are not affected by the canopies, in the case of 0° from the main axis. However, the influence on the pressure distribution is noticeable for wind incidence perpendicular to the main axis of the arch roofs and for other incidences as well.

Uematsu et al. (2007) tested three types of roof geometries, (i.e. gable, troughed and mono sloped roofs). Wind pressures were measured at many points both on the top and bottom surfaces of the roof model at various wind directions. The conclusions at which Uematsu and co-workers arrived based on their investigation and those of other authors may be summarized as:

a) The roof pitch affects the wind forces significantly.
b) There are significant differences in the results when the roof pitch is smaller than 15°.
c) The influence of roof aspect ratio (length/width from 1 to 4) on the wind force coefficients is small.
d) The experimental data for mono sloped and gable roofs is limited.
e) Roof thickness and supporting systems significantly affects the results.

Roof is supported by slender columns and no walls, so that wind action is directly exerted on the top and bottom surfaces. These roofs seem to be more vulnerable to wind actions than

those of enclosed buildings. Local wind pressures and overall wind forces and moments acting on free standing canopy roofs have been investigated experimentally. Based on the results for the distribution of the most critical positive and negative peak pressure difference coefficients irrespective of wind direction, the peak wind force coefficients for the design of cladding and its immediately supporting structures were proposed in Uematsu et al. (2007).

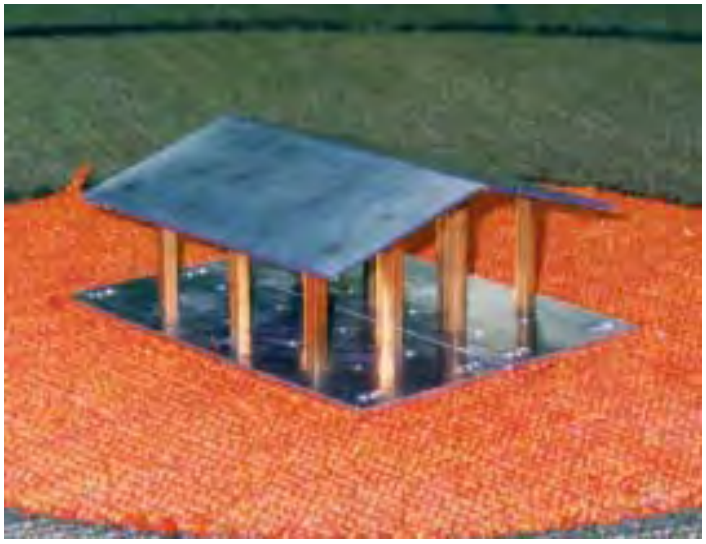

Figure 2.3: Wind tunnel model (Uematsu et al. 2008)

Figure 2.3 shows a canopy roof model on the turntable of the wind tunnel of Concordia University. Special care was taken in decreasing the roof thickness and column width to avoid the distortion of the flow around the roof. The roof model is made of two galvanized steel sheets 0.3 mm thick and consists of a sandwich structure.

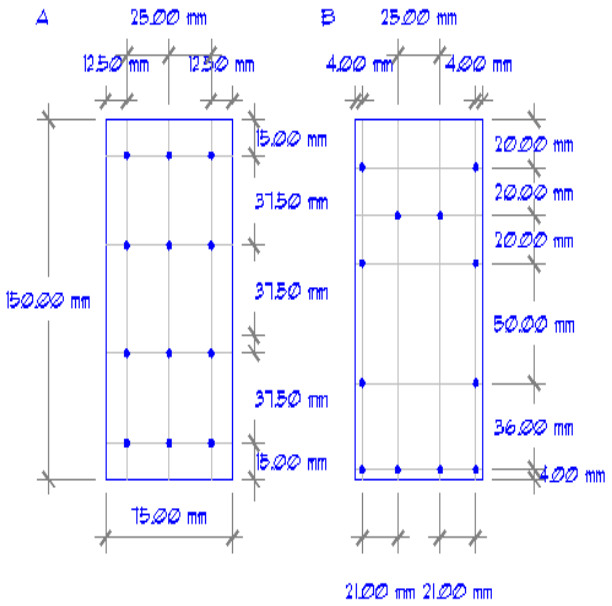

Figure 2.4: Pressure taps arrangement (Uematsu, et al. 2008)

Twelve pressure taps of 0.4 mm diameter were drilled on each side of the basic model. Taping locations were identical on both the upper and lower surfaces so that the net pressure difference could be obtained. Two types of tap arrangements were used; one is for overall wind measurements and the other is for the local pressure measurements.

Very large negative peak values are induced in the leeward ridge corner for the gable roof and in the windward eave corner for the troughed and mono-sloped roofs. The most critical values, both positive and negative, generally increase in magnitude with an increase in β, the roof pitch. When the roof pitch is the same, larger peak values are induced in mono-sloped roofs than in gable and troughed roofs (Uematsu et al. 2008).

2.3 Computational Fluid Dynamics (CFD)

Computational fluid dynamics (CFD) in Wind Engineering was initiated and has progressed over the past two decades. The rapid growth of computer power, which makes possible power acquisition and analysis of large amounts of experimental data, has led to the increasing use of CFD techniques (Baker 2007). The ultimate goal of CFD is to represent the physical events that occur in the fluids flow around and within designated objects. These events are related to the action and interaction of dissipation, diffusion, convection, shock waves, slip surfaces, boundary layers and turbulence. In the field of aerodynamics all these phenomena are governed by the Navier-Stokes equations (Lomax and Pulliam, 1999).

Computational fluid dynamics constitutes a new approach in the study and development of fluid dynamics, which was previously dominated by wind tunnel testing. At present, most researchers in the field of wind engineering agree that there is a need to have better theory and experiments in order to gain understanding of wind acting on structures. The recent success obtained through CFD simulations are indicative that both, physical and numerical approaches can be used as complementary techniques, rather than on eliminating the other. Computational fluid dynamics results are analogous to wind tunnel results obtained in a laboratory, in the sense that they both provide data for given flow configurations. However, unlike a wind tunnel which is generally heavier, a computer program can be carried on and accessed remotely by computers (Anderson, 1995).

Computational fluid dynamics (CFD) has recently made enormous strides. However, techniques for obtaining time dependent pressures induced by turbulent flows do not allow the routine and confident use of CFD as a substitute for wind tunnel testing of structures, although

can be a compliment for such testing. The role of CFD in structural engineering applications may be expected to become more important in the future (Simiu and Miyata 2006).

Use is often made of commercially available CFD codes because of their ready availability, well developed interfaces and broad verification and validation. The atmospheric boundary layer (ABL) extends for a considerable distance above the earth's surface relative to the average building height. CFD can only represent a smaller finite distance because of hardware limitation and the complexity of including a meteorological model. Currently, smaller features such as vegetation and small buildings cannot be included in the computational grid using personal computers. The k-ε model, that includes energy dissipation, is generally incorporated through a wall function approach that is based on boundary layer theory (Hargreaves and Wright 2007).

Accurate simulation of ABL flow in the computer domain is imperative to obtain accurate and reliable predictions of the related atmospheric process. In a CFD simulation, the flow profiles of mean wind speed and turbulence quantities that are applied at the inlet plane of the computational domain are generally fully developed profiles. These profiles should be representative of the roughness characteristics of that part of the upstream terrain that is not included in the computational domain. This is expressed by the presence of either the appropriate aerodynamic roughness length or the appropriate power law exponent of the terrain (Blocken et al. 2007).

The most common CFD techniques are capable of predicting the mean pressures on buildings with reasonable accuracy, but are not sufficiently accurate at evaluating the fluctuating and peak pressures. The poor representation of the pressure fluctuations is primarily because it is necessary to incorporate over simplified representations of the turbulence in the fluid flow

equations. However, CFD techniques are capable of providing useful insights into wind flow around building for environmental considerations (Holmes, 2001).

The lack of validation with the full scale, as was done in the early years on wind tunneling, could easily mislead a well intentioned structural engineer into thinking that the CFD package is generating real design loads. Engineers need to take the lead to ensure that non-validated data are non taken as gospel (Cochran, 2006).

2.4 Wind Tunnel Testing

Wind tunnel testing was mostly carried out in aeronautical wind tunnels in smooth uniform flow. There were some isolated exceptions where the variation of wind speed with height was simulated. Although there were significant differences in the pressures between uniform and boundary layer flows, it appeared to be of academic interest only (Davenport, 2002).

A significant development during the 1950s was due to Jensen, who undertook a comparison of the mean pressures on small buildings in full scale and in wind tunnel model experiments. They were carried out in a variety of boundary layers, and he stated his model law, “The correct model test for phenomena in the wind must be carried out in a turbulent boundary layer and the model law requires the boundary layer to be scaled as regards the velocity profile” (Davenport, 2002).

Wind tunnel test on wind loading on structures require the simulation of the atmospheric boundary layer (ABL). Several methods have been proposed since 1960’s to reproduce the atmospheric flow. It is accepted that the best atmospheric boundary layer simulation is obtained with rough floor surface, although simulation scales reached by this method are too small for

usual applications in structural aerodynamics. It has been shown that when comparing with atmospheric data, it is preferable to use comparative procedures, which do use the boundary layer thickness as a scaling factor (De Bortoli et al. 2002).

Wind tunnels have evolved as an indispensable aid to the practice of civil engineering. Boundary layer wind tunnels and currently data acquisition systems reveals that such tests continue to provide even more comprehensive wind load information for structural design (Cermark 2003).

With the basics of the aerodynamics of bluff bodies and the detailed characteristics of the atmospheric surface layer discussed in the previous sections, one can now approach the wind tunnel simulation process with confidence. The important element in the section on bluff body aerodynamics is the role played by the turbulence (small scale and large scale) in the formation of vortices under separated shear layers (Tieleman, 2003).

Independent tests conducted at six prominent wind tunnel laboratories on models of two industrial buildings showed that test results can vary significantly from laboratory to laboratory. Because of some variations in results, some structural engineering firms have engaged in the design of important structures, commission wind tunnel tests to more than one laboratory (Simiu and Miyata 2006).

2.5 Parapet Pressures

The influence of parapets has been investigated for closed structures, perhaps in relation to wind effects on closed buildings. It is clear that low parapets may significantly increased the roof corner suctions for oblique wind directions. Data indicates that, in general, the higher the

parapet, the lower are the pressure coefficients. This is due to the fact that the parapet tends to lift the vortices away from the roof surface. A wind study reflecting a comparison with existing wind code provisions, NBCC (National Building Code of Canada) and ANSI 1985, against obtained experimental results on wind pressures and suctions on flat roofs with parapets (Stathopoulos and Baskaran, 1987).

Pressure studies have shown that parapet height can influence pressure coefficients at the roof edge. Low parapets, of the order of 0.5m in height, have been found to increase peak suction on the roof in comparison to a roof without a parapet. On the other hand, higher parapets, in the order of 1 m or higher, cause a significant reduction in peak suction (Stathopoulos et al. 2002).

The parapets tend to raise the corner vortex above the roof surface. For lower parapets, this acts to increase the local suctions; for higher parapets, the loads are decreased below those of no parapets. In all cases, the extents of the vortices on the roofs are expanded. The results of a systematic study on the effects of parapets on structural loads for low buildings indicate that parapets are no benign. The distance from the flow separation at the eave's edge to the first reattachment point on the roof for normal wind increases significantly. This leads to an increased load of about 10% in interior frames. Bay uplift is increased on end bays by similar amounts (Kopp et al. 2005).

CHAPTER 3. SIMULATION OF WIND FLOW USING COMPUTIONAL FLUID DYNAMICS (CFD)

There are several ways to represent wind flow on structural components, either through a physical representation of the structure (as would be done in a wind tunnel) or else using computer modeling. This chapter deals with the computational simulation of wind flow on structures using what is known as Computational Fluid Dynamics (CFD), whereas wind tunnel representations are discussed in the next chapter.

3.1 Theoretical background

Computational fluid dynamics (CFD) techniques have been under development for a number of years (Holmes 2001) as a branch of fluid dynamics. At present, CFD constitutes a new approach in the study of wind effects on structures. The introduction of fast digital computers, together with the development of accurate numerical algorithms for solving numerical problems, has revolutionized the way researchers study and practice fluid dynamics today. This complements the approaches of the pure theory and pure experiments but, as Anderson (1995) states, it will never fully replace either of these approaches.

CFD results are directly analogous to wind tunnel results obtained in a laboratory; they both represent sets of data for given flow configurations at different Mach numbers, Reynolds numbers, etc. A CFD computer program is, therefore, a readily transportable tool, and could be thought as analogous to a transportable wind tunnel (Anderson 1995).

The physical aspects of fluid flows are governed by three fundamental postulates:

1. Mass is conserved

2. Newton's second law is satisfied, force = mass × acceleration

3. Energy is conserved

The first step in a CFD problem is to specify the problem to be solved; second, an appropriate set of governing equations must be selected for the domain and boundary conditions; third, appropriate numerical approximations should be made. To obtain basic equations of fluid motion, one need to identify the relevant physical features, apply these features to a model of the flow and, from this application, extract the mathematical equations. The resulting equations are the well known Navier-Stokes equation, which are discussed in the following for the sake of completeness.

For convenience of the presentation, a Cartesian coordinate system is adopted here, where velocity and density (ρ) are functions of space (*x, y, z*) and time *t*, which considers the flow through an infinitesimal element of sides *dx*, *dy*, and *dz*. The scalar density is given by

$$\rho = \rho(x, y, z, t) \tag{3.1}$$

Using the chain rule from differential calculus, it is possible to obtain $d\rho$:

$$d\rho = \frac{\partial \rho}{\partial x} dx + \frac{\partial \rho}{\partial y} dy + \frac{\partial \rho}{\partial z} dz + \frac{\partial \rho}{\partial t} dt \tag{3.2}$$

From equation (3.2), the rate of change of density with time is represented by:

$$\frac{d\rho}{dt} = \frac{\partial \rho}{\partial t} + \frac{\partial \rho}{\partial x}\frac{dx}{dt} + \frac{\partial \rho}{\partial y}\frac{dy}{dt} + \frac{\partial \rho}{\partial z}\frac{dz}{dt} \tag{3.3}$$

Since $\frac{dx}{dt} = u, \frac{dy}{dt} = v, \frac{dz}{dt} = w$, where u, v, w are velocity components, equation (3.3) becomes

$$\frac{d\rho}{dt} = \frac{\partial \rho}{\partial t} + u\frac{\partial \rho}{\partial x} + v\frac{\partial \rho}{\partial y} + w\frac{\partial \rho}{\partial z} \qquad 3.4$$

In CFD this equation is called the substantial derivative and represents a total derivative with respect to time. The governing flow equations are frequently expressed in terms of the substantial derivative.

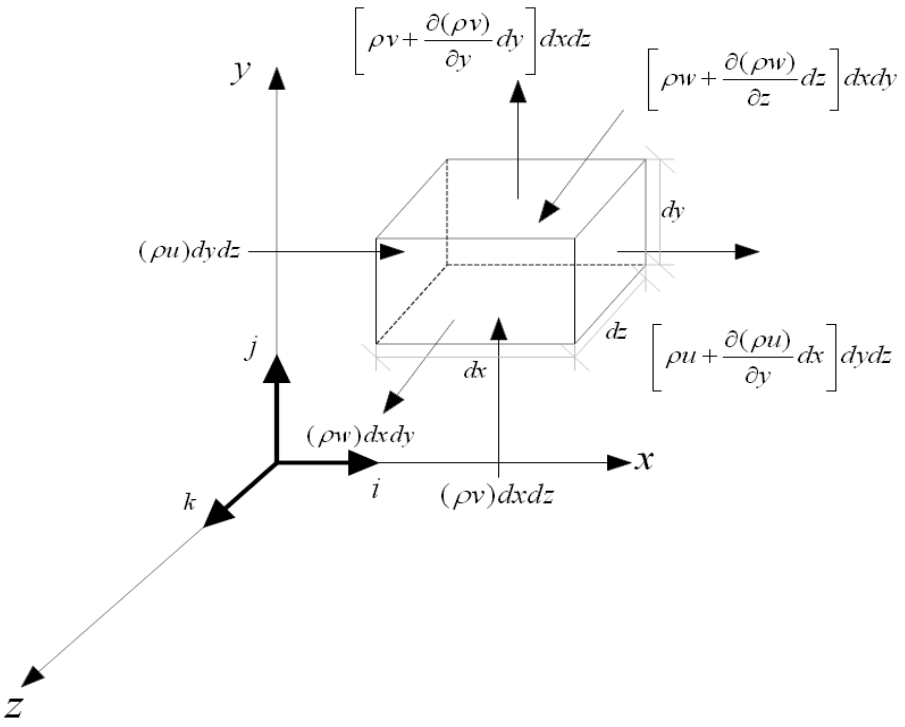

Figure 3.1: Model of an infinitesimal small element assumed fixed in space.

Consider a flow model like the one shown in Figure 3.1, namely, an infinitesimal element fixed in space, with the fluid moving through it, for which a mass flow occurs through this element. From Figure 3.1 we have a net outflow in the x direction given by (Anderson 1995),

$$\left[\rho u + \frac{\partial(\rho u)}{\partial x}dx\right]dydz - (\rho u)\,dydz = \frac{\partial(\rho u)}{\partial x}dxdydz \tag{3.5}$$

The net outflow in the y direction is given by

$$\left[\rho v + \frac{\partial(\rho v)}{\partial y}dy\right]dxdz - (\rho v)\,dxdz = \frac{\partial(\rho v)}{\partial y}dxdydz \tag{3.6}$$

Finally, the net outflow in the z direction is

$$\left[\rho w + \frac{\partial(\rho w)}{\partial z}dz\right]dxdy - (\rho w)\,dxdy = \frac{\partial(\rho w)}{\partial z}dxdydz \tag{3.7}$$

Hence, the net mass flow out of the element is given by

$$\text{Net mass flow} = \left[\frac{\partial(\rho u)}{\partial x} + \frac{\partial(\rho v)}{\partial y} + \frac{\partial(\rho w)}{\partial z}\right]dxdydz \tag{3.8}$$

The physical principle that mass is conserved, when applied to a fixed element, must equal the time rate of decrease of mass inside the element. Denoting the mass decrease by a negative quantity, this statement can be expressed as,

$$\left[\frac{\partial(\rho u)}{\partial x} + \frac{\partial(\rho v)}{\partial y} + \frac{\partial(\rho w)}{\partial z}\right]dxdydz = -\frac{\partial\rho}{\partial t}(dxdydz) \tag{3.9}$$

Or

$$\frac{\partial\rho}{dt} + \left[\frac{\partial(\rho u)}{\partial x} + \frac{\partial(\rho v)}{\partial y} + \frac{\partial(\rho w)}{\partial z}\right] = 0 \tag{3.10}$$

In Equation (3.10) the terms in brackets are $\nabla \cdot (\rho V)$ where the operator ∇ is the divergence operator. Then, equation 3.10 becomes

$$\frac{\partial \rho}{\partial t} + \nabla \cdot (\rho V) = 0 \qquad 3.11$$

V is the flow velocity. Equation (3.11) is the partial differential equation form of the continuity equation, which was derived on the assumption of an infinitesimal small element fixed in space, as shown in Figure 3.1.

The second postulate is Newton's Law, $F = ma$, the momentum equation. Newton's second law, when applied to the moving fluid element states that the net force on the fluid element equals its mass times the acceleration of the element. This is a vector relation and can be split into three scalars relations in the x, y and z directions. Let us consider the x component of Newton's second law; the total force in the x direction is given by (Anderson 1995),

$$Fx = \left[-\frac{\partial p}{\partial x} + \frac{\partial \tau_{xx}}{\partial x} + \frac{\partial \tau_{xy}}{\partial y} + \frac{\partial \tau_{zx}}{\partial z} \right] dxdydz + \rho f_x dxdydz \qquad 3.12$$

where f_x is the body force per unit mass acting on the element, p =surface pressure and τ are the components of the stress tensor: τ_{xy} and τ_{zx} are the shear stress related to the time of change of shearing deformation of the fluid element in the xy and zx, respectively and τ_{xx} the normal stress is related to the time rate of change of volume of the fluid element. The mass m of the fluid element is given by,

$$m = \rho dxdydz \qquad 3.13$$

Since we are following a moving fluid element, the rate of change with respect to time in the *x* direction is given by,

$$a_x = \frac{Du}{Dt} \tag{3.14}$$

Combining equations (3.12), (3.13) and (3.14), we can obtain the x component of the momentum equation for a viscous flow. The x, y and z components are the components of the momentum equations (Anderson 1995).

$$\rho \frac{Du}{Dt} = -\frac{\partial p}{\partial x} + \frac{\partial \tau_{xx}}{\partial x} + \frac{\partial \tau_{yx}}{\partial y} + \frac{\partial \tau_{zx}}{\partial z} + \rho f_x \tag{3.15}$$

$$\rho \frac{Dv}{Dt} = -\frac{\partial p}{\partial y} + \frac{\partial \tau_{xy}}{\partial x} + \frac{\partial \tau_{yy}}{\partial y} + \frac{\partial \tau_{zy}}{\partial z} + \rho f_y \tag{3.16}$$

$$\rho \frac{Dw}{Dt} = -\frac{\partial p}{\partial z} + \frac{\partial \tau_{xz}}{\partial x} + \frac{\partial \tau_{yz}}{\partial y} + \frac{\partial \tau_{zz}}{\partial z} + \rho f_z \tag{3.17}$$

The partial differential equations were obtained from an application of the fundamental physical principle to an infinitesimal fluid element. These are scalar equations and are called the Navier-Stokes equations. These equations are (Anderson 1995),

$$\frac{\partial(\rho u)}{\partial t} + \nabla(\rho u V) = -\frac{\partial p}{\partial x} + \frac{\partial \tau_{xx}}{\partial x} + \frac{\partial \tau_{yx}}{\partial y} + \frac{\partial \tau_{zx}}{\partial z} + \rho f_x \tag{3.18a}$$

$$\frac{\partial(\rho v)}{\partial t} + \nabla(\rho v V) = -\frac{\partial p}{\partial y} + \frac{\partial \tau_{xy}}{\partial x} + \frac{\partial \tau_{yy}}{\partial y} + \frac{\partial \tau_{zy}}{\partial z} + \rho f_y \tag{3.18b}$$

$$\frac{\partial(\rho w)}{\partial t} + \nabla(\rho w V) = -\frac{\partial p}{\partial z} + \frac{\partial \tau_{xz}}{\partial x} + \frac{\partial \tau_{yz}}{\partial y} + \frac{\partial \tau_{zz}}{\partial z} + \rho f_z \tag{3.18c}$$

For virtually all practical aerodynamics problems, Stokes in 1845 obtained the constitutive conditions in the form (Anderson 1995)

$$\tau_{xx} = \lambda(\nabla \cdot V) + 2\mu \frac{\partial u}{\partial x} \tag{3.19a}$$

$$\tau_{yy} = \lambda(\nabla \cdot V) + 2\mu \frac{\partial v}{\partial y} \tag{3.19b}$$

$$\tau_{zz} = \lambda(\nabla \cdot V) + 2\mu \frac{\partial w}{\partial z} \tag{3.19c}$$

$$\tau_{xy} = \tau_{yx} = \mu \left[\frac{\partial v}{\partial x} + \frac{\partial u}{\partial y} \right] \tag{3.19d}$$

$$\tau_{xz} = \tau_{zx} = \mu \left[\frac{\partial u}{\partial z} + \frac{\partial w}{\partial x} \right] \tag{3.19e}$$

$$\tau_{yz} = \tau_{zy} = \mu \left[\frac{\partial w}{\partial y} + \frac{\partial v}{\partial z} \right] \tag{3.19f}$$

where μ is the molecular viscosity coefficient and λ is the second viscosity coefficient. Stokes made the hypothesis that $\lambda = \frac{2}{3}\mu$. Substituting (3.19) into (3.18) we obtain the complete Navier-Stokes equations in conservation form. In the CFD literature, a "Navier-Stokes solution" means a solution of a viscous flow problem using the full governing equations. This includes the solution for the momentum, energy and mass equations. They are a system of nonlinear partial

differential equations, and hence are difficult to solve analytically, with the consequence that no general closed form solution exist to these equations at present.

The third postulate states that the energy is conserved. The first law of thermodynamics states that when applied to the flow model of a fluid element moving with the flow, the rate of change of energy inside the fluid element is equal to the heat into the element, plus the rate of work done on the element due to body and surface forces. The rate of doing work by a force exerted on a moving body is equal to the product of the force and the component of velocity in the direction of the force.

Finally, a numerical method and a strategy for dividing the flow domain into cells or elements must be selected. Many different gridding strategies exist, including structured, unstructured, hybrid, composite, and overlapping grids. The most common choices of a numerical method are finite difference, finite volume, finite element, and spectral methods (Zingg 1999).

The most common finite difference representations of derivatives are based on Taylor's series expansions. The majority of the partial differential equations on the governing equations can be replaced by a system of algebraic difference equations for the dependent variables of a difference equation. Finite volume methods have become very popular in CFD as a result of two major advantages: First, they ensure that the discretization of the governing equations is conservative and second, the volume methods do not require transformations in order to be applied to irregular meshes. The basic idea of the finite-volume method is to satisfy the integral form of the conservation law to some degree of approximation for many continuous control volumes, which cover the domain of interest. For this research, the finite volume method is used

(as implemented by the software developer), to satisfy the conservation law to some degree of approximation for contiguous control volumes, which cover the domain of interest.

3.2 EFD.Lab program description

The wind flow on an open canopy structure with parapets can be represented and modeled with the use of CFD. The specific CFD software used in this research is named EFD.Lab (Engineering Fluid Dynamics), developed by Flomerics Inc. (Flomerics 2009). EFD.Lab solves the Navier-Stokes equations, which include the formulations of mass, momentum and energy conservation laws for fluid flows. The equations are supplemented by fluid state equations defining the nature of the fluid and by empirical dependencies of fluid density, viscosity and thermal conductivity on temperature (Flomerics 2009).

EFD.Lab solves the governing equations using the finite volume method (FVM) on a prismatic rectangular computational mesh drawn in a 3D Cartesian coordinate system with the planes orthogonal to its axes. To improve the results, the mesh is refined locally at the solid/fluid interface. Turbulence is incorporated by means of turbulent intensity and turbulent length parameters, which were obtained from the wind tunnel and used in the CFD computations in order to emulate the wind tunnel conditions.

3.3 CFD model

The initial computational mesh used for the simulation is created in a prismatic domain, as shown in Figure 3.2. The domain dimensions assumed in this initial example are 300 ft (91.4 m) in the x direction, 85 ft (25.9 m) in the z direction, and 80 ft (24.4 m) in the y direction. The surface area on the left is defined as the inlet boundary, in which it is possible to introduce the

non-uniform values of a wind profile. The specific wind profile adopted in the first model investigated in this research is a power law (as defined by ASCE 7 05),

$$V(z) = V(z_{ref})(\frac{z}{z_{ref}})^{1/\alpha}$$

This velocity profile has been investigated for the specific wind tunnel used in the research at Universidad Nacional del Nordeste (UNNE) in Resistencia, Argentina, and a value of $1/\alpha$=0.24 is recommended by the researchers of that wind tunnel (De Bortoli et al. 2002). The exponent $1/\alpha$ depends on the surface roughness and on the wind speed averaging time. z_{ref} is the reference height, namely 10 m (32.8 ft). $V(z_{ref})$ is the velocity of reference at the height of reference.

The simulation of a wind flow on a canopy requires the definition of a flow model and an element mesh; each one has been considered in order to identify a mesh providing acceptable results. Our first model considered is shown in Figure 3.2, in which the incoming flow has a velocity profile which follows the power law. Different velocities on the left inlet entrance of Figure 3.2 indicate that a wind profile using the power law was used as a wind velocity input. The canopy induces significant changes to the flow, and the program calculates wind pressures and Cp values on the model surfaces.

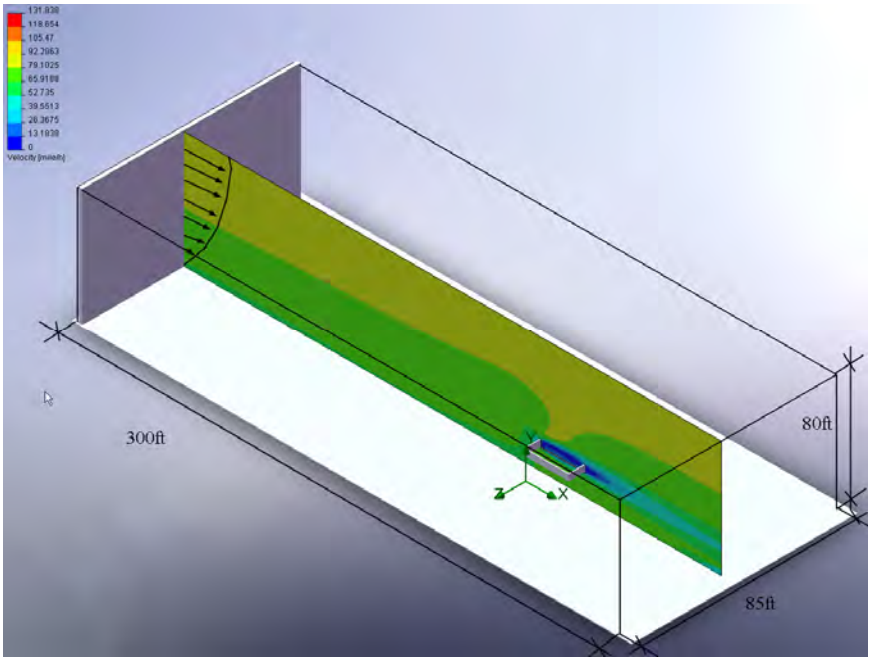

Figure 3.2: Computational domain for Model #1, with boundary definition and laminar wind profile. The inlet condition is defined in the plane on the left.

EFD.Lab determines for external flows, the boundary conditions for all the boundaries of the computational domain. The boundary conditions on any CFD problem define the solutions to be obtained from the governing equations. In this particular model, the inlet surface has been defined as mentioned before, a power law wind profile, with different wind velocities specified through the height. The bottom boundary condition is automatically defined based on surface roughness. The outlet boundary is defined as away from the surface boundary as possible, simulating the real physical boundary condition. The rest of the boundaries assume a zero relative velocity between the surface and the fluid immediately at the surface. This is called the no-slip condition at the surface for a viscous flow.

A second computational model, named Model #2, with the same mesh configuration as Model #1, was also built, in which a uniform flow was assumed, i.e. a uniform velocity profile in height was assumed at the inlet boundary (see Figure 3.3). Although the inlet conditions between a power law and a uniform velocity profile are very different, in the present case in which the canopy is a thin body located at a given distance from the terrain, the results in terms of pressures acting on the canopy are remarkably similar. The reasons for this similarity are that the canopy is located away from the turbulence generated at the ground level, and the pressures are dominated by the pressures and velocities that occur at the canopy height. Such similarity is only specific of this case and does not occur in enclosed structures.

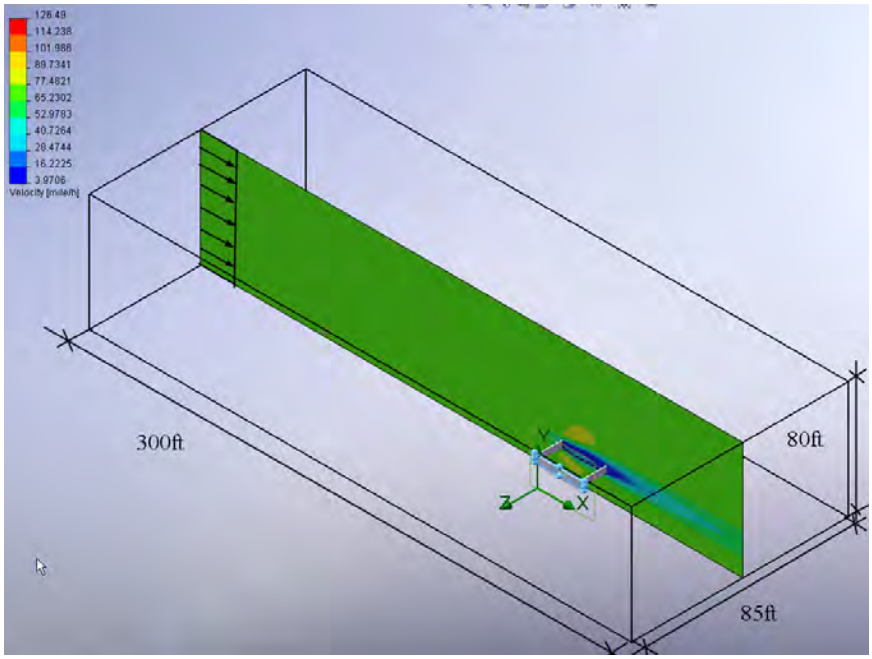

Figure 3.3: Computational domain for Model #2, without boundary definition and uniform wind profile.

To investigate the sensitivity of the solution to changes in the number of elements adopted, the laminar model was considered. A third computational model (see Figure 3.4), named Model #3 was also created. This model has a smaller computational domain in which

laminar flow was assumed with a constant velocity profile in height at the inlet boundary. The domain dimensions assumed in this initial example are 150 ft (45.7 m) in the x direction, 85 ft (25.9 m) in the z direction, and 80 ft (24.4 m) in the y direction. This computational model was created to verify if similar results can be obtained with a smaller computational domain and number of fluid cells compared to the computational domain on Model #2 and Model #1.

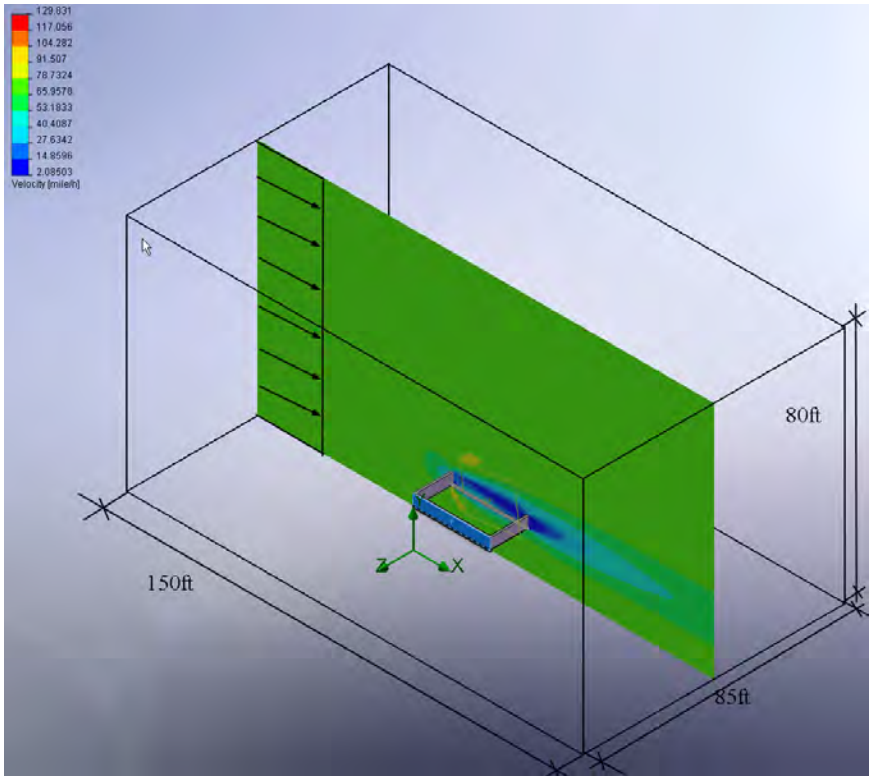

Figure 3.4: Computational domain for Model #3, without boundary definition and uniform wind profile.

The results from the initial computational domain, Model #1, with the use of the inlet boundary layer calculated with the power law, were compared against a similar domain in terms of geometry and number of fluid cells. The number of fluid cells generated for Model #1 and Model #2 was 303,123. The domain for Model #3 generated a number of cells of 54,954. The computational time on a personal computer was drastically reduced from 3 hours and 27 minutes

for Model #1 and Model #2, to 23 minutes for Model #3. In addition, Cp values on top surfaces on each canopy model were compared (See Figure 3.5 to 3.7) and the results obtained were similar. Based on these results, it was decided that further analysis would be performed with the smaller domain of Model #3 using a uniform velocity profile at the inlet surface, as shown in Figure 3.4.

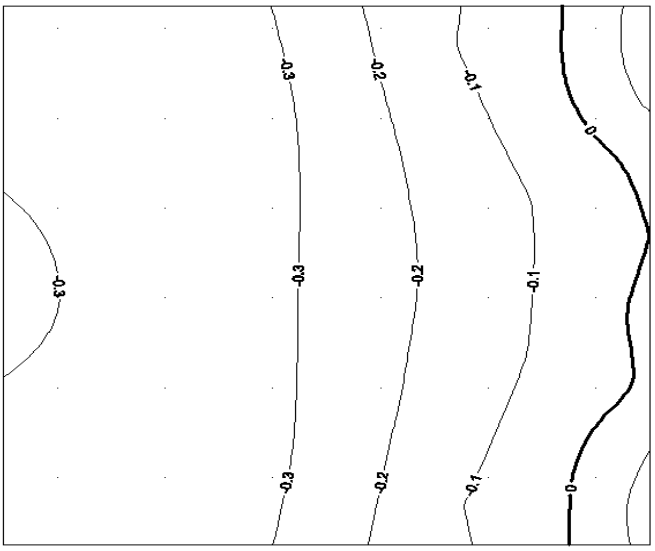

Figure 3.5: Model #1 top surface Cp values.

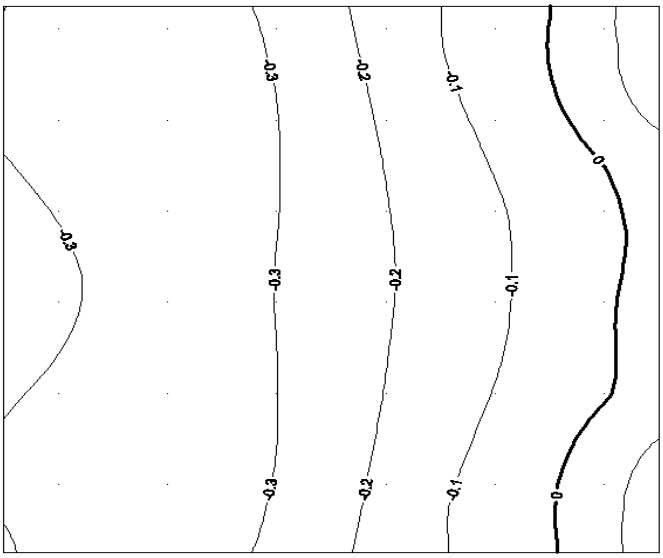

Figure 3.6: Model #2, top surface Cp values.

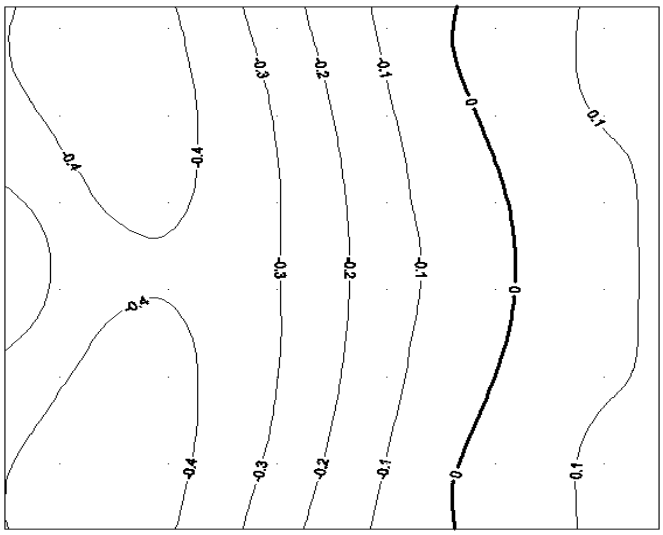

Figure 3.7: Model #3, top surface Cp values.

The significance of velocity in the model and in real situations is not self-evident and needs some clarification. The sustained wind velocity used for analysis on Model #2 and Model #3 was obtained from the wind velocity in Model #1, with the use of the power law formula. The wind speed velocity calculation with an hourly wind speed of 96 mph (145 mph 3 sec gust wind speed, same as ASCE 7-05 basic wind speed for Puerto Rico) was obtained using Figure C6-2, in the ASCE 7-05 Commentary (ASCE 2005).

$$V(z) = (Vz_{ref})(\frac{z}{z_{ref}})^{1/\alpha} = 96mph(\frac{12\,ft}{32.8\,ft})^{1/4.16} = 75mph \qquad 3.21$$

Vz_{ref} = hourly wind speed wind speed (mph), z = mean roof height (ft), z_{ref} = reference height = 32.8 ft (10 m), $1/\alpha$ = power law exponent = 1/4.16 = 0.24 for open terrain on the UNNE wind tunnel.

This result is based on the power law and the result is the hourly wind speed at 12 ft averaged over one hour. The averaged one hour wind speed is commonly used as a reference wind speed in wind tunnel simulations. The hourly wind speed obtained will be used in the CFD simulations for Model #2 and Model #3.

The wind speed in Model #1 at the canopy roof height was approximately 75 mph. The same wind velocity of 75 mph, but sustained, instead of a wind profile calculated by the power law, was applied to Model #2 and Model #3. This means that the same wind velocity was applied on all investigated models at open canopy height. The results for laminar (Figure 3.5) and for uniform velocity flow (Figure 3.6) are virtually identical in terms of values and distributions. Based on the agreement and on the significant differences in computer time required, it was decided that the detailed investigations and comparisons with wind tunnel would be done using uniform velocity flow. Regarding the use of a different number of cell elements in the uniform velocity flow (Figures 3.6 and 3.7), some small differences were obtained in the results. The area of exposure of both models against the wind at the same canopy heights is similar. Further analysis was performed with the smaller domain of Model #3, using a uniform velocity profile at the inlet surface. The CFD Reynolds number calculated for the simulation is 8.52×10^7.

The CFD software yields results of wind pressures on the external (top and bottom) surfaces of the structure. In this case, a wind velocity similar to those specified by design codes has been adopted, with an hourly wind speed of 33.5 m/s (75 mph) for all simulations. This sustained wind speed is equivalent to 64.8 m/s (145 mph) 3 second gust wind speed, as required by ASCE 7-05 for Puerto Rico. Within the context of this research, CFD simulations were extremely useful to identify and define the geometric characteristics of the canopies to be investigated prior to the construction of physical models that were tested in a wind tunnel facility. Preliminary investigations allowed the identification of the high-pressure areas, which were in turn used to specify the location of the wind pressure taps that were used in the small scale models.

The initial geometry of the canopy analyzed consists of a 7.6 m (25 ft) x 7.6m (25ft) with a 1.2m (4ft) parapet. The roof height is located at 3.6m (12ft). The proposed geometry was decided after comparing photographs and visits through many existing gas stations in Puerto Rico. The proposed geometry is very common and used in many gas stations in Puerto Rico.

The mesh cells sides used on the program are orthogonal to the specified axes on the coordinate system. The mesh can be automatically created using a mesh generator, but the mesh in this simulation was specified so that it could be refined on the exposed surfaces. Further sub-meshing was assigned for refinement on all exposed surfaces. Refer to Figure 3.8 and Figure 3.9 for meshing and sub-meshing images.

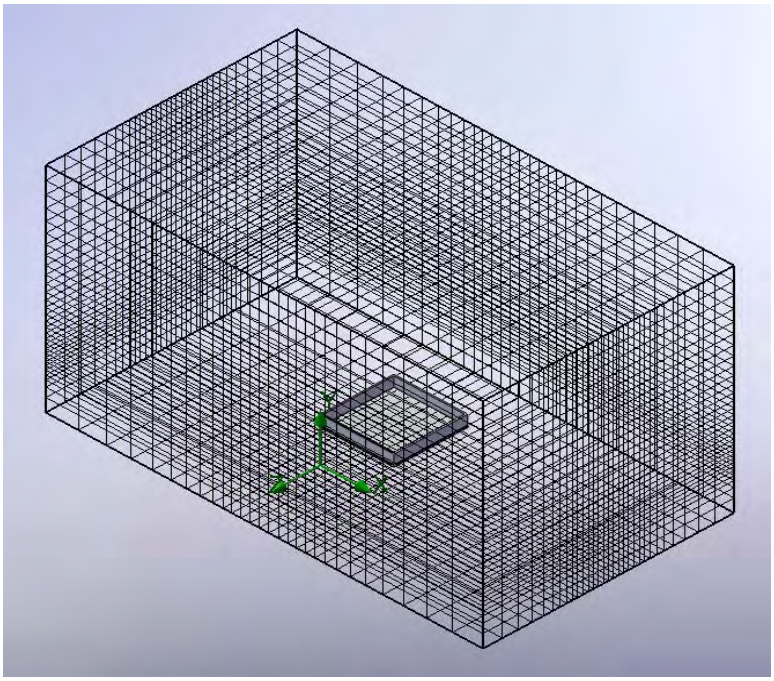

Figure 3.8: Computational domain and meshing used in Model #3.

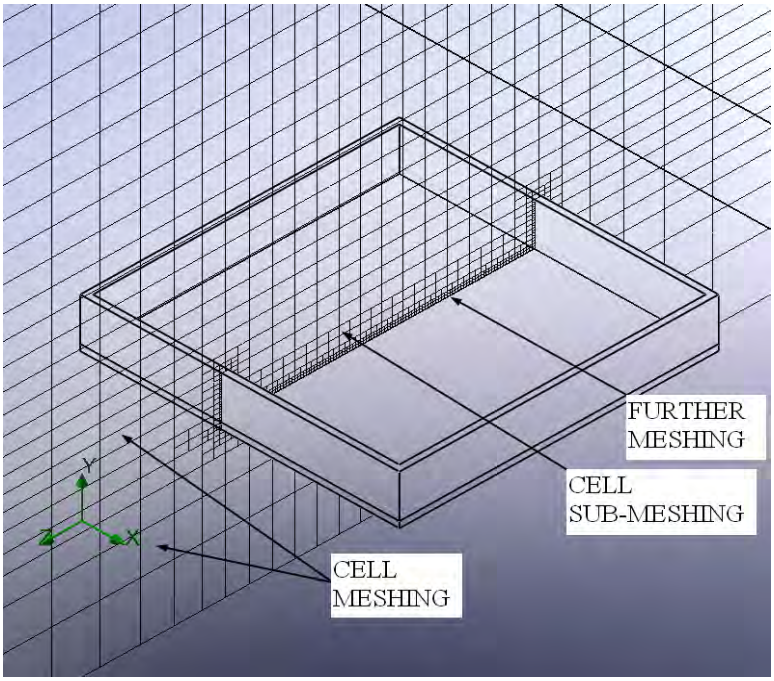

Figure 3.9: Open canopy showing fluid cell mesh, submeshing and further meshing at Model #3, domain intercept.

Wind pressures coefficients Cp's were obtained from the CFD simulations. To compare the results from the wind tunnel, data was obtained at the same geometric location where the pressure taps were located in the scale model. Specifically, pressure taps were located on the top surface, bottom surface and on all parapets covering inside and outside surfaces, and their locations as indicated in Figure 3.10. The same tab locations were used in the CFD models to specify mesh points. Results of the Cp (pressure coefficient factor) were obtained from the CFD simulation, and have been represented in Figure 3.11 in terms of contour lines. The expression used in EFD.Lab to evaluate the pressure coefficients is:

$$Cp = \frac{p - p_0}{\frac{1}{2}\rho V^2} \qquad 3.22$$

where V=reference wind speed (fps), ρ = air density (slugs), p= pressure measured at point of interest (psf), p_0 = reference pressure (psf).

The CFD model with the location of the pressure taps has is shown in Figure 3.12. As mentioned before, the pressure taps are at the same locations as in the model tested at the wind tunnel. Results from those simulations will be reported in Chapter 6 of this dissertation.

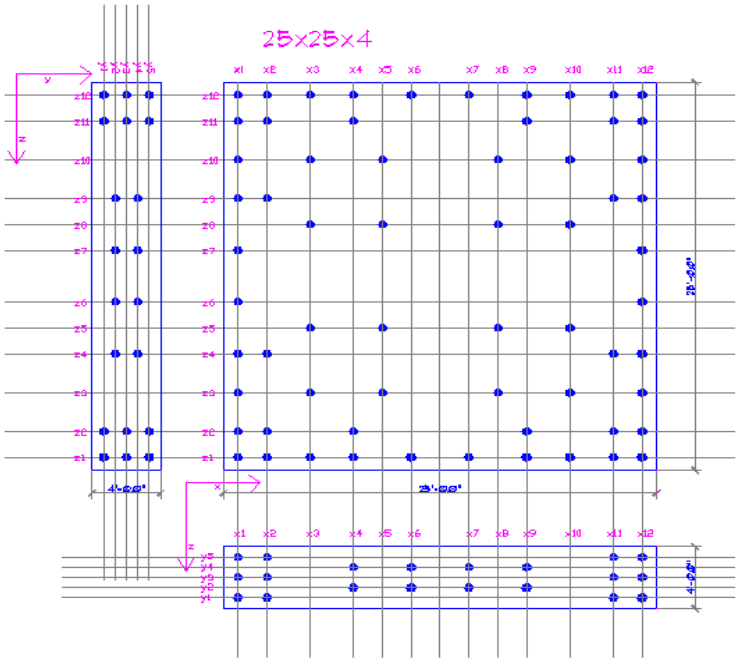

Figure 3.10: Pressure tap locations on top, bottom and parapet surfaces used for CFD and wind tunnel scale model.

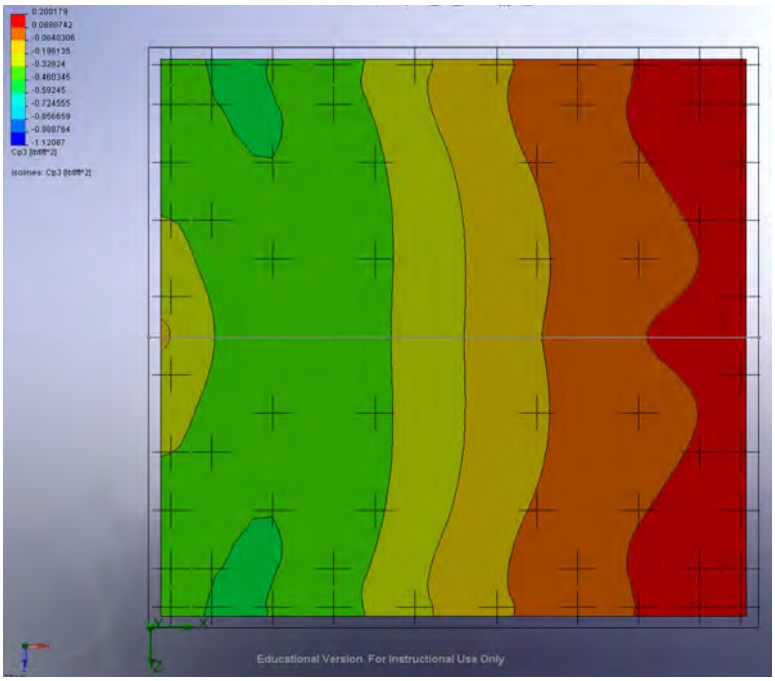

Figure 3.11: Location of pressure taps and measured wind pressures on the top surface. Wind direction acting from the right (0 degrees).

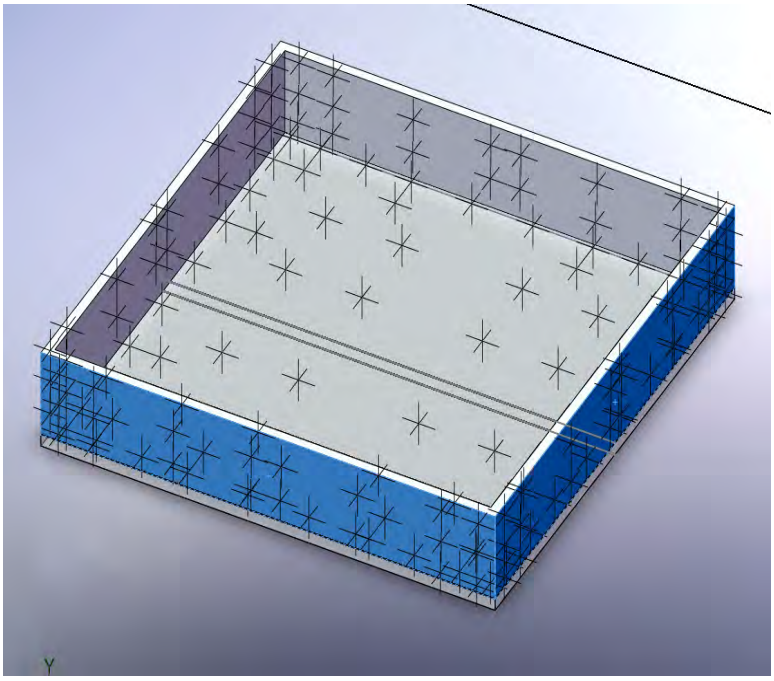

Figure 3.12: Model pressure taps on the canopy model.

Two wind directions were used for the computational model, which were the same wind directions used in the wind tunnel. Following Gumley (1981, 1982), and Letchford (1992), one direction was assumed at 0 degrees (see Figure 3.13) and the second one at 30 degrees of the long axis of the canopy (see Figure 3.14). Verification was done with the use of CFD and running one model with the wind applied at different directions, and we confirmed that the choice of 0 degrees and 30 degrees leads to extreme values in terms of Cp. Considerations regarding the use of CFD models will be made again in Chapter 6, where numerical and experimental results are compared.

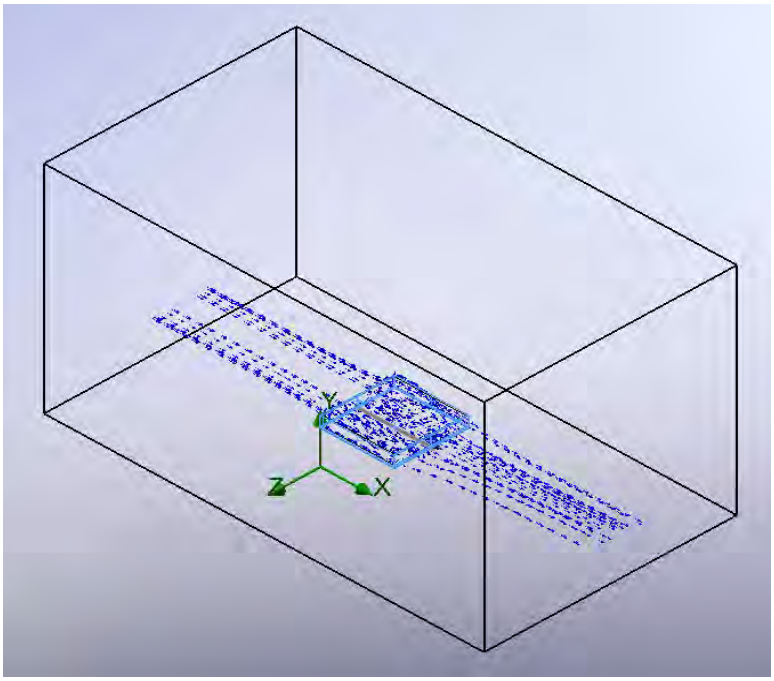

Figure 3.13: Wind direction in CFD model at 0 degrees.

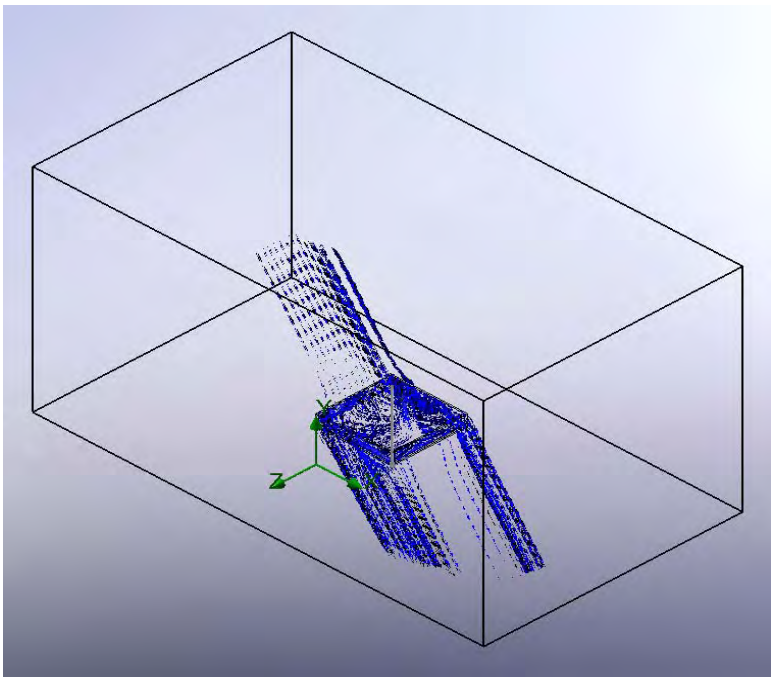

Figure 3.14: Wind direction in CFD model at 30 degrees.

CHAPTER 4. WIND TUNNEL TESTING

4.1 General features of wind tunnel studies

The use of wind tunnels to aid in civil engineering, structural design and planning has been increasing in recent years. The purpose of wind tunnel tests is to provide designers with information on local wind parameters, and wind loads having an accuracy far exceeding that which can be obtained from predictions based on other less expensive means such as theory, numerical analysis, and consulting (Liu 1991).

Some structures warrant a wind tunnel test, like skyscrapers, large structures, constructions having unusual shapes or major structures located in special locations. Examples of special locations are those affected by topographical features, such as hills, cliffs or valleys. In these situations, the use of wind tunnel tests is used to improve the final design. Failure to conduct tests or investigate using the wind tunnel may result in an unsafe design.

A wind tunnel model test conducted in the United States may approximately cost in the order of forty thousand dollars, so that most companies cannot afford a wind tunnel test for every structure to be analyzed. A wind tunnel test cannot be financially justified, unless the expected savings from such a test are far greater that the cost of conducting it. Safety in most of the cases is not the motivation for wind tunnel tests. Savings in cladding are the primary motivation in terms of analyzing structures with complex geometries. In several cases, wind tunnel testing can produce thousands of dollars in savings when actual wind pressures can be obtained from it.

Numerous criteria exist to categorize wind tunnels. According to the flow circuit, a tunnel may be classified as either an open or closed circuit tunnel. An open circuit tunnel is normally a

straight structure. Air is drawn into the tunnel from a funnel-shape intake at one end of the tunnel, and the air exits the tunnel through a funnel shape outlet. The enlarged cross-sectional areas at the two ends prevent undesirable strong winds from being generated outside the tunnel near the inlet or outlet. The closed circuit type is a recirculation loop. It may occupy a small space if the loop is vertical. Advantages of closed circuit tunnels are, (1) they do not cause undesirable winds in laboratories housing the wind tunnels; (2) they generate less noise. Both open and closed circuit tunnels are often used for testing structural models. The tunnel used in this investigation, was an open circuit tunnel at UNNE.

A boundary layer wind tunnel must have a test section that is sufficiently long to generate a thick vertical boundary layer, sufficiently high so that the boundary layer generated will not touch the tunnel ceiling and sufficiently wide so that neighboring structures and topographical features can be incorporated into the model. Furthermore, the blockage ratio, which is the ratio of the cross sectional area of the model blocking the flow and the cross sectional area of the tunnel test section, must be less than one tenth. These requirements necessitate rather large tunnels. The boundary layer tunnels used in commercial testing of structural models normally have a minimum width of 2.4 m (8ft), minimum height of 1.5 m (5 ft), and a minimum length of 10 m (33 ft), all measures referring to test sections.

To facilitate the rapid growth of a vertical boundary layer along the tunnel test section, roughness elements must be placed on the tunnel floor, and additional devices, such as spires, must be installed upstream. The roughness and the spires must be designed to produce the type of velocity profile and the type of turbulence similar to that encountered by the prototype structure. Typically, the model tested in a wind tunnel is placed on a turntable so that it can be

studied for winds from different directions. To simulate the wind field correctly, the model should include the terrain and structure features.

Major components of a wind tunnel include fan, test section, nozzle, diffuser, honeycomb, flow strengtheners, guide vanes, screens, turntable, spires and roughness elements on the floor. The fan is needed for all types of wind tunnels. The test section is where the model is tested and where the atmospheric boundary layer is simulated. The model is always placed near the downstream end of the test section where the boundary layer thickness is maximum. The turntable is round and has a diameter slightly smaller than the width of the test section. The turntable is covered with the structure to be tested. Further upstream the floor is covered with roughness elements to generate and maintain a turbulent boundary layer. The roughness elements are normally cubic elements attached to the tunnel floor (Liu 1991).

4.2 Wind tunnel description

Wind tunnels are equipment designed to obtain air flow conditions, so that similarity studies can be performed, with the confidence that actual operational conditions can be reproduced. The wind tunnel testing was performed during 2008/2009 academic year at Universidad Nacional del Nordeste (UNNE) in Resistencia, Argentina. The UNNE wind tunnel facility is a low velocity atmospheric boundary layer wind tunnel, built with the aim to perform aerodynamic studies of structural models. The distribution of the flow on the structural model must be such that the atmospheric boundary layer at the actual location is reproduced. This is obtained with the help of turbulence promoters and vortex generators, so that wind simulations could be performed (Wittwer and Moller 2000).

Figure 4.1: View the UNNE wind tunnel facility. (Photograph by the Author)

The facility is an open circuit tunnel with a length of 22.8 m (74.8 ft), the testing chamber being a rectangular section of 2.4 m (7.87 ft) width and 1.8 m (5.9 ft) in height and uses a 2.25 m diameter (7.38 ft) fan with a 92 kW motor. The maximum wind velocity that may be obtained in this tunnel is 25 m/s (55.9 mph) when the testing section is empty (the section is empty when there is no model in the testing chamber). Further details regarding this wind facility are given by Wittwer and Möller (2000).

All models were tested under a wind simulation corresponding to a suburban area. The simulation of the natural wind on the atmospheric boundary layer was performed by means of the Counihan and Standen methods with velocity distributions defined as ground covered by several closely spaced obstacles in forest or urban territory (Wittwer and Moller 2000). The Counihan and Standen methods are techniques developed to thicken boundary layers on wind

tunnels. These techniques are generally known as roughness, barrier and mixing-device methods (Natalini et al. 1998). Surface roughness was obtained on 17 m (55.7 ft) test floor section with prismatic 30x30x22 mm (1.18x1.18x.89 in) elements, 80 mm (3.14 in) apart. The choice of element size and packing density was based on the works of Counihan, Fang and Sill, Gartshore and Cross (Natalini et al. 1998).

Representative values of power law exponent $1/\alpha = 0.24$ and the roughness length parameter $z_0 = 0.7\,\mathrm{m}$ were adopted in order to obtain a scale of 1:500, a usual scale in simulations. Consequently, the design value in the wind tunnel for the specified scale is $z_0 = 1.4mm$. The same suburban terrain exponent was used on the CFD simulation. The suburban terrain condition corresponds to open terrain with scattered obstructions having heights of less than 9.1 m (30 ft). According to the ASCE 7-05, it corresponds to Exposure B. In order to obtain a boundary layer depth of $\delta = 1.3\,\mathrm{m}$ artificial simulation methods were applied. This technique called natural simulation produces simulation scales higher than 1:500, and it requires the use of long wind tunnels. The simulation hardware consisted of two modified Irwin's spires, as shown in Figure 4.2 and 4.3. Figure 4.4 shows the tunnel plan at UNNE.

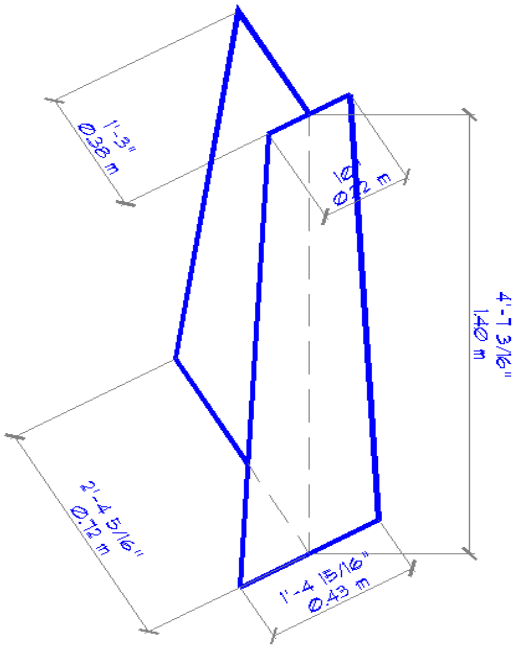

Figure 4.2: Typical Irwin spires used on the UNNE wind tunnel.

Figure 4.3:View the UNNE surface roughness and Irwin spires. (Photograph by the Author)

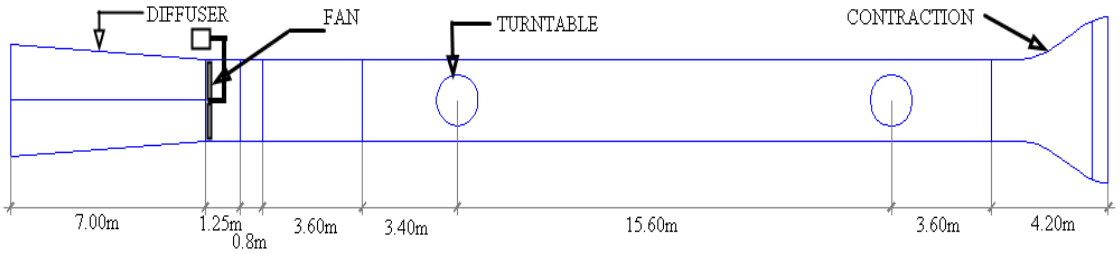

Figure 4.4: Wind tunnel plan at UNNE (reproduced from Wittwer and Moller 2000).

In this way, a part-depth boundary layer simulation of neutrally stable atmosphere was obtained. Mean velocities, when fitted to a potential law, with an exponent of 0.24 obtained at UNNE are shown on Figure 4.5.

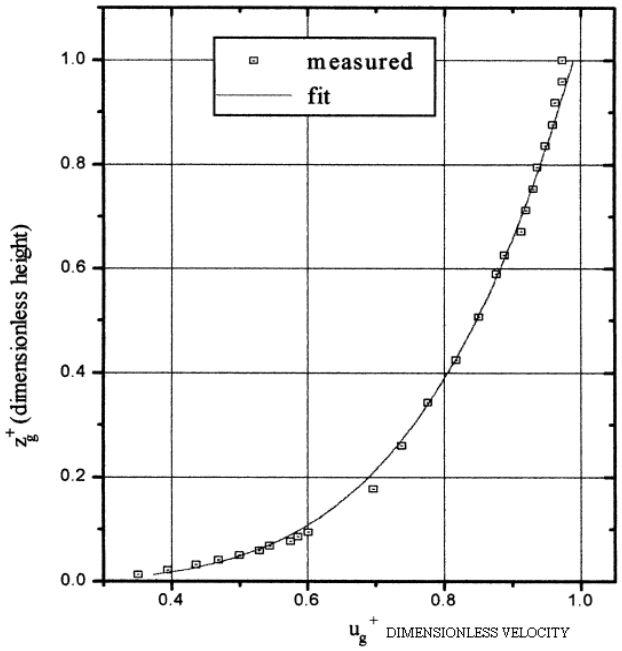

Figure 4.5: Mean velocity profiles at the UNNE wind tunnel (Wittwer and Moller 2000).

4.3 Construction of models

The similitude theory in fluid mechanics requires that all model tests must be conducted under geometric, kinematic and dynamic similarities. Geometrical similarity requires that the shape of the model must be the same as that of the prototype. Kinematic similarity means the velocity field must be similar. Dynamic similarity means the pressure distribution and the generated forces must be similar too (Liu 1991). These three similarities are not independent of each other. For example, in this research a scale ratio of 1:50 is proposed. Making the Reynolds number identical for the model as for the CFD model yields

$$R_m = R_p \Rightarrow \frac{\rho_m V_m L_m}{\mu_m} = \frac{\rho_p V_p L_p}{\mu_p}$$

where R_m=Reynolds number for the model, R_p=Reynolds number for CFD, $\rho =$ air density, $\mu =$ dynamic viscosity, $V =$ velocity and $L =$ length. Air density and viscosity are similar on both cases, consequently

$$\frac{V_m}{V_p} = \frac{L_p}{L_m} = 50$$

This simple calculation shows that to maintain the same Reynolds number the wind speed for the wind tunnel needs to be 50 times of the prototype velocity. This is very hard to obtain on a wind tunnel. The Reynolds number on the wind tunnel is 3.67×10^6. The calculated Reynolds number on the CFD simulation is 8.52×10^7. As long as the Reynolds number is not smaller than 10^4, it will allow the flow around the model to remain turbulent, and kinematic and dynamic similarities will prevail (Liu 1991).

Experiments were conducted on one 1:50 scale model of a 7.5 m (25 ft) × 7.5 m (25 ft) square roof with parapets of 1.2 m (4 ft) high, having an eave height of 3.6 m.(12 ft). The usual

scale for wind tunnel testing of open structures varies from 1:50 to 1:100. In this particular research, a scale of 1:50 was chosen in order to install all the PVC tubes to be connected to the testing instruments without any interference.

First, experiments were carried out without parapets in order to compare with other wind tunnel results available in the open literature. Wind load coefficients were measured under wind blowing at angles of 0° and 30° relative to one of the symmetry axis, since, as demonstrated by Gumley (1981, 1982) and Letchford et al. (1992) among others, these directions produce the most severe loads on planar canopy roofs with no parapets. In the absence of additional information, it was expected that such angles would still be relevant for canopies with parapets.

The roof of the model and the parapets were made with a 2 mm thick aluminum plate, and the columns with a 2.5 mm diameter steel rod. As the models have two axes of symmetry, only a quarter of the roof model was instrumented with pressure taps in place, thus reducing the number of tubes needed. In addition, all the tubes were led towards the farthest corner, where they formed a bundle that went into a horizontal pipe through which they went away from the model to finally go under the floor. In this way, the scale distortion in both columns and roof thickness and the possible interference of the tubes upon the measurements were minimized. The model is shown in Figures 4.6 to 4.8.

Figure 4.6: Model with parapets with PVC tubes and columns. (Photograph by the Author)

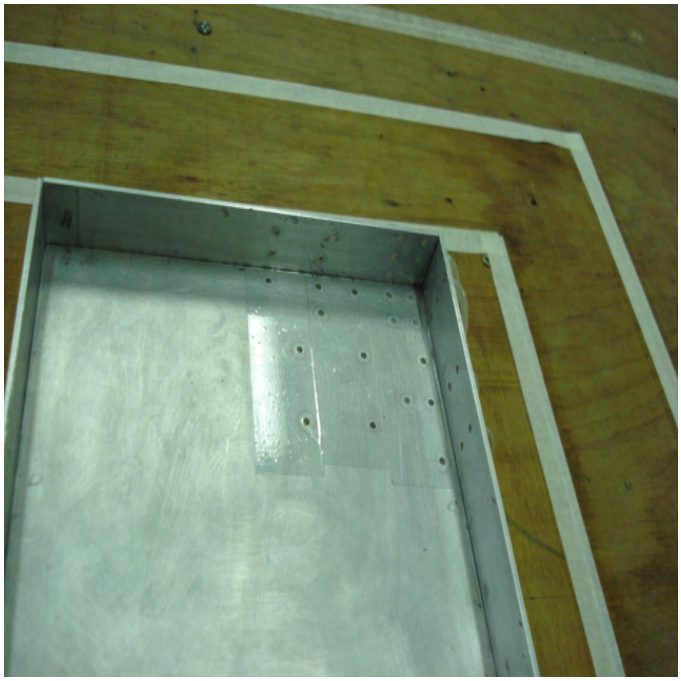

Figure 4.7: Top view of the model, showing the distribution of 16 pressure taps on the top surface of the canopy and parapets. (Photograph by the Author)

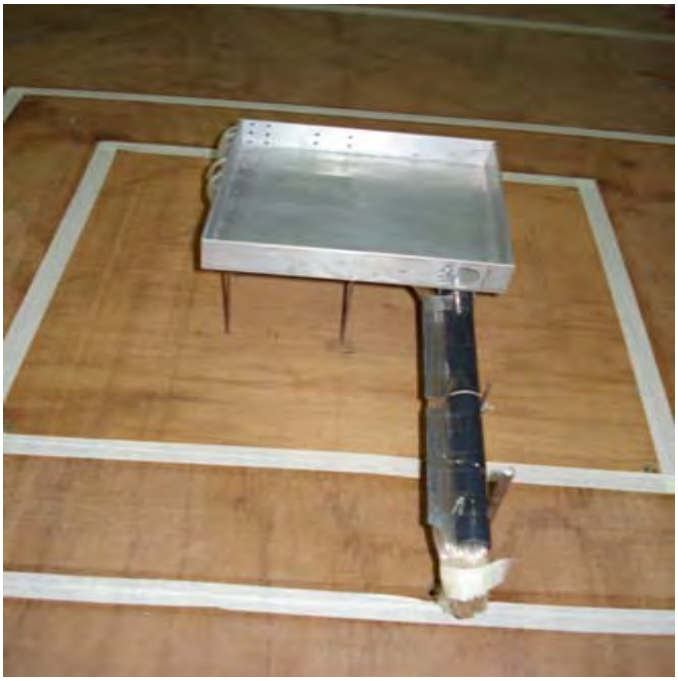

Figure 4.8: Distribution of pressure taps on the model with bundle of tubes and columns. (Photograph by the Author)

Sixteen pressure taps were spread on the roof and twenty on the parapets. The specific locations of the taps were influenced by the previous computational results which indicated, and suggested places of special interest in terms of pressure values. Figure 4.9 shows the position of the pressure taps on the top surface of the model and Figure 4.10 shows the model placed in the turntable. The turntable is a round table of 1.5 m (4.9 ft) of width, which is rotated during the wind test in order to obtain the desired wind pressures.

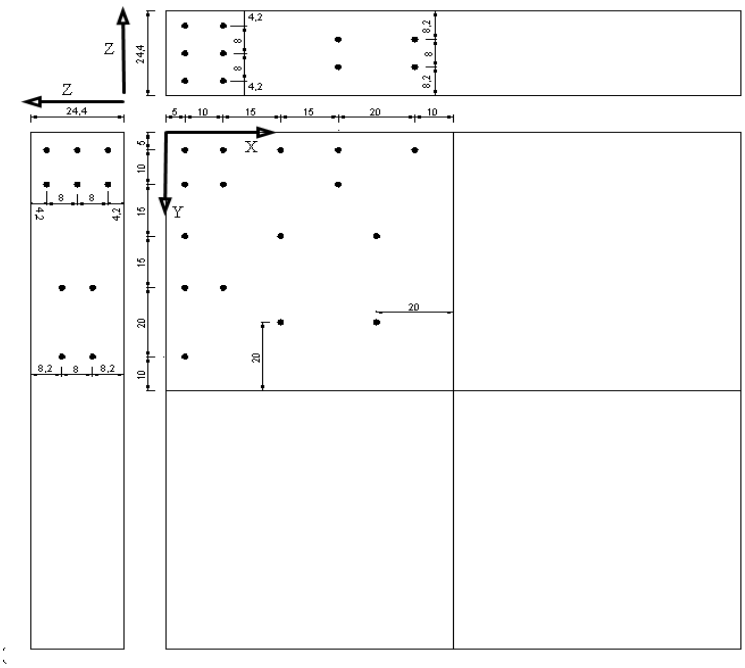

Figure 4.9: Distribution of pressure taps on the model.

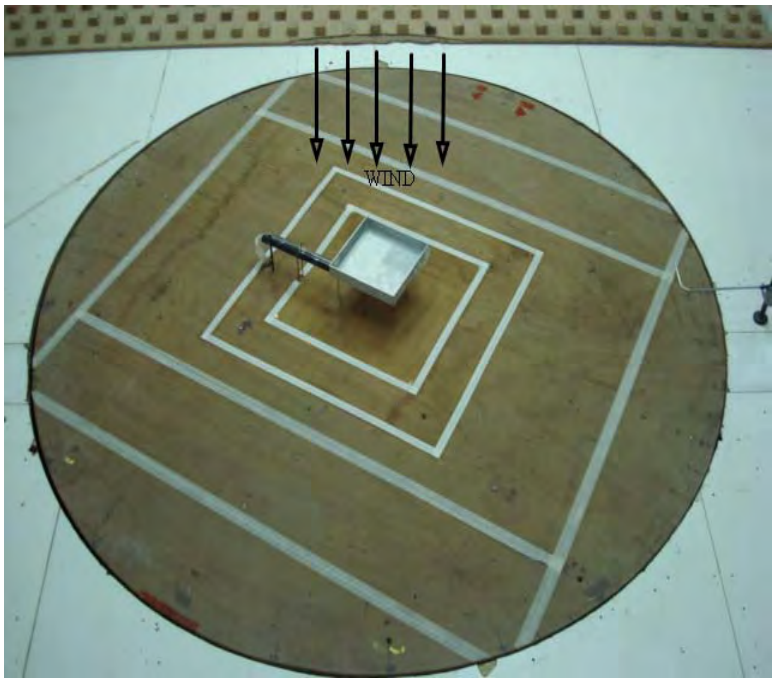

Figure 4.10: View of the model with parapets on the turntable (Photograph by the Author).

4.4 Instrumentation

Pressures were measured using a differential pressure electronic transducer. The brand used in this tunnel is Micro Switch Honeywell 163 PC (Figure 4.11). The transducer converts the pressure differences from the model and the reference static pressures, to differences in voltage.

Figure 4.11: View of the pressure electronic transducer Honeywell 163PC. (Photograph by the Author)

A sequential switch Scanivale 48 D9-1/2, which was driven by means of a CTLR2 / S2-S6 solenoid controller, connected the pressure taps to the transducer through PVC tubes of 1.5 mm internal diameter and 650 mm in length (Figure 4.12). The Scanivale system is the only working system available in this tunnel. It has some disadvantages in the sense that measurements cannot be taken simultaneously but should be obtained following a sequence. Each PVC tube connected to the Scanivale is connected to a pressure tap on the scale model. For this experiment, each pressure tap data was acquired once at a time following a numerical order.

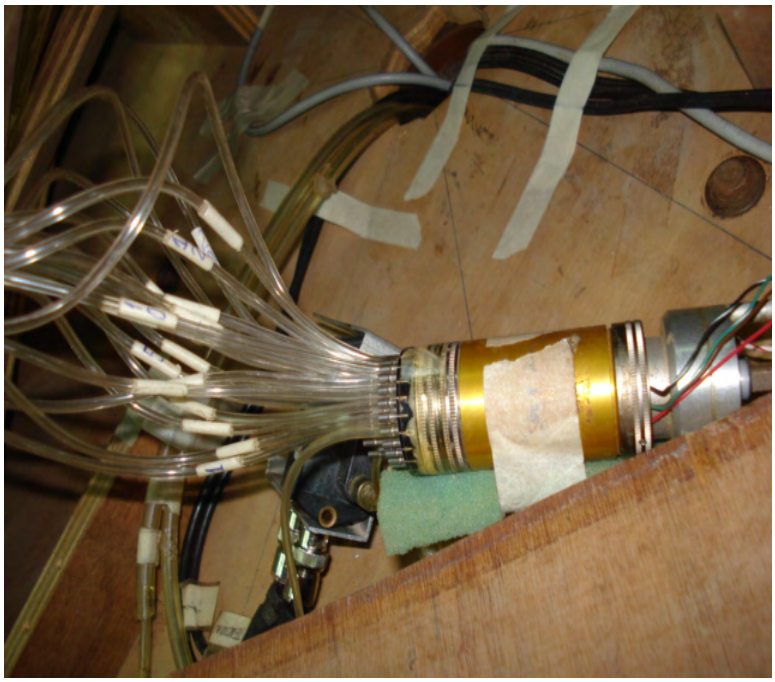

Figure 4.12: View of the Scanivale 48 D9-1/2 w/PVC tubes (Photograph by the Author).

No resonance problems were detected for tubes of that length. Therefore, restrictors for the tubes were not used for filtering. When a fluctuating signal flows through the tubes in order to reach the Scanivale, verification that the signal is not amplified or with distortion is done through comparison with previous results. Those signals go to the DC transducer output and were read with the aid of a Keithley 2000 digital multimeter. The integration time operation rate of the A/D converter was set to produce mean values over 15 seconds of time integration (Figure 4.13). The multimeter was configured to read and store the values every 0.6 seconds, and every 25 readings and average are recorded every 15 seconds. This procedure can obtain variances in the order of +/- 0.02 of the pressure coefficient.

Figure 4.13: View of the UNNE Keithley 2000 digital multimeter (Photograph by the Author).

Simultaneously to the pressure measurements being taken on any of the roof surfaces, the reference dynamic pressure, q_{ref}, was measured at the eave's height with a Pitot-Prandtl tube connected to a Van Essen 2500 Betz differential micro-manometer of 1 Pa resolution (Figure 4.14). The probe stayed beside the model at a distance of about 0.70 m to avoid mutual interference. The reference static pressure was obtained from the static pressure taps of the same Pitot-Prandlt tube (Figure 4.15).

Figure 4.14: View of the Van Essen 2500 Betz differential micro manometer. (Photograph by the Author)

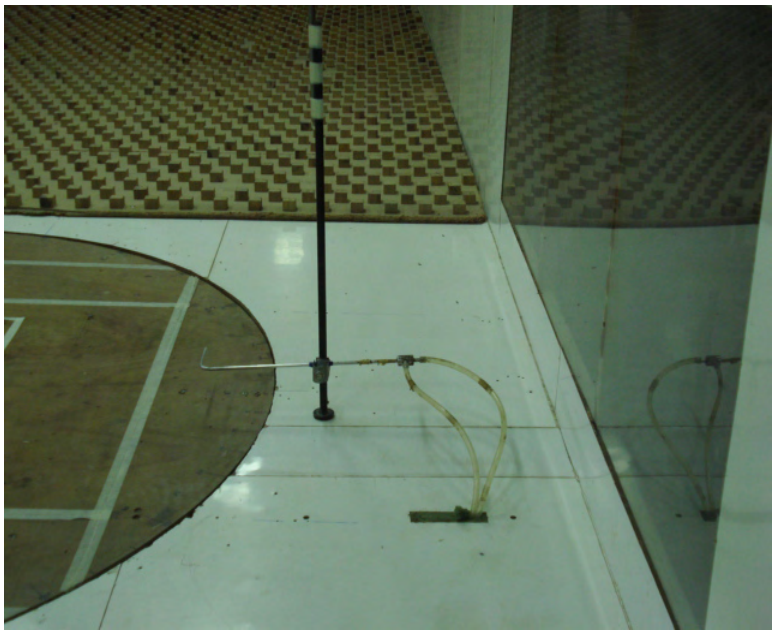

Figure 4.15: View of the Pitot-Prandtl tube. (Photograph by the Author)

The wind tunnel fan is an axial type, Aerofol model 88-J with a velocity of rotation of 720 rpm. The motor has a power of 100 kW generating a maximum wind velocity of 25 m/s (55.9 mph). Refer to Figure 4.16 for a photograph of the tunnel fan.

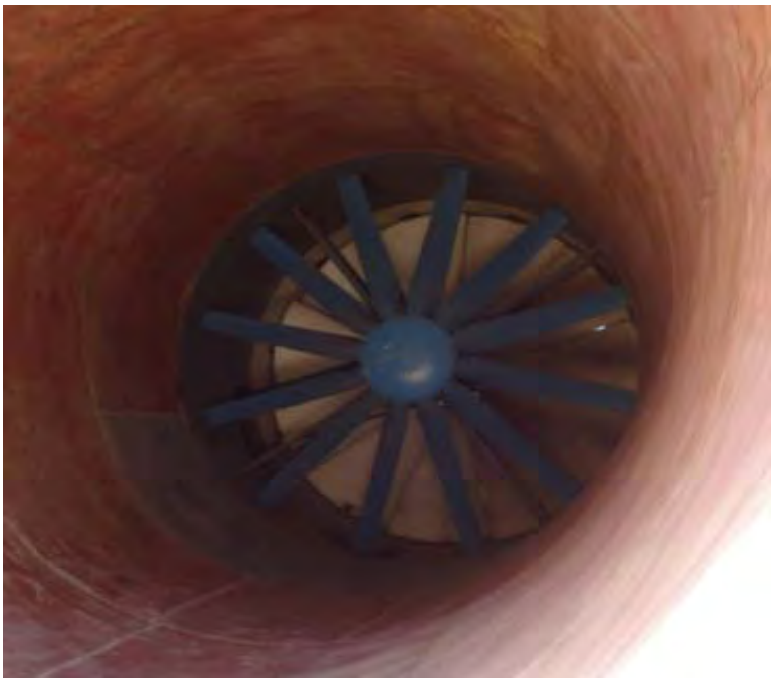

Figure 4.16: View of the UNNE tunnel fan. (Photograph by the Author).

4.5 Data processing

In order to obtain pressure coefficients from the wind tunnel at the UNNE, the following procedure has been used. The first step is to calibrate the electronic transducer. Inducing pressure and suction on the differential micromanometer, readings from the multimeter on each of the induced pressures are obtained. Figure 4.17 shows the data obtained from the multimeter on the

model without parapets. The procedure is done at the beginning of the test and at the end to verify that there were no sudden pressure changes that can affect the measured data.

CALIBRACION DE TRANSDUCTOR

PRESION [Pa]	Lecturas [voltios]	
	Inicio	Fin
0	3.509	3.510
20	3.548	3.550
40	3.588	3.590
60	3.628	3.630
-10	3.488	3.490
-20	3.468	3.470
-30	3.449	3.451
-40	3.429	3.431
-50	3.409	3.410
	16:44	18:57

Figure 4.17: Calibration data on model without parapets.

Figure 4.18: Photograph showing the author taking data from the wind tunnel test.

With the data obtained for the calibration, and using a spreadsheet we can obtain the linear relation between the pressure differential and the voltage obtained. The manufacturer of the electronic transducer guarantees that there is a lineal relationship in order to obtain the slope and intercept in the form of:

$$P = a + b * Voltage$$

This processed calibration data is then used for the calculation of the pressure coefficients, Cp factors. Cn values are computed from the difference of Cp values. Figure 4.19 shows a sample of the processed transducer calibration data.

Test February 25 2009				
Exterior α = 30		Exterior α = 210		
Exterior α = 330		Exterior α = 150		
Pressure[Pa]	Voltage		P=a+b.Volt.	
0	3.509	b	501.8434	
20	3.548	a	-1761.1235	
40	3.588			
60	3.628	Test	-50.339333	
-10	3.488			
-20	3.468			
-30	3.449		Error Analysis	
-40	3.429	a=	-1762.7048	1.5813
-50	3.409	a=	-1760.1208	-1.0027
0	3.51	b=	502.4224	-0.5789
20	3.55	b=	501.4299	0.4135
40	3.59			
60	3.63		Least square method	
-10	3.49		to fit data	
-20	3.47			
-30	3.451			
-40	3.431			
-50	3.41			

Figure 4.19: Processed data for the calibration of the transducer.

The pressure electronic transducer receives from the PVC tubes a pressure from the model and a pressure from the static pressure Pitot-Prandlt, which is used to measure q_{ref} or the

dynamic pressure of reference. This potential difference is measured with the digital multimeter. This signal is fluctuating due to the fluctuation of the wind. As mentioned before, the multimeter was configured to read and store the values every 0.6 seconds, and after 25 readings, an average is recorded (every 15 seconds). Figure 4.20 shows the processed data after the transducer was calibrated. The pressure difference, for example, is obtained using the previous equation:

$$P = a + b*Voltage = +(-1761.12 + 501.84*(3.504)) = 2.664Pa$$

Exterior, interior and total pressures on Model 1				
Without parapets				
α = 30				
Exterior pressures				
Tap number	Potential [ ]	Pres.Dif.[Pa]	q_{ref} [Pa]	c_e
1	3.504	-2.664	108.7	-0.025
2	3.476	-16.716	108.6	-0.154
3	3.477	-16.214	108.5	-0.149
4	3.463	-23.240	108.4	-0.214
5	3.458	-25.749	108.3	-0.238
6	3.505	-2.162	108.2	-0.020
7	3.512	1.351	108.1	0.012
8	3.507	-1.159	108.0	-0.011
9	3.494	-7.683	107.9	-0.071
10	3.516	3.358	107.8	0.031
11	3.514	2.354	107.7	0.022
12	3.487	-11.196	107.6	-0.104
13	3.516	3.358	107.5	0.031
14	3.492	-8.686	107.4	-0.081
15	3.517	3.860	107.3	0.036
16	3.515	2.856	107.2	0.027

Figure 4.20: Processed data for the pressure coefficient Cp.

The dynamic pressure of reference, q_{ref}, is measured with the differential micromanometer. The final pressure coefficient is the dynamic pressure/q_{ref}. The net pressure coefficient (Cn) is the difference between the external pressure coefficient and the internal pressure coefficient. Appendix B through E shows the complete data sets, and the procedure with the calculated values on spreadsheets. The results from the wind tunnel tests will be presented and discussed in Chapter 6.

CHAPTER 5. AVAILABLE DESIGN CODE INFORMATION

5.1 General Code Information

Open structures have been designed and constructed in many countries for a number of years. In each case, the designer follows national standards based on best practices. However, little help is found with reference to the problem posed in this dissertation. For the sake of completeness, the design of open structures according to current building codes has been investigated during this research. Several design codes and standards are currently in use worldwide, such as the Uniform Building Code (1997 Edition), the ASCE 7-05 standard, the Eurocode, the Australian Code and the Japanese Code. Those were investigated to identify their current design criteria for the design of open structures. First, American codes (the UBC 97 and the ASCE 7-05) will be discussed in order to investigate current design criteria for the analysis of open canopy structures with parapets. Next, we will mention other design codes used worldwide, and whether they have available information in the design of open canopy structures with parapets.

5.2 UBC 97

The Uniform Building Code, (1997 Edition) is a design code still in use in the West of the United States, and it is also the required building code in use in Puerto Rico. The UBC 97 is complemented in Puerto Rico with the use of the ASCE 7-05 for the calculation of wind pressures. The Uniform Building code covers the design of many types of structures. The open canopy structures will be included on what is called by the code, “unenclosed structures” as defined by Section 1616.

The basic wind speed is the fastest mile wind speed associated with an annual probability of occurrence of 0.02 measured at a point 33 feet above the ground for an exposure category C (UBC 1997), as defined by Section 1618. Design wind pressures are defined on Section 1620. Wind pressure for buildings and calculations are obtained in accordance to

$$P = C_e C_q q_s I_w \qquad \text{(UBC 20-1)}$$

where C_e = Gust factor coefficient, as given in UBC Table 16-G, C_q = Pressure coefficient, as given in UBC Table 16-H, I_w = Importance factor in UBC, Table 16-K, P = Design wind pressure, q_s = Wind stagnation pressure, as set forth in UBC Table 16-F.

The primary load resisting system of every structure shall be designed for the pressures using UBC formula 20-1. Two primary methods, Method 1 (normal force method) and Method 2 (projected area method), are the two methods commonly used for the calculation of wind pressures. No specific design procedure is available for the design of open structures with parapets in the Uniform Building Code, 1997 edition.

5.3 ASCE 7-05

The American Society of Civil Engineers provisions, ASCE 7-05, provide three procedures for the calculation of wind loads. Method 1 or the simplified procedure is discussed in Section 6.4 of the ASCE document, Method 2, the analytical procedure is found in Section 6.5 of the document and Method 3, is the wind tunnel procedure which is described in Section 6.6.

The basic wind speed is the 3-second gust speed at 33 ft (10 m) above the ground in open terrain. The basic wind speeds are specified in the ASCE wind maps in their Figure 6-1. In

Puerto Rico the basic 3-second gust wind is 145 mph. The wind speeds are assumed to be the same for all horizontal directions.

Method 2, the analytical procedure on Section 6.5 describes the procedures for determining the wind pressures. Method 1 cannot be used for the design of open structures due to Section 6.4.1.1 item 3, which describes that it can only be used for enclosed structures.

Section 6.5.10 describes the formula for the calculation of the velocity pressure as follows:

$q_z = .00256 K_z K_{zt} K_d V^2 I$ (ASCE 6-15)

where K_z =velocity pressure exposure coefficient, defined in Section 6.5.6.6, K_{zt} =topographic factor, defined in Section 6.5.7.2, K_d =wind directionality factor, defined in Section 6.5.4.4, V = velocity from Figure 6-1, I = Importance factor for the building or other structure which is determined from Table 6-1.

Regarding exposure, for each wind direction being considered, the upwind exposure category shall be based on ground surface roughness, which is determined from the natural topography, vegetation or surrounding constructed facilities (ASCE 7-05). Surface roughness categories are defined in Section 6.5.6.2. Surface roughness C is used for the wind tunnel simulation and CFD model simulation. Gust effect factor is determined on section 6.5.8. For rigid structures, one should use Section 6.5.8.1 and for flexible of dynamically sensitive structures, Section 6.5.8.2.

Enclosure classifications are defined in Section 6.5.9 in such a way that all buildings shall be classified as enclosed, partially enclosed or open. Section 6.5.13 covers the design of wind loads for open buildings with monoslope, pitched or troughed roofs. Parapets shall be designed as explained in Section 6.5.12.2.4. The ASCE 7-05 does not provide coefficients for structures

that combine both, open canopy and parapets in the same structure. No previous studies have been done evaluating the proposed code coefficients.

5.4 IBC 2006

The most recent design code in the United States is the International Building Code, 2006 Edition. This code is used in the entire nation, and almost all the states are adopting it, or are in the process of incorporating the code to their standards. The IBC 2006 makes reference to the ASCE 7-05 for wind design procedures. It uses all the standards, formulas and coefficients of the ASCE 7, which were briefly described in the previous section.

5.5 Additional Building Codes

Building codes in different parts of the world were investigated, to verify if there was available information for the design of open canopy structures. The Eurocode (CEN TC 250, date: 2002-06, prEN 1991-1-4.6, Eurocode 1: Actions on structures - Part 1-4: General actions – Wind actions), which is used in Europe and many Caribbean islands, does not include any information for the design of open canopy structures with parapets.

The Australian Code, Standards Association of Australia, AS 1170.2-1989, Minimum design loads on structures (known as the SA Loading Code) - Wind loads, 1989, does not include any information for the design of open canopy structures with parapets.

Additional codes include the Japanese Code, which is composed of the Building Standard Law, and the Building Standard Law Enforcement Order. The Building Standard Law, in which objectives of the code, definitions of terms, fundamental concepts are described, was revised in 1998, leading to the performance-based regulation. Following the revision, technical regulations

such as load provisions, and structural calculation provisions, were modified in 2000. They are in the Building Standard Law Enforcement Orders (cabinet orders), the Building Standard Law Enforcement Regulations (Ministry of Land, Infrastructure and Transportation). The former is Ministry of Construction and Notifications of the Ministry of Construction. The revision of the wind load provisions was very drastic, but it was based on the Architectural Institute of Japan (AIJ) recommendations, and it does not include any information for the design of open canopy structures with parapets.

The last two codes explored, the Brazilian Code (Associação Brasileira de Normas Técnicas published “Forças devidas ao vento em edificações NBR 6123”, Jun/1988), and the Canadian Code (NRC-CNRC National Building Code of Canada, Canadian Commission on Building and Fire Codes, 1995), do not provide any information for the design of open canopy structures with parapets.

CHAPTER 6. RESULT OF WIND PRESSURES IN CANOPIES

6.1 Comparison between wind tunnel results and previous work

First, wind tunnel experiments were carried out at UNNE on a canopy without parapets, in order to compare the measurement with other wind tunnels results already available in the open literature. This provides the opportunity to check the accuracy of the tunnel boundary layer and the instrumentation available at UNNE. Wind load coefficients were measured under wind blowing at angles of 0º and 30º relative to one of the symmetry axis, since, as demonstrated by Gumley (1981, 1982) and Letchford et al. (1992), among others, these wind directions produce the most severe loads on planar canopy roofs with no parapets.

Results are next compared against previous work of Ginger and Letchford (1994). It can be seen from Figure 6.1 to Figure 6.4 that both sets of contour lines are very close in both qualitative and quantitative terms. Note that in the present study (Figure 6.2 and Figure 6.4) the interference of the columns has been eliminated in order to prevent the interference caused by the column sizes.

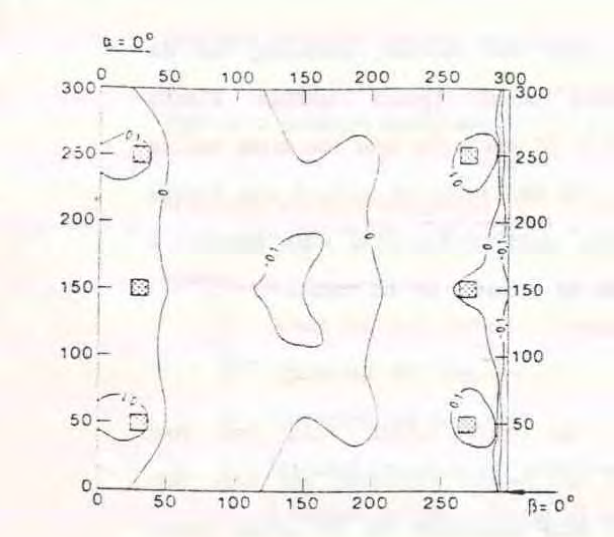

Figure 6.1: No parapets, net pressures, wind direction of 0º from Ginger et al. (1994)

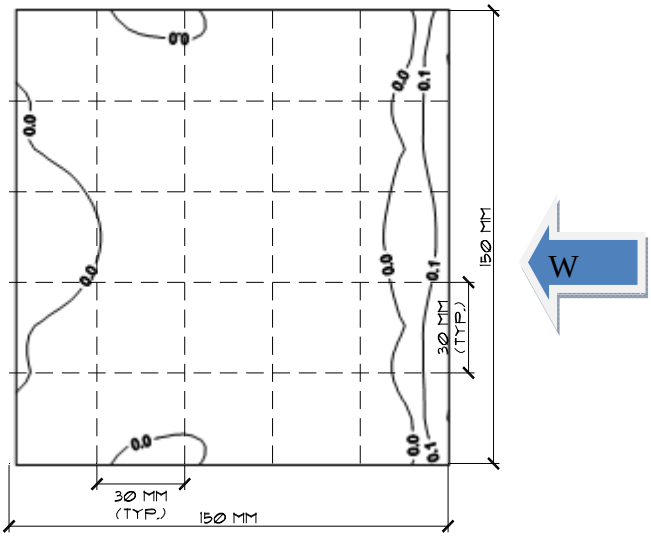

Figure 6.2: No parapets, wind tunnel net pressures, wind direction of 0°, present research.

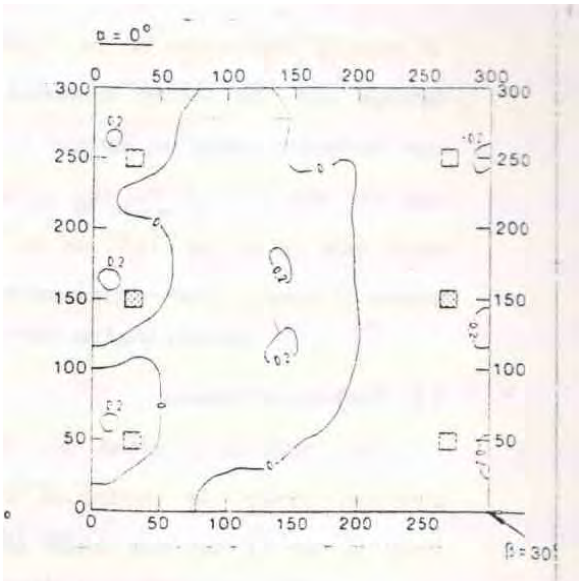

Figure 6.3: No parapets, wind tunnel net pressures, wind direction of 30º (Ginger et al. 1994)

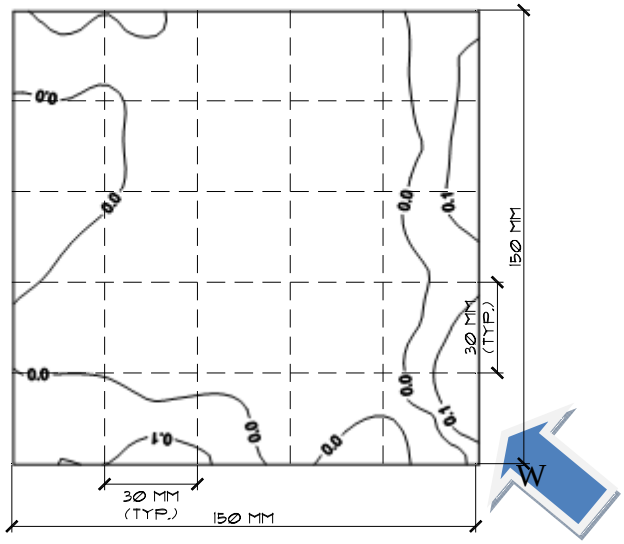

Figure 6.4: No parapets, wind tunnel net pressures, wind direction of 30°, present research.

Data from the wind tunnel (and also from computational models) were recorded on the top and bottom surfaces at 64 pressure points, from which Cp values were obtained for each surface. Two wind conditions were considered in this experimental part of the research: one with

an incident wind oriented along the long axis direction (0°), as shown in Figure 6.1 and 6.2 whereas a second case was considered by rotating the turntable to 30° with respect to the structural axis (see Figure 6.3 and 6.4). Blue arrows in the figures indicate the wind direction in the present study.

6.2 CFD and wind tunnel results for top surface, wind at 0 degrees

Data from the wind tunnel and computational models were obtained on the top and bottom surfaces at 64 pressure points leading to Cp values for each surface. Refer to Figure 4.9 for pressure tap distribution. Two wind conditions were considered: one with incident wind oriented in the long axis direction (0°), whereas a second case was considered by rotating the wind to 30° with respect to the structural axis. Refer to Figure 3.13 and Figure 3.14 for wind direction representation on EFD.Lab.

Figure 6.5 shows the designations of the canopy surfaces used in this chapter, including the top, bottom and all the parapet surfaces. All exterior parapet surfaces are identified by an odd number, whereas all interior parapet surfaces are identified by even numbers. The wind direction at 0 degrees is also represented. For the CFD computations and the wind tunnel tests, only one configuration has been tested, the canopy with dimensions 7.6 m (25ft) x 7.6 m (25 ft) and parapet of 1.22 m (4 ft)

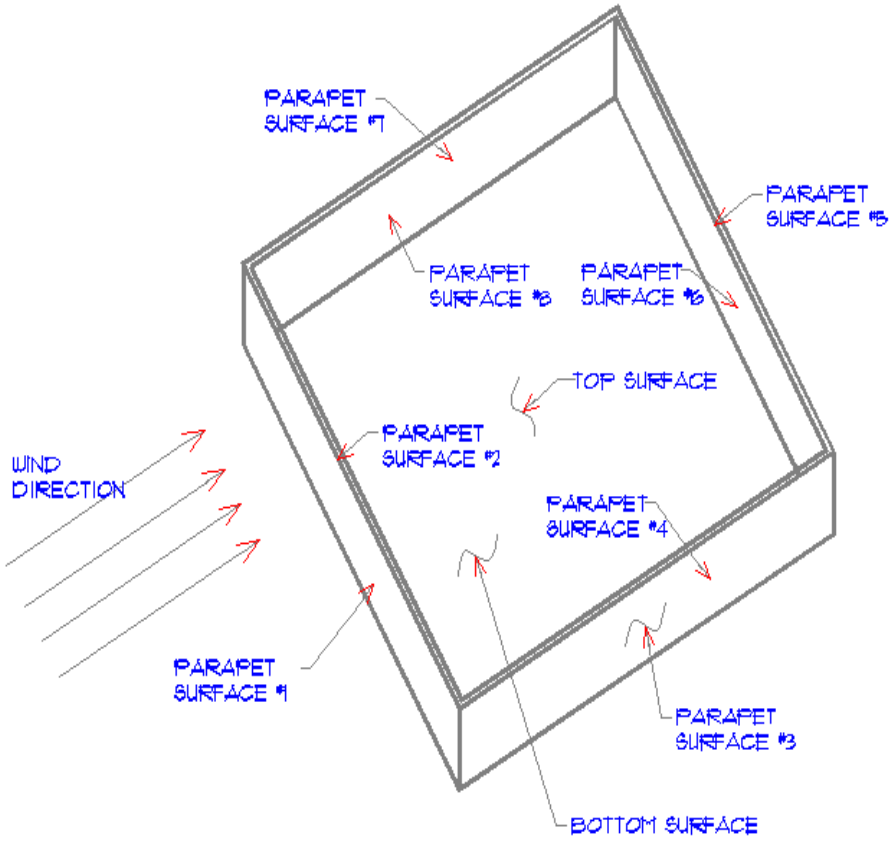

Figure 6.5: Canopy surface nomenclature.

Figure 6.6a shows the Cp values for the top surface of the open canopy, from the CFD simulations Cp results for wind at 0°. A blue arrow in the figures indicates the wind direction on both models. In the CFD simulation, the top surface shows an uplift almost until the end of the surface where a downward pressure is clearly shown at the end of the current figure.

Figure 6.6b shows Cp results obtained from the wind tunnel for the top surface of the canopy. Again, the wind tunnel measurements on the top surface show uplift almost until close to the end of the surface where a downward pressure is noticed. Thus, approximately 1/6 of the canopy is under positive pressures and the rest is under suction. Some changes in Cp values are

noticed in the transverse direction, appearing from boundary effects on the sides of the canopy, generally, the pattern of contours follows fairly regular lines parallel to each other.

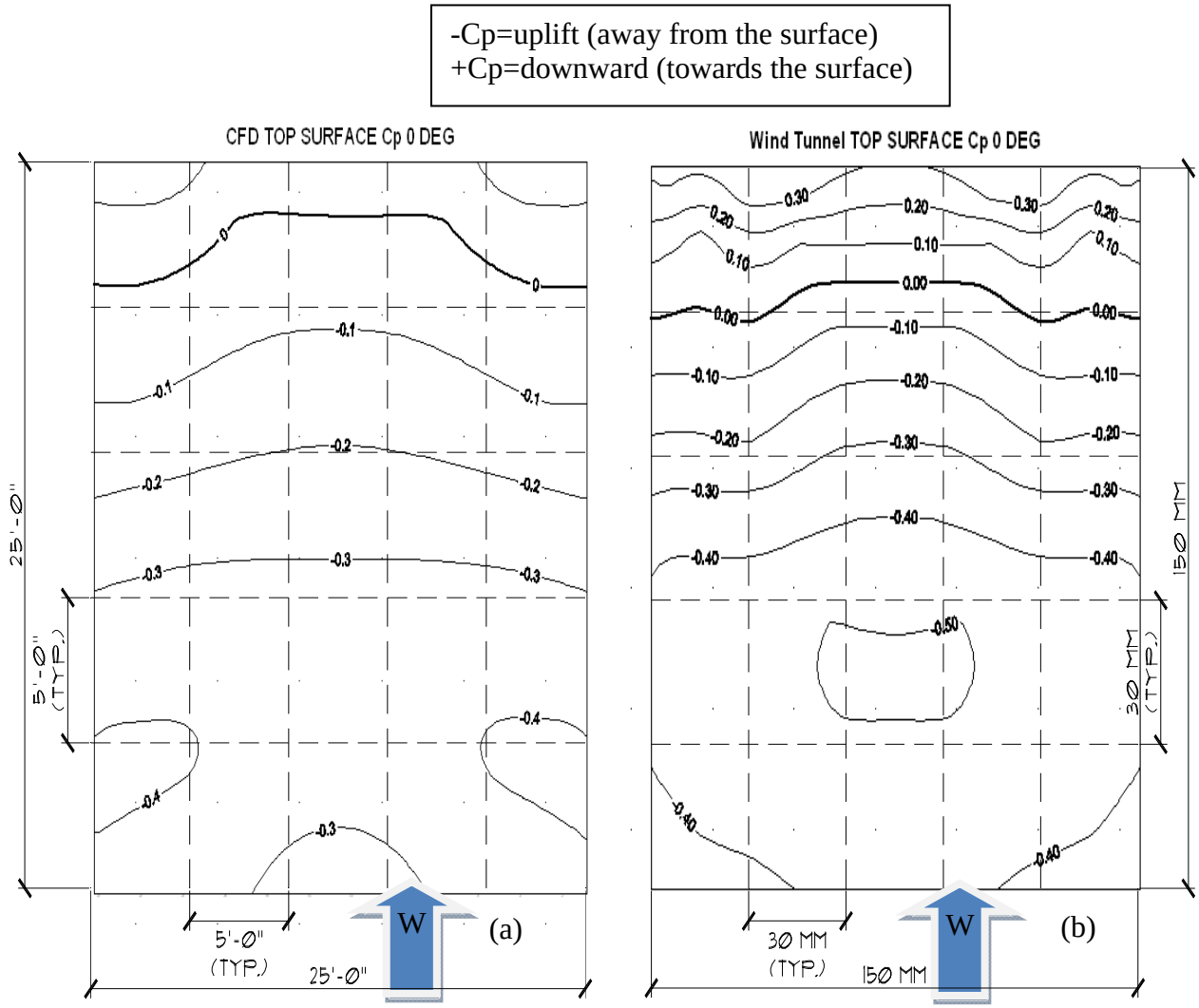

Figure 6.6: Cp results from top surface from CFD (a) and wind tunnel (b) model for incident wind at 0 degrees from the structural axis.

6.3 CFD and wind tunnel results for bottom surface, wind at 0 degrees

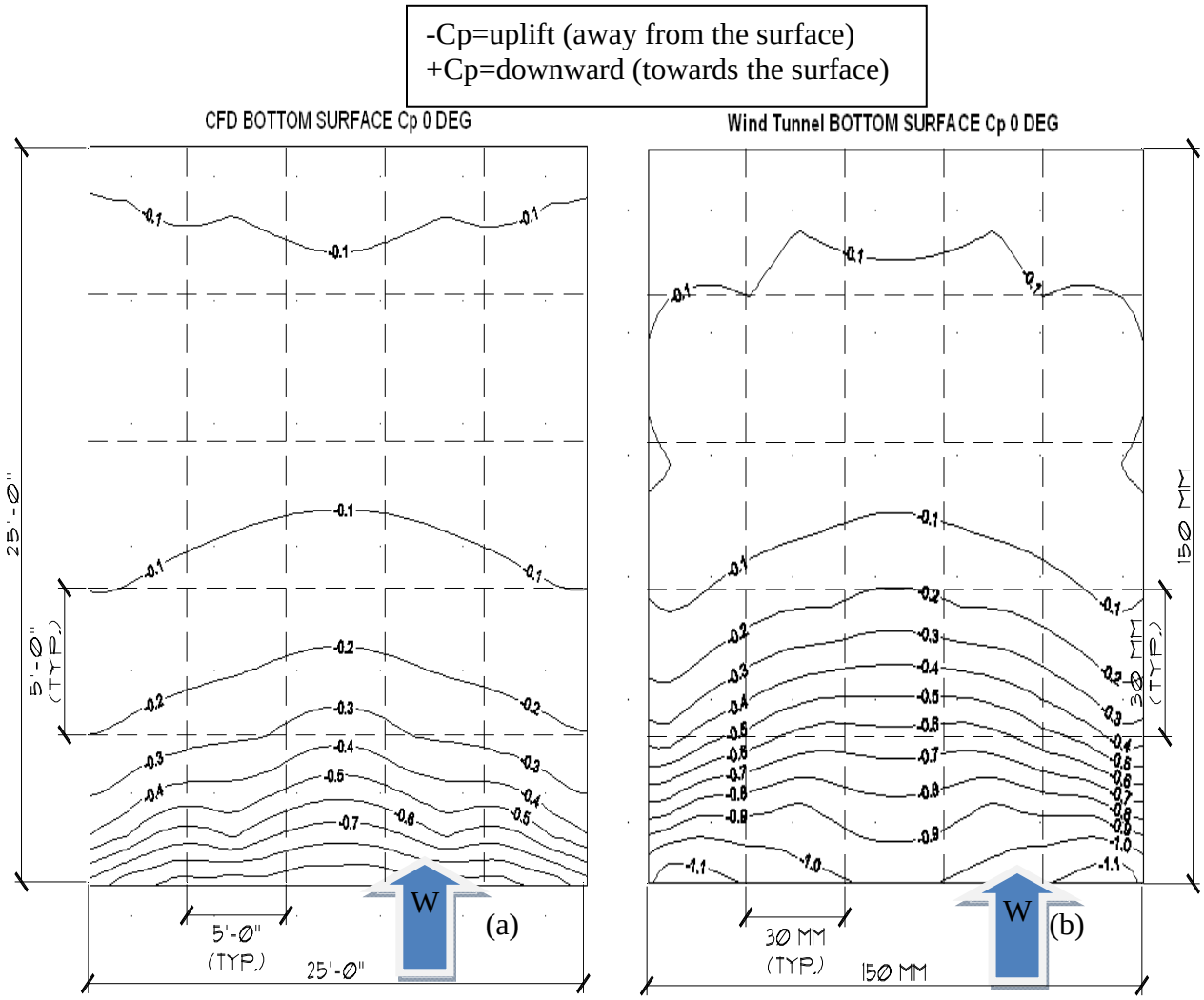

Figure 6.7: Cp results from bottom surface CFD (a) and wind tunnel (b) model for incident wind at 0 degrees from the structural axis.

Figure 6.7a show the Cp values for the bottom surface of the canopy using CFD, for the wind at 0°. The bottom surface shows on both, the wind tunnel and the CFD simulation, uniform downward pressure through the entire bottom surface.

The Cp values for the bottom surface of the canopy at the wind tunnel for the wind at 0° are shown in Figure 6.7b. The wind tunnel results have an almost uniform downward pressure gradient affecting the entire bottom surface. The comparisons indicate that Cp values derived

from the CFD and the wind tunnel tests are in good agreement. A t-sample statistical analysis, where the difference of the two set of data is compared, indicate a difference of less than 5 percent through the present research for the Cp and Cn values for top and bottom surfaces. Refer to Appendix G for an example of the statistical analysis procedure.

6.4 CFD and wind tunnel results for top surface, wind at 30 degrees

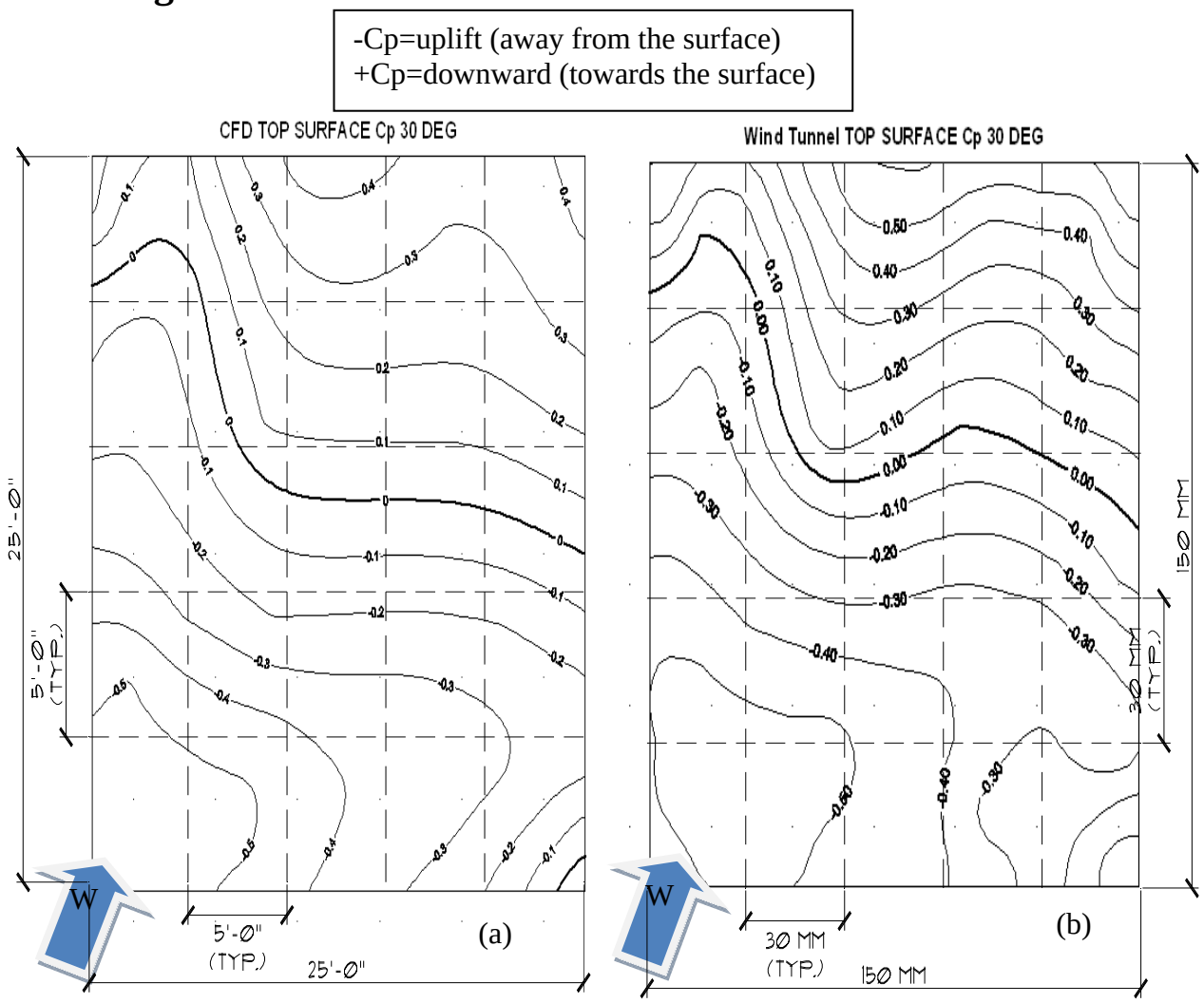

Figure 6.8: Cp results from top surface CFD (a) and wind tunnel (b) model for incident wind at 30 degrees from the structural axis.

Figure 6.8a shows the Cp values for the top surface of the canopy, obtained with CFD, for the wind at 30°. The CFD simulation on the top surface shows an uplift for the first half of the top surface (windward region) and a downward pressure on the other half (leeward).

Next, a configuration at 30° was investigated by rotating the turntable in the wind tunnel. Figure 6.8b shows the Cp values for the top surface of the canopy from the wind tunnel for the wind at 30°, indicating that there is an uplift on the first half (windward region) of the top surface and a downward pressure on the other half (leeward). This effect is clearly shown on both of the previous figures (Figure 6.8a and 6.8b).

6.5 CFD and wind tunnel results for bottom surface, wind at 30 degrees

Figure 6.9a shows the CFD Cp values for the bottom surface of the canopy for the wind at 30°. The bottom surface shows uniform negative Cp values, meaning that there is an uplift pressure on the surface, i.e. downward pressure (suction) through the entire bottom surface.

Figure 6.9b shows the Cp values for the bottom surface of the canopy for the wind tunnel for the wind at 30° incident angle. The bottom surface shows on the wind tunnel and uniform downward pressure through the entire bottom surface. Both figures are in good agreement regarding the values obtained.

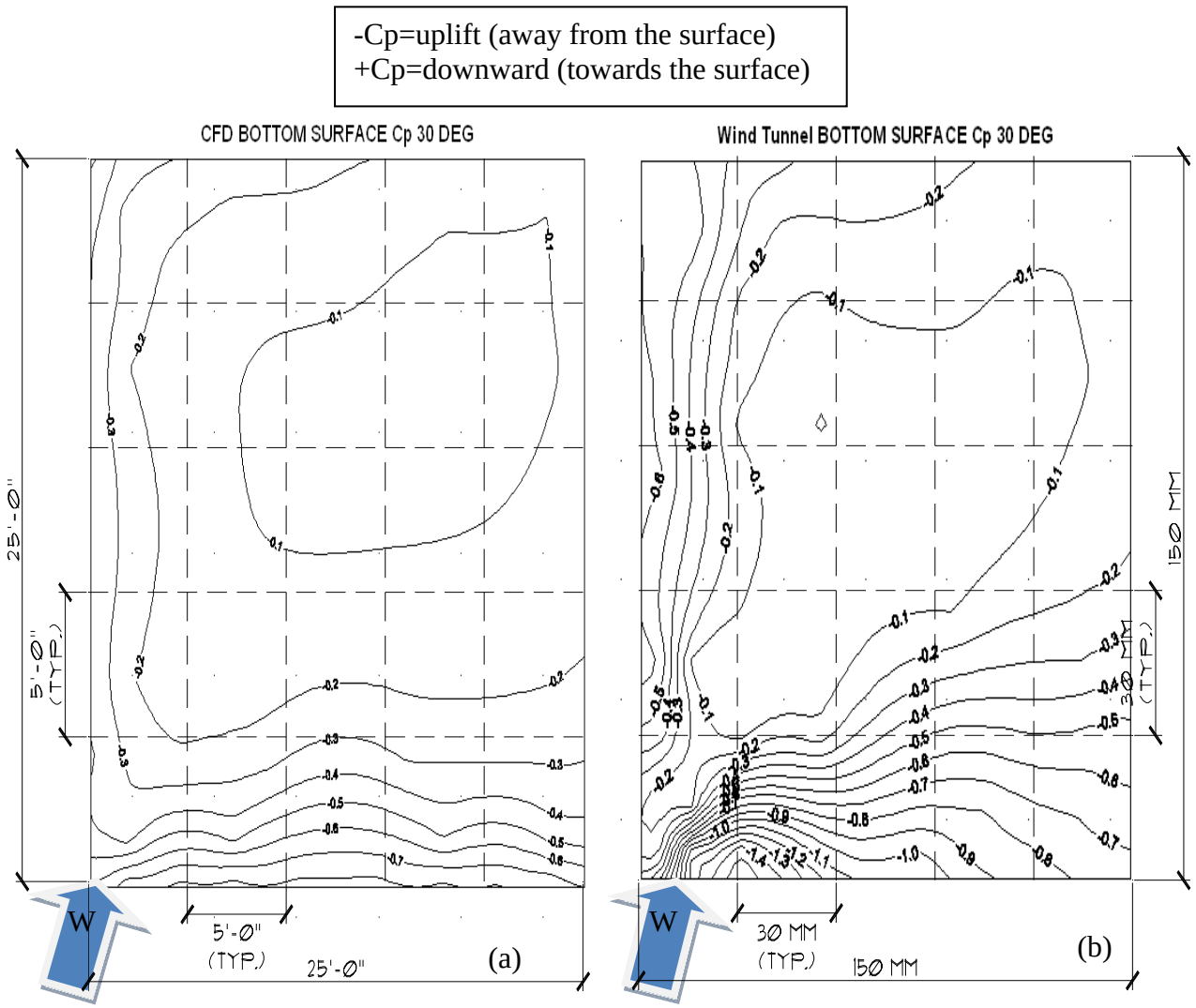

Figure 6.9: Cp results from bottom surface CFD (a) and wind tunnel (b) model for incident wind at 30 degrees from the structural axis.

Net values, denoted by Cn, were calculated as the difference between the Cp values obtained at the same location and on the top and bottom surfaces. Figure 6.10a shows the Cn results for the wind at 0° for the CFD simulation, and Figure 6.10b was drawn using the wind tunnel results. Both figures show an initial downward pressure through the first 1/3 of the length, and uplift for the next 1/3 of the length, and a downward pressure for the last 1/3 of the surface.

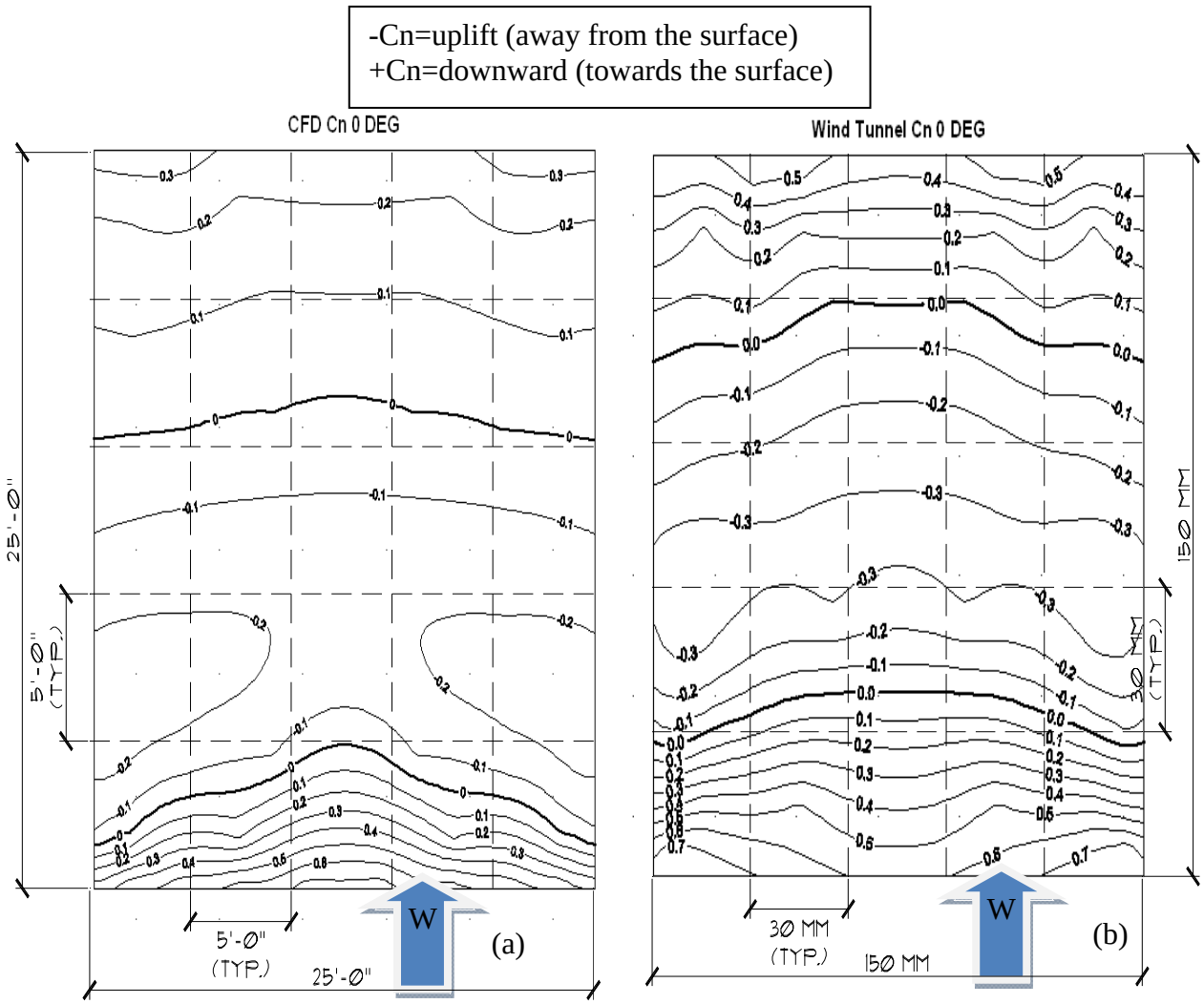

Figure 6.10: Cn results from CFD (a) and wind tunnel (b) model for incident wind at 0 degrees from the structural axis.

Cn results for the wind at 30° are shown on Figure 6.11a and Figure 6.11b. The net pressures in this case show an uplift area located in the center of the surface, with a downward pressure zone around that uplift center area. The wind in both studies, the CFD and the wind tunnel, are in good agreement in the location of the areas where uplift and downward pressure are located.

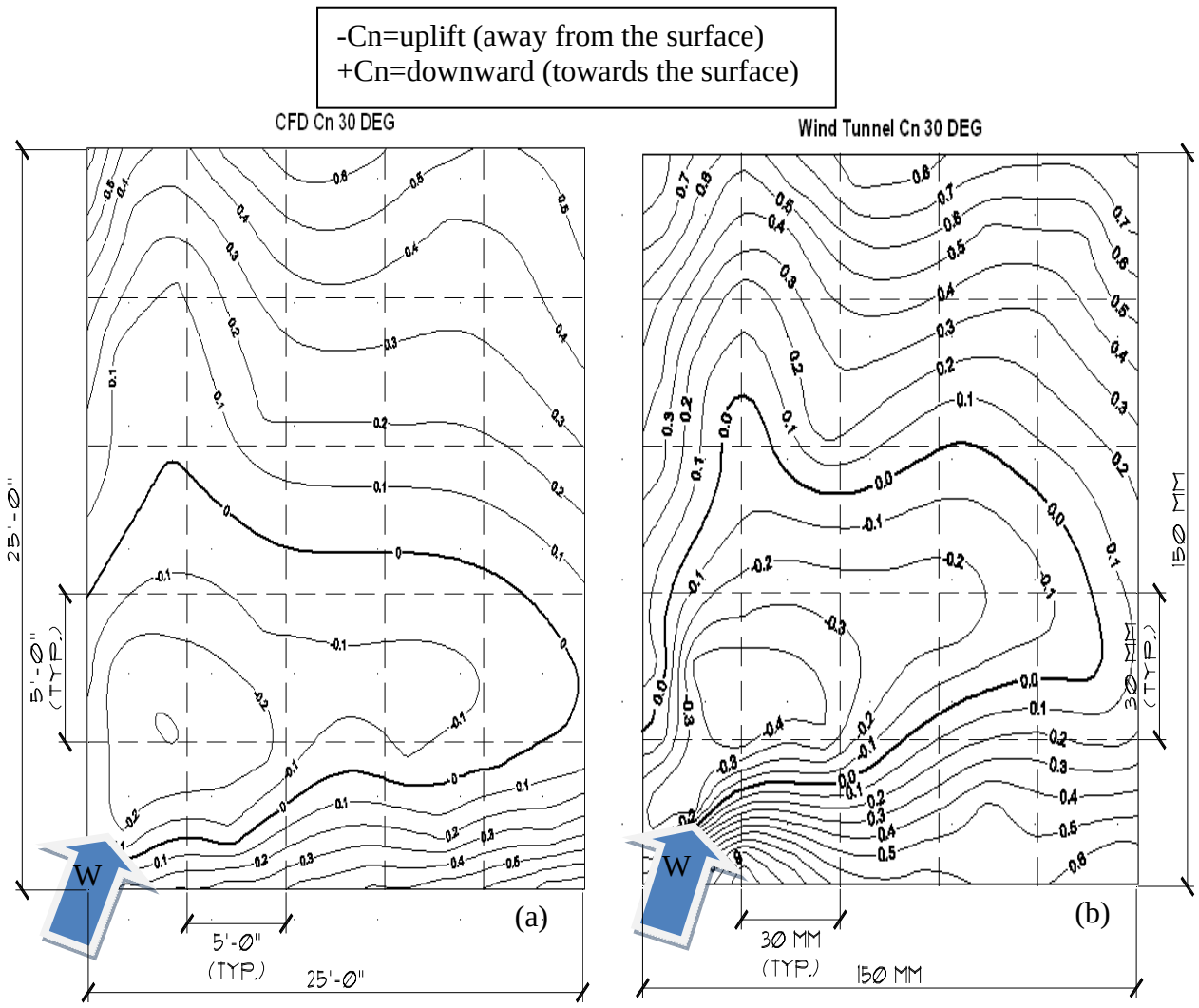

Figure 6.11: Cn results from CFD (a) and wind tunnel model (b) for 30 degrees from the structural axis.

The extreme values for Cp and Cn along the wind axis are shown in Figure 6.12. Values of Cp TP (Cp at the top surface), Cp BP (Cp at the bottom surface), and Cn for the canopy with a wind at 0° are plotted. The Cn values show a Cp of +1.3 maximum behind the parapet. The Cn values changes along the center of the roof to a Cn of -0.5, whereas at the end of the surface it changes to a Cn of +0.5. The Cn values change from + (positive=downward) to – (negative=uplift) and to + (positive=downward) Cn values along the roof geometry.

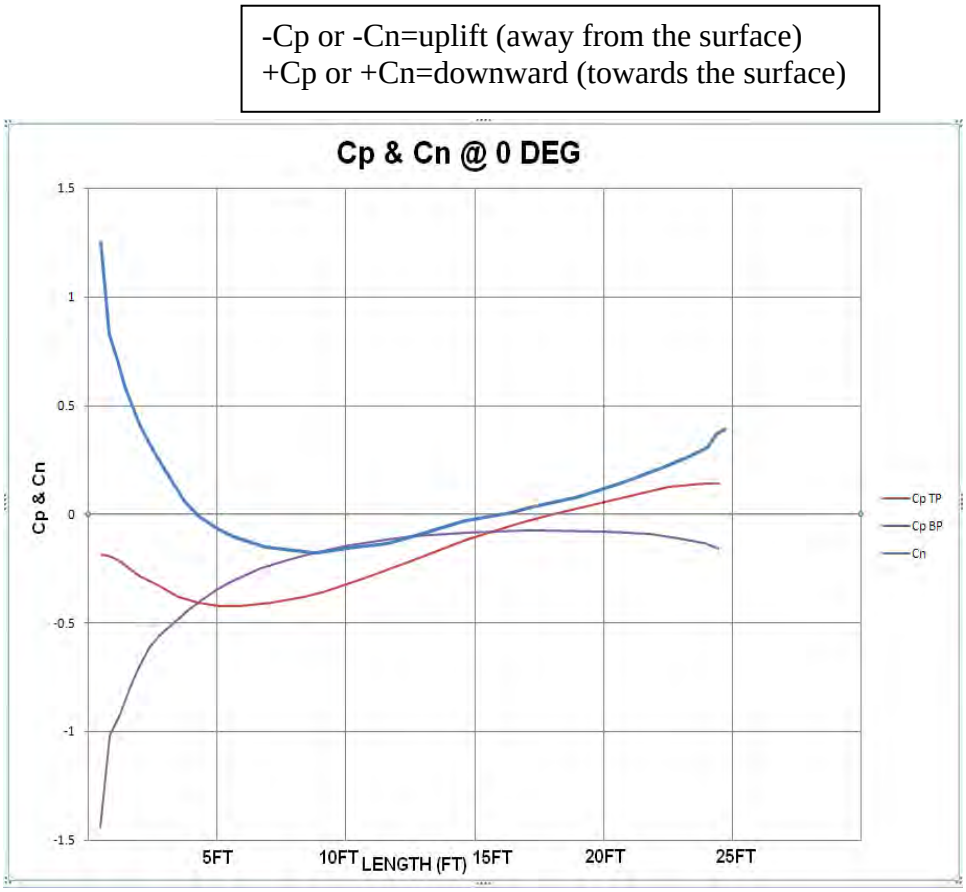

Figure 6.12: Cp and Cn results for CFD model at 0 degrees for (25x25x4 ft) canopy.

6.6 CFD and wind tunnel results for parapets, wind at 0 degrees

Cp values for the parapet surface #1 at 0° for CFD and wind tunnel are shown in Figure 6.13a and Figure 6.13b. Positive Cp values indicating pressure downward on the surface. Values vary from +0.9 to +1.1.

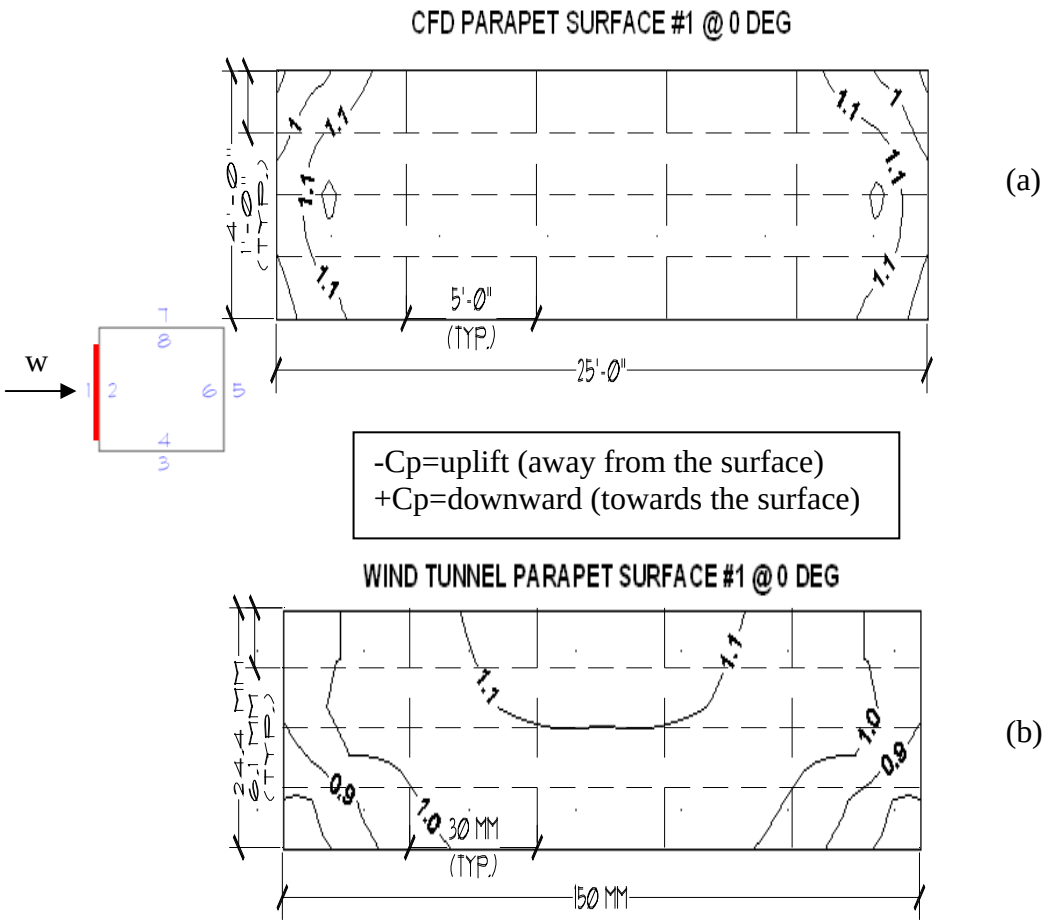

(a)

(b)

Figure 6.13: Cp results at parapet surface #1 at 0 degrees from CFD (a) and wind tunnel (b).

Cp values for the parapet surface #2 at 0° for CFD and wind tunnel are shown in Figure 6.14a and Figure 6.14b. Negative Cp values indicating uplift pressure away from the surface. Values vary from -0.3 to -0.4.

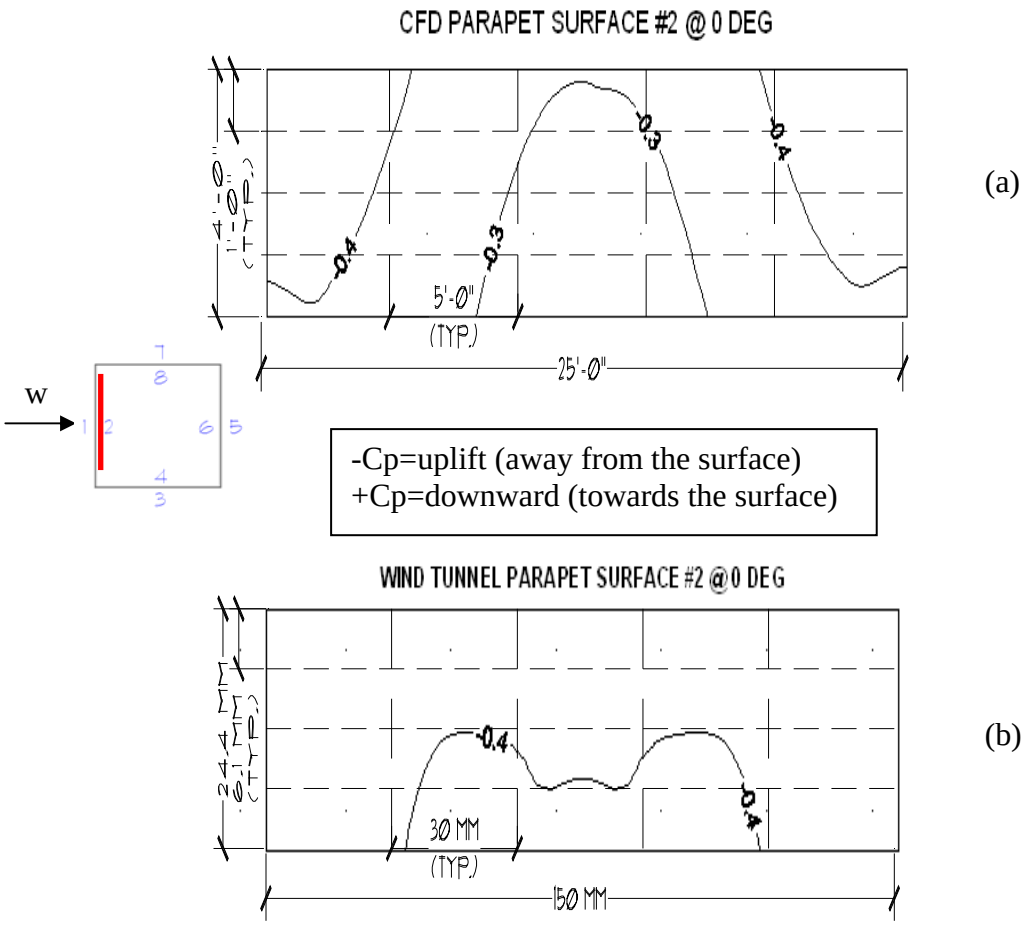

(a)

(b)

Figure 6.14: Cp results at parapet surface #2 at 0 degrees for CFD (a) and wind tunnel (b).

Cp values for the parapet surface #3 and parapet surface #7 at 0° for CFD and wind tunnel are shown in Figure 6.15a and Figure 6.15b. Negative Cp values indicating uplift pressure away from the surface. Values vary from -0.9 to -0.1.

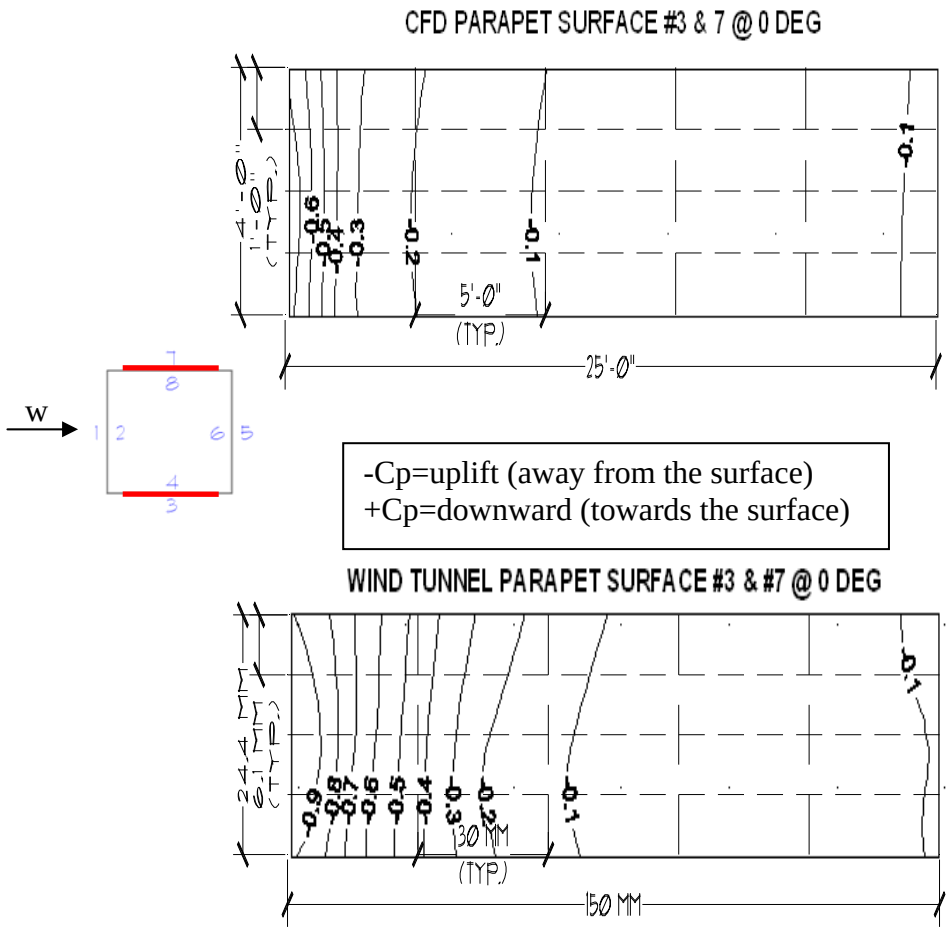

(a)

(b)

Figure 6.15: Cp results at parapet surface #3 and #7 at 0 degrees for CFD (a) and wind tunnel (b).

Cp values for the parapet surface #4 and parapet surface #8 at 0° for CFD and wind tunnel are shown in Figure 6.16a and Figure 6.16b. Negative Cp values indicating uplift, or pressure away from the surface. Positive Cp values indicating pressure towards on the surface. There is a transition from negative to positive values at 2/3 of the horizontal surface. Values vary from -0.4 to +0.2.

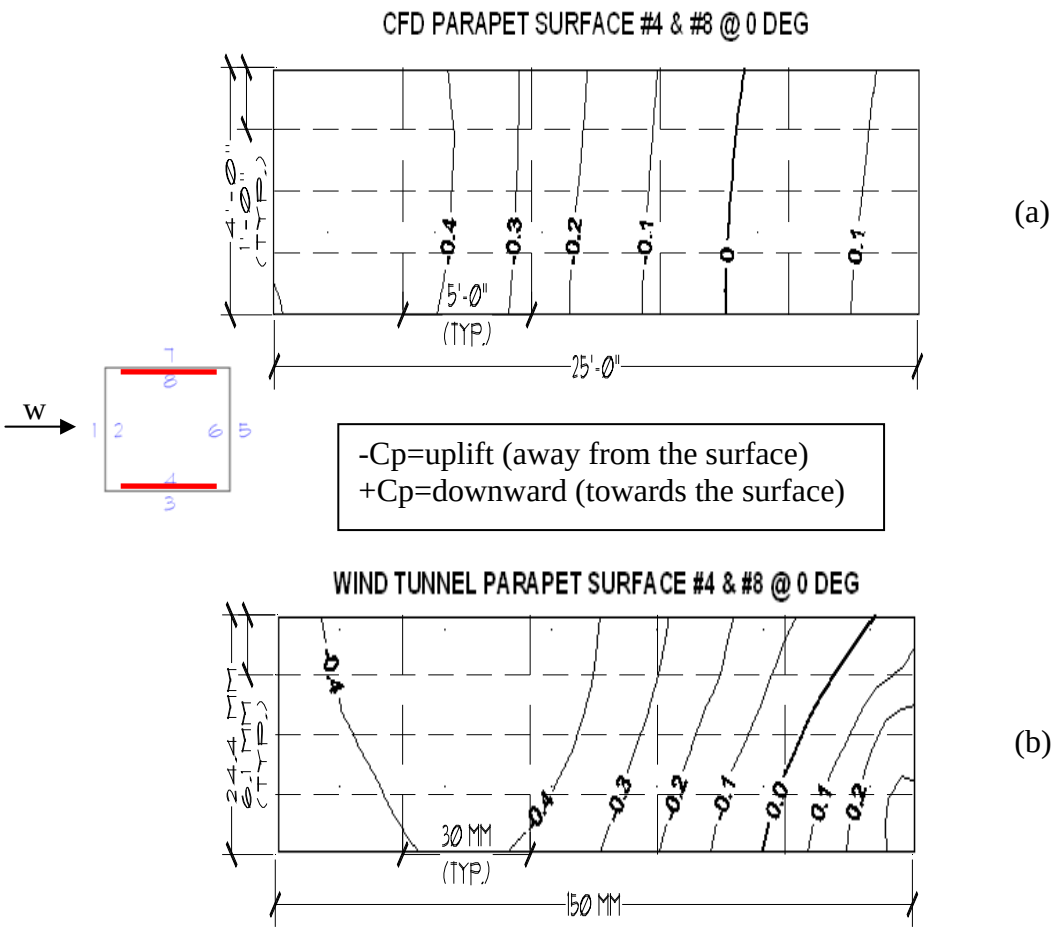

(a)

(b)

Figure 6.16: Cp results at parapet surface #4 and #8 at 0 degrees for CFD (a) and wind tunnel (b).

Cp values for the parapet surface #5 at 0° for CFD and wind tunnel are shown in Figure 6.17a and Figure 6.17b. Negative Cp values indicating uplift, pressure away from the surface are shown on both figures. Values are -0.3 on both simulations.

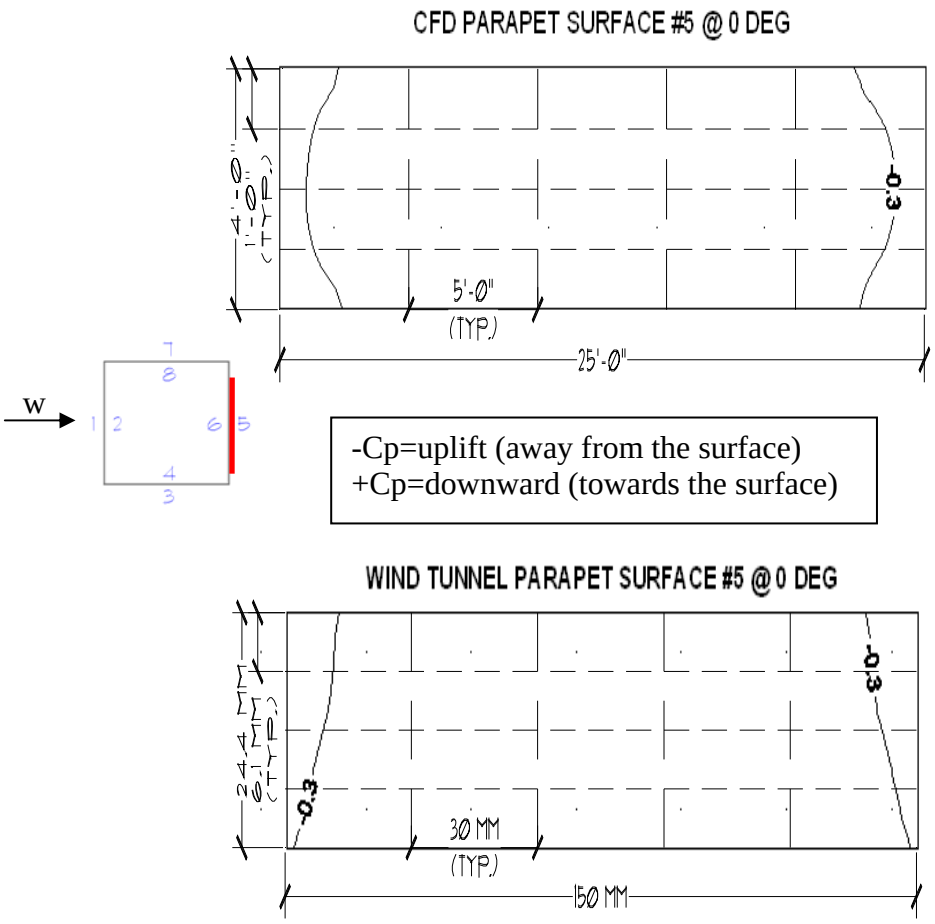

(a)

(b)

Figure 6.17: Cp results at parapet surface #5 at 0 degrees for CFD (a) and wind tunnel (b).

Cp values for the parapet surface #6 at 0° for CFD and wind tunnel are shown in Figure 6.18a and Figure 6.18b. Positive Cp values indicating pressure downward on the surface are shown on both figures. Values vary from +0.1 to +0.2.

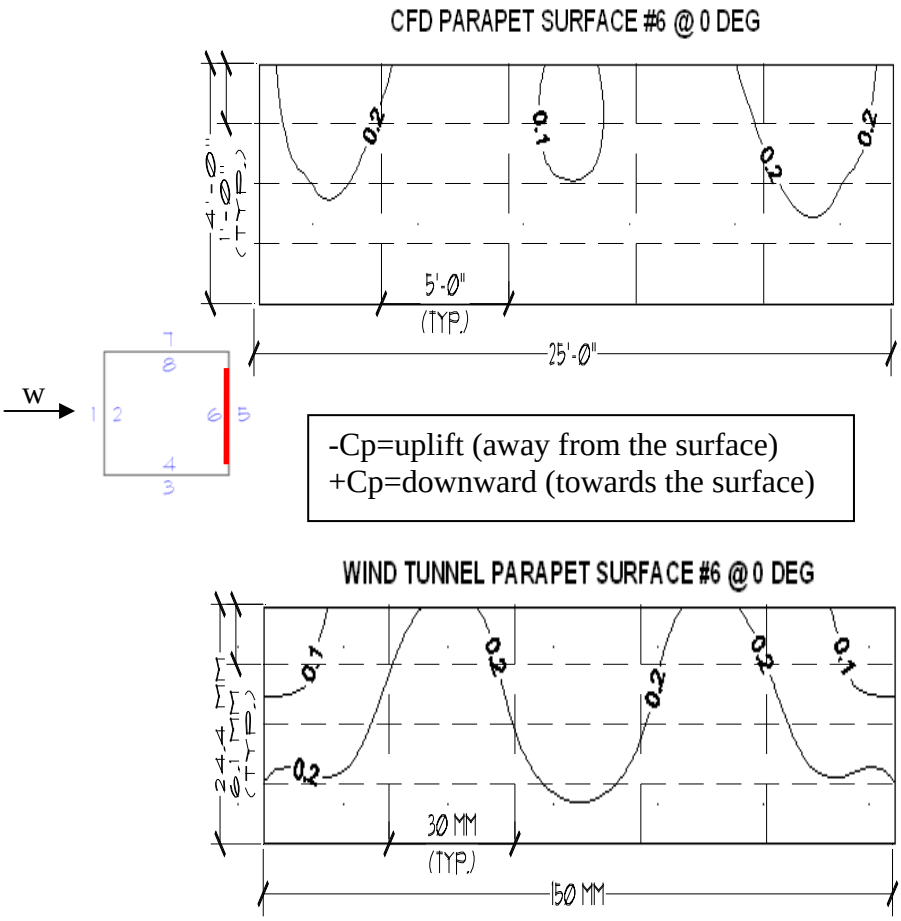

(a)

(b)

Figure 6.18: Cp results at parapet surface #6 at 0 degrees for CFD (a) and wind tunnel (b).

Cn values for the parapet surface #1 and parapet surface #2 at 0° for CFD and wind tunnel are shown in Figure 6.19a and Figure 6.19b. Net positive values indicating pressure downward on the surface is shown on both figures. Values vary from +1.2 to +1.5.

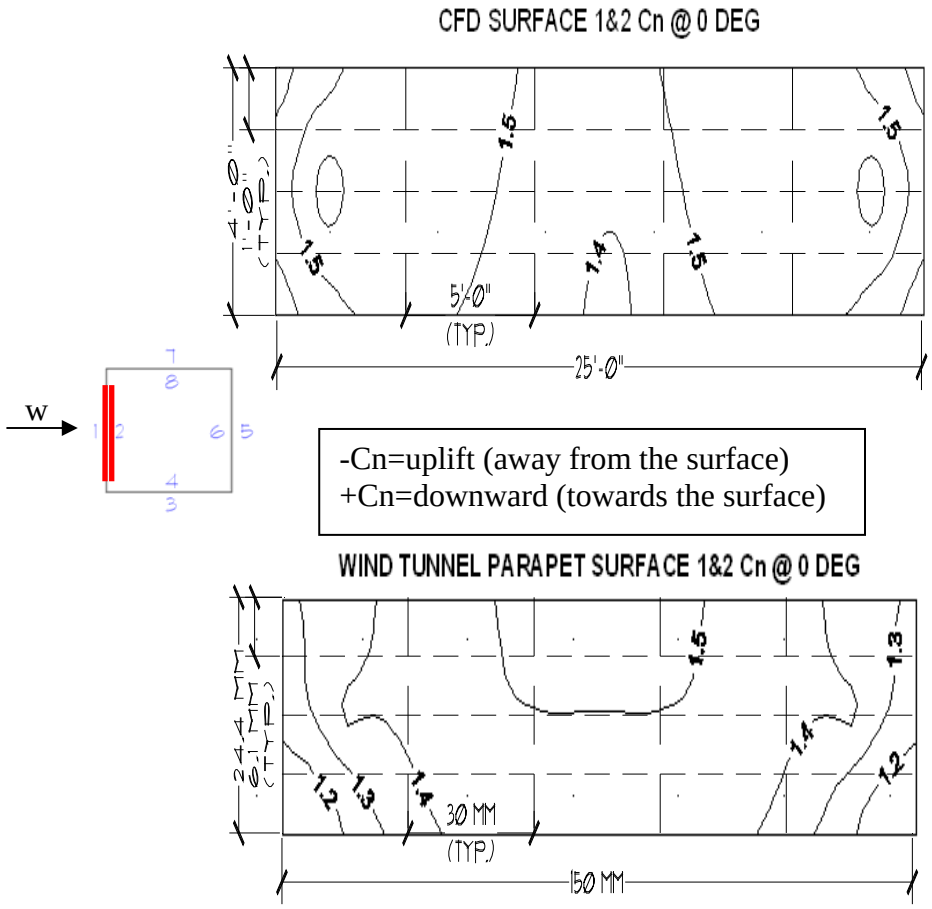

(a)

(b)

Figure 6.19: Cn results at parapet surface #1 and 2 at 0 degrees for CFD (a) and wind tunnel (b).

Cn values for the parapet surface #3 and parapet surface #4 at 0° for CFD and wind tunnel are shown in Figure 6.20a and Figure 6.20b. Net negative and positive values indicating changes in pressure downward and uplift on the surface is shown in both figures. Values vary from -0.5 to be 0.0 the first 1/3 of the horizontal surface. Cn values for the parapet surface #3 and parapet surface #4 at 0° for CFD and wind tunnel are shown in Figure 6.20a and Figure 6.20b.

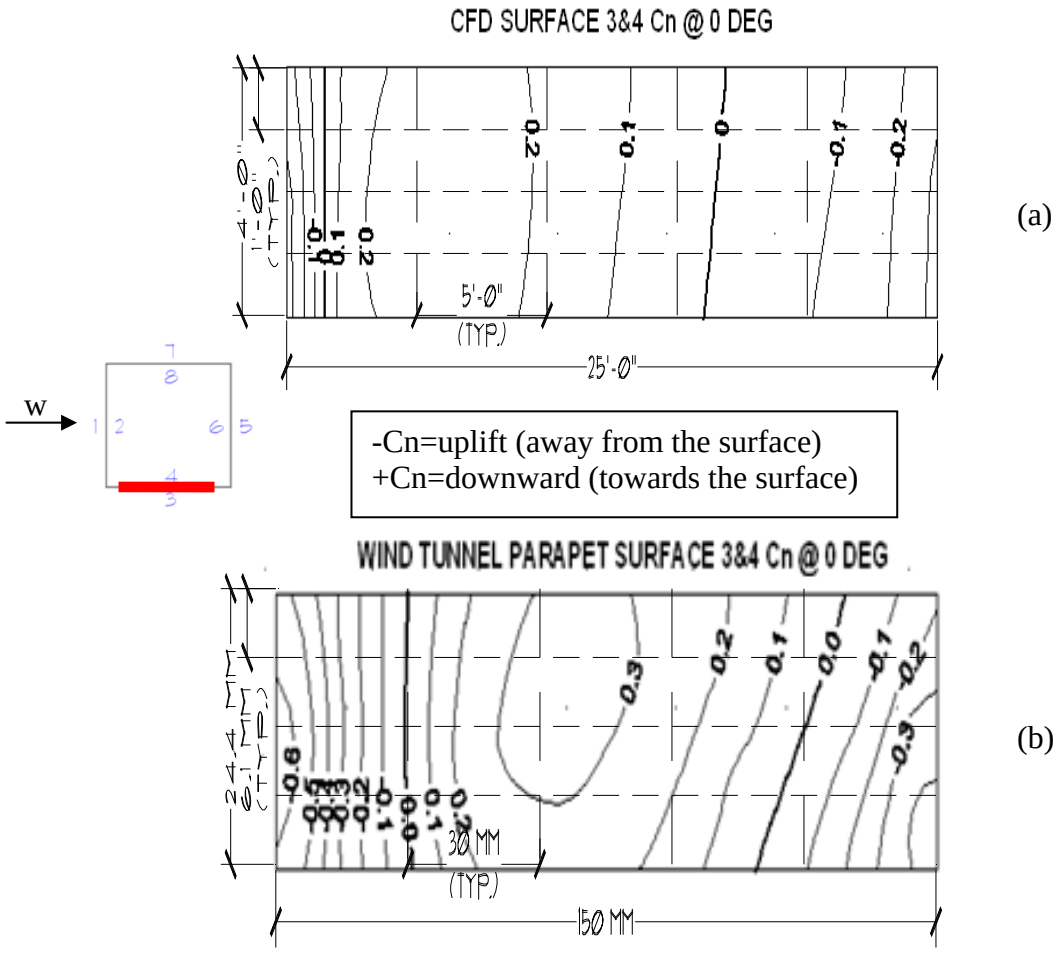

(a)

(b)

Figure 6.20: Cn results at parapet surface #3 and 4 at 0 degrees for CFD (a) and wind tunnel (b).

Net negative and positive values indicating changes in pressure downward and uplift on the surface is shown in both figures. Values vary from -0.5 to be 0.0 the first 1/3 of the horizontal surface. The values continue changing from 0.0 to +0.3 and to 0.0 for 2/3 of the horizontal surface. The last 1/3 of the horizontal surface, Cn surface values changes from 0.0 to -0.3. The CFD simulation is able to capture the transition between the changes in downward pressure and uplift. The values at the beginning of the horizontal surface are higher on the wind tunnel parapet surface.

Cn values for the parapet surface #5 and parapet surface #6 at 0° for CFD and wind tunnel are shown on Figure 6.21a and Figure 6.21b. Net negative values indicating uplift on the surface is shown on both figures. Values vary from -0.5 to -0.4.

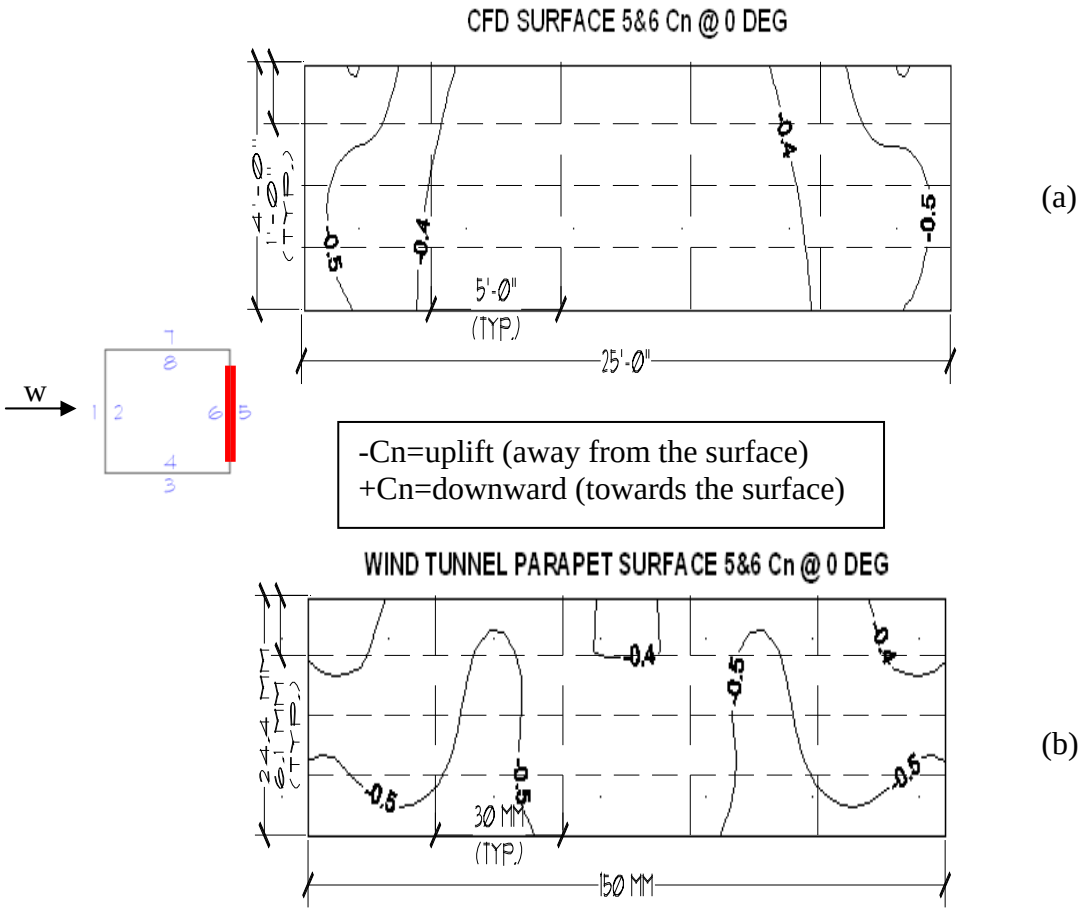

Figure 6.21: Cn results at parapet surface #5 and 6 at 0 degrees for CFD (a) and wind tunnel (b).

Cn values for the parapet surface #7 and parapet surface #8 at 0° for CFD and wind tunnel are shown on Figure 6.22a and Figure 6.22b. Net negative and positive values indicating changes in pressure towards and away on the surface are shown on both figures.

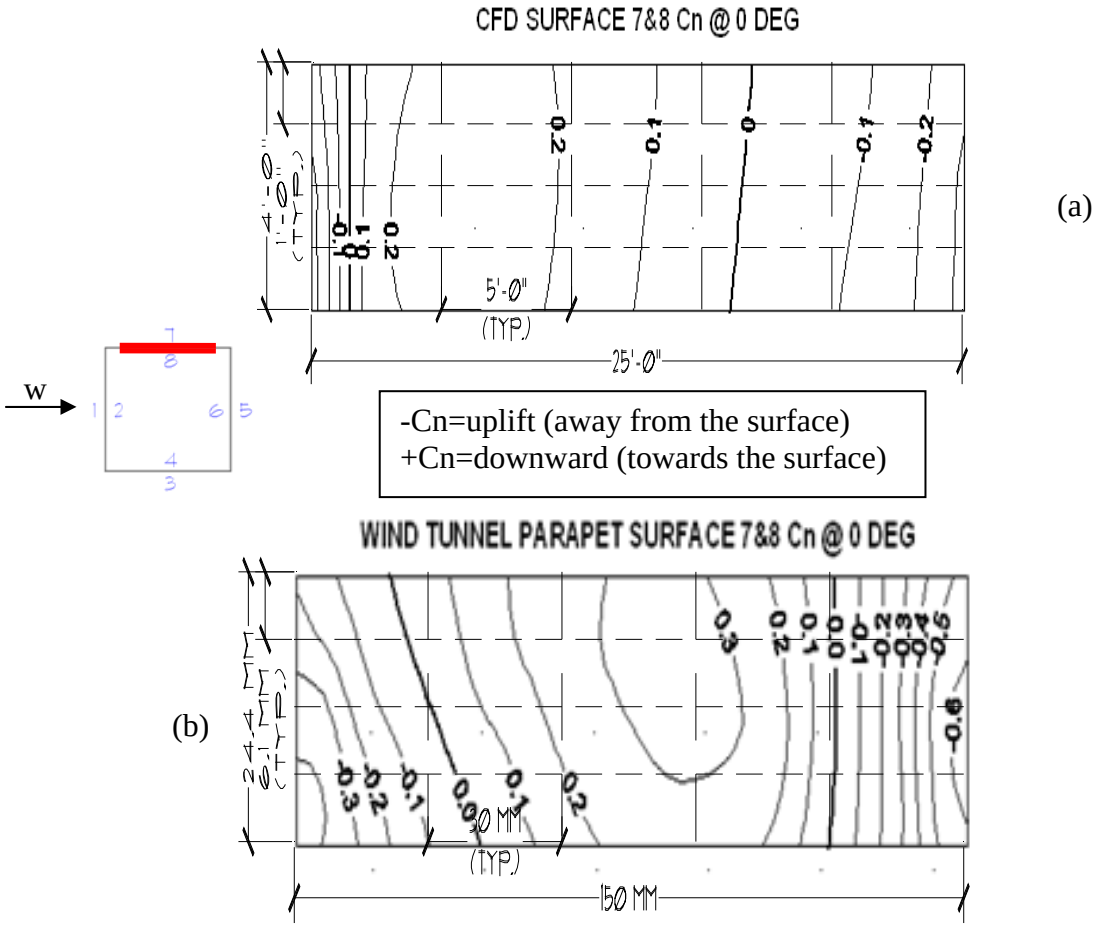

Figure 6.22: Cn results at parapet surface #7 and 8 at 0 degrees for CFD (a) and wind tunnel (b).

Values vary from -0.6 to 0.0 at the first 1/3 of the horizontal surface. The values continue changing from 0.0 to +0.3, going back to 0.0 for 2/3 of the horizontal surface. The last 1/3 of the horizontal surface, Cn surface values changes from 0.0 to -0.3. The CFD simulation is able to capture the transition between the changes in towards pressure and away from surface. The higher values at the beginning of the horizontal surface are higher on the wind tunnel parapet surface.

6.7 CFD and wind tunnel results for parapets, wind at 30 degrees

Cp values for the parapet surface #1 at 30° for CFD and wind tunnel are shown in Figure 6.23a and Figure 6.23b. Positive Cp values indicating pressure downward on the surface. Values vary from +0.5 to +1.1.

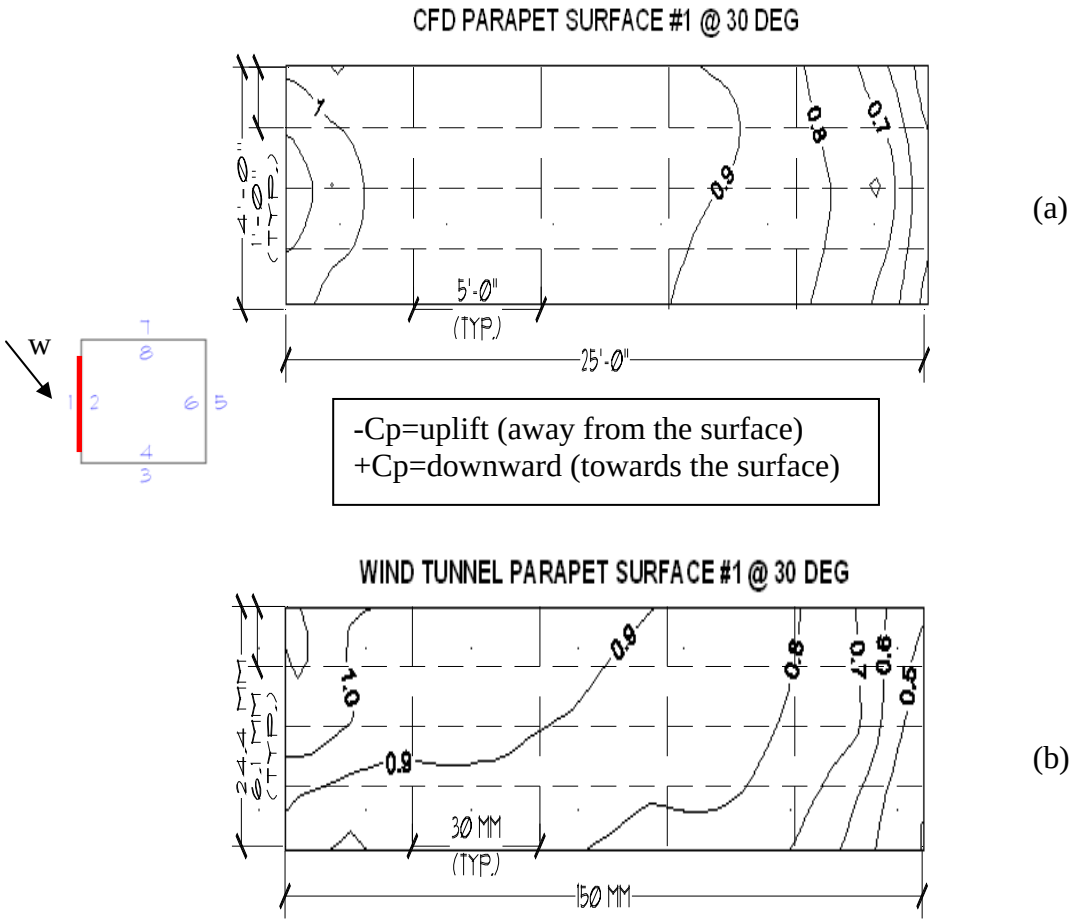

(a)

(b)

Figure 6.23: Cp results at parapet surface #1 at 30 degrees for CFD (a) and wind tunnel (b).

Cp values for the parapet surface #2 at 30° for CFD and wind tunnel are shown in Figure 6.24a and Figure 6.24b. Negative Cp values indicating uplift pressure away from the surface and

a transition zone where the Cp values changes from negative to positive values at the last 1/6 of the horizontal surface. Values vary from -0.5 to +0.1.

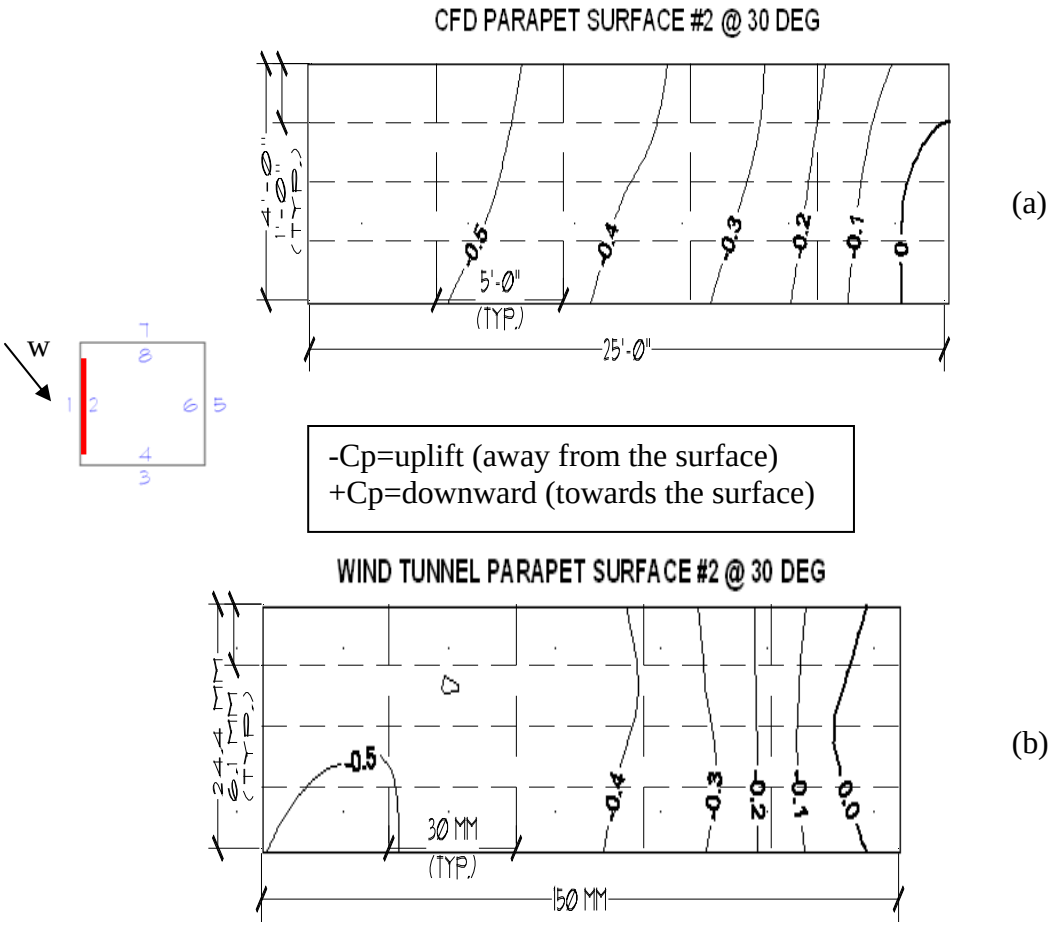

(a)

(b)

Figure 6.24: Cp results at parapet surface #2 at 30 degrees for CFD (a) and wind tunnel (b).

Cp values for the parapet surface #3 and parapet surface #7 at 30° for CFD and wind tunnel are shown in Figure 6.25a and Figure 6.25b. Negative Cp values indicating uplift pressure away from the surface. Values vary from -0.7 to -0.2.

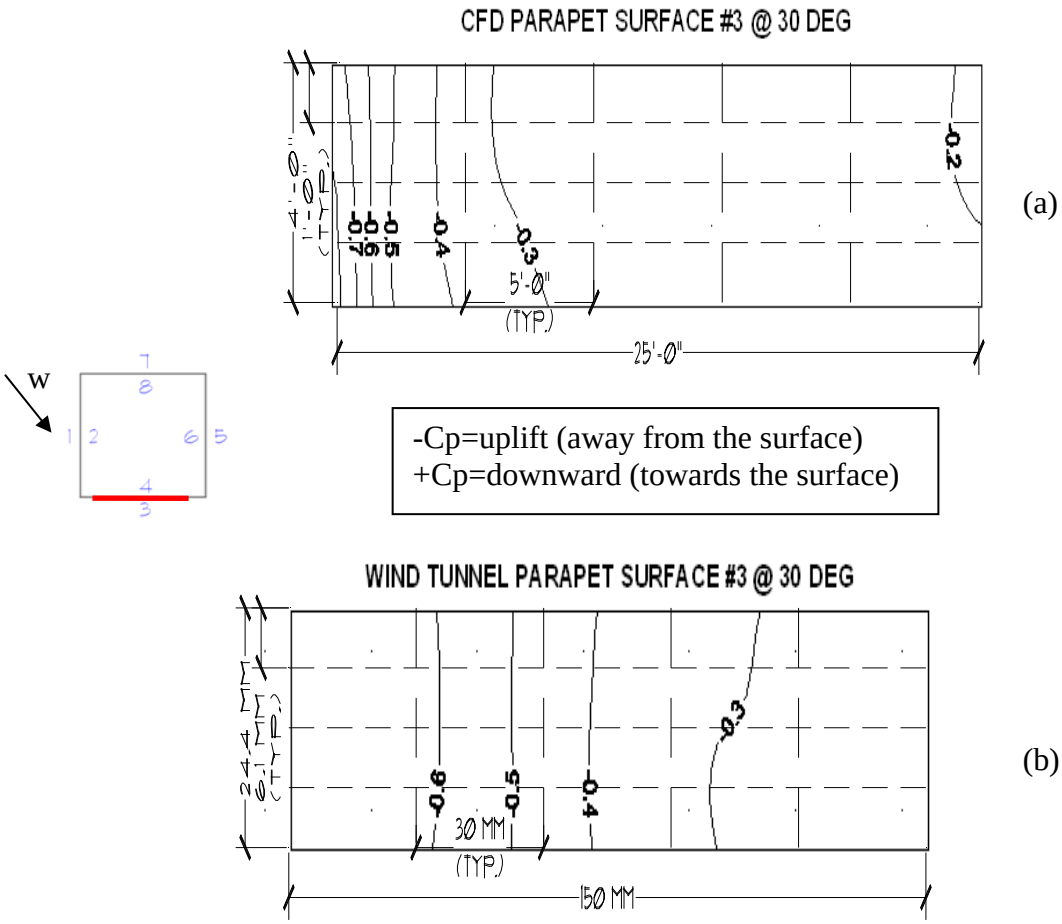

(a)

(b)

Figure 6.25: Cp results at parapet surface #3 at 30 degrees for CFD (a) and wind tunnel (b).

Cp values for the parapet surface #4 at 30° for CFD and wind tunnel are shown in Figure 6.26a and Figure 6.26b. Negative Cp values indicating uplift, pressure away from the surface. Positive Cp values indicating pressure downward on the surface. There is a transition from negative to positive values at 1/2 of the horizontal surface. Values vary from -0.2 to 0.0 on the first half, and from 0.0 to 0.7 on the second half.

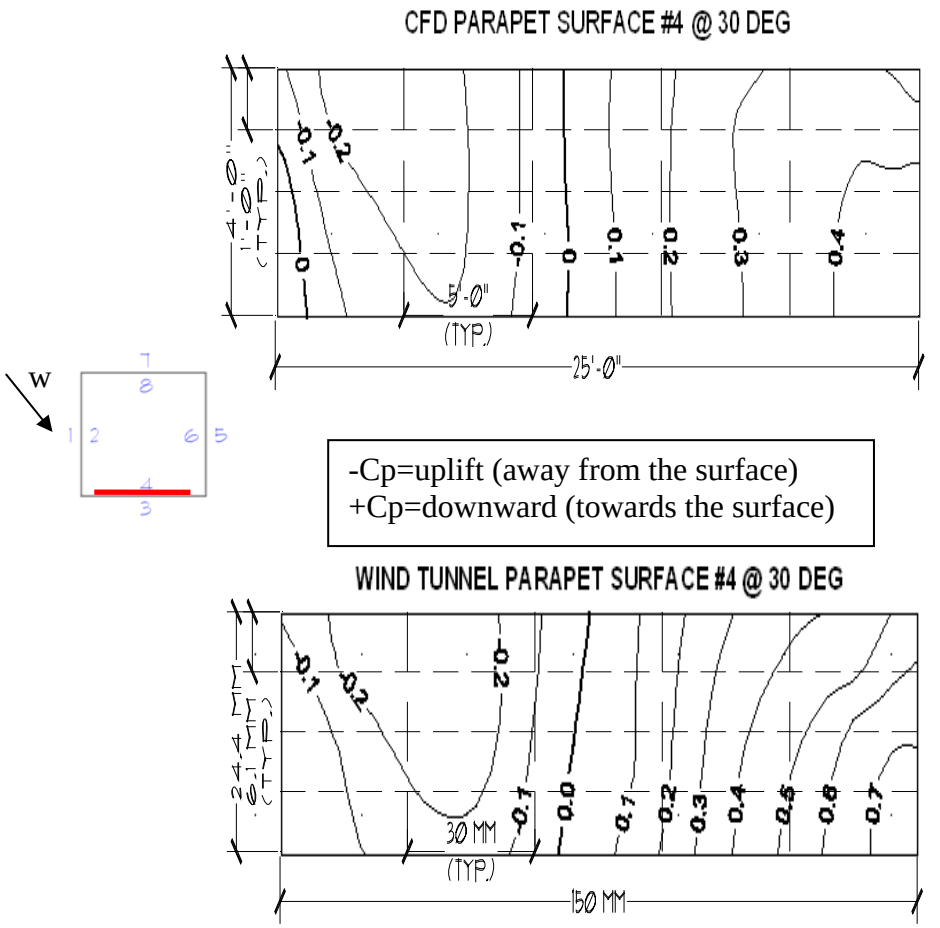

(a)

(b)

Figure 6.26: Cp results at parapet surface #4 at 30 degrees for CFD (a) and wind tunnel (b).

Cp values for the parapet surface #5 at 30° for CFD and wind tunnel are shown in Figure 6.27a and Figure 6.27b. Net negative values indicating uplift on the surface is shown on both figures. Values vary from -0.6 to -0.2.

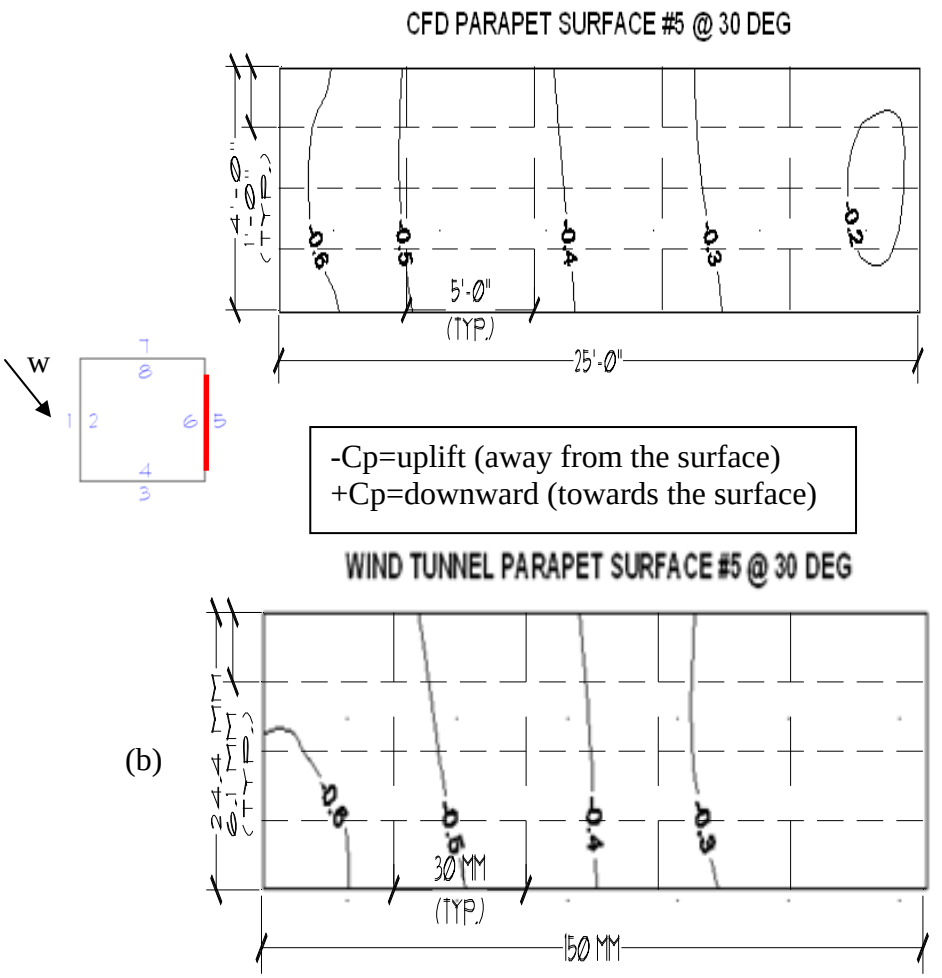

(a)

(b)

Figure 6.27: Cp results at parapet surface #5 at 30 degrees for CFD (a) and wind tunnel (b).

Cp values for the parapet surface #6 at 30° for CFD and wind tunnel are shown in Figure 6.28a and Figure 6.28b. Positive net values indicating downward pressure on the surface is shown on both figures. There is a small region where the values changes from positive to negative Cp values at the end of the horizontal surface. Values vary from +0.6 to 0.0.

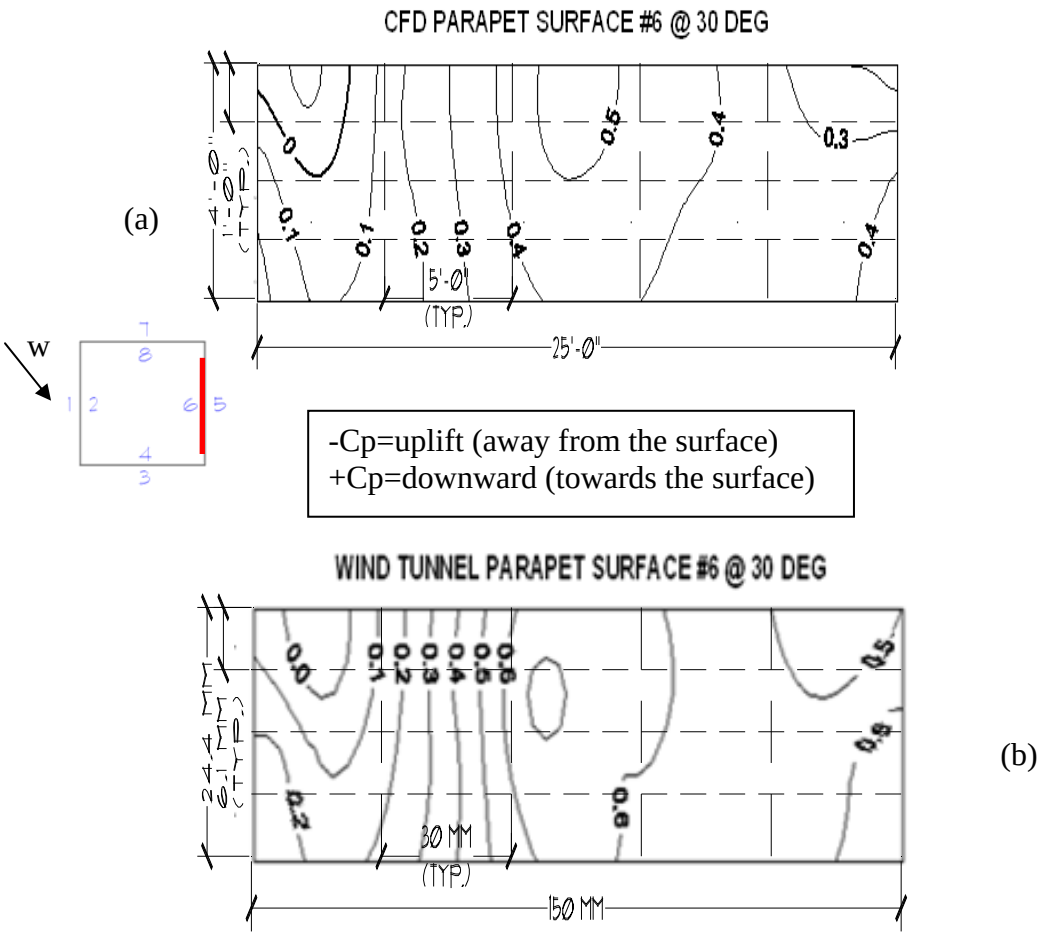

Figure 6.28: Cp results at parapet surface #6 at 30 degrees for CFD (a) and wind tunnel (b).

Cp values for the parapet surface #7 at 30° for CFD and wind tunnel are shown in Figure 6.29a and Figure 6.29b. Positive Cp values indicating towards pressure on the surface are shown on both figures. Values vary from +0.4 to +0.1.

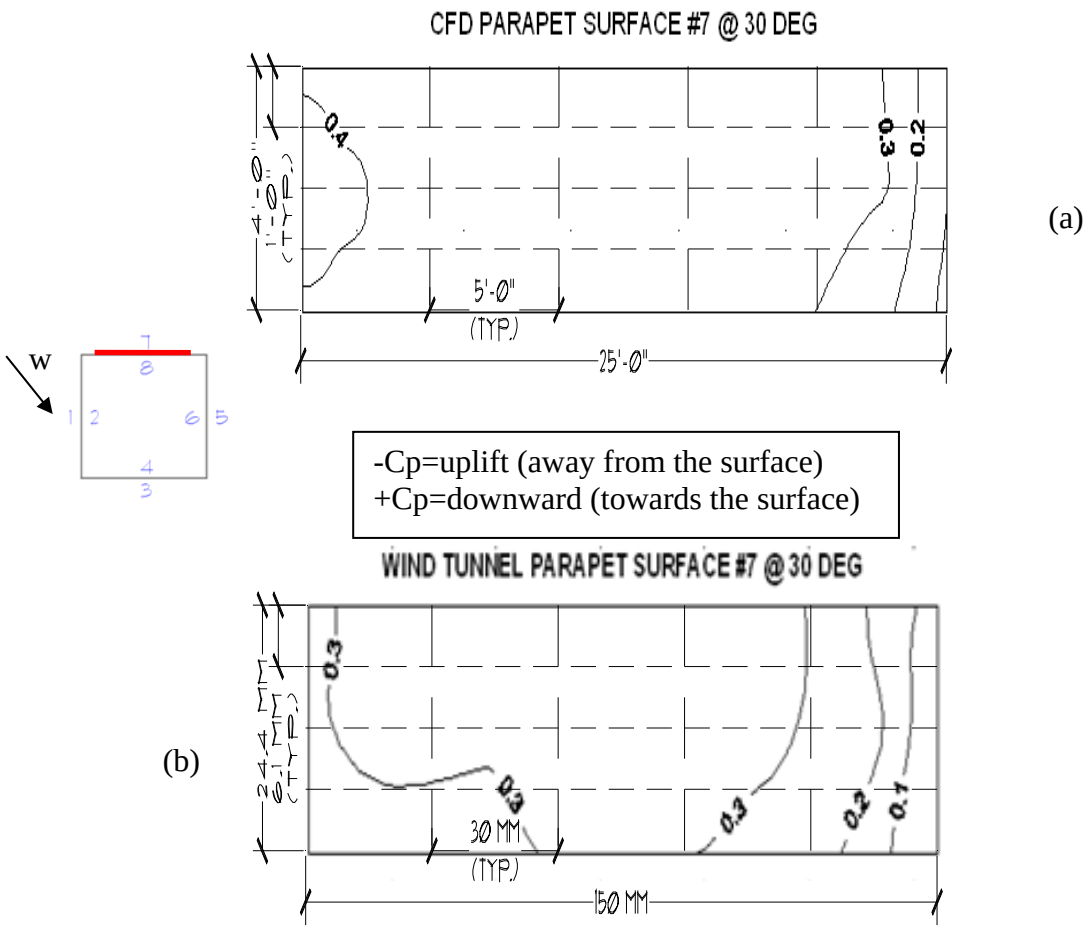

(a)

(b)

Figure 6.29: Cp results at parapet surface #7 at 30 degrees for CFD (a) and wind tunnel (b).

Cp values for the parapet surface #8 at 30° for CFD and wind tunnel are shown in Figure 6.30a and Figure 6.30b. Negative Cp values indicating uplift, pressure away from the surface. Positive Cp values indicating pressure downward on the surface. There is a transition from negative to positive values at 2/3 of the horizontal surface. Values vary from -0.4 to 0.0 and from 0.0 to +0.3.

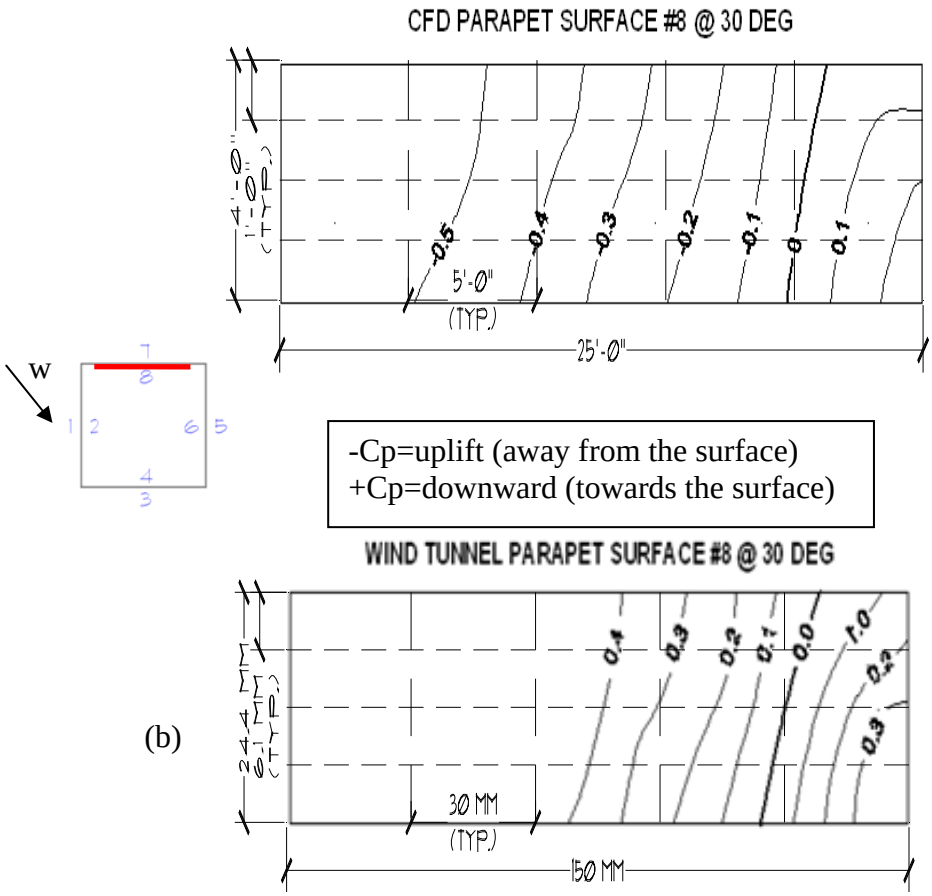

Figure 6.30: Cp results at parapet surface #8 at 30 degrees for CFD (a) and wind tunnel (b).

Cn values for the parapet surface #1 and parapet surface #2 at 30° for CFD and wind tunnel are shown in Figure 6.31a and Figure 6.31b. Net positive values indicating pressure downward on the surface is shown on both figures. Values vary from +1.5 to +0.5.

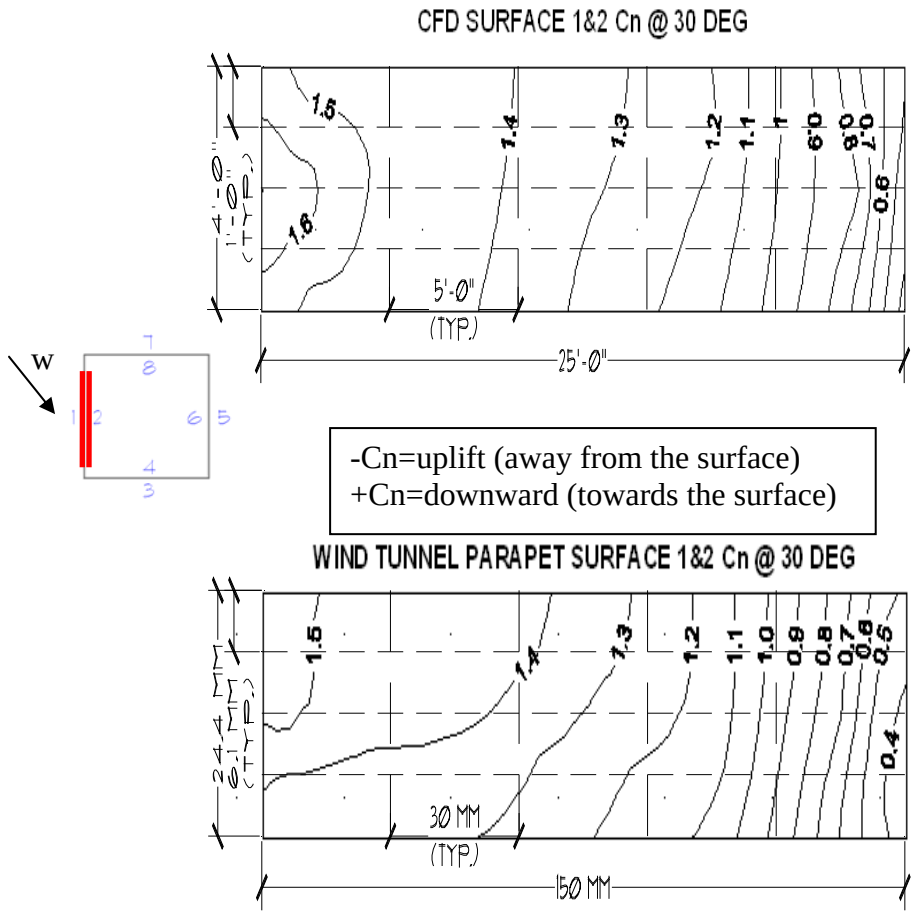

(a)

(b)

Figure 6.31: Cn results at parapet surface #1 and 2 at 30 degrees for CFD (a) and wind tunnel (b).

Cn values for the parapet surface #3 and parapet surface #4 at 30° for CFD and wind tunnel are shown in Figure 6.32a and Figure 6.32b. Net negative values indicating changes in pressure and uplift on the surface are shown on both figures. Values vary from -0.9 to -0.3 for the first 1/2 of the horizontal surface. The values continue changing from -0.3 to -0.6 at the end of the horizontal surface.

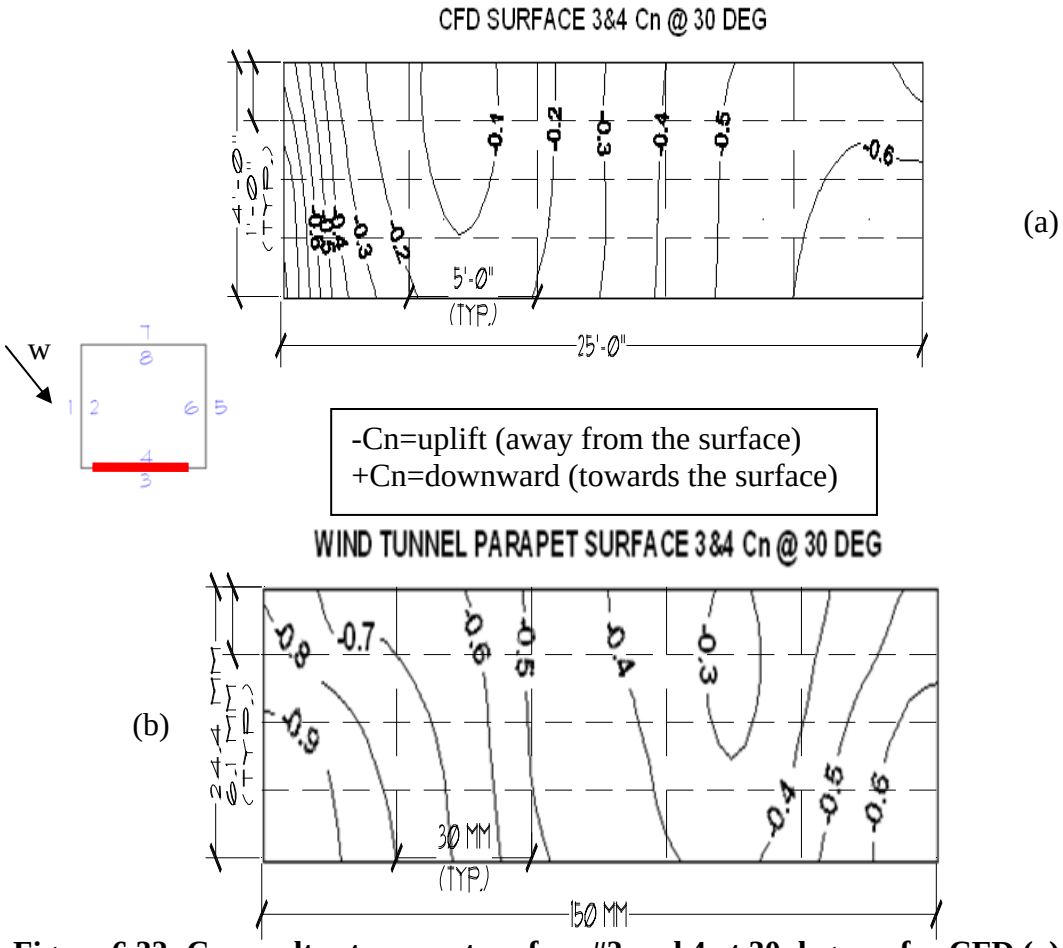

Figure 6.32: Cn results at parapet surface #3 and 4 at 30 degrees for CFD (a) and wind tunnel (b).

Cn values for the parapet surface #5 and parapet surface #6 at 30° for CFD and wind tunnel are shown in Figure 6.33a and Figure 6.33b. Net negative values indicating uplift on the surface is shown on both figures. Values vary from -1.1 to -0.6.

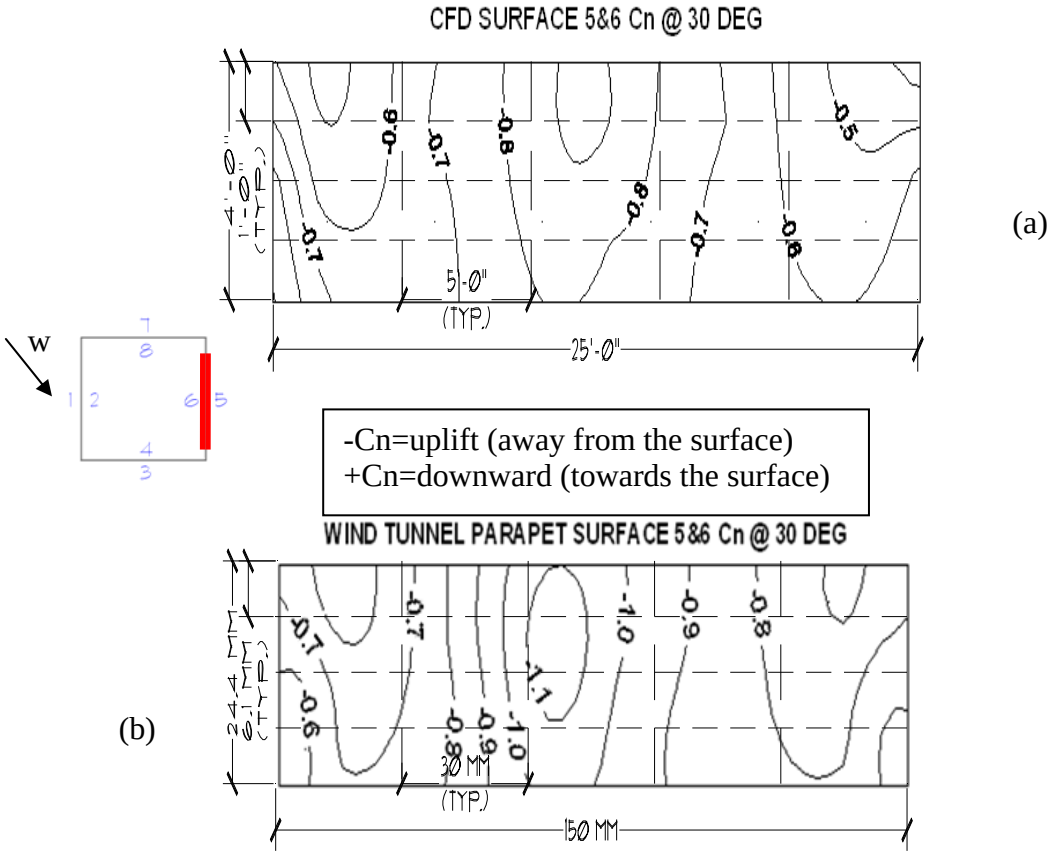

(a)

(b)

Figure 6.33: Cn results at parapet surface #5 and 6 at 30 degrees for CFD (a) and wind tunnel (b).

Cn values for the parapet surface #7 and parapet surface #8 at 30° for CFD and wind tunnel are shown in Figure 6.34a and Figure 6.34b. Net positive and negative values indicating changes in uplift and pressure downward are shown on both figures. Values vary from +0.9 to 0.0 until the last 1/6 of the horizontal surface. The values continue changing from 0.0 to -0.3 on the last 1/6 of the horizontal surface.

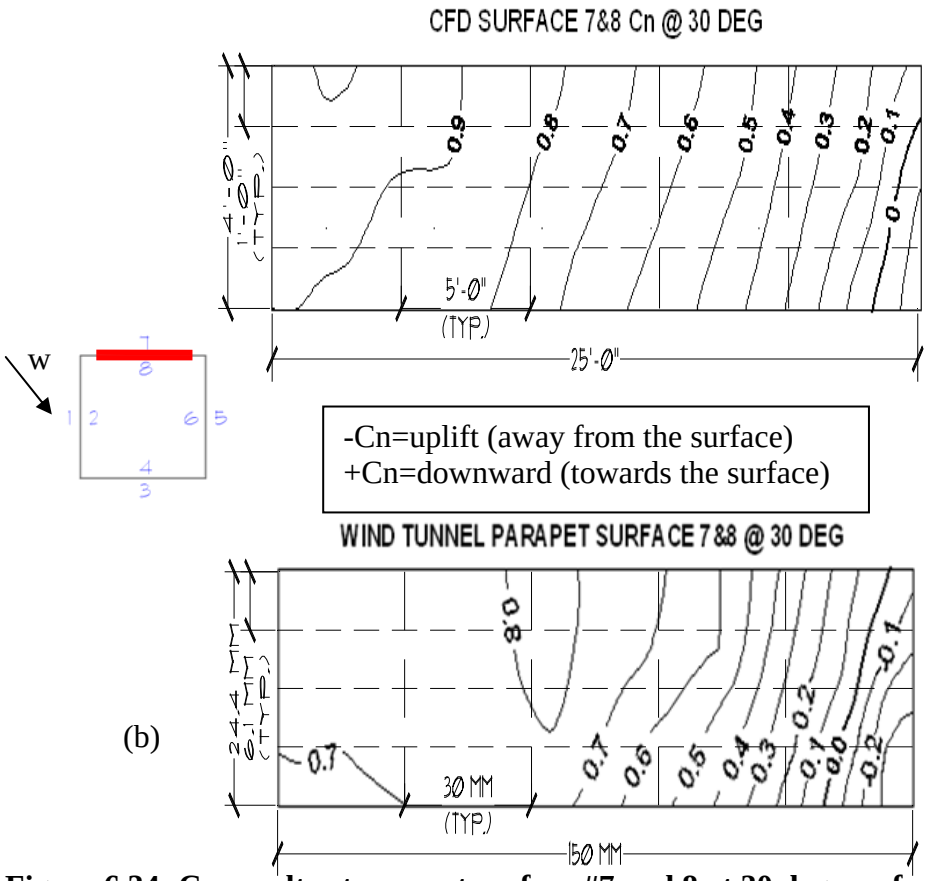

(a)

(b)

Figure 6.34: Cn results at parapet surface #7 and 8 at 30 degrees for CFD (a) and wind tunnel (b).

CHAPTER 7. PARAMETRIC STUDIES OF PRESSURE COEFFICIENTS IN CANOPIES USING CFD

7.1 Description

The results of the previous chapter shows that EFD.Lab, the CFD computer program used in this investigation, can generate similar Cp values in comparison to the wind tunnel results. For the CFD computations and the wind tunnel tests, only one configuration has been tested, the canopy with dimensions 7.6 m (25ft) x 7.6 m (25 ft) and parapet of 1.22 m (4 ft). However, it is necessary to investigate different geometries in order to determine how the Cp and the Cn values vary with the plan geometry and parapet differences, and establish design Cn values based on those results.

Three different configurations are investigated in this chapter. Each configuration is investigated individually with four different parapet heights. Figure 7.1 indicates the nomenclature used for the canopy geometry. Four different parapet heights are investigated in combination with the different plan models. Parapet heights attempt to represent realistic cases and vary from 0.91 m (3 ft), 1.22 m (4 ft), 1.52 m (5 ft) and 1.83 m (6 ft). Two different wind directions are modeled using the CFD program, 0 and 30 degrees as done on the wind tunnel. The combination of all the plan and parapet geometries generates a total of 24 models to be investigated.

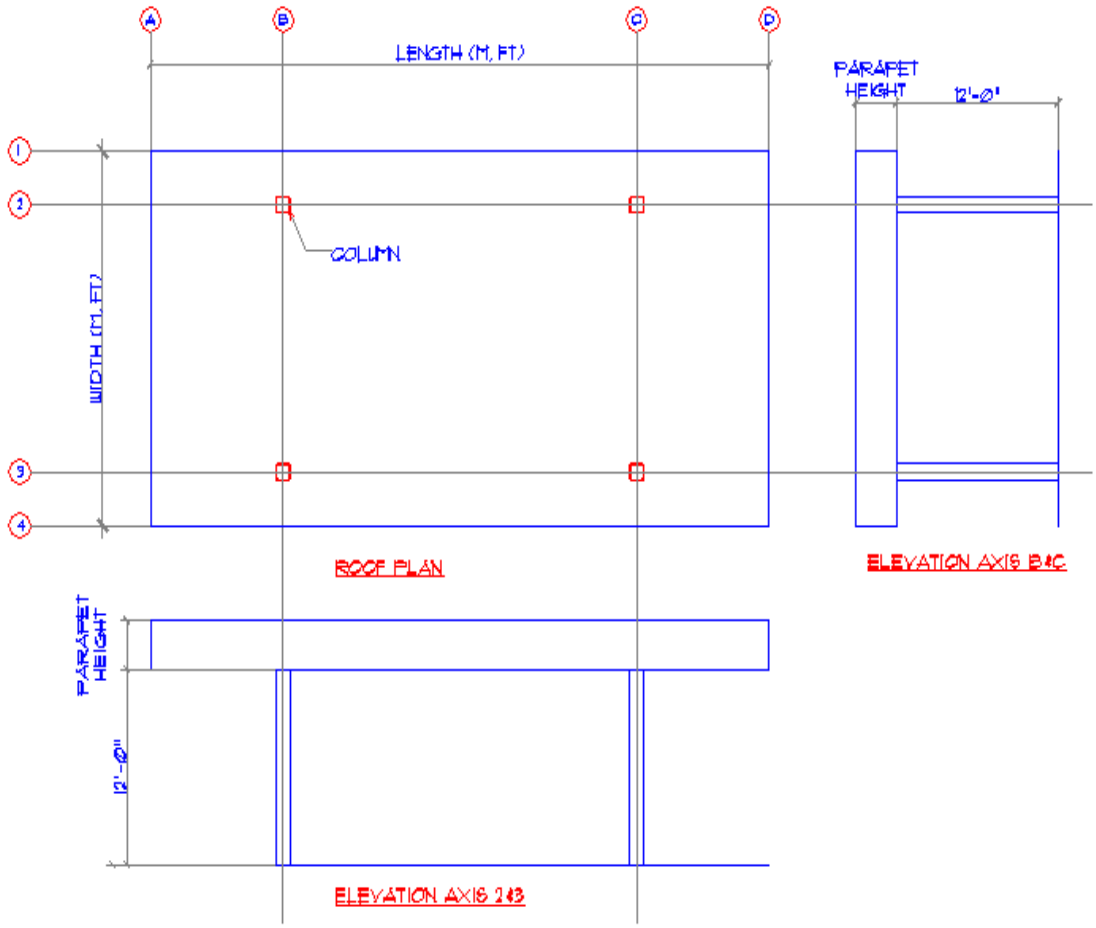

Figure 7.1: Nomenclature used for description of open canopy investigation.

Table 7.1 indicates the number of models and geometry description. A total of twenty four (24) models were generated and investigated. Values for Cp and Cn were obtained for each model, and results for all models are presented on the following sections.

Table 7.1: Model geometry description for the CFD parametric study.

Model #	Model Description (LxWxPH)	Width		Length		Parapet height		Wind Angle
		m	ft	m	ft	m	ft	degrees
1	25x25x3 0 DEG	7.62	25	7.62	25	0.91	3	0
2	25x25x3 30 DEG	7.62	25	7.62	25	0.91	3	30
3	25x25x4 0 DEG	7.62	25	7.62	25	1.22	4	0
4	25x25x4 30 DEG	7.62	25	7.62	25	1.22	4	30
5	25x25x5 0 DEG	7.62	25	7.62	25	1.52	5	0
6	25x25x5 30 DEG	7.62	25	7.62	25	1.52	5	30
7	25x25x6 0 DEG	7.62	25	7.62	25	1.83	6	0
8	25x25x6 30 DEG	7.62	25	7.62	25	1.83	6	30
9	25x40x3 0 DEG	7.62	25	12.19	40	0.91	3	0
10	25x40x3 30 DEG	7.62	25	12.19	40	0.91	3	30
11	25x40x4 0 DEG	7.62	25	12.19	40	1.22	4	0
12	25x40x4 30 DEG	7.62	25	12.19	40	1.22	4	30
13	25x40x5 0 DEG	7.62	25	12.19	40	1.52	5	0
14	25x40x5 30 DEG	7.62	25	12.19	40	1.52	5	30
15	25x40x6 0 DEG	7.62	25	12.19	40	1.83	6	0
16	25x40x6 30 DEG	7.62	25	12.19	40	1.83	6	30
17	25x50x3 0 DEG	7.62	25	15.24	50	0.91	3	0
18	25x50x3 30 DEG	7.62	25	15.24	50	0.91	3	30
19	25x50x4 0 DEG	7.62	25	15.24	50	1.22	4	0
20	25x50x4 30 DEG	7.62	25	15.24	50	1.22	4	30
21	25x50x5 0 DEG	7.62	25	15.24	50	1.52	5	0
22	25x50x5 30 DEG	7.62	25	15.24	50	1.52	5	30
23	25x50x6 0 DEG	7.62	25	15.24	50	1.83	6	0
24	25x50x6 30 DEG	7.62	25	15.24	50	1.83	6	30

CFD model results are represented in two different graphical formats. First, top view of the contour surface representing the Cn values is presented for each model. Second, a 3D contour plot showing the Cn values are also represented. The purpose of that graphical representation is that it helps the visualization of the Cn values. The maximum and minimum are clearly represented, especially when the wind is applied at 30 degrees from the structural axis to the model.

After each group of four models is discussed, a 2D graph is shown to plot the Cn values for each parapet height, for each of the geometries. Observations and comments for each graphical result are in the following sections.

The importance of this parametric study is to investigate the effects of different geometries on the Cn values, with the aim of using them for structural design.

7.2 Open canopy models, 7.6 m (25 ft) x7.6 m (25 ft) at 0 degrees

Model #1 is a canopy with dimensions of 7.6 m (25 ft) x 7.6 m (25 ft) x 0.91 m (3 ft) with the wind at 0 degrees, as shown in Figure 7.2. Values of pressure coefficients were computed for this case and the results in terms of contour lines are plotted in Figure 7.2. Figure 7.3 shows a 3D view of the Cn values of the canopy. Values range from a maximum of +0.6 close the windward (and due to turbulence generated by the front parapet) to a minimum of -0.3. The results plotted show clear bounds with equal pressure values in the transverse direction, and only close to the front parapet does turbulence generate a small transverse variation.

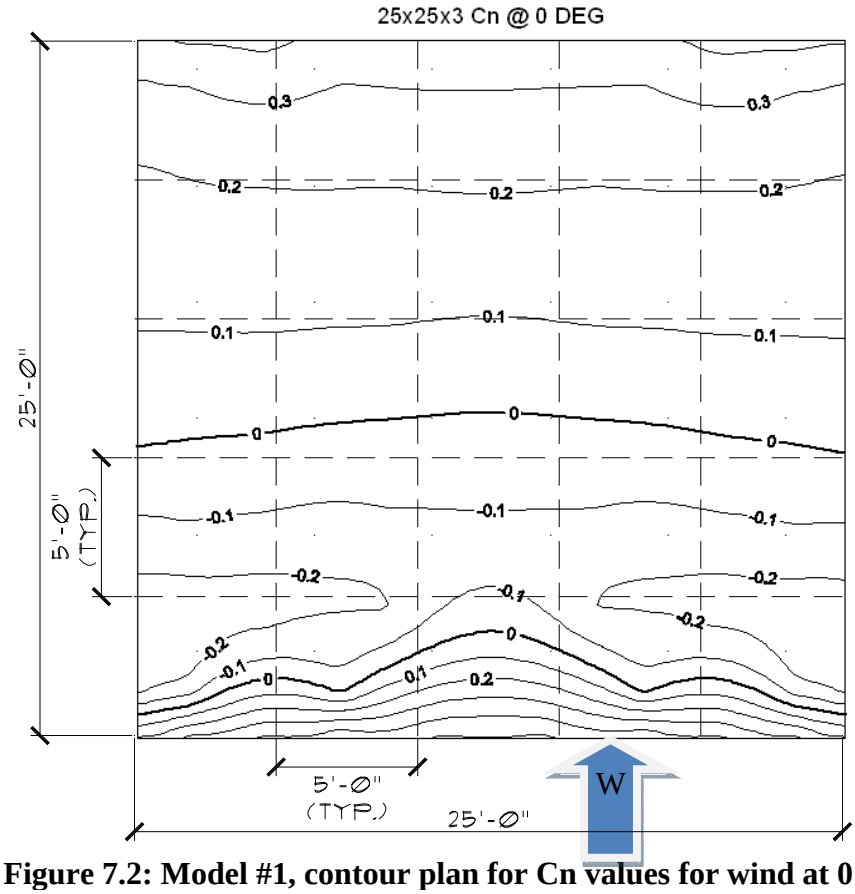

Figure 7.2: Model #1, contour plan for Cn values for wind at 0 degrees.

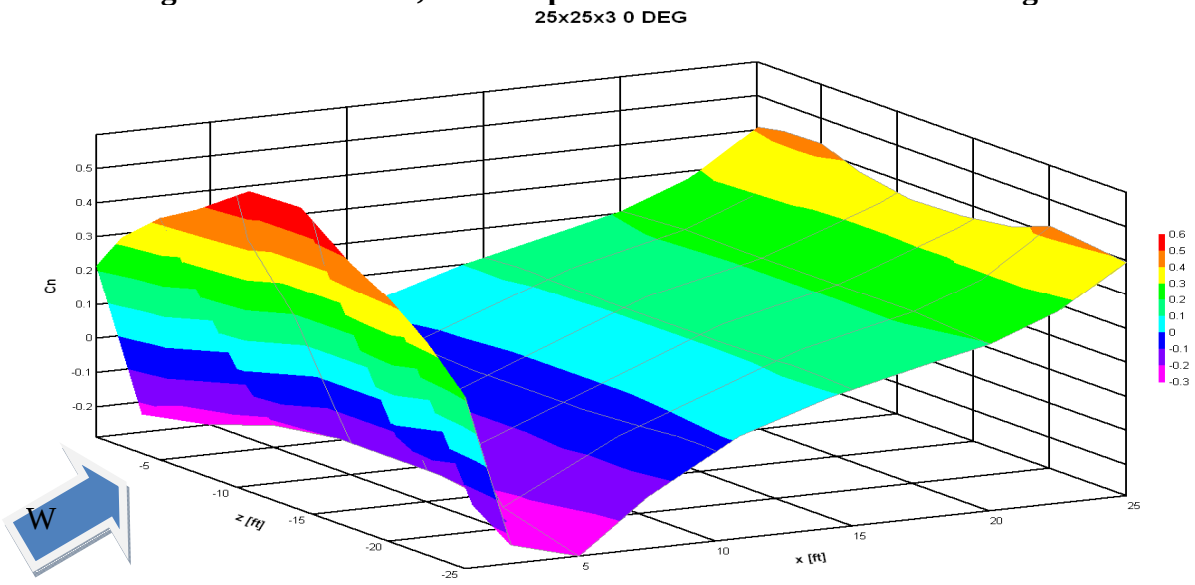

Figure 7.3: Model #1, 3D contour plot for Cn values for wind at 0 degrees.

For the same dimensions in plan, the new model has a higher parapet. Cn values for contour plan for Model #3, with dimensions of 7.6 m (25 ft) x 7.6 m (25 ft) x 1.22 m (4 ft) with the wind at 0 degrees are shown in Figure 7.4. Figure 7.5 shows a 3D view of the Cn values of the canopy. Values range from a maximum of +0.8 to a minimum of -0.3. In comparison with the previous model with a shorter parapet, the maximum positive values have increased from 0.6 to 0.8 for a change of parapet from 3 to 4 ft.

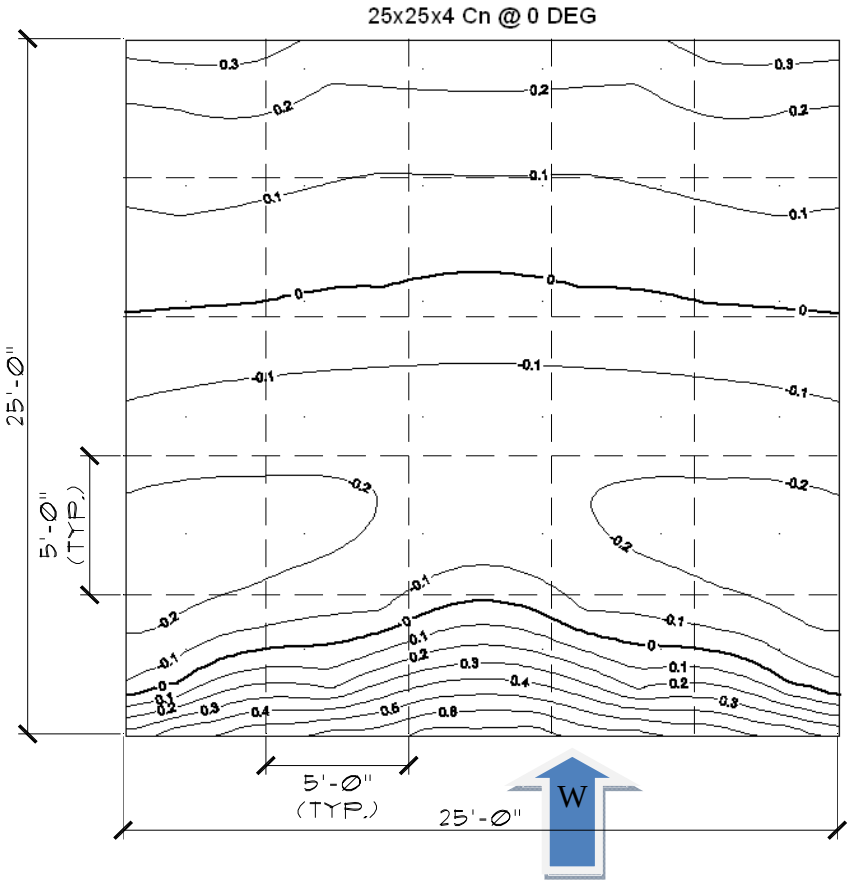

Figure 7.4: Model #3, contour plan for Cn values for wind at 0 degrees.

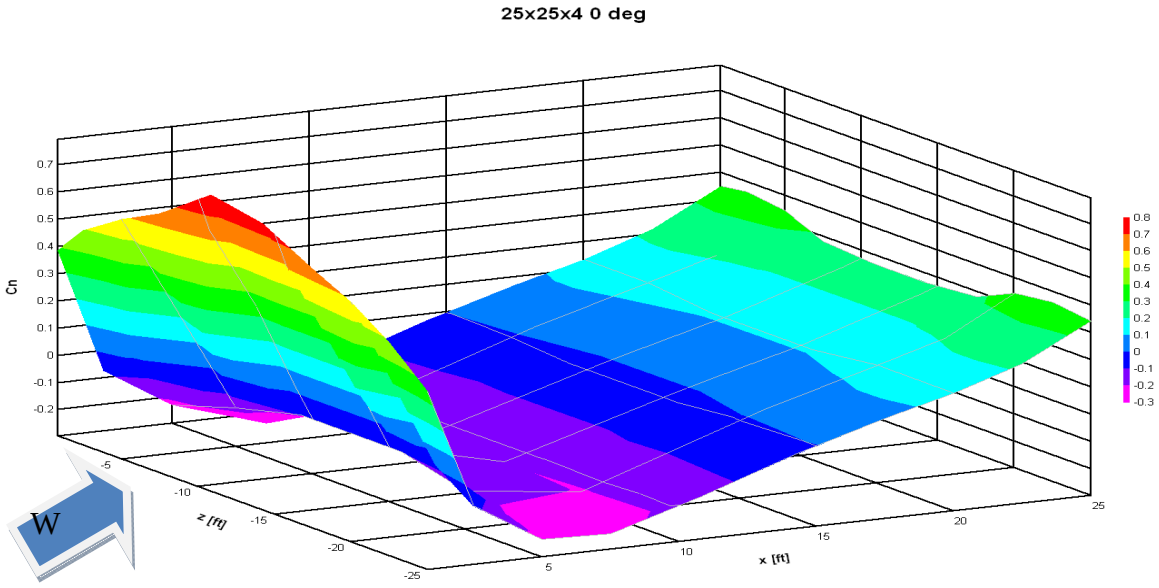

Figure 7.5: Model #3, 3D contour plot for Cn values for wind at 0 degrees.

A higher parapet is investigated in the next configuration. Cn values for contour plan for Model #5, with dimensions of 7.6 m (25 ft) x 7.6 m (25 ft) x 1.52 m (5 ft) with the wind at 0 degrees are shown on Figure 7.6. Figure 7.7 shows a 3D view of the Cn values of the canopy. Values range from a maximum of +0.9 to a minimum of -0.3.

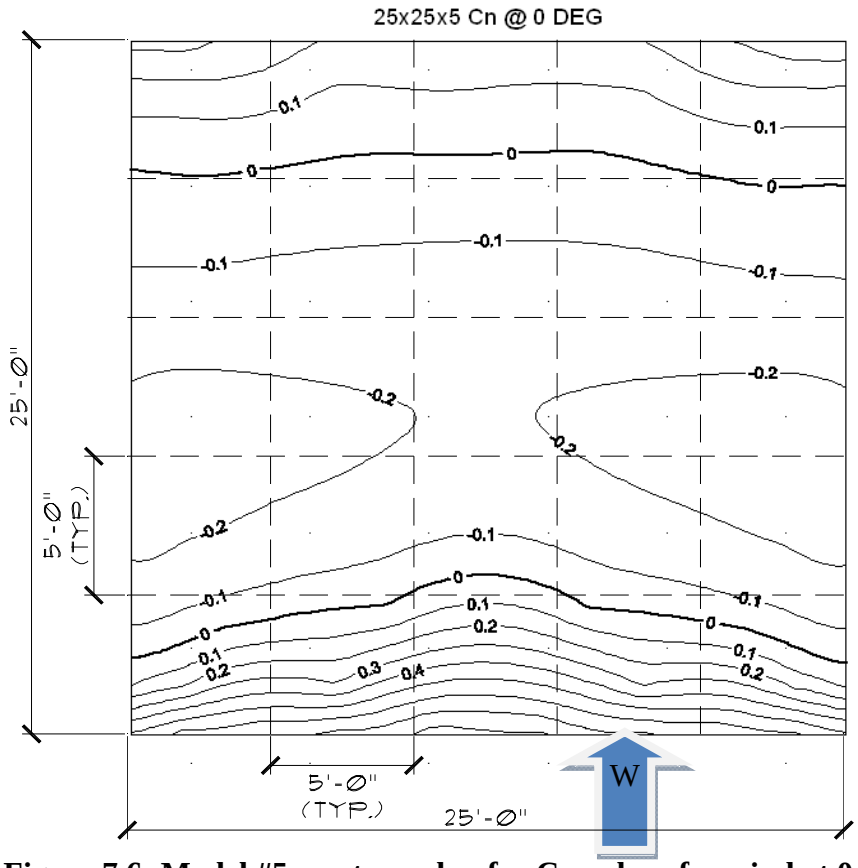

Figure 7.6: Model #5, contour plan for Cn values for wind at 0 degrees.

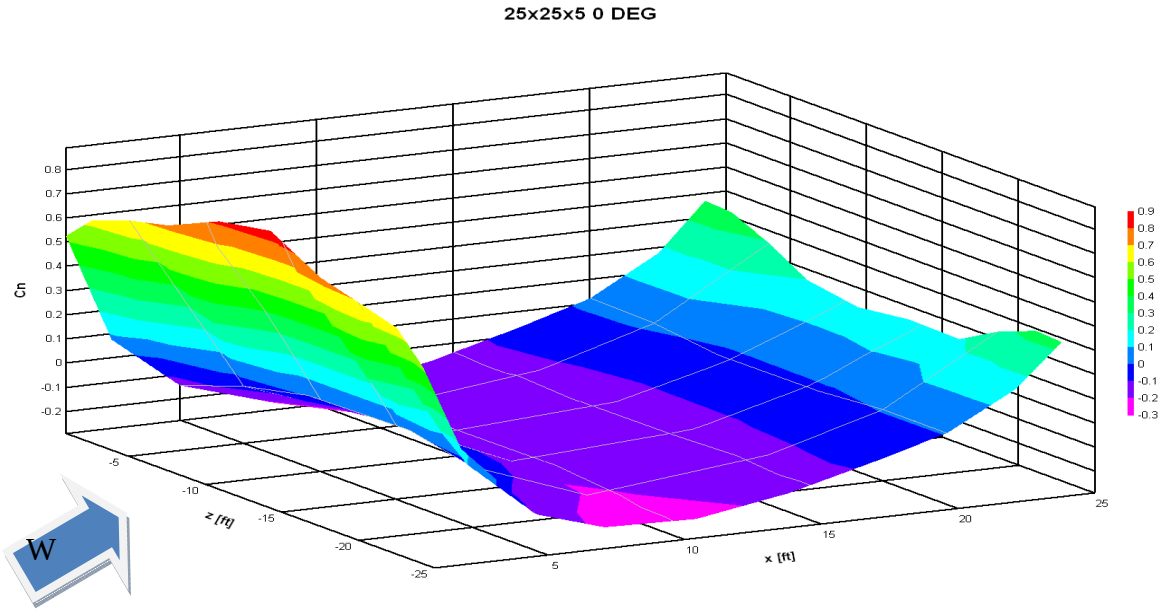

Figure 7.7: Model #5, 3D contour plot for Cn values for wind at 0 degrees.

Finally, the parapet is increased with respect to the previous models. Cn values for contour plan for Model #7, with dimensions of 7.6 m (25 ft) x 7.6 m (25 ft) x 1.82 m (6 ft) with the wind at 0 degrees, are shown on Figure 7.8. Figure 7.9 shows a 3D view of the Cn values of the canopy. Values ranges from a maximum of +0.9 to a minimum of -0.3.

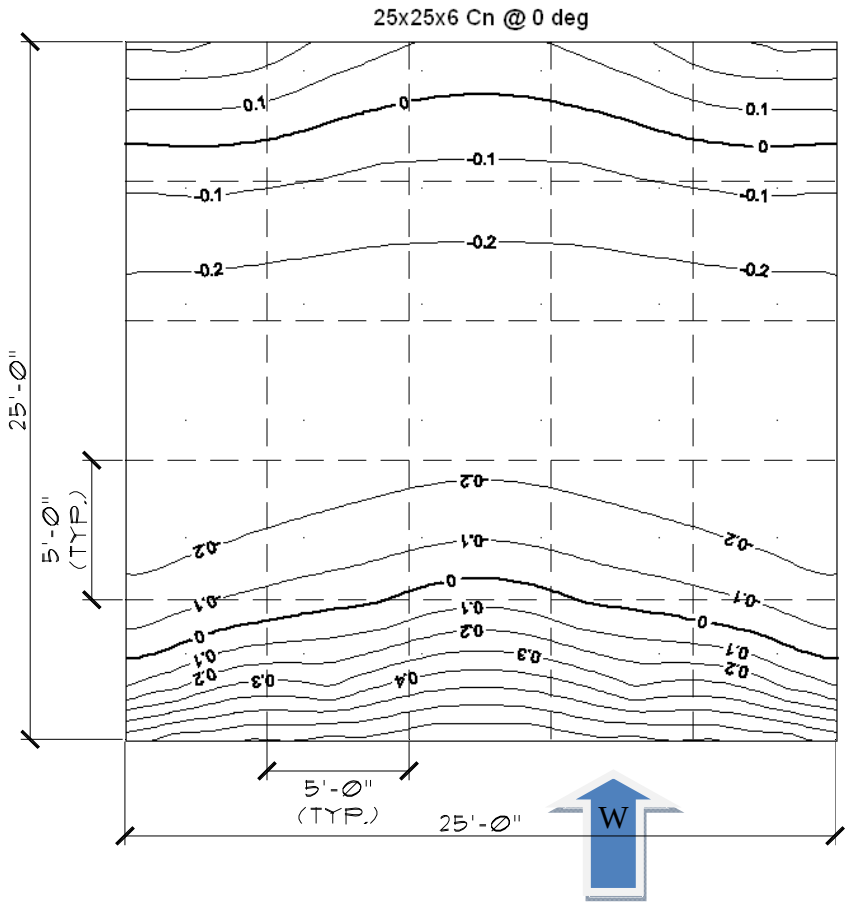

Figure 7.8: Model #7, contour plan for Cn values for wind at 0 degrees.

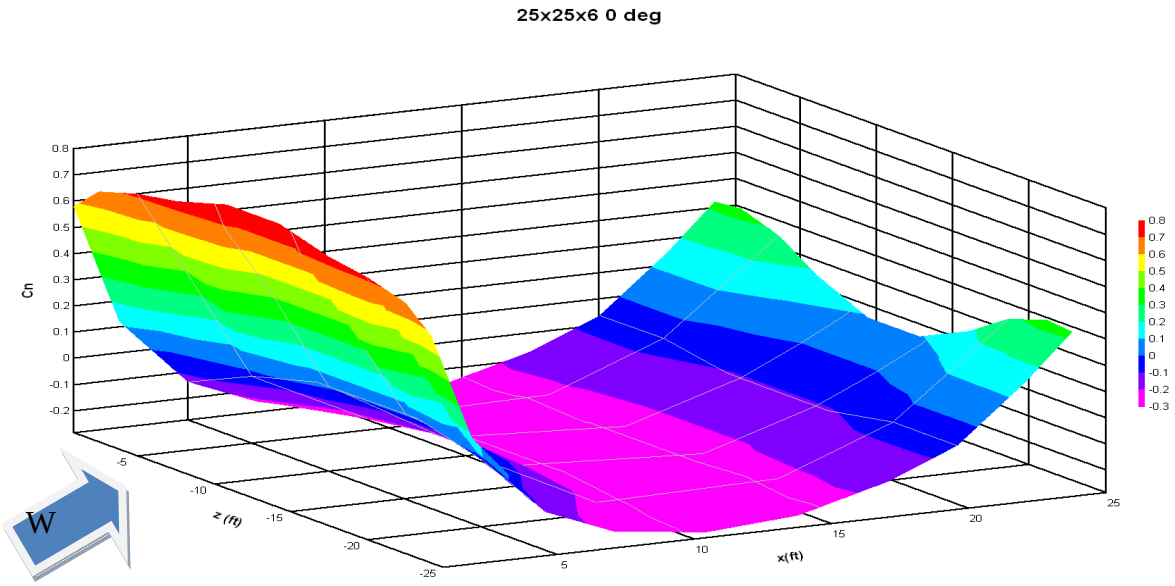

Figure 7.9: Model #7, 3D contour plot for Cn values for wind at 0 degrees.

Figure 7.10 shows four Cn graphs, one for each parapet height on the 7.6 m (25 ft) x 7.6 m (25 ft) open canopy. The 2D graph data was obtained at the center of the canopy width in the principal axis direction. Every parapet height exhibits in the graph a segment of positive Cn values (acting downward) on the first L/5 of the horizontal length. After the downward segment, uplift pressure acting on a length of L/3 followed, to end with a downward pressure for the rest of the horizontal distance. It may be seen that the downward values on the area close to windward are larger than those computed on the leeward zone.

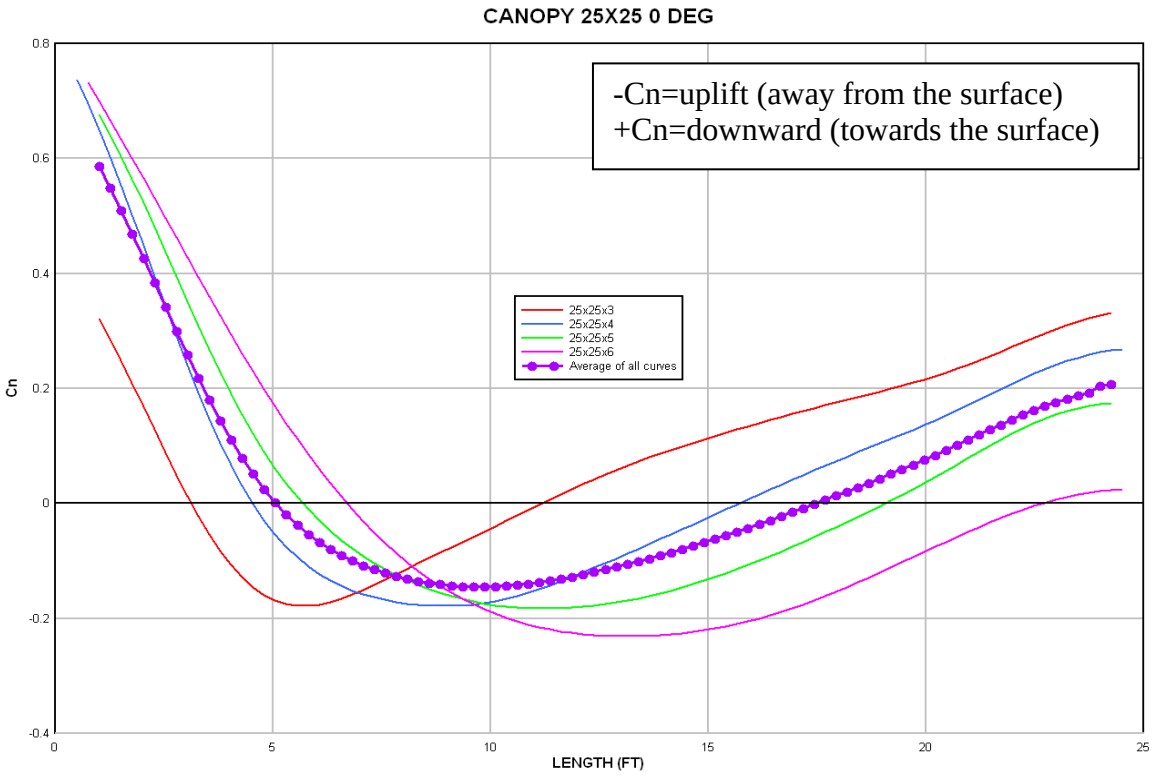

Figure 7.10: Influence of parapet height. 2D graph of Cn values for all 7.6 m (25 ft) x 7.6 m (25 ft) @ 0 degrees.

7.3 Open canopy models, 7.6 m (25 ft) x7.6 m (25 ft) at 30 degrees

The configuration in the previous section was aligned with the wind direction; however, other wind directions may lead to more stringent pressure values. Cn values for contour plan for Model #2, with dimensions of 7.6 m (25 ft) x 7.6 m (25 ft) x 0.91 m (3 ft) with the wind at 30 degrees are shown in Figure 7.11. Figure 7.12 shows a 3D view of the Cn values of the canopy. The results indicate an asymmetric pressure pattern in the canopy, in which two parapets seen to play a role. Values range from a maximum of +0.8 to a minimum of -0.6. These values are significantly higher than those computed for Model #1, which were +0.6 and -0.3 respectively.

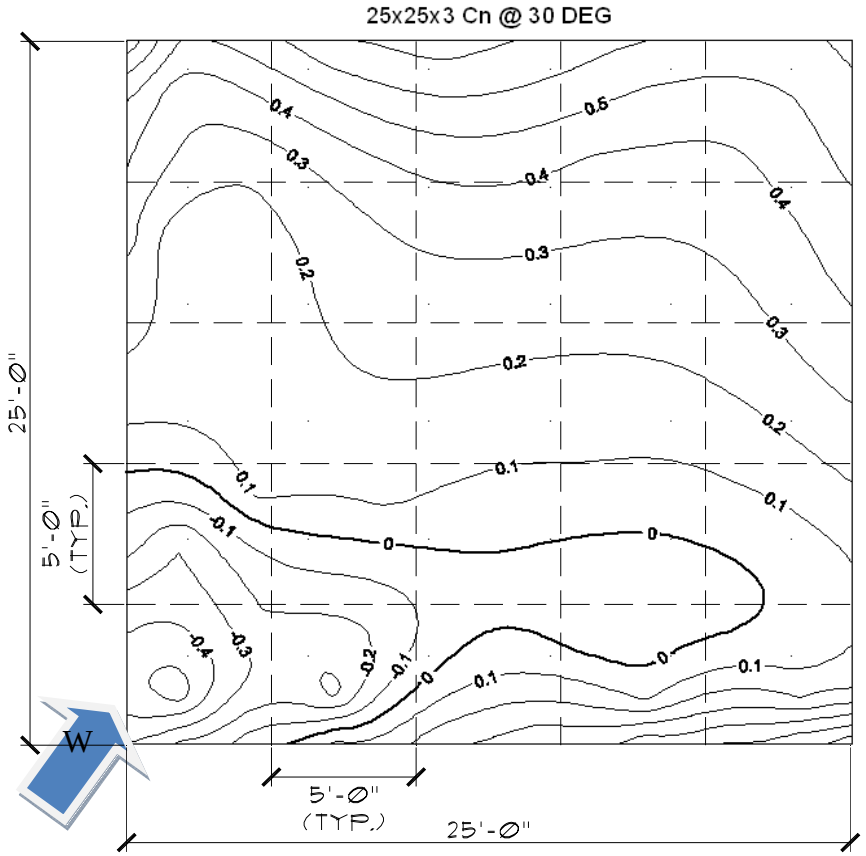

Figure 7.11: Model #2, contour plan for Cn values for wind at 30 degrees.

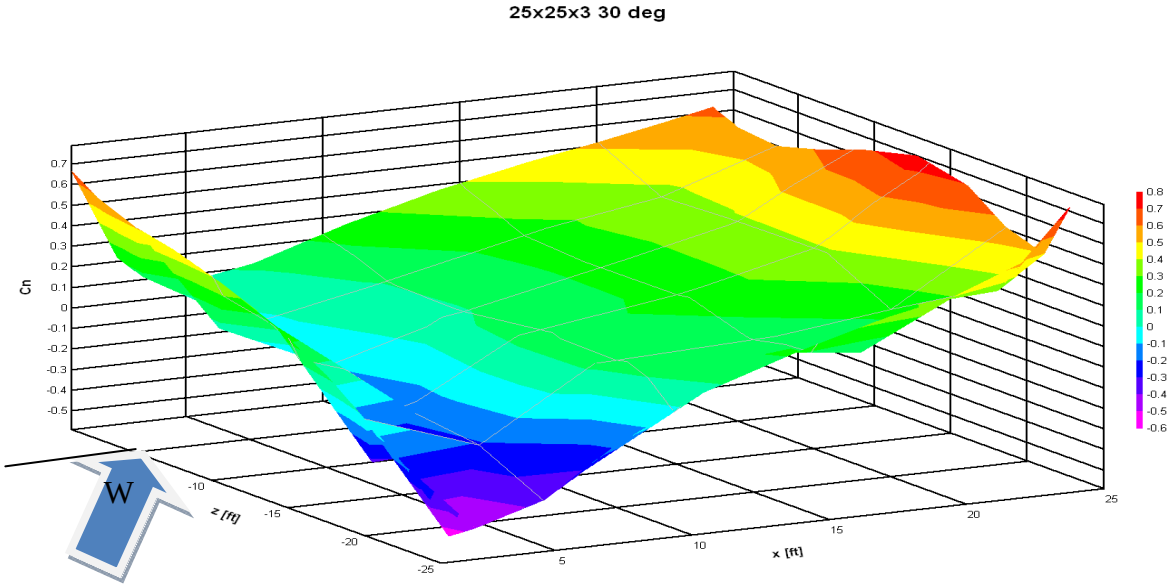

Figure 7.12: Model #2, 3D contour plot for Cn values for wind at 30 degrees.

Cn values for contour plan for Model #4, with dimensions of 7.6 m (25 ft) x 7.6 m (25 ft) x 1.22 m (4 ft) with the wind at 30 degrees are shown in Figure 7.13. Figure 7.14 shows a 3D view of the Cn values of the canopy. Values range from a maximum of +0.8 to a minimum of -0.3. Those are the same extreme values computed for the wind incidence at 0°.

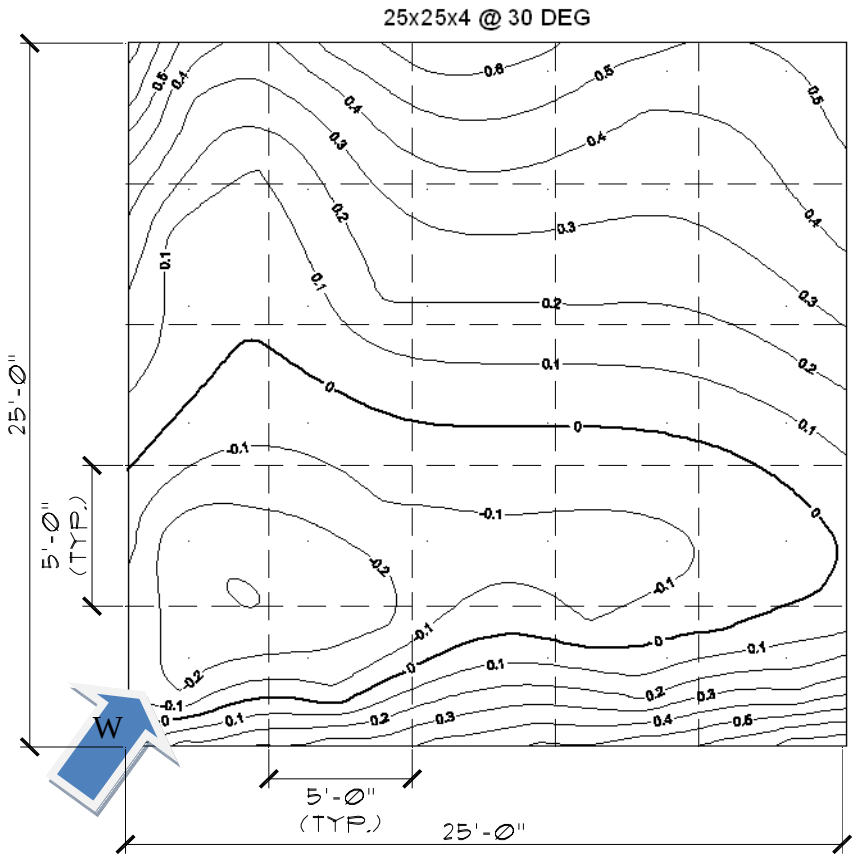

Figure 7.13: Model #4, contour plan for Cn values for wind at 30 degrees.

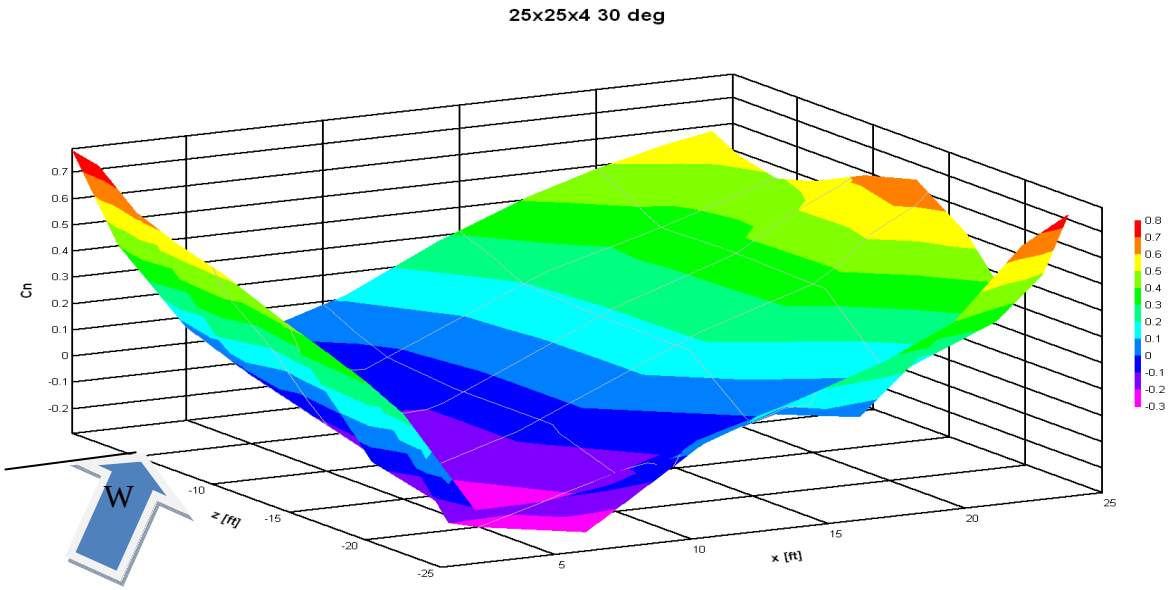

Figure 7.14: Model #4, 3D contour plot for Cn values for wind at 30 degrees.

Cn values for contour plan for Model #6, with dimensions of 7.6 m (25 ft) x 7.6 m (25 ft) x 1.52 m (5 ft) with the wind at 30 degrees are shown in Figure 7.15. Figure 7.16 shows a 3D view of the Cn values of the canopy. Values range from a maximum of +0.9 to a minimum of -0.2, which are similar to the values computed for Model #5 (with 0°).

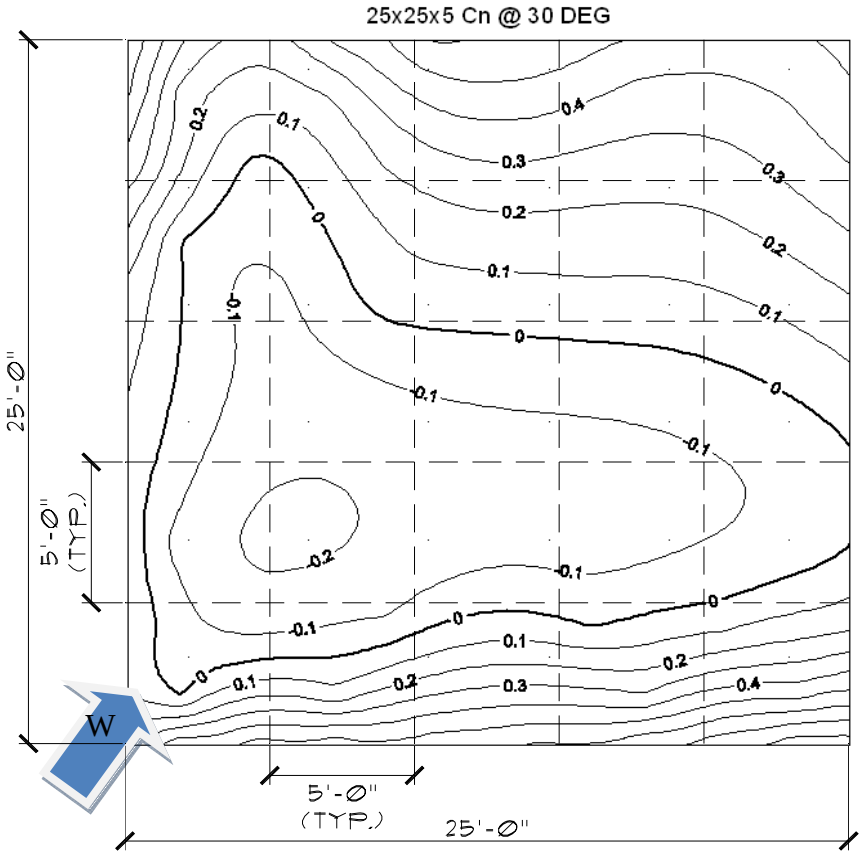

Figure 7.15: Model #6, contour plan for Cn values for wind at 30 degrees.

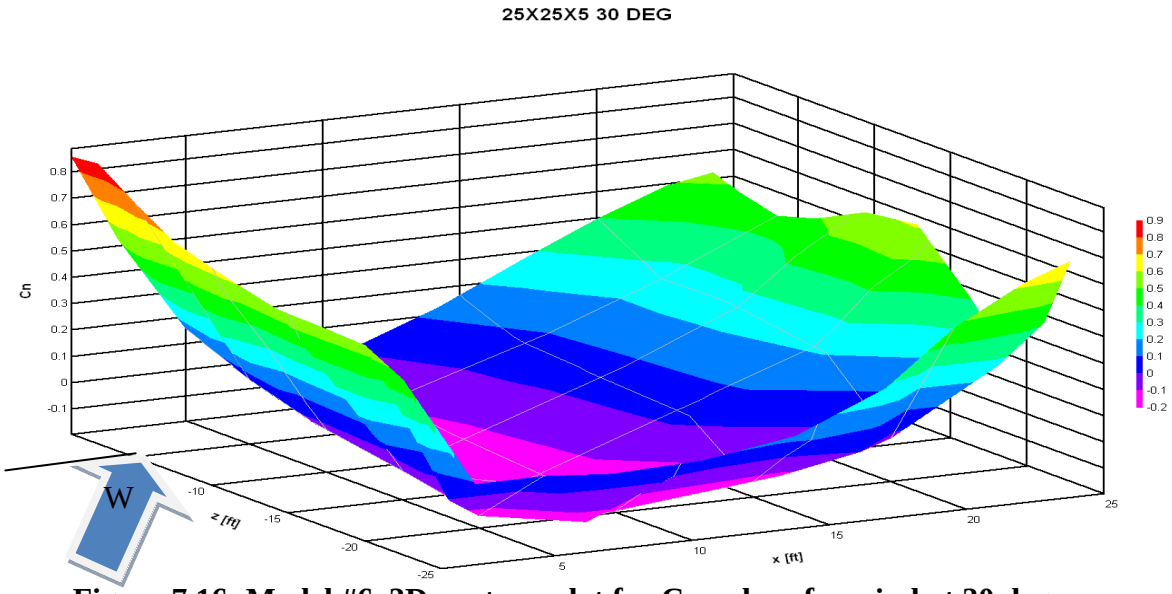

Figure 7.16: Model #6, 3D contour plot for Cn values for wind at 30 degrees.

Cn values for contour plan for Model #8, with dimensions of 7.6 m (25 ft) x 7.6 m (25 ft) x 1.82 m (6 ft) with the wind at 30 degrees are shown in Figure 7.17. Figure 7.18 shows a 3D view of the Cn values of the canopy. Values range from a maximum of +0.9 to a minimum of -0.2, which are smaller than those computed at 0° (+1.0 and -0.2 respectively).

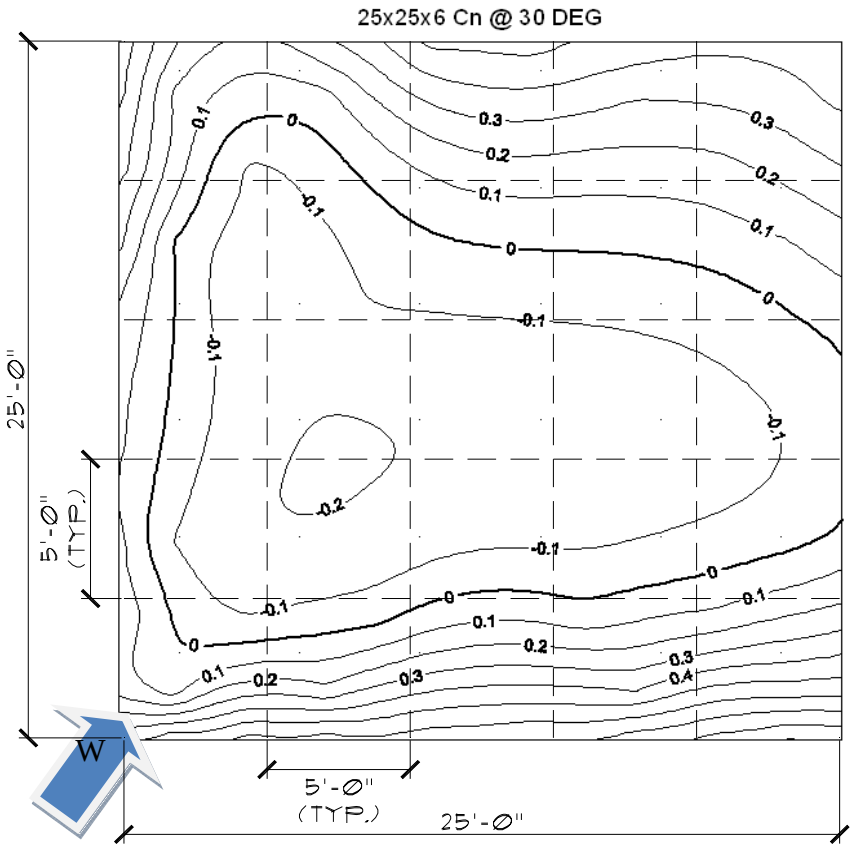

Figure 7.17: Model #8, contour plan for Cn values for wind at 30 degrees.

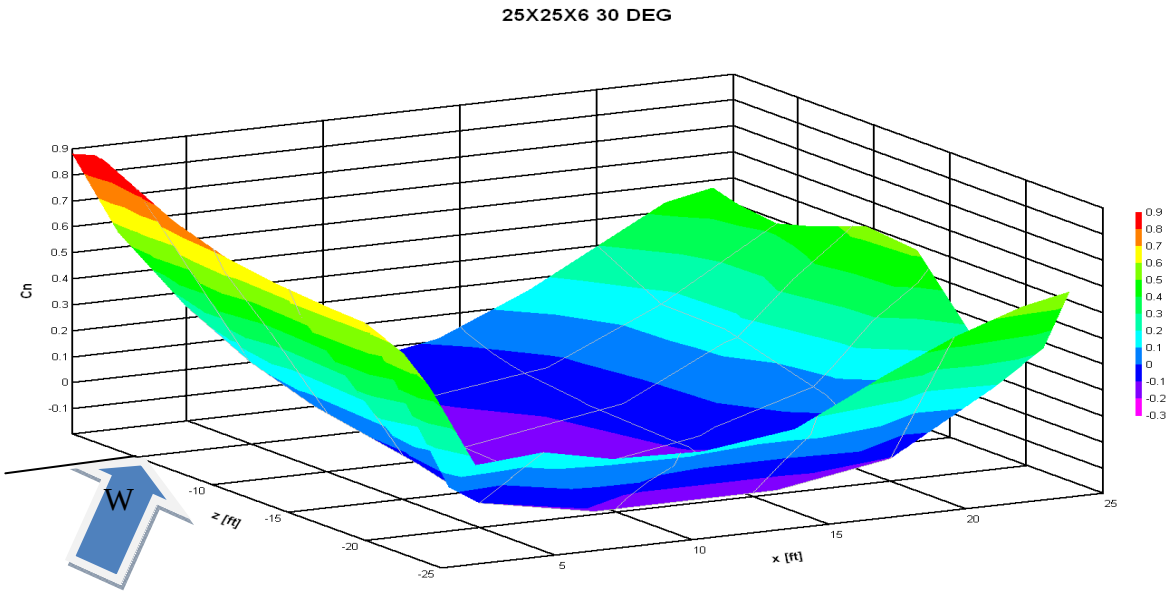

Figure 7.18: Model #8, 3D contour plot for Cn values for wind at 30 degrees.

Figure 7.19 shows four Cn graphs, one for each parapet height on the 7.6 m (25 ft) x 7.6 m (25 ft) open canopy. The 2D graph data was obtained at the center of the canopy width in the angle of the applied wind, in these case thirty (30) degrees from the principal axis direction. All parapet height exhibit on the graph a segment of positive Cn values (downward) on the first L/5, except for the parapet height of 0.91 m (3 ft) and 1.22 m (4 ft), which were all negative Cn values. After the uplift segment, an uplift pressure length of L/3 followed a downward for the rest of the horizontal distance. As said before, the extreme values shown by 0° and 30° are similar, but the actual distributions are the same, as can be seen from comparisons of Figures 7.10 and 7.19.

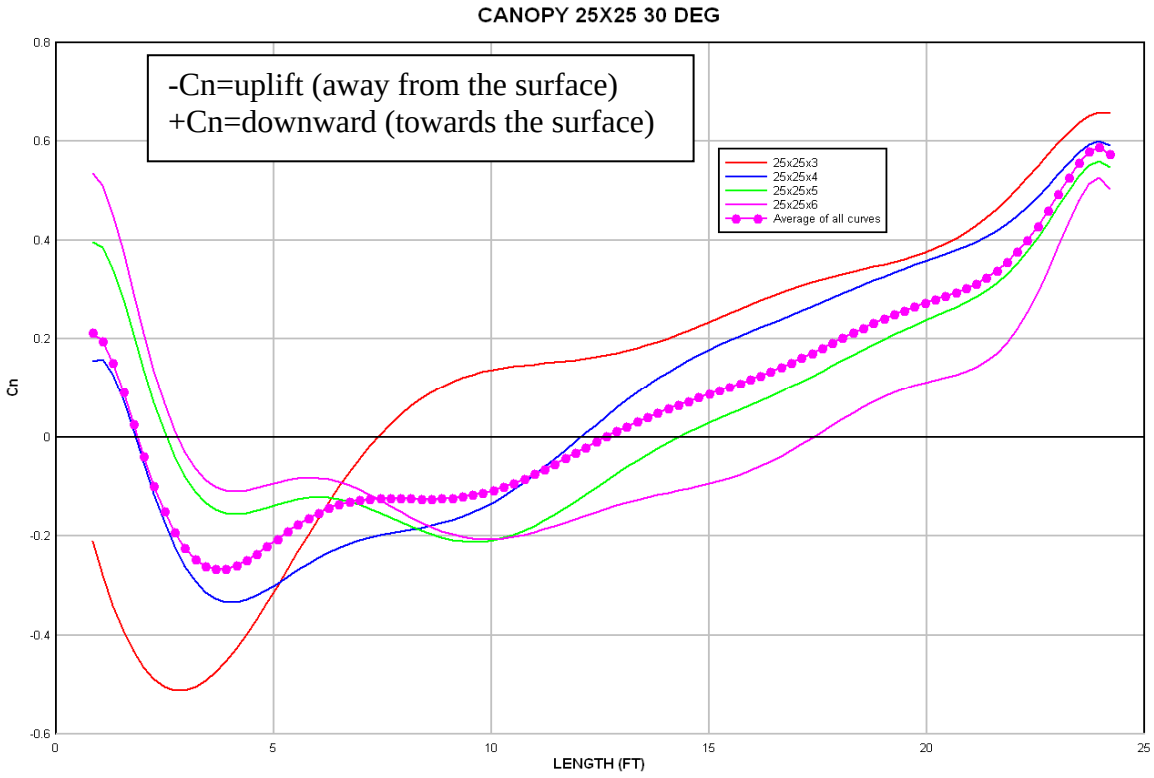

Figure 7.19: 2D graph of Cn values for all 7.6 m (25 ft) x 7.6 m (25 ft) @ 30 degrees.

7.4 Open canopy models, 7.6 m (25 ft) x12.2 m (40 ft) at 0 degrees

The previous configurations were representative of square canopies, and the influence of having a rectangular configuration is investigated next. Again, the influence of parapet height is taken into account. Cn values for contour plan for Model #9, with dimensions of 7.6 m (25 ft) x 12.2 m (40 ft) x 0.91 m (3 ft) with the wind at 0 degrees are shown in Figure 7.20. Figure 7.21 shows a 3D view of the Cn values of the canopy. Values range from a maximum of +0.7 to a minimum of -0.4. The values are slightly higher than in the square configuration #1 (+0.6 and -0.3 respectively).

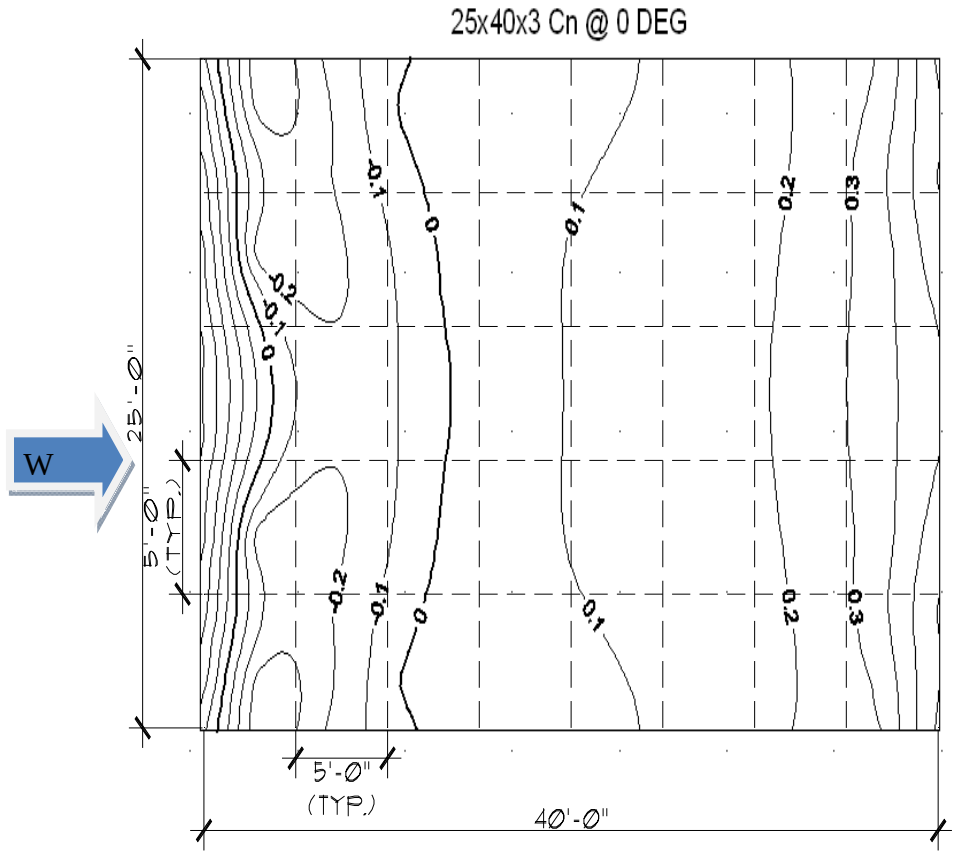

Figure 7.20: Model #9, contour plan for Cn values for wind at 0 degrees.

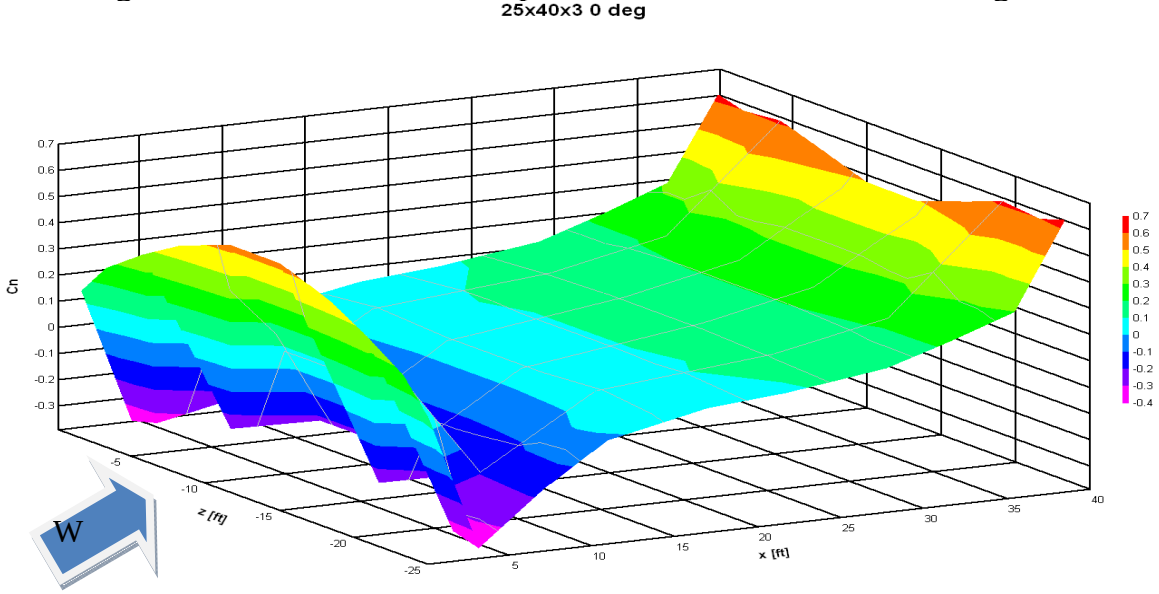

Figure 7.21: Model #9, 3D contour plot for Cn values for wind at 0 degrees.

Cn values for contour plan for Model #11, with dimensions of 7.6 m (25 ft) x 12.2 m (40 ft) x 1.22 m (4 ft) with the wind at 0 degrees are shown in Figure 7.22. Figure 7.23 shows a 3D

view of the Cn values of the canopy. Values range from a maximum of +0.7 to a minimum of -0.3. In the square configuration, we reported extreme values of +0.8 and -0.3.

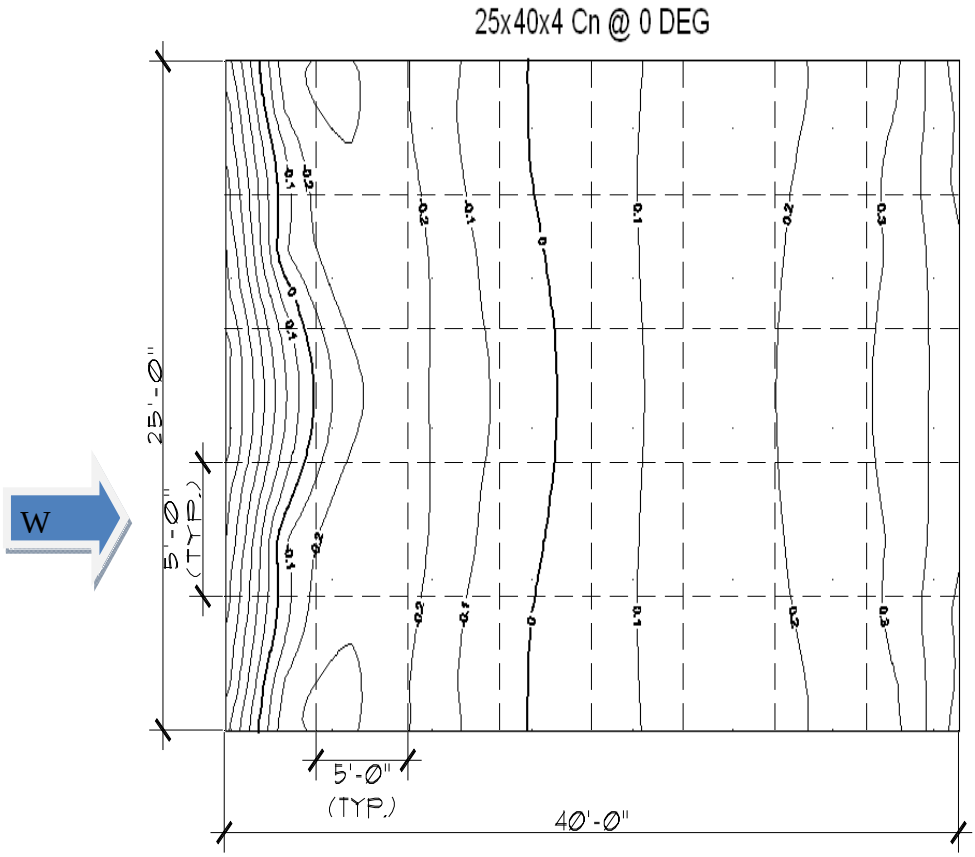

Figure 7.22: Model #11, contour plan for Cn values for wind at 0 degrees.

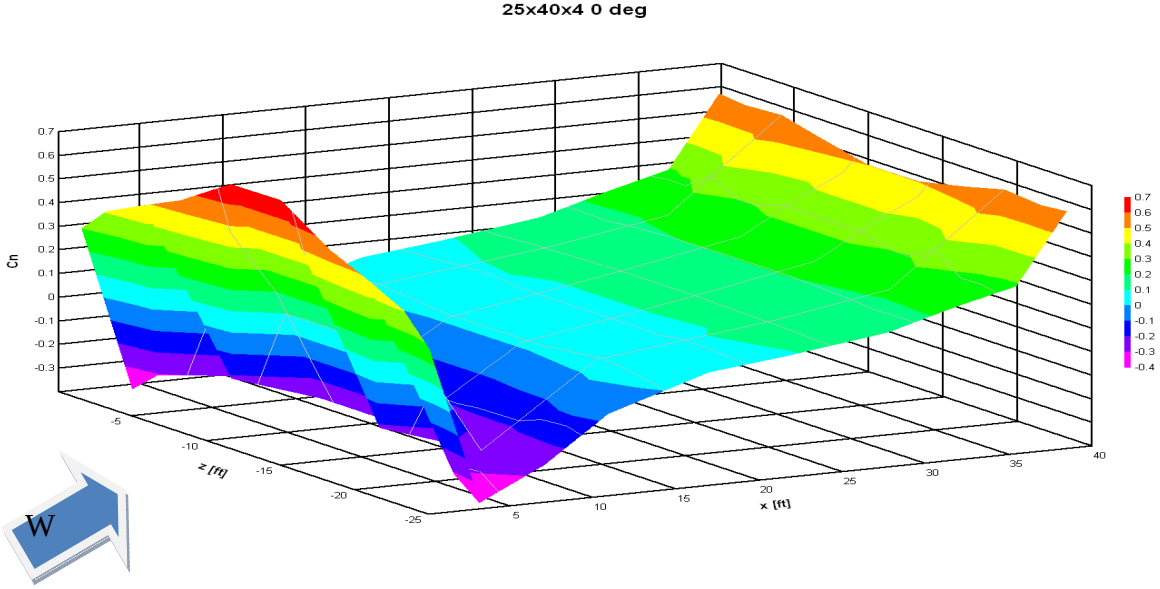

Figure 7.23: Model #11, 3D contour plot for Cn values for wind at 0 degrees.

Cn values for contour plan for Model #13, with dimensions of 7.6 m (25 ft) x 12.2 m (40 ft) x 1.52 m (5 ft) with the wind at 0 degrees are shown in Figure 7.24. Figure 7.25 shows a 3D view of the Cn values of the canopy. Values range from a maximum of +0.9 to a minimum of -0.3. The same extreme values were obtained in the square canopy.

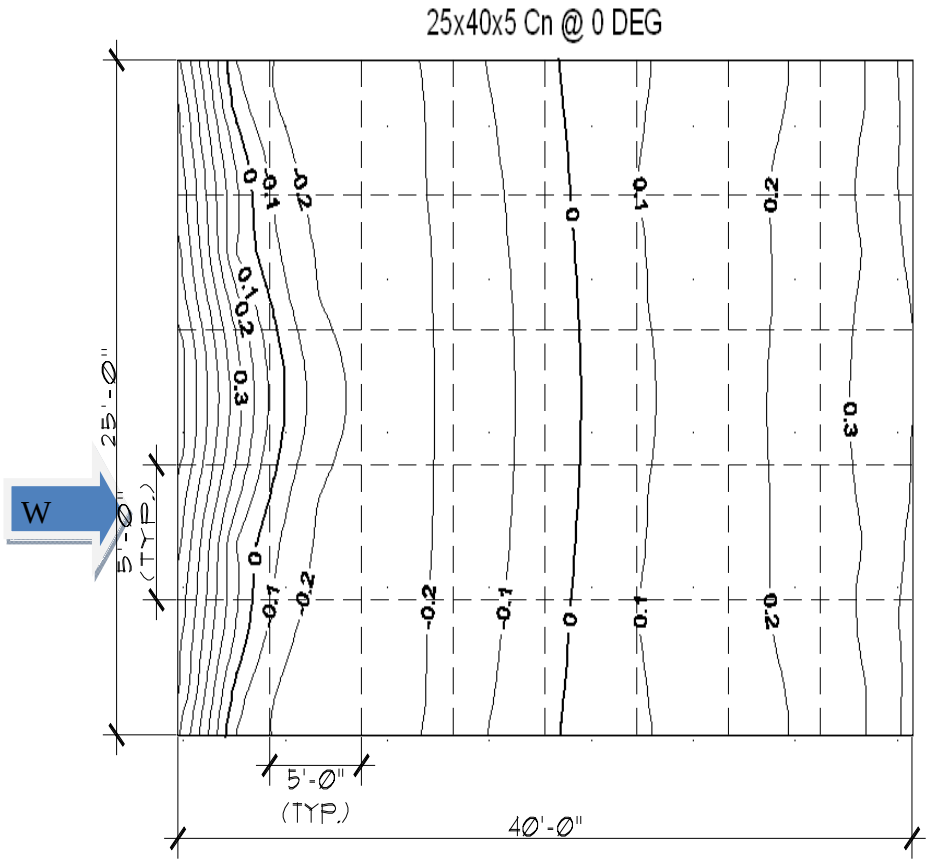

Figure 7.24: Model #13, contour plan for Cn values for wind at 0 degrees.

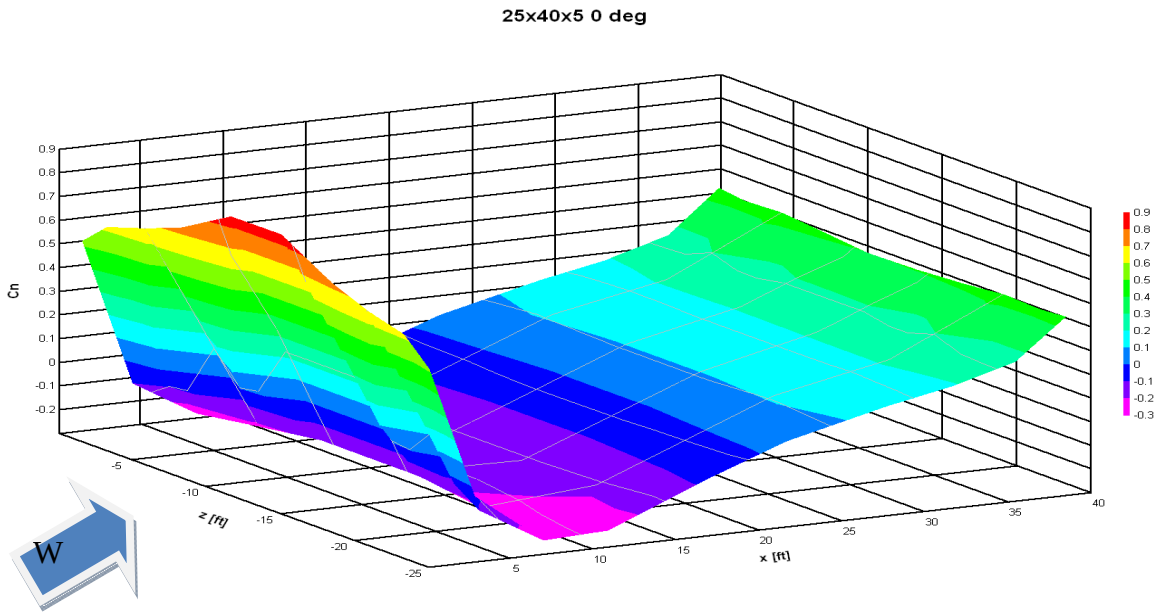

Figure 7.25: Model #13, 3D contour plot for Cn values for wind at 0 degrees.

Cn values for contour plan for Model #15, with dimensions of 7.6 m (25 ft) x 12.2 m (40 ft) x 1.82 m (6 ft) with the wind at 0 degrees are shown in Figure 7.26. Figure 7.27 shows a 3D view of the Cn values of the canopy. Values range from a maximum of +0.9 to a minimum of -0.3. As a reference value, values of +1.0 and -0.2 resulted for the square configuration.

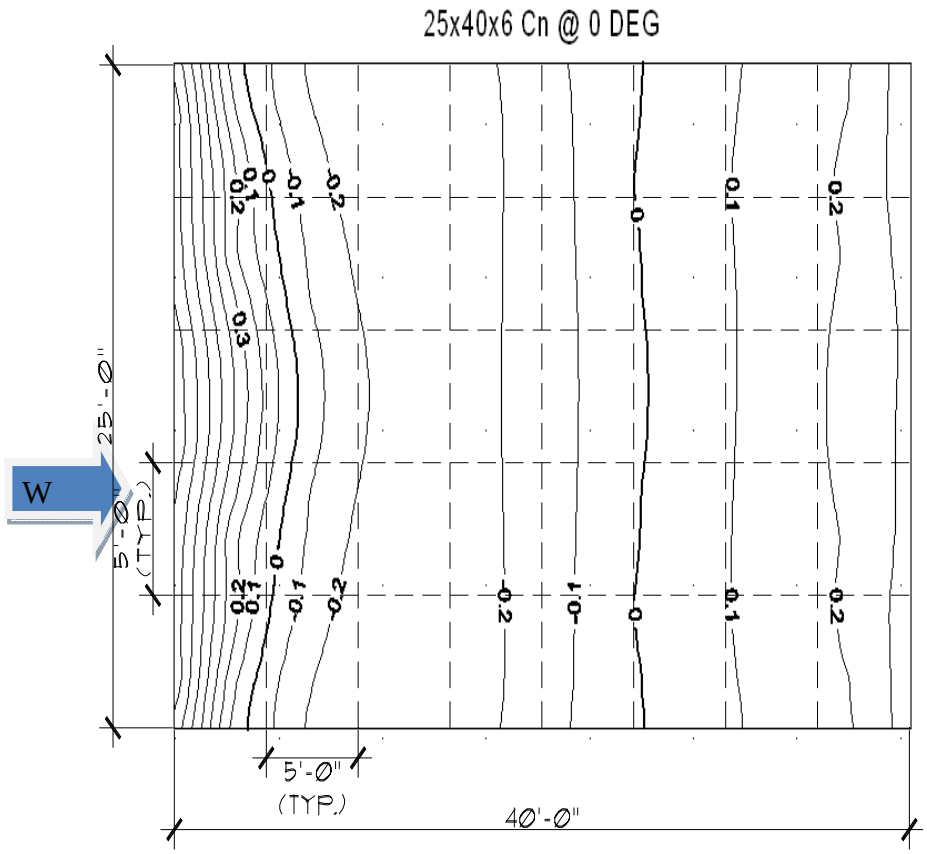

Figure 7.26: Model #15, contour plan for Cn values for wind at 0 degrees.

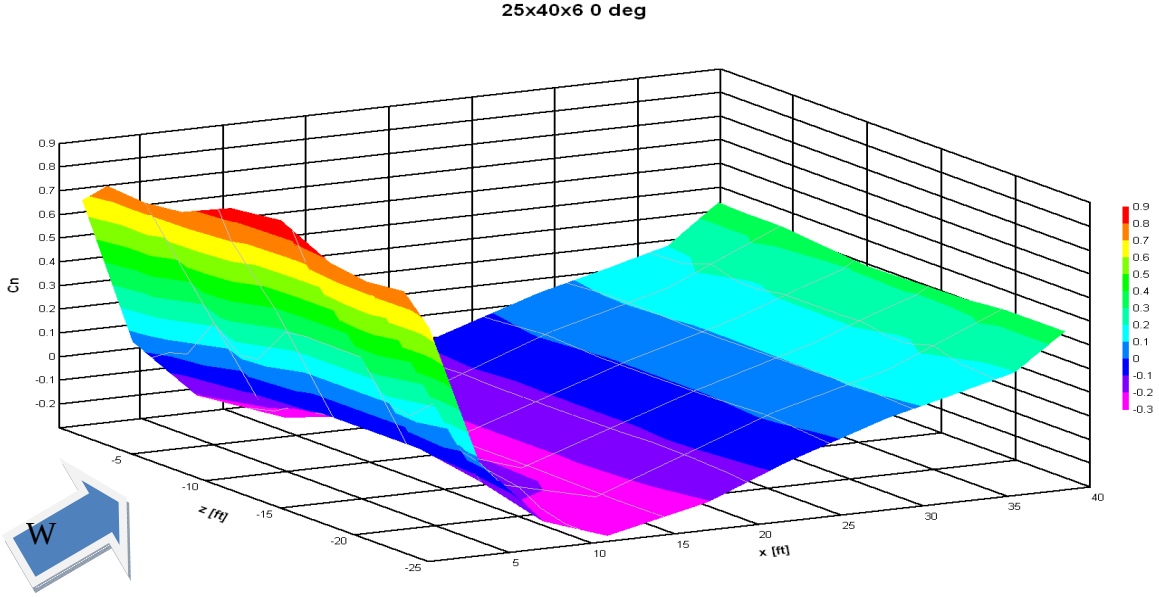

Figure 7.27: Model #15, 3D contour plot for Cn values for wind at 0 degrees.

Figure 7.28 shows four Cn graphs, one for each parapet height on the 7.6 m (25 ft) x 12.2 m (40 ft) open canopy. The 2D graph data was obtained from the middle of the canopy width in the principal axis direction. All parapet heights exhibit a segment of positive Cn values (downward) for the first L/5 of the horizontal length. After the downward segment, an uplift pressure length of L/3 occurs, followed by a downward segment for the rest of the horizontal distance.

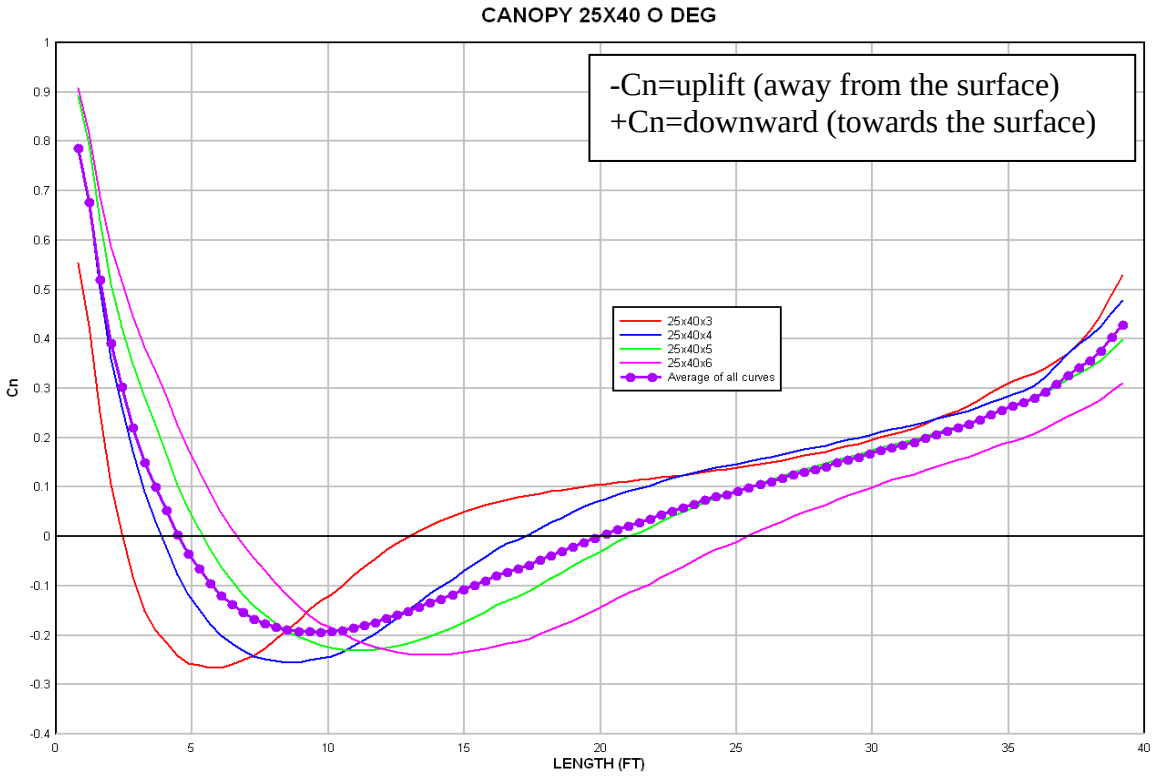

Figure 7.28: 2D graph of Cn values for all 7.6 m (25 ft) x 12.2 m (40 ft) @ 0 degrees.

7.5 Open canopy models, 7.6 m (25 ft) x12.2 m (40 ft) at 30 degrees

Cn values for contour plan for Model #10, with dimensions of 7.6 m (25 ft) x 12.2 m (40 ft) x 0.91 m (3 ft) with the wind at 30 degrees are shown in Figure 7.29. Figure 7.30 shows a 3D view of the Cn values of the canopy. Values range from a maximum of +0.9 to a minimum of -

0.7. The values are slightly higher than in the square configuration #2 (+0.7 and -0.4 respectively).

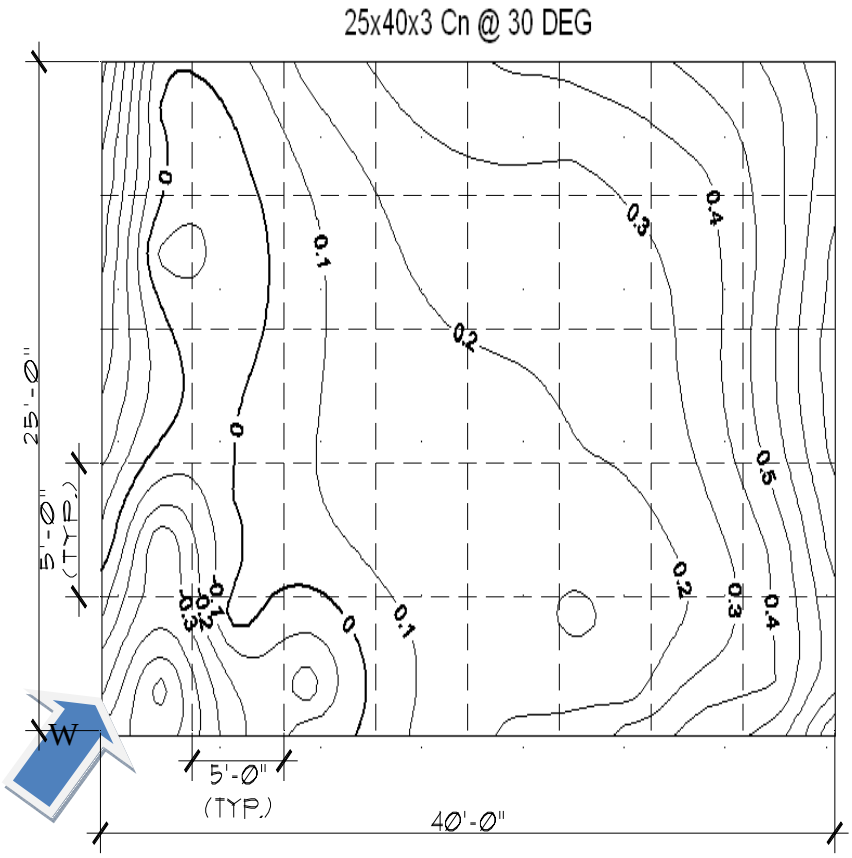

Figure 7.29: Model #10, contour plan for Cn values for wind at 30 degrees.

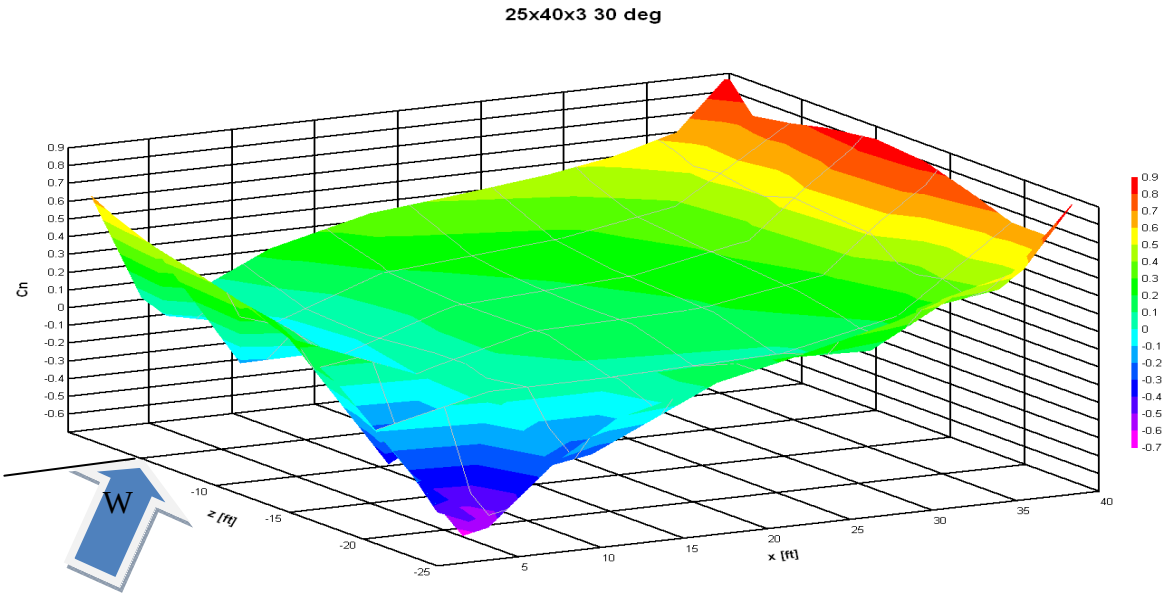

Figure 7.30: Model #10, 3D contour plot for Cn values for wind at 30 degrees.

Cn values for contour plan for Model #12, with dimensions of 7.6 m (25 ft) x 12.2 m (40 ft) x 1.22 m (4 ft) with the wind at 30 degrees are shown in Figure 7.31. Figure 7.32 shows a 3D view of the Cn values of the canopy. Values range from a maximum of +1.0 to a minimum of -0.6. The values are slightly higher than in the square configuration Model #4 (+0.8 and -0.3 respectively).

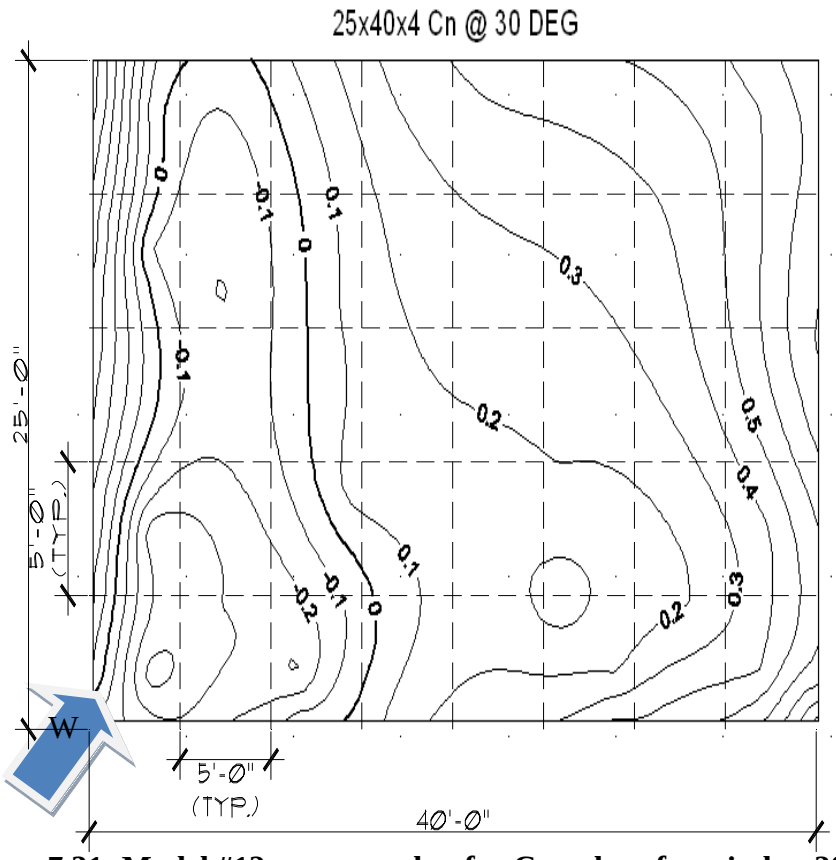

Figure 7.31: Model #12, contour plan for Cn values for wind at 30 degrees.

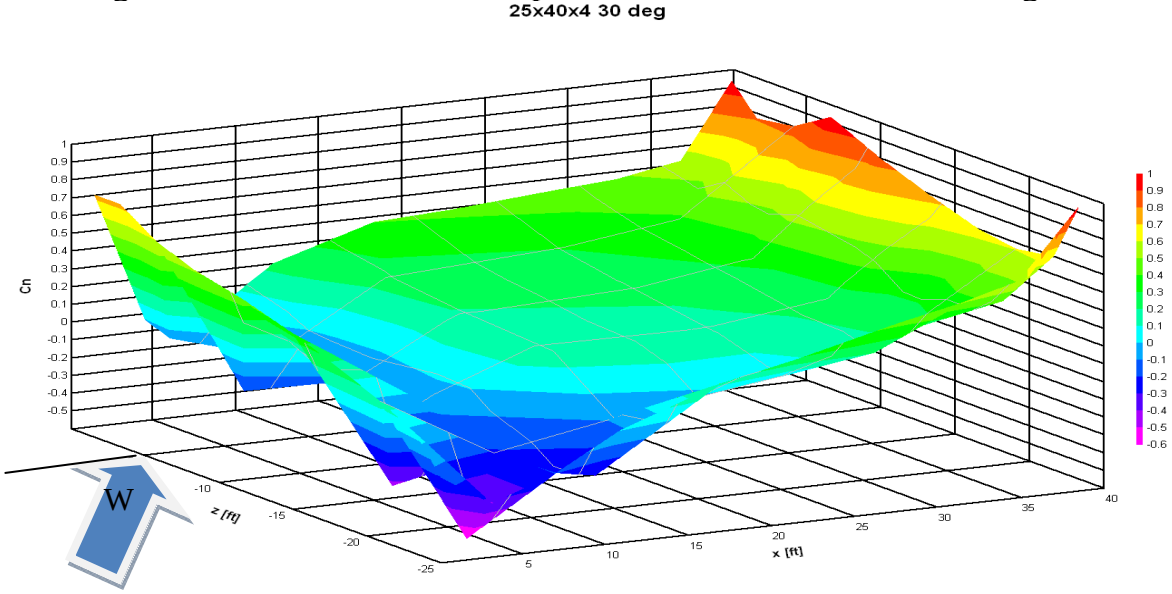

Figure 7.32: Model #12, 3D contour plot for Cn values for wind at 30 degrees.

Cn values for contour plan for Model #14, with dimensions of 7.6 m (25 ft) x 12.2 m (40 ft) x 1.52 m (5 ft) with the wind at 30 degrees are shown in Figure 7.33. Figure 7.34 shows a 3D view of the Cn values of the canopy. Values range from a maximum of +0.9 to a minimum of -0.3. The values are very similar compared to the square configuration Model #6 (+0.9 and -0.2 respectively).

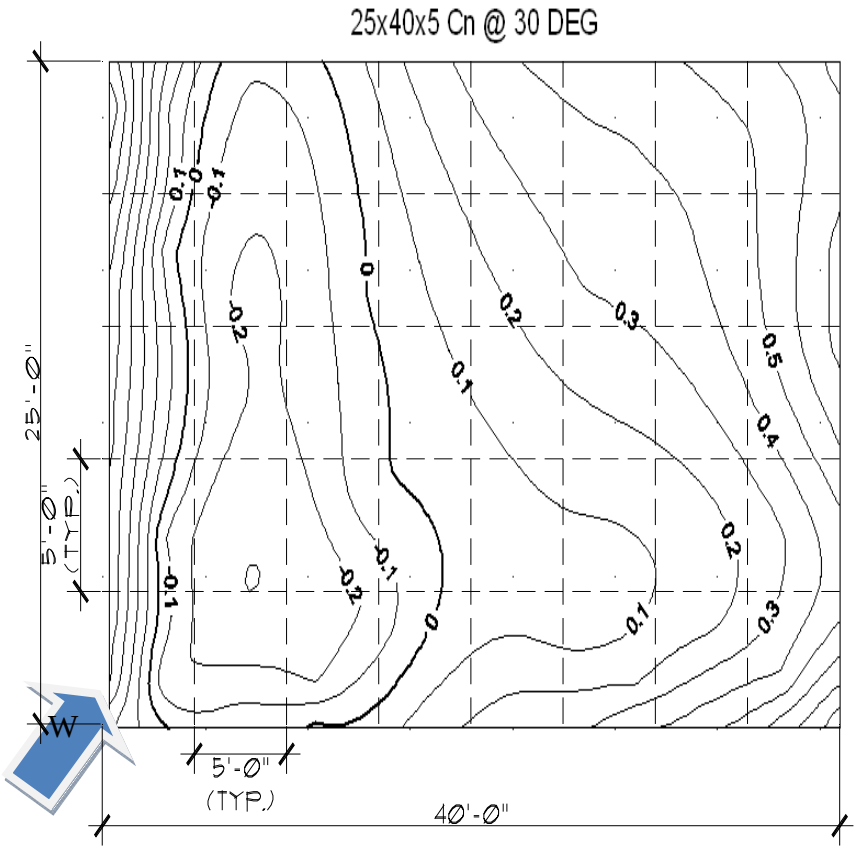

Figure 7.33: Model #14, contour plan for Cn values for wind at 30 degrees.

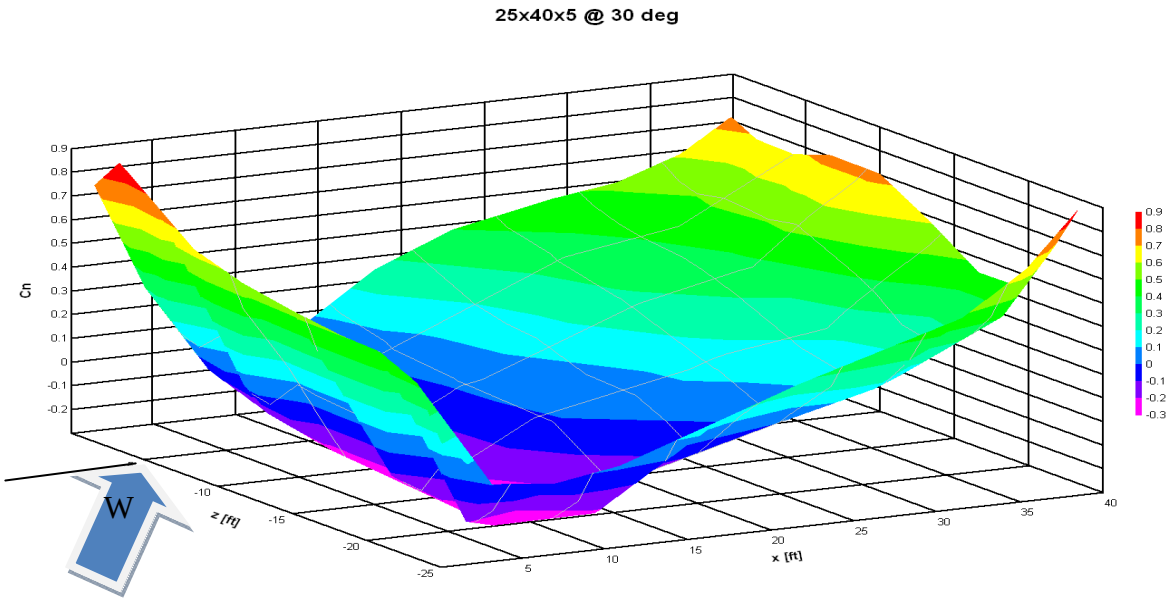

Figure 7.34: Model #14, 3D contour plot for Cn values for wind at 30 degrees.

Cn values for contour plan for Model #16, with dimensions of 7.6 m (25 ft) x 12.2 m (40 ft) x 1.82 m (6 ft) with the wind at 30 degrees are shown in Figure 7.35. Figure 7.36 shows a 3D view of the Cn values of the canopy. Values range from a maximum of +1.0 to a minimum of -0.3. The values are slightly higher than in the square configuration #8 (+0.9 and -0.2 respectively).

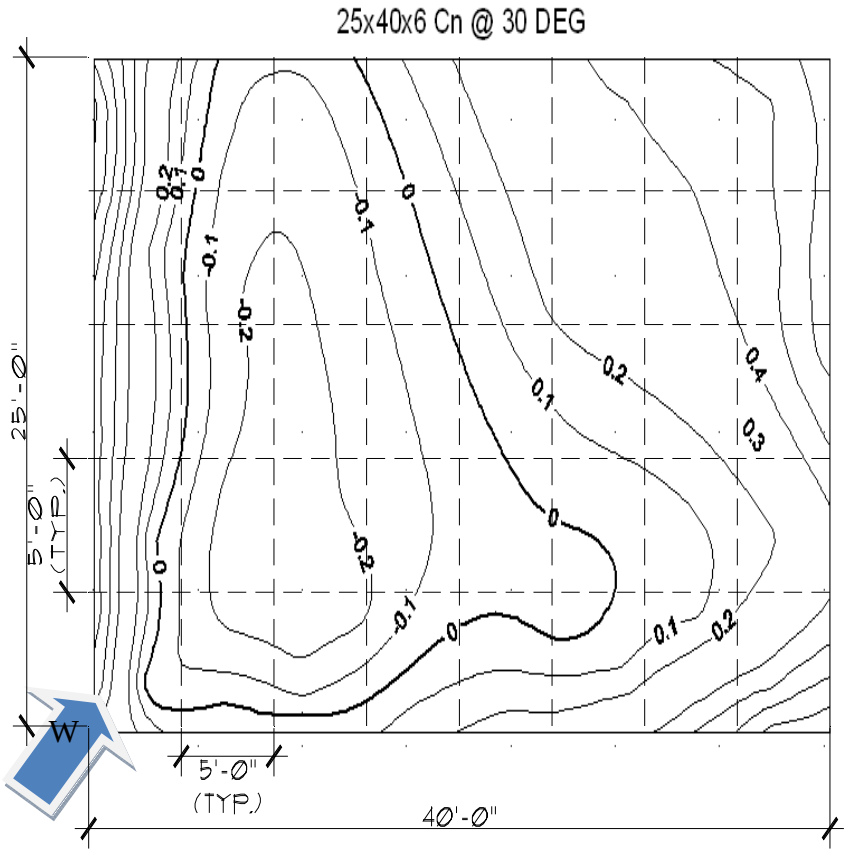

Figure 7.35: Model #16, contour plan for Cn values for wind at 30 degrees.

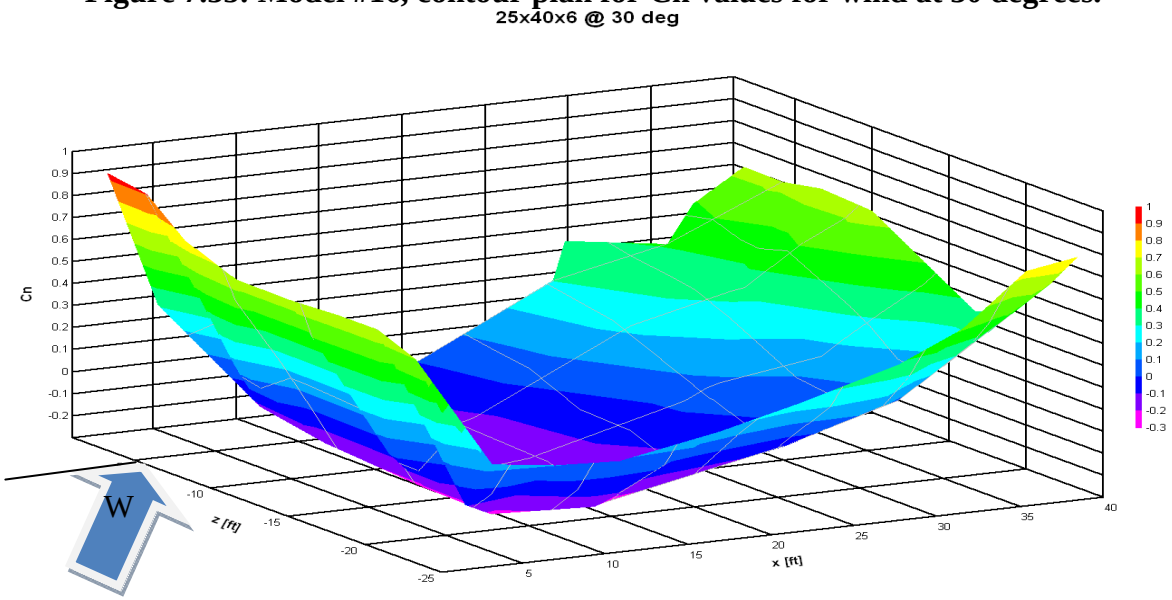

Figure 7.36: Model #16, 3D contour plot for Cn values for wind at 30 degrees.

Figure 7.37 shows four Cn graphs, one for each parapet height on the 7.6 m (25 ft) x 12.2 m (40 ft) open canopy. The 2D graph data was obtained from the middle of the canopy width in the angle of the applied wind, in these case thirty (30) degrees from the principal axis direction. All parapet height exhibits on the graph a segment of positive and negative Cn values. Depending on the parapet height, downward and uplift pressure is reflected. This is shown on the first L/5, except the parapet height of 0.91 m (3 ft) and 1.22 m (4 ft), which were all negative Cn values. After the downward and uplift segment, an uplift pressure length of L/3 occurs followed by a downward pressure for the rest of the horizontal distance.

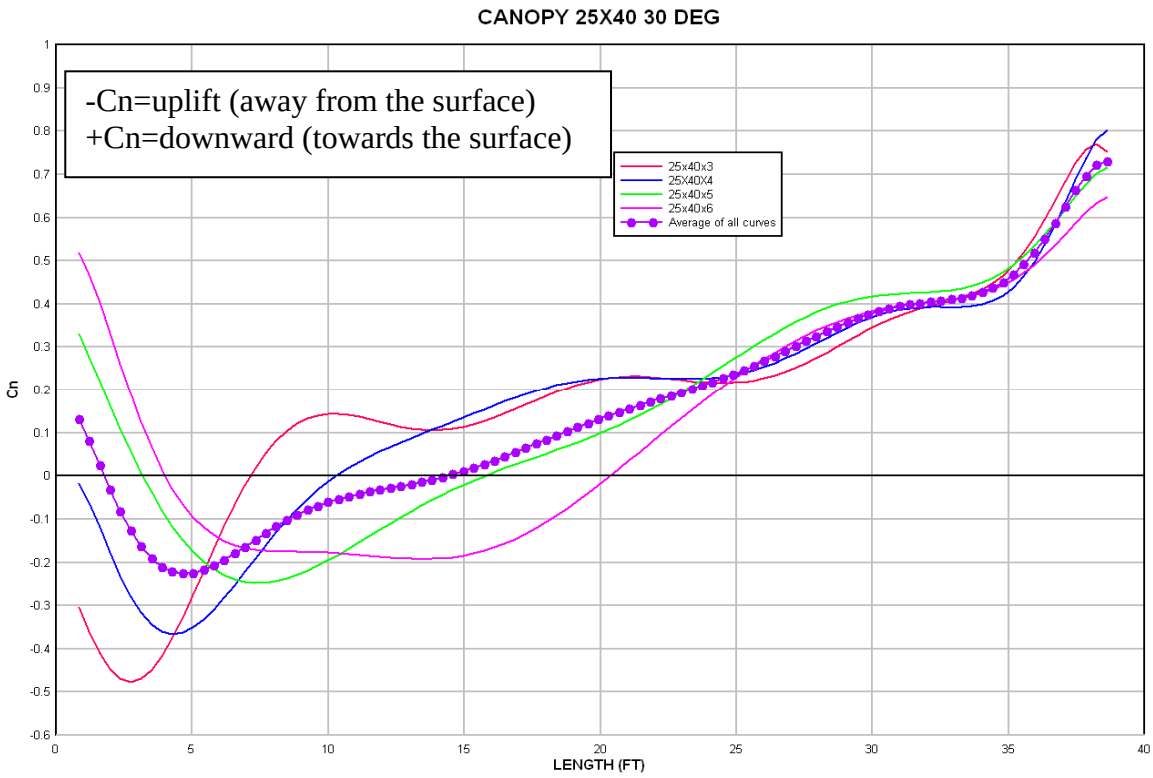

Figure 7.37: Graph of Cn values for all 7.6 m (25 ft) x 12.2 m (40 ft) @ 30 degrees.

7.6 Open canopy models, 7.6 m (25 ft) x15.2 m (50 ft) at 0 degrees

An even longer canopy in the transverse direction is investigated in this section, in which the length is increased to 50 ft. Cn values for contour plan for Model #17, with dimensions of 7.6 m (25 ft) x 15.2 m (50 ft) x 0.91 m (3 ft) with the wind at 0 degrees are shown in Figure 7.38. Figure 7.39 shows a 3D view of the Cn values of the canopy. Values range from a maximum of +0.7 to a minimum of -0.4. (Same as in Model #9).

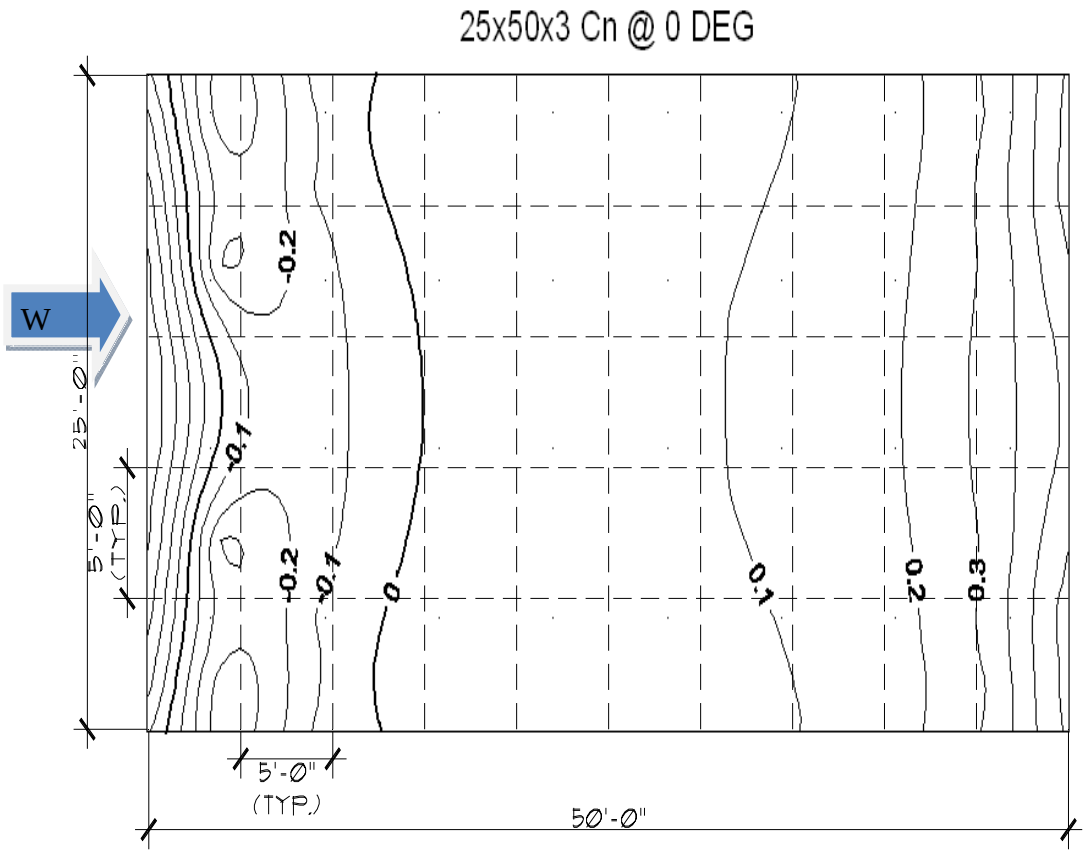

Figure 7.38: Model #17, contour plan for Cn values for wind at 0 degrees.

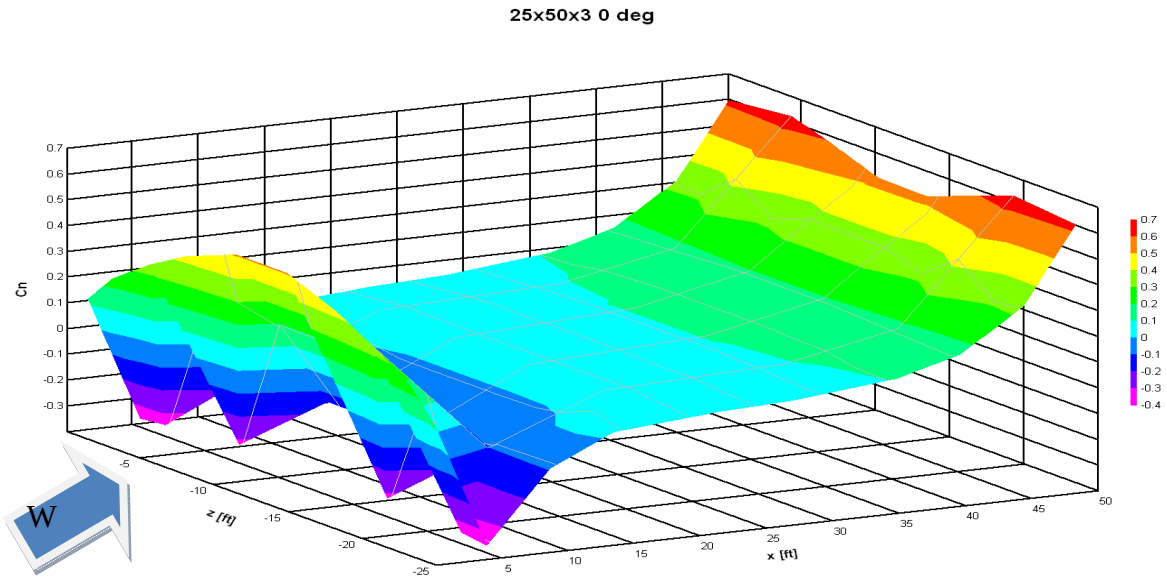

Figure 7.39: Model #17, 3D contour plot for Cn values for wind at 0 degrees.

Cn values for contour plan for Model #19, with dimensions of 7.6 m (25 ft) x 15.2 m (50 ft) x 1.22 m (4 ft) with the wind at 0 degrees are shown in Figure 7.40. Figure 7.41 shows a 3D view of the Cn values of the canopy. Values range from a maximum of +0.7 to a minimum of -0.4. (Similar to Model #11).

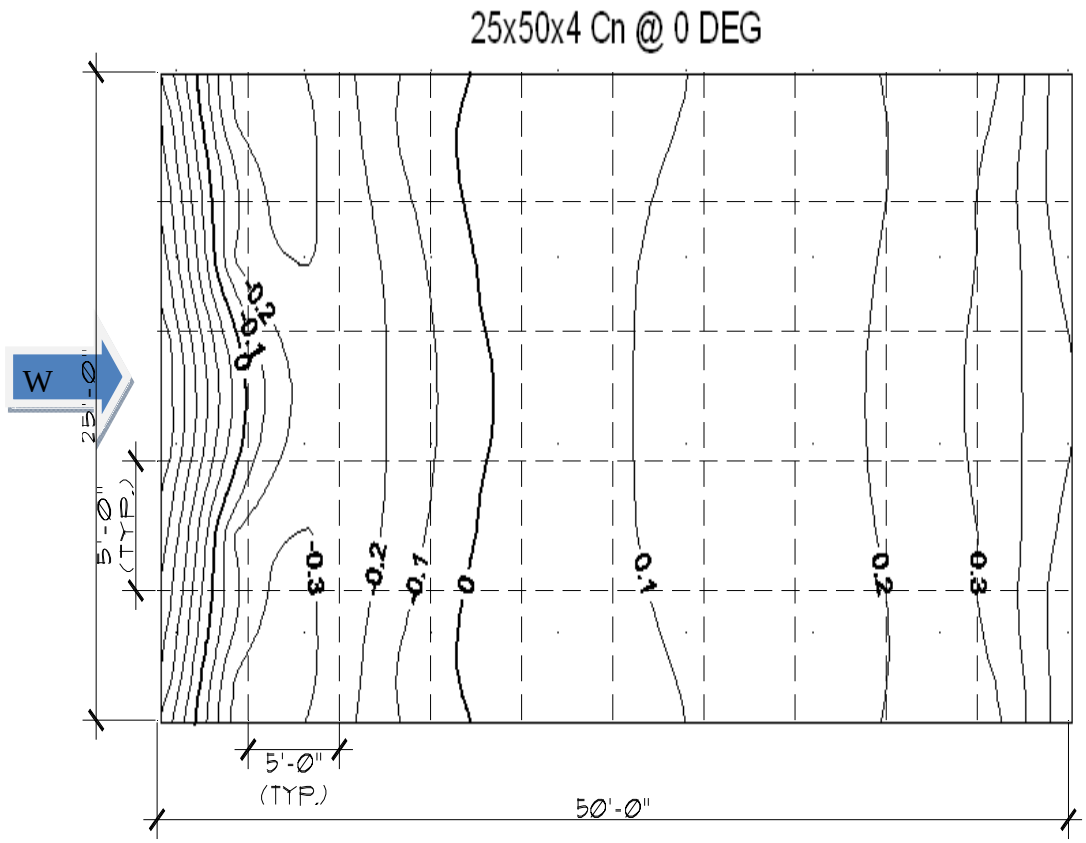

Figure 7.40: Model #19, contour plan for Cn values for wind at 0 degrees.

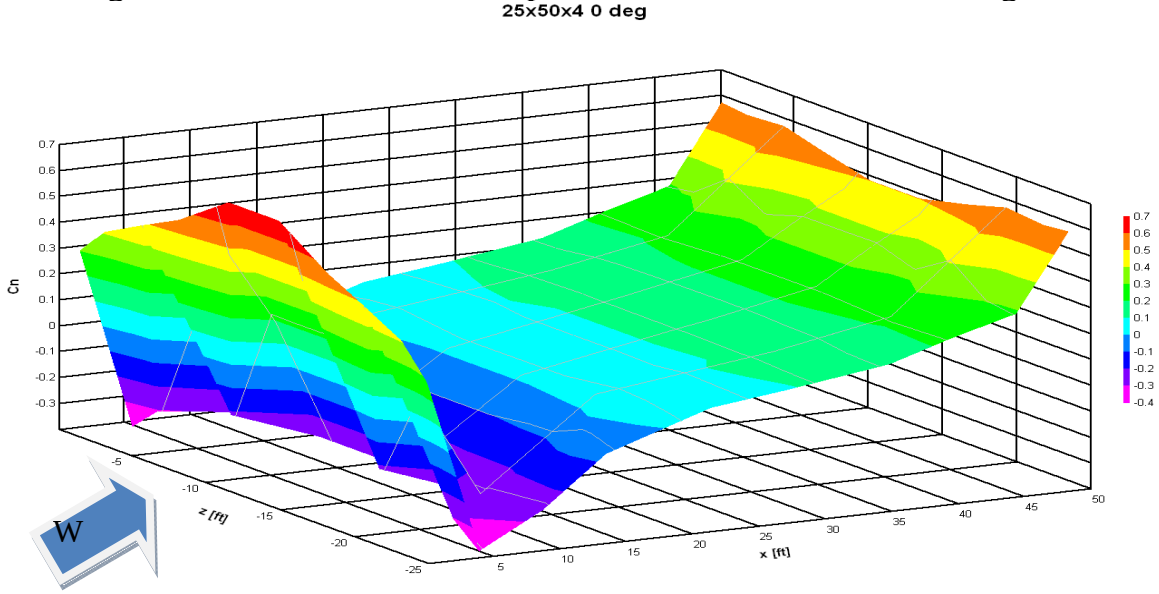

Figure 7.41: Model #19, 3D contour plot for Cn values for wind at 0 degrees.

Cn values for contour plan for Model #21, with dimensions of 7.6 m (25 ft) x 15.2 m (50 ft) x 1.52 m (5 ft) with the wind at 0 degrees are shown in Figure 7.42. Figure 7.43 shows a 3D view of the Cn values of the canopy. Values range from a maximum of +0.9 to a minimum of -0.3. (Similar to Model #13).

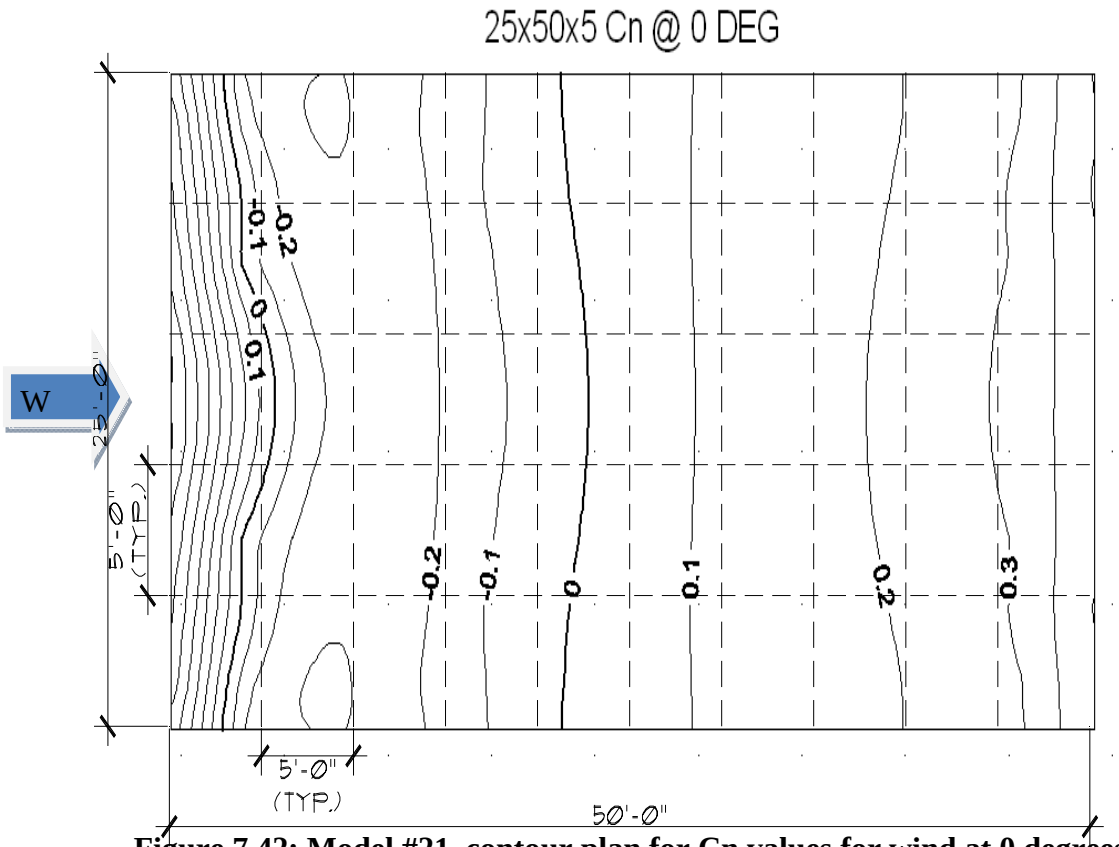

Figure 7.42: Model #21, contour plan for Cn values for wind at 0 degrees.

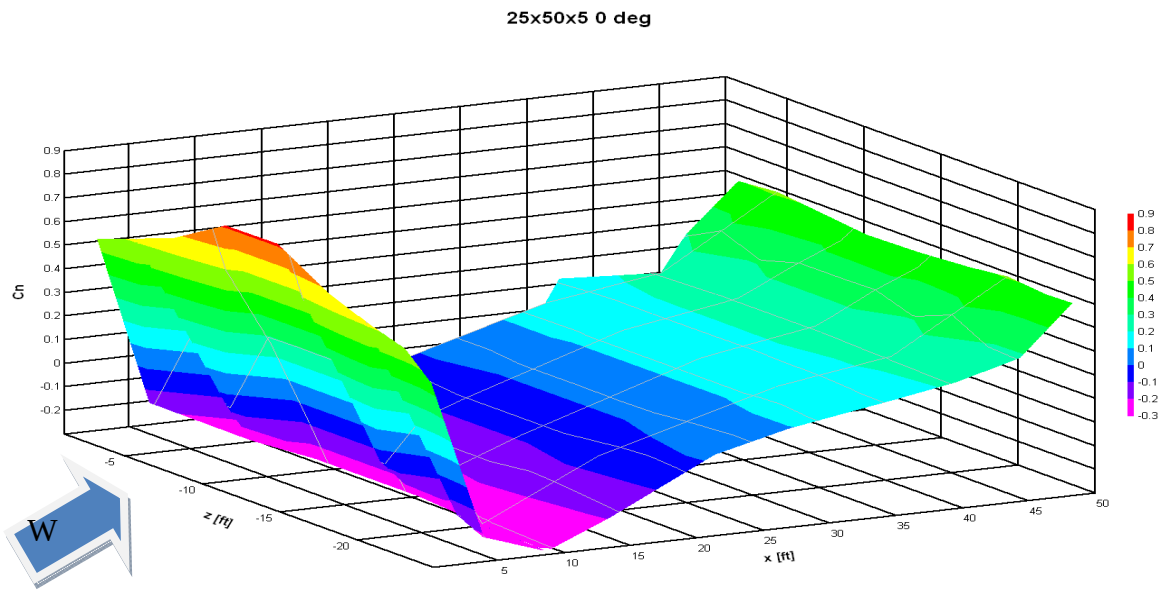

Figure 7.43: Model #21, 3D contour plot for Cn values for wind at 0 degrees.

Cn values for contour plan for Model #23, with dimensions of 7.6 m (25 ft) x 15.2 m (50 ft) x 1.82 m (6 ft) with the wind at 0 degrees are shown in Figure 7.44. Figure 7.45 shows a 3D view of the Cn values of the canopy. Values range from a maximum of +0.9 to a minimum of -0.3. (Identical values as in Model #15).

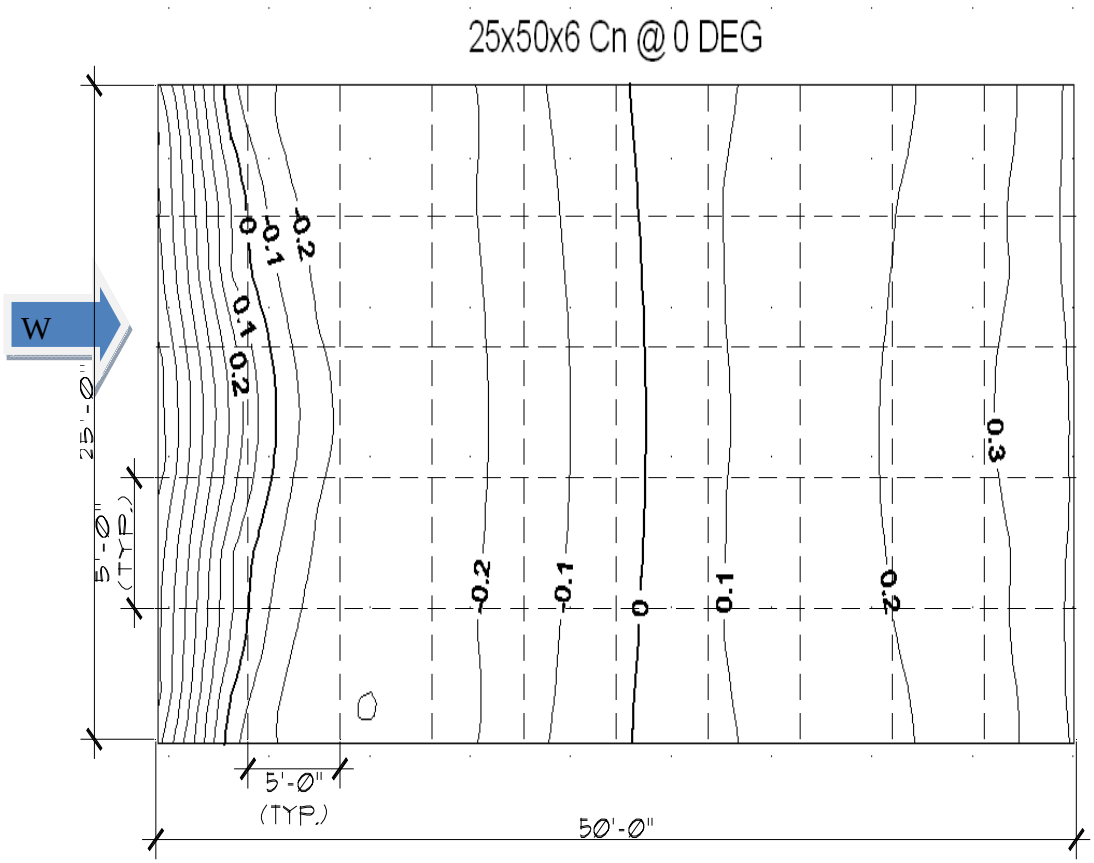

Figure 7.44: Model #23, contour plan for Cn values for wind at 0 degrees.

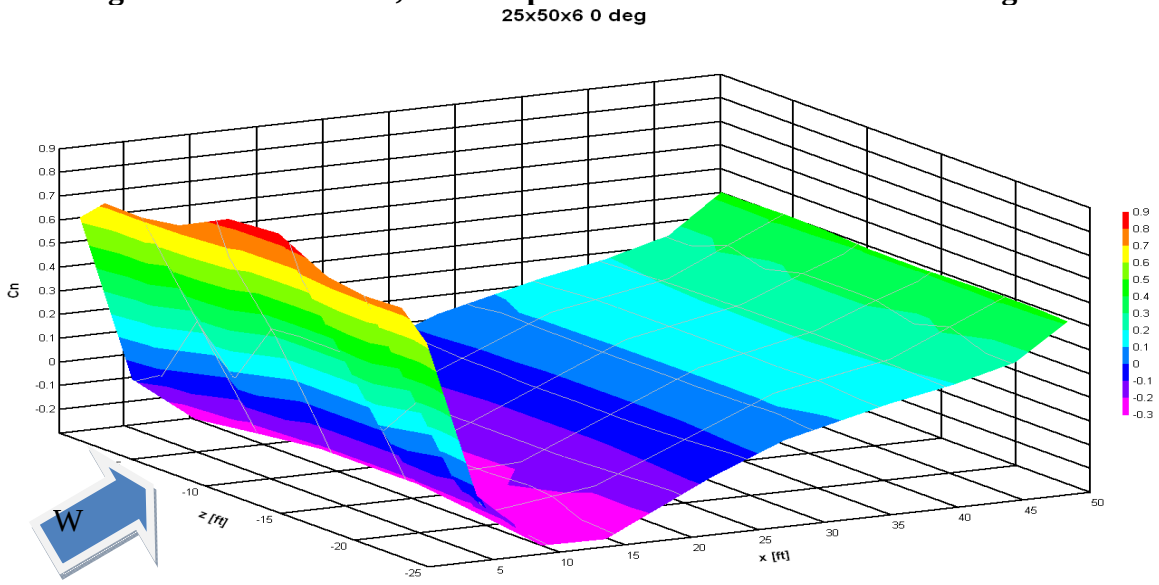

Figure 7.45: Model #23, 3D contour plot for Cn values for wind at 0 degrees.

Figure 7.46 shows four Cn graphs, one for each parapet height on the 7.6 m (25 ft) x 15.2 m (50 ft) open canopy. The 2D graph data was obtained from the middle of the canopy width in the principal axis direction. All parapet height exhibits on the graph a segment of positive Cn values (downward) for the first L/5 of the horizontal length. After the downward segment, an uplift pressure length of L/3 occurs, followed by a downward for the rest of the horizontal distance. The results computed for the canopy with 50 ft in the transverse direction are almost identical to those computed for the 40 ft canopy.

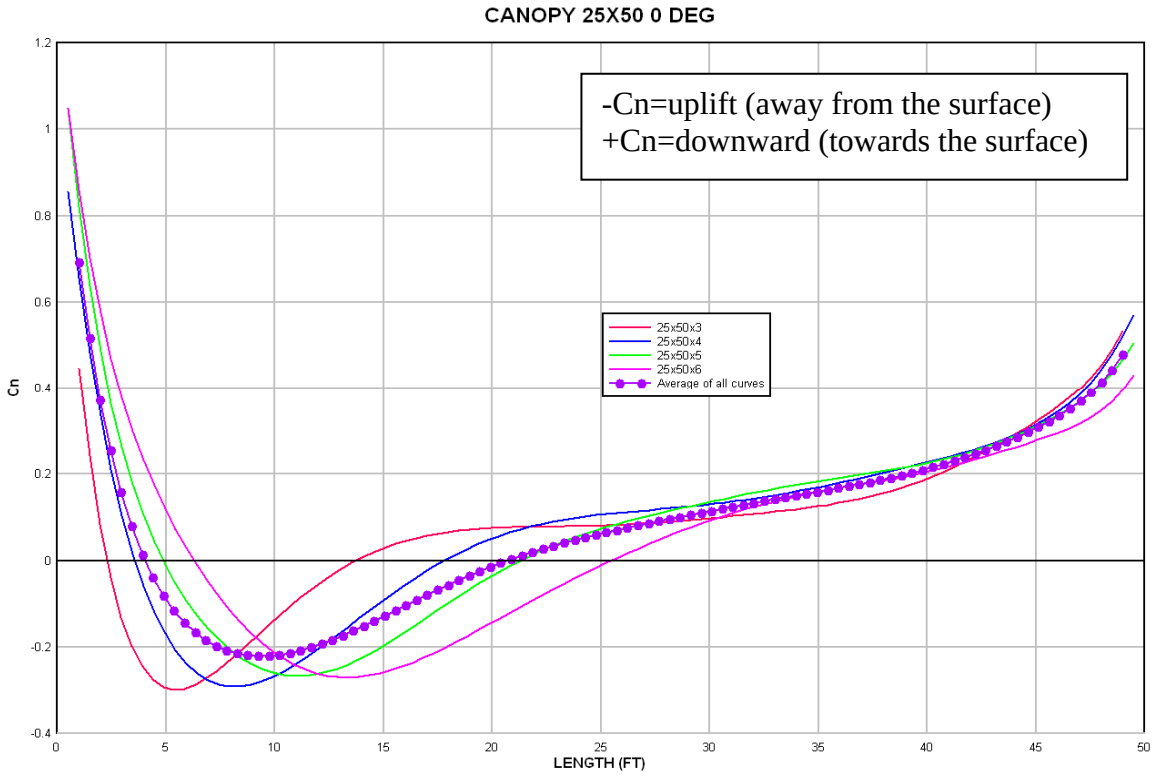

Figure 7.46: 2D graph of Cn values for all 7.6 m (25 ft) x 15.2 m (50 ft) @ 0 degrees.

7.7 Open canopy models, 7.6 m (25 ft) x15.2 m (50 ft) at 30 degrees

Cn values for contour plan for Model #18, with dimensions of 7.6 m (25 ft) x 15.2 m (50 ft) x 0.91 m (3 ft) with the wind at 30 degrees are shown in Figure 7.47. Figure 7.48 shows a 3D view of the Cn values of the canopy. Values range from a maximum of +1.0 to a minimum of -0.6. The values are similar compared to the configuration Model #10 (+1.0 and -0.7 respectively).

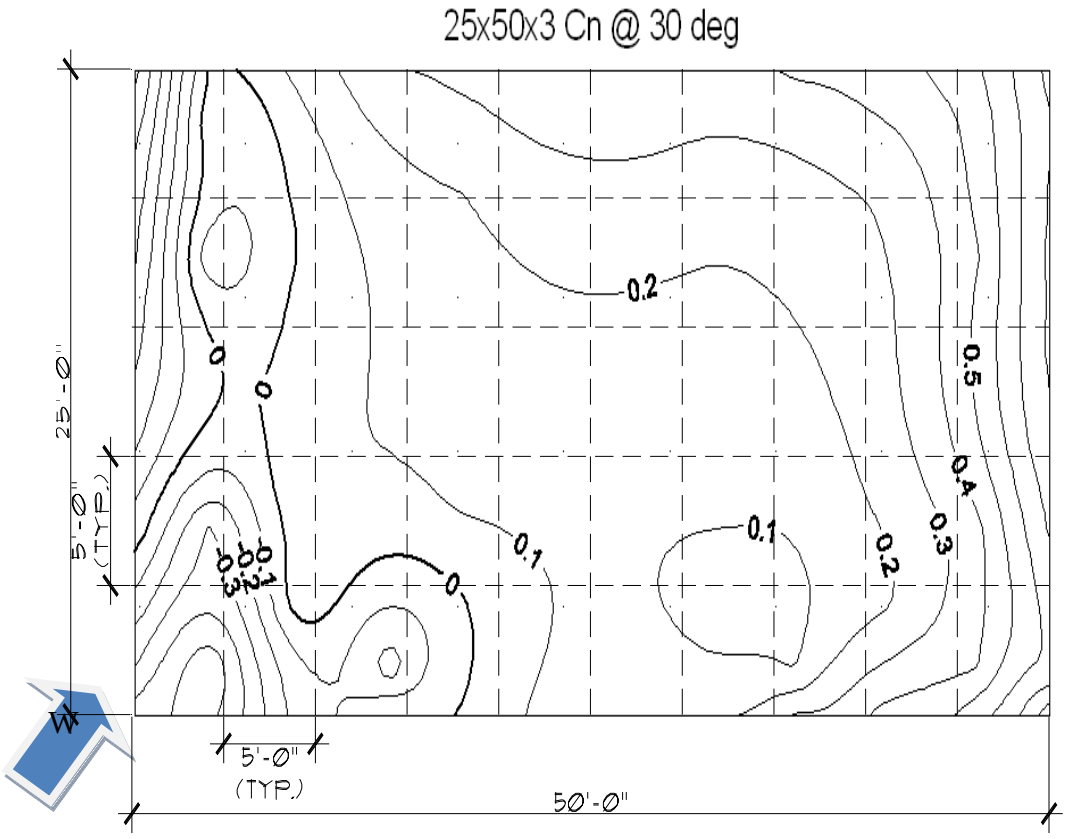

Figure 7.47: Model #18, contour plan for Cn values for wind at 30 degrees.

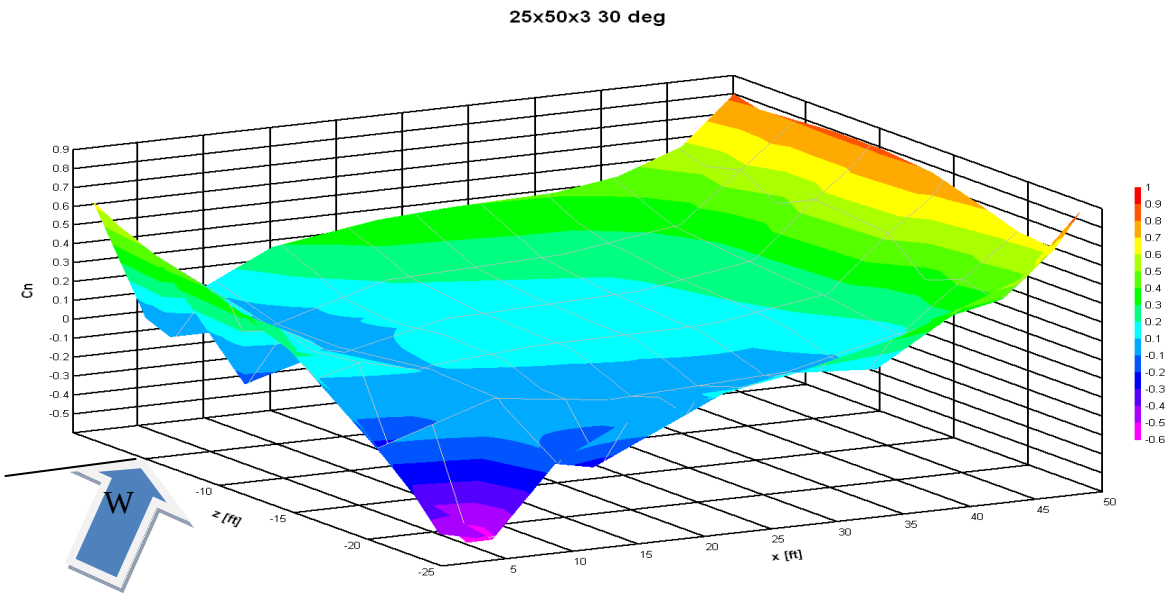

Figure 7.48: Model #18, 3D contour plot for Cn values for wind at 30 degrees.

Cn values for contour plan for Model #20, with dimensions of 7.6 m (25 ft) x 15.2 m (50 ft) x 1.22 m (4 ft) with the wind at 30 degrees are shown in Figure 7.49. Figure 7.50 shows a 3D view of the Cn values of the canopy. Values range from a maximum of +1.0 to a minimum of -0.6. The values are identical compared to the square configuration Model #12 (+1.0 and -0.6 respectively).

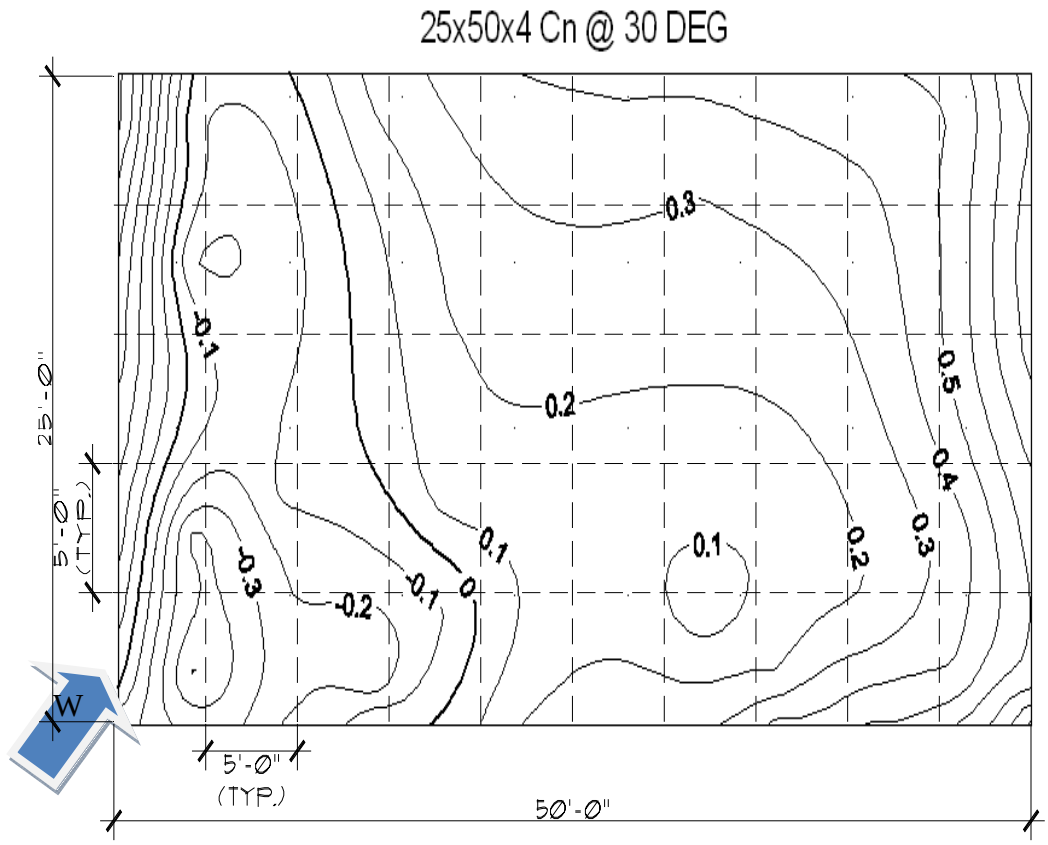

Figure 7.49: Model #20, contour plan for Cn values for wind at 30 degrees.

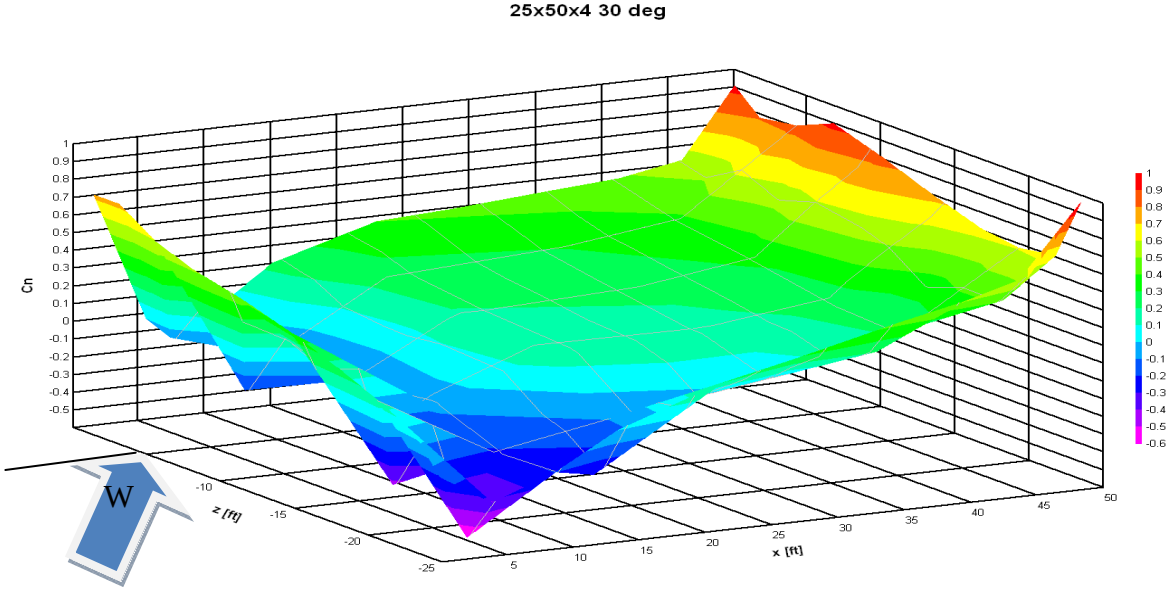

Figure 7.50: Model #20, 3D contour plot for Cn values for wind at 30 degrees.

Cn values for contour plan for Model #22, with dimensions of 7.6 m (25 ft) x 15.2 m (50 ft) x 1.52 m (5 ft) with the wind at 30 degrees are shown in Figure 7.51. Figure 7.52 shows a 3D view of the Cn values of the canopy. Values range from a maximum of +1.0 to a minimum of -0.4. The values are very similar compared to the configuration Model #14 (+0.9 and -0.3 respectively).

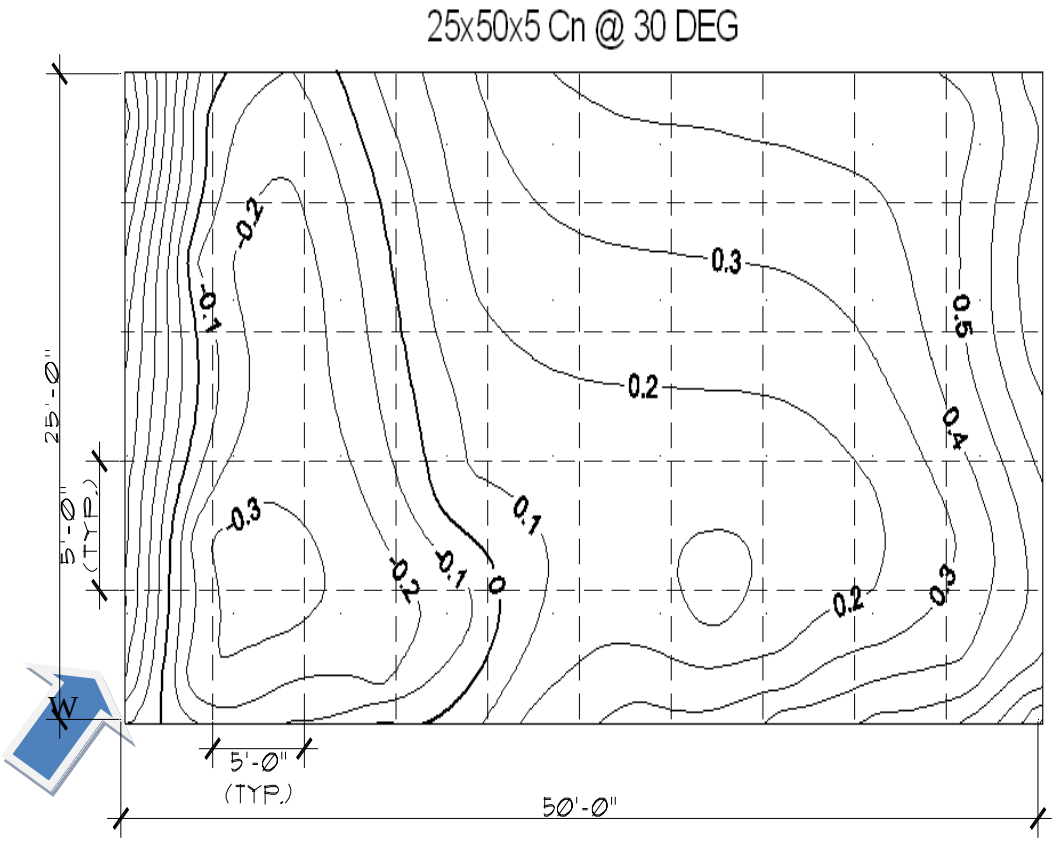

Figure 7.51: Model #22, contour plan for Cn values for wind at 30 degrees.

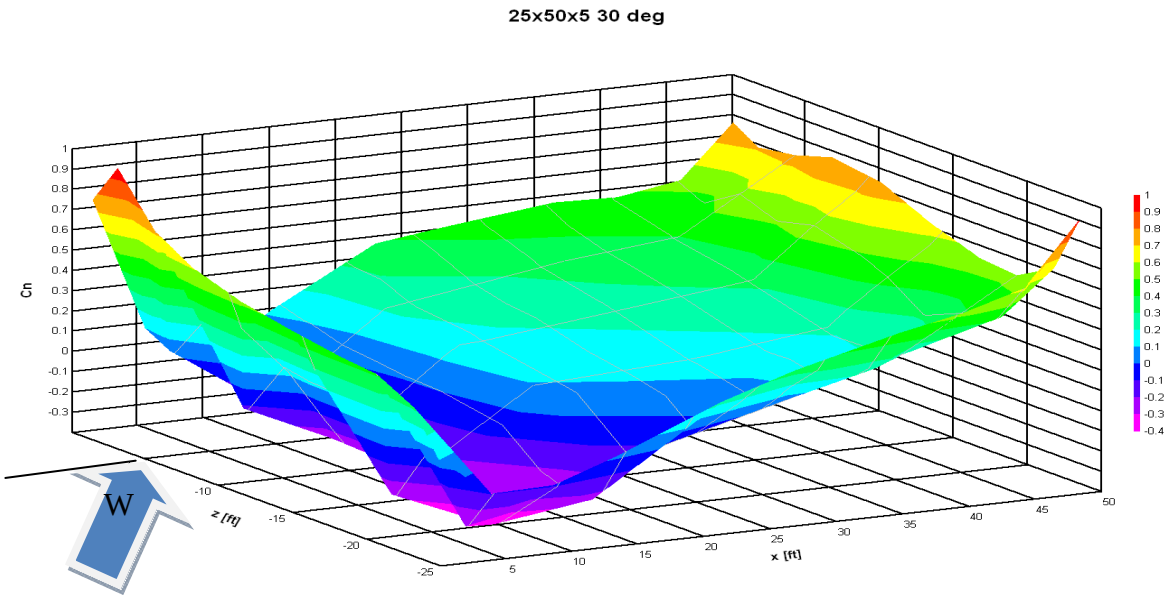

Figure 7.52: Model #22, 3D contour plot for Cn values for wind at 30 degrees.

Cn values for contour plan for Model #24, with dimensions of 7.6 m (25 ft) x 15.2 m (50 ft) x 1.82 m (6 ft) with the wind at 30 degrees are shown in Figure 7.53. Figure 7.54 shows a 3D view of the Cn values of the canopy. Values range from a maximum of +0.9 to a minimum of -0.3. The values on the configuration Model #14 are +1.0 and -0.3 respectively.

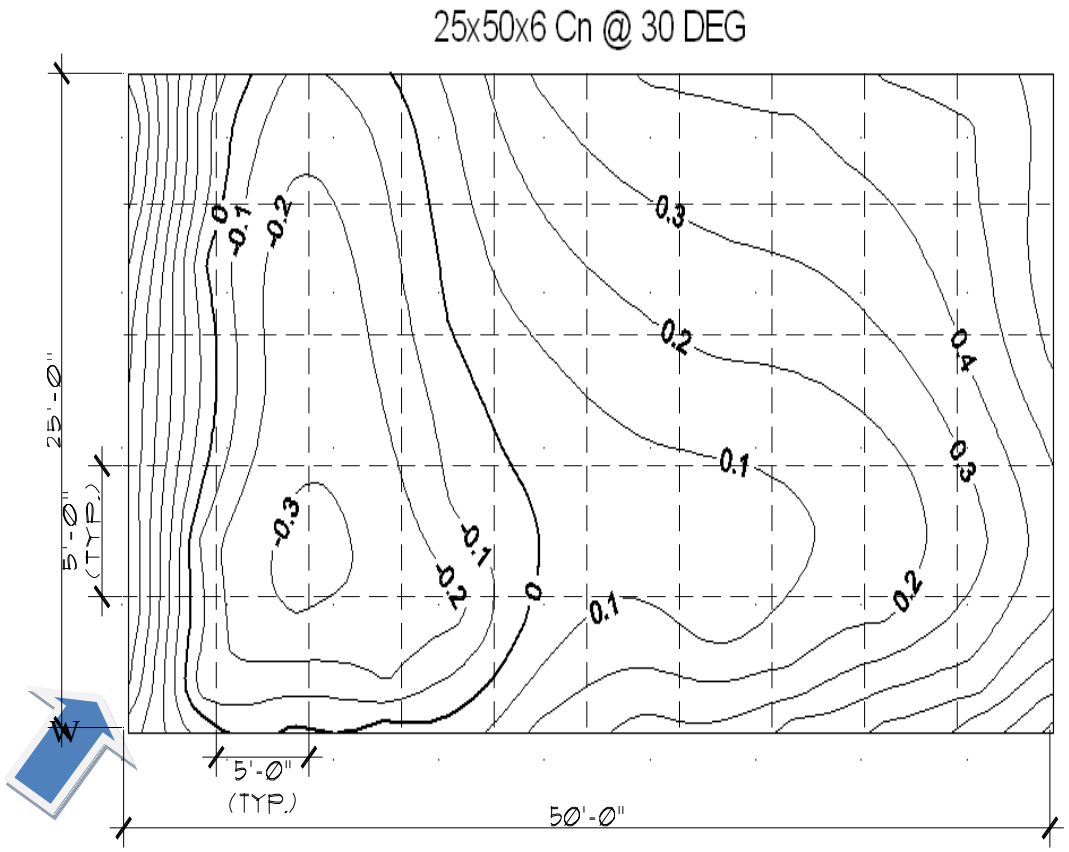

Figure 7.53: Model #24, contour plan for Cn values for wind at 30 degrees.

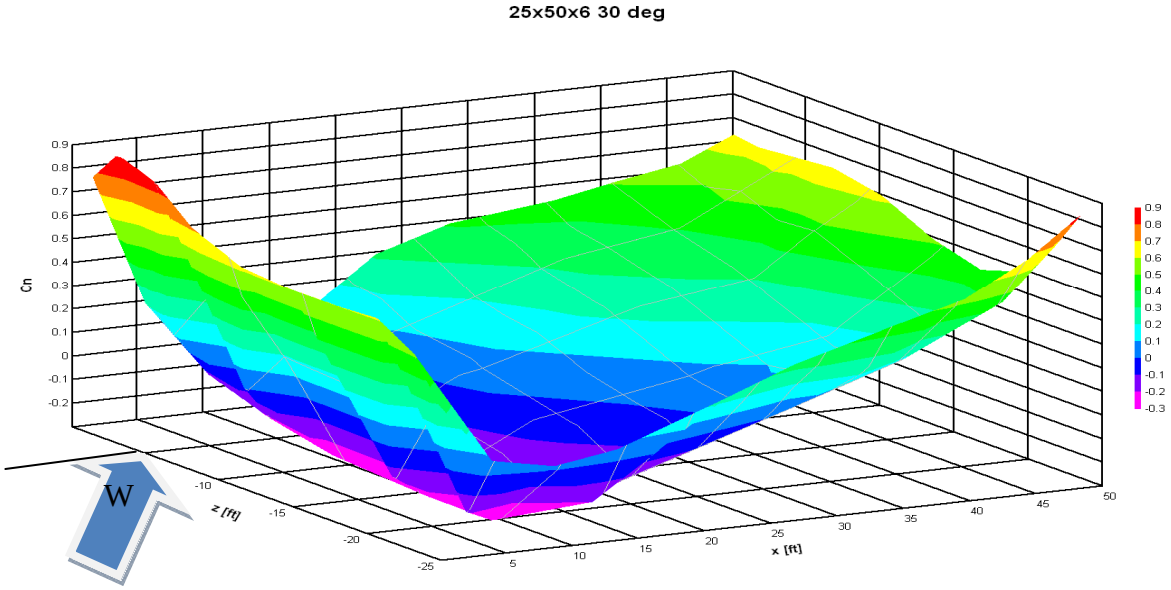

Figure 7.54: Model #24, 3D contour plot for Cn values for wind at 30 degrees.

Figure 7.55 shows four Cn graphs, one for each parapet height on the 7.6 m (25 ft) x 15.2 m (50 ft) open canopy. The 2D graph data was obtained at the center of the canopy width in the angle of the applied wind, in this case, 30 degrees from the principal axis direction. All parapet height exhibits on the graph a segment of positive and negative Cn values. Depending on the parapet height, downward and uplift is reflected. This is shown on the first L/5, except the parapet height of 0.91 m (3 ft) and 1.22 m (4 ft), which were all negative Cn values. After the downward and uplift segment, an uplift pressure length of L/3 occurs followed by a downward for the rest of the horizontal distance.

-Cn=uplift (away from the surface)
+Cn=downward (towards the surface)

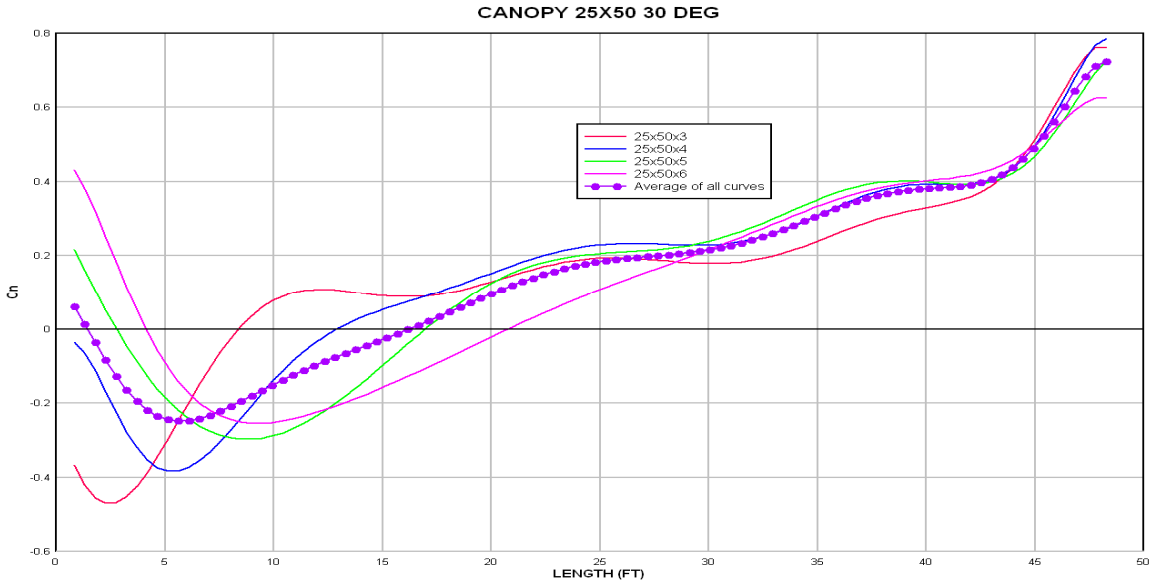

Figure 7.55: Graph of Cn values for all 7.6 m (25 ft) x 15.2 m (50 ft) @ 30 degrees.

7.8 Conclusions

Three canopy configurations were investigated in this chapter using CFD simulations, in which wind incidence angle, parapet height, and transverse direction were changed to understand pressure coefficient distributions. High changes are associated with parapet height, as expected,

as shown in Figures 7.10, 7.19, 7.28, 7.37, 7.46 and 7.55. The influence of wind direction is also important in terms of values and pressure distributions, to visualize that it is necessary to compare pairs of Figures, such as 7.10 and 7.19; 7.28 and 7.37; and 7.46 and 7.55. Finally, the relative dimension of the canopy in plan has been investigated for a square configuration and two rectangular ones. To visualize changes, one should compare Figures 7.10, 7.28 and 7.46; and Figures 7.19, 7.37 and 7.55.

A warning should be made that differences between configurations used to compute pressure values will lead the differences in structural response; however this is not a linear effect and at this point in the thesis it is not clear how the detected differences will affect the response of the structure. This the subject of Chapter 8.

CHAPTER 8. CASE STUDIES OF CANOPIES AND COMPARISONS WITH FIELD EVIDENCE

8.1 Structural Analysis

From the point of view of this research, the structural analysis of open canopies that suffered the effect of wind forces is very important for several reasons. First, a structural analysis based on the previous pressure coefficients derived in this research work is extremely useful in order to validate the proposed Cn wind coefficients on this type of structure. Second the definitions of pressures due to wind make engineering sense in the context of structural analysis and behavior. From the engineering point of view, the relevance of the pressure coefficients depends on the performance of the structures affected by wind. For example, details of pressure coefficients in given zones of a structure would not be relevant if the structural response is not sensitive to those changes. Thus, we estimate wind speed data in order to make structural analysis and improve structural behavior. The importance of wind pressures in the collapse of canopies can be highlighted with reference to the multiple cases of failure identified following hurricanes Katrina and Rita in 2005 (NIST, 2006). From reconnaissance missions to affected areas by Hurricanes Katrina and Rita in 2005, four open canopies have been selected to perform a structural analysis in this chapter. In the cases selected, wind velocity data was not available and could only be estimated based on information available for neighboring areas. Current wind velocity for the comparison of the selected case studies was estimated based on ASCE 7-05, Figure 6-1A, page 34 that uses a 3 second gust speed. Wind speeds in Case 1, 2 and 4 have been estimated to be about 130 mph. Wind speed in case 3 was estimated to be about 110 mph. The wind velocities were used to obtain the wind pressures, and those pressures were used for the

structural analysis. This is a sequential methodology, in which the evaluation of wind pressures is uncoupled for the structural response.

In order to propose and develop a methodology to analyze and calculate the structural response of an open canopy, first we apply the wind pressure obtained from the Cn results on Chapter 7. The structural effects of the applied wind pressures were analyzed considering two main wind directions, at 0 and 30 degrees from the main horizontal axis. This procedure, in which a detailed distribution of Cp values, based on contour levels is used, is called Method #1 and is similar to the methodology followed by Portela (2004). A second procedure, in which the values from Method #1 are simplified, so that three zones of uniform pressure are identified with their maximum values. Again, wind directions at 0 and 30 degrees were investigated. This procedure was called Method #2. There is a third level of modeling attempted, which is based on the same methodology employed by the ASCE 7-05, Section 6.5.13. The Cn values used on the structural analysis for this method are the extreme values found in Chapter 7. This procedure was called Method #3. Cn values vary from +1.2 to -0.6 and to +0.8 on this proposed method. Typical proposed Cn values for Method #3 are summarized in Figure 8.1.

With the wind pressures obtained with all three methods, a structural analysis of the open canopy was performed. The importance of doing structural analysis on case studies this is a firsthand opportunity of analyzing a structure that has actually collapsed and see if that could be anticipated (and prevented) with the use of the proposed Cn values.

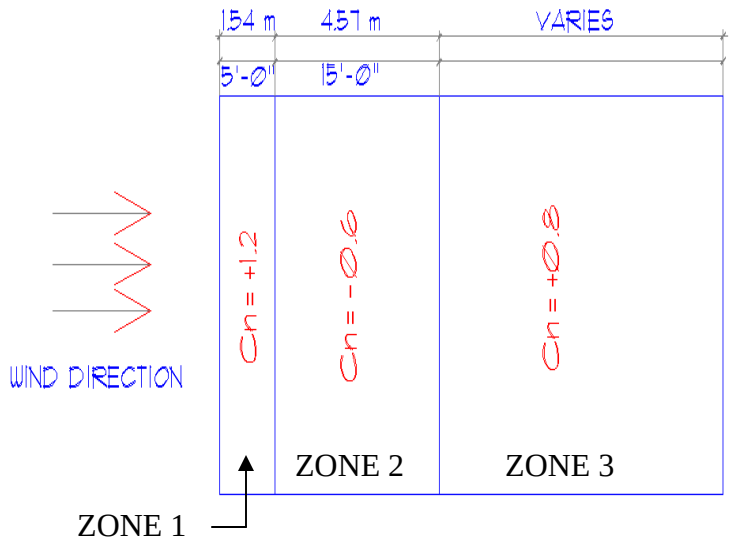

Figure 8.1: Proposed Cn values to be applied for Method #3 to the structural analysis model.

8.2 Case study #1, Shell Gas Station in Pt. Arthur, Texas, Method #1

The case study number 1 is a Shell gas station located in Pt. Arthur, Texas. A roof plan and elevations are illustrated in Figure 8.2. The dimensions were taken from measurements in the field. The floor plan dimensions are approximately 14 m (46 ft) in length by 7 m (23 ft) in width and 4.3 m (14 ft) in height. It has a system of four steel columns of 0.3 m (1 ft) x 0.3 m (1 ft) with wide flange steel beams and channels for the gravity system of the structure. Smallest thickness of steel columns and beams were used for the analysis. A steel deck was used for the roof cladding. A parapet of 0.91 m (3 ft) is on the roof perimeter. There is no available data of the foundation size and depth.

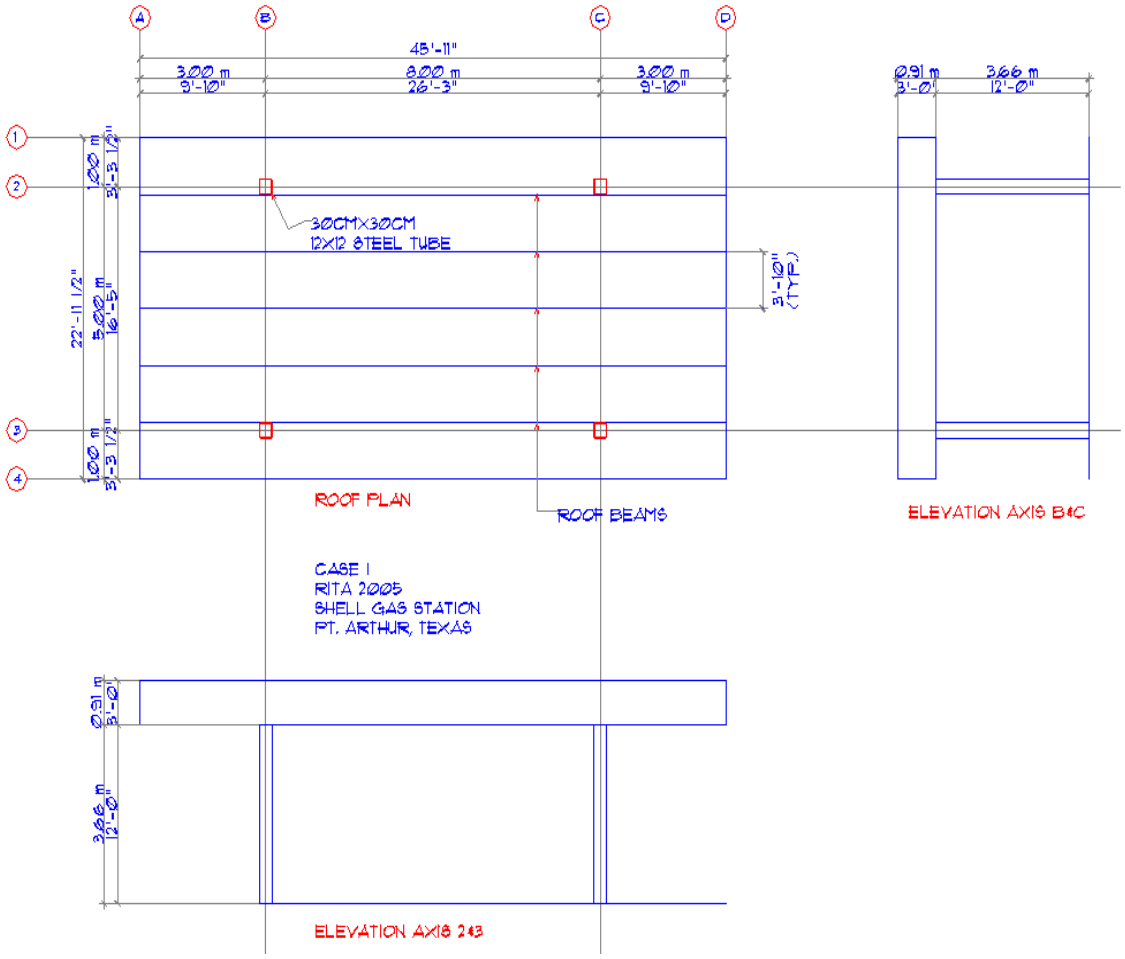

Figure 8.2: Canopy floor plan and elevations for Case study #1.

On Chapter 7, Cn values were obtained for the open canopy geometry for Case study #1. Those Cn values were converted to wind pressures in pounds per square foot (psf) for two wind cases, one wind direction at 0 and another one at 30 degrees, as shown on Figures 8.3 and 8.4, respectively the negative values indicate uplift pressure and positive values indicate downward pressures.

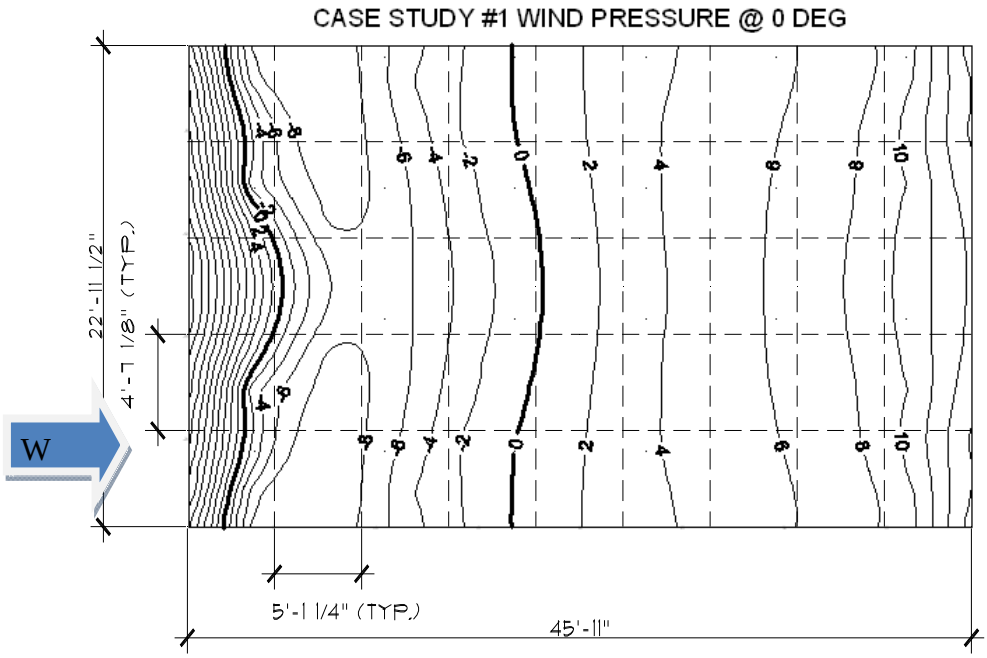

Figure 8.3: Contours for wind pressures for open canopy case #1 at 0 degrees.

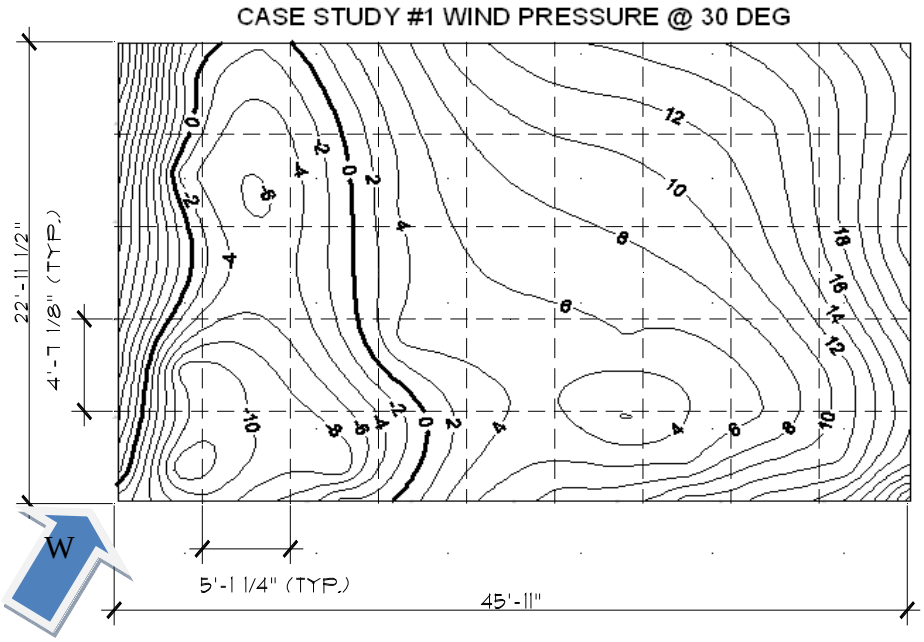

Figure 8.4: Contours for wind pressures for open canopy case #1 at 30 degrees.

The resultant wind pressures for each wind case were applied to a computational model using the structural analysis software ETABS (CSI 2009). Using a refined mesh for the roof

cladding, it was possible to input all the wind pressure values on the roof surface as shown on Figures 8.5 and 8.6. The darker lines indicate the contours for wind pressures from the previous figures.

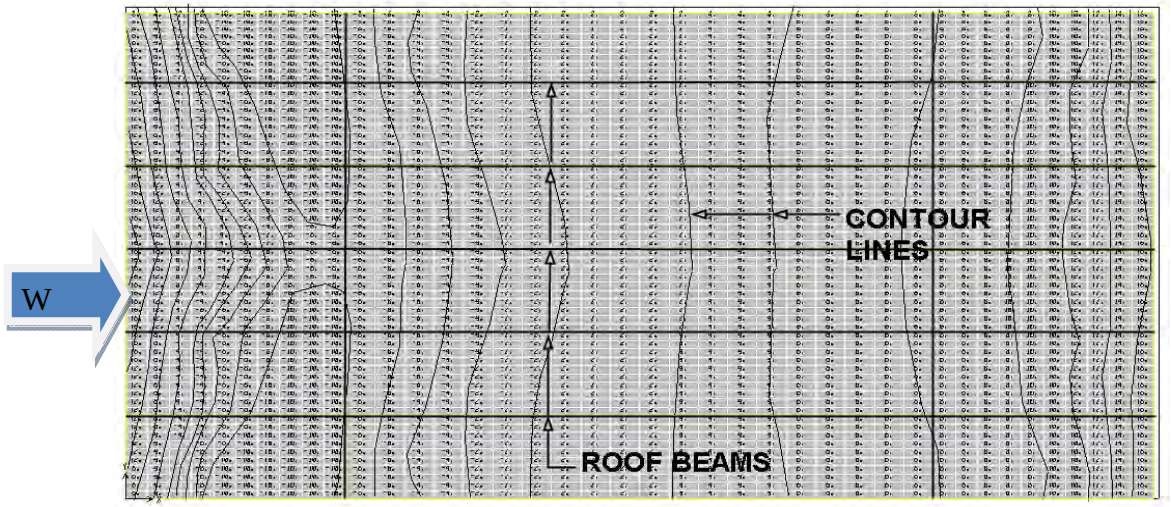

Figure 8.5: Computer model with wind pressures applied to roof surface at 0 degrees.

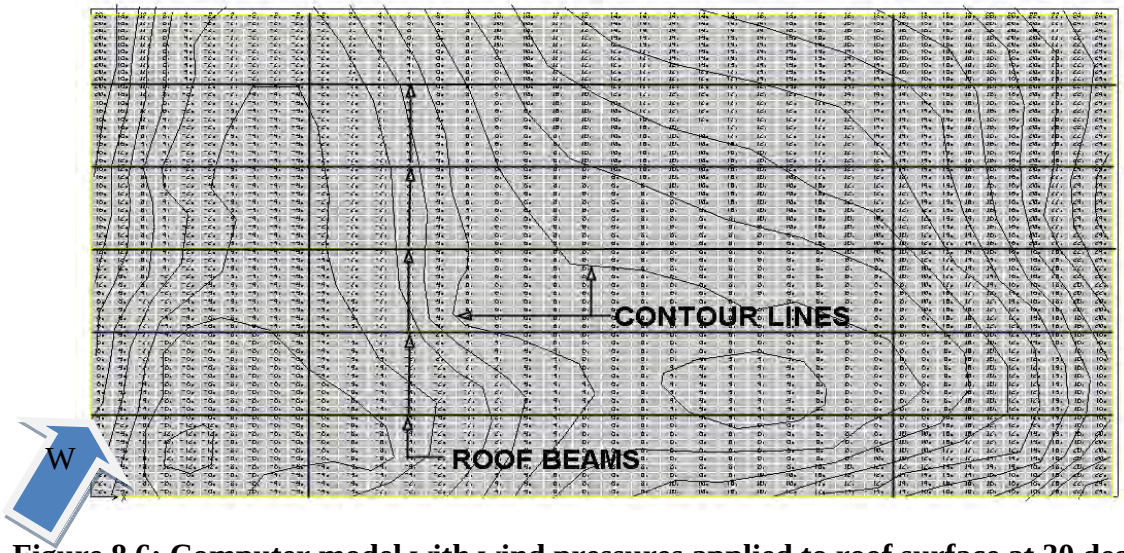

Figure 8.6: Computer model with wind pressures applied to roof surface at 30 degrees.

The results of the applied wind load conditions at 0 and 30 degrees were obtained with the use of ETABS, and Figure 8.7a and 8.7b show the deflected roof surface due to winds at 0

and 30 degrees, respectively. The deflected surfaces show differences between the applied wind pressures for the wind directions tested in this study.

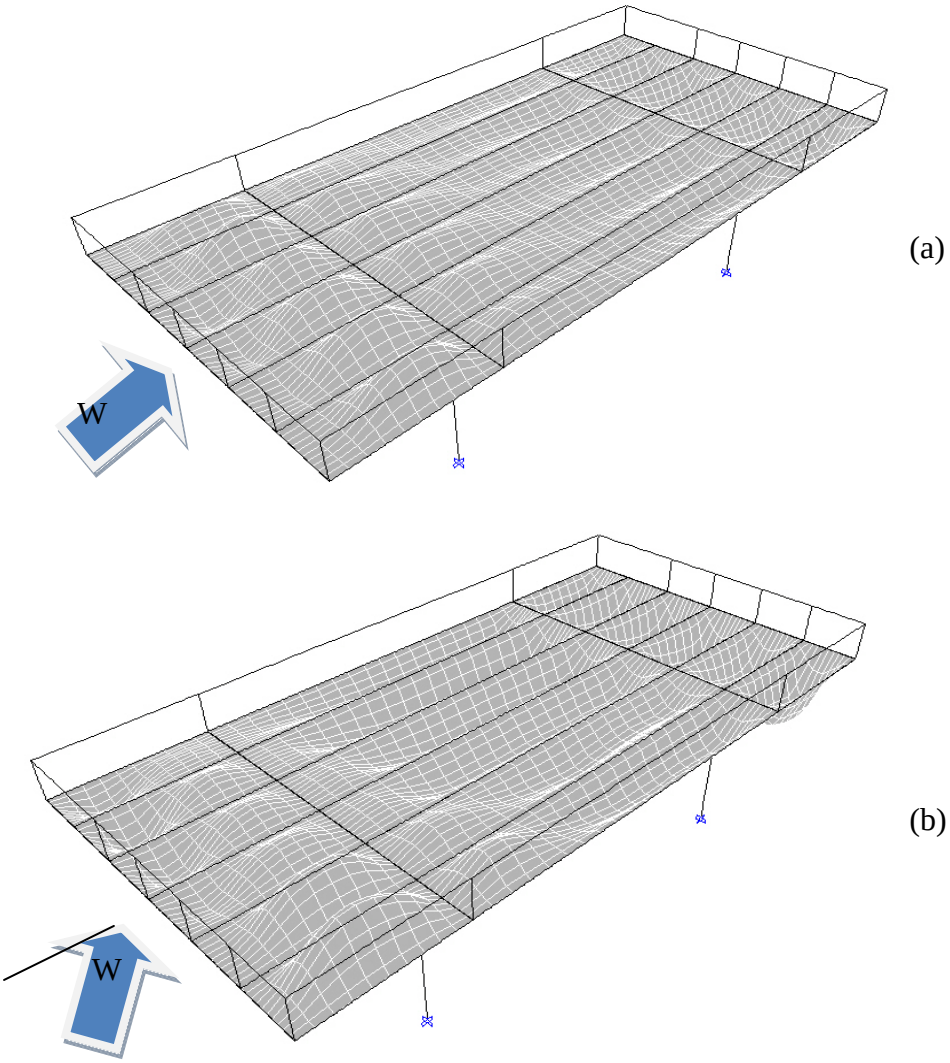

Figure 8.7: ETABS model for Case #1 showing the refined roof mesh and deflected shape of the wind loading at (a) 0 degrees (b) 30 degrees.

Figures 8.8a and 8.8b show the steel stress ratios based on ASD 1989 steel code (AISC, 1989) for the wind at 0 and 30 degrees, respectively. A stress ratio is the relation between a given stress state in a structural member and its capacity using plasticity considerations. For this particular canopy, the results in Figures 8.8a and 8.8b show that in both cases there are beam

members with stress factors larger than 1. Wind direction at 30 degrees, produce higher stress ratios than wind at 0 degrees. For example, the transverse beam on the leeward side of the roof has a stress ratio of 1.515 for wind blowing at 0 degree, whereas for 30 degrees the ratio is 1.667, that is, a 9.1 % difference. The long beams on the roof are also under conditions of severe stress, showing values of 1.01 for 0° and 1.19 for 30°. The available evidence for this canopy, which can be seen in Figures 8.18 to 8.22, indicate that the columns were still standing after the structure failed and did not show signs of damage. The transverse beams, on the other hand, had clearly failed, and this is in agreement with the computations carried out with Method #1 (also with Methods #2 and #3, as will be seen next). The columns do not seem to be severely compromised by the wind conditions considered. Method #1 has some disadvantages because the wind load input for Method #1 is very complicated. A large number of elements need to be included in the model to represent the contours and this has to be done by hand. Input has to be done one by one, on each of the individual mesh elements, with the consequence that a total of 2400 roof shell elements were assigned wind loading pressures, one at a time. In addition, a considerable amount of computational time is required to solve the model. The wind loading computed and input, represents the calculated wind pressures on the open canopy, for a specific parapet height. The need for a simpler design method is obvious and a second method, Method #2 is proposed and investigated in the following section.

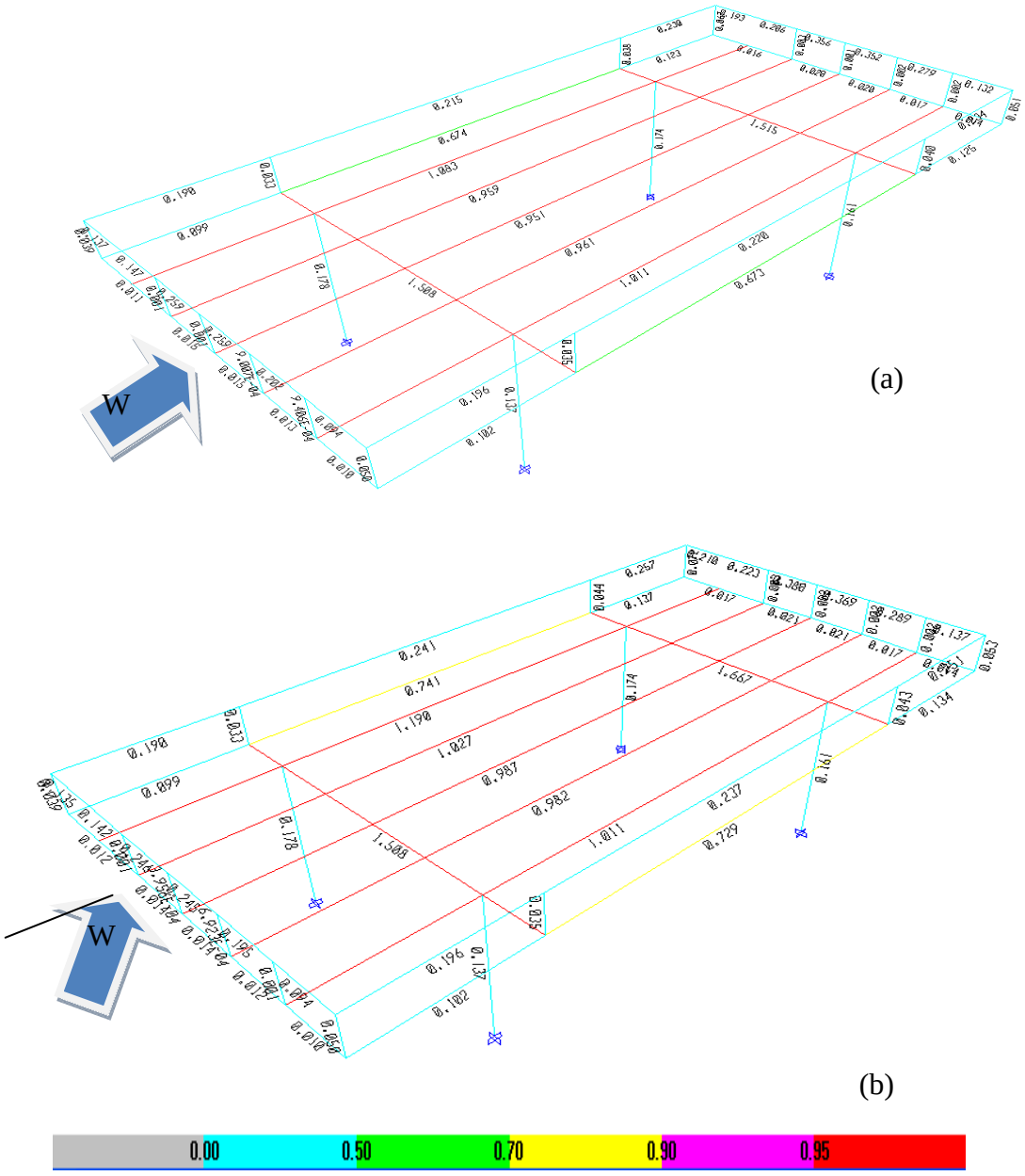

Figure 8.8: Structural steel results from ETABS for Case #1, showing members stress ratios using Method #1 for (a) wind at 0 degrees (b) wind at 30 degrees.

8.3 Case study #1, Shell Gas Station in Pt. Arthur, Texas, Method #2

Case study #1 was investigated using a simplified loading procedure, named Method #2. It was proposed that instead of input all the contours on the roof surface, the new approach will be to use the maximum wind pressure on the downward and uplift segments, from the extreme wind pressures that were used in Method #1. This method simplifies the wind load input on a structural model. Following recommendations in the literature for identifying the most critical conditions, two wind directions were investigated, the wind at 0 degrees and 30 degrees. The input wind pressures to be used on the structural model are shown on Figures 8.9 for 0° angle of attack and Figure 8.10 for the 30° condition.

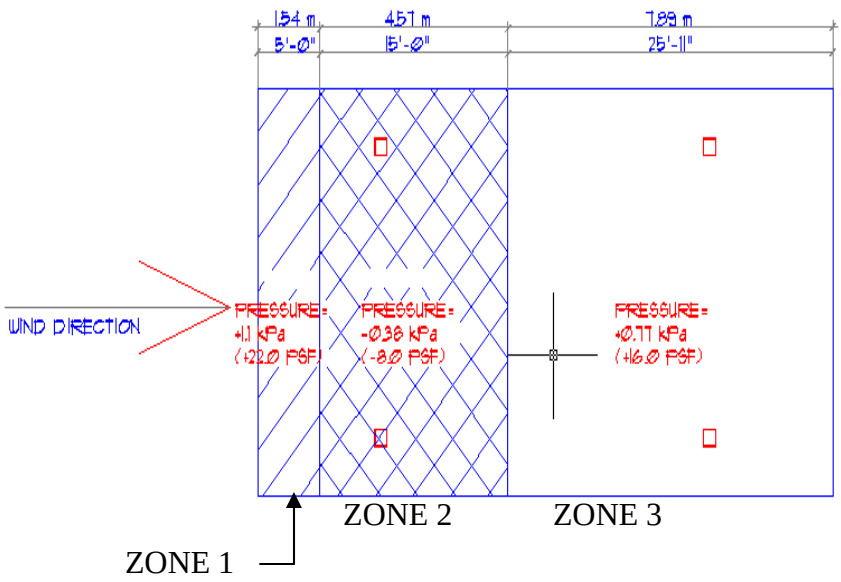

Figure 8.9: Roof canopy wind pressures for case #1, Method 2, wind at 0 degrees, + means downward pressure, - means uplift pressure.

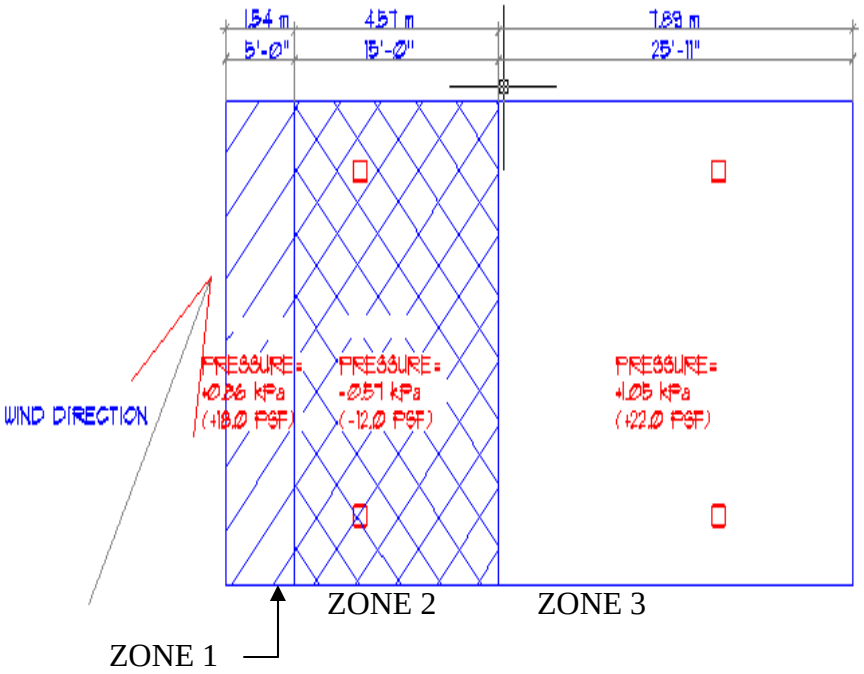

Figure 8.10: Roof canopy wind pressures for case #1, Method 2, wind at 30 degrees, + means downward pressure, - means uplift pressure.

The wind pressures from both wind load conditions were input on the ETABS program for Case #1. The stress ratios are shown on Figure 8.12a and 8.12b, using wind direction at 0 and 30 degrees, respectively. Higher stress ratios were obtained using Method #2 in comparison with Method #1, and in this sense the method is conservative (similar conclusions were obtained for other cases investigated). For example, the transverse beam on the leeward side receives a stress ratio of 1.515 for wind blowing at 0 degree and Method #1, whereas using Method #2 the ratio becomes 1.889, which is 19.8% higher. For wind at 30 degrees the same beam changes from 1.667 to 2.144 (22.2% higher). Significant changes are detected in the long beams in this method, with higher values of 1.38 for 0° and 1.47 for 30°. The proposed second method used to solve Case #1, is simpler and easier to use, but it needs to include two separate load conditions for wind each time which is not what designers are used to.

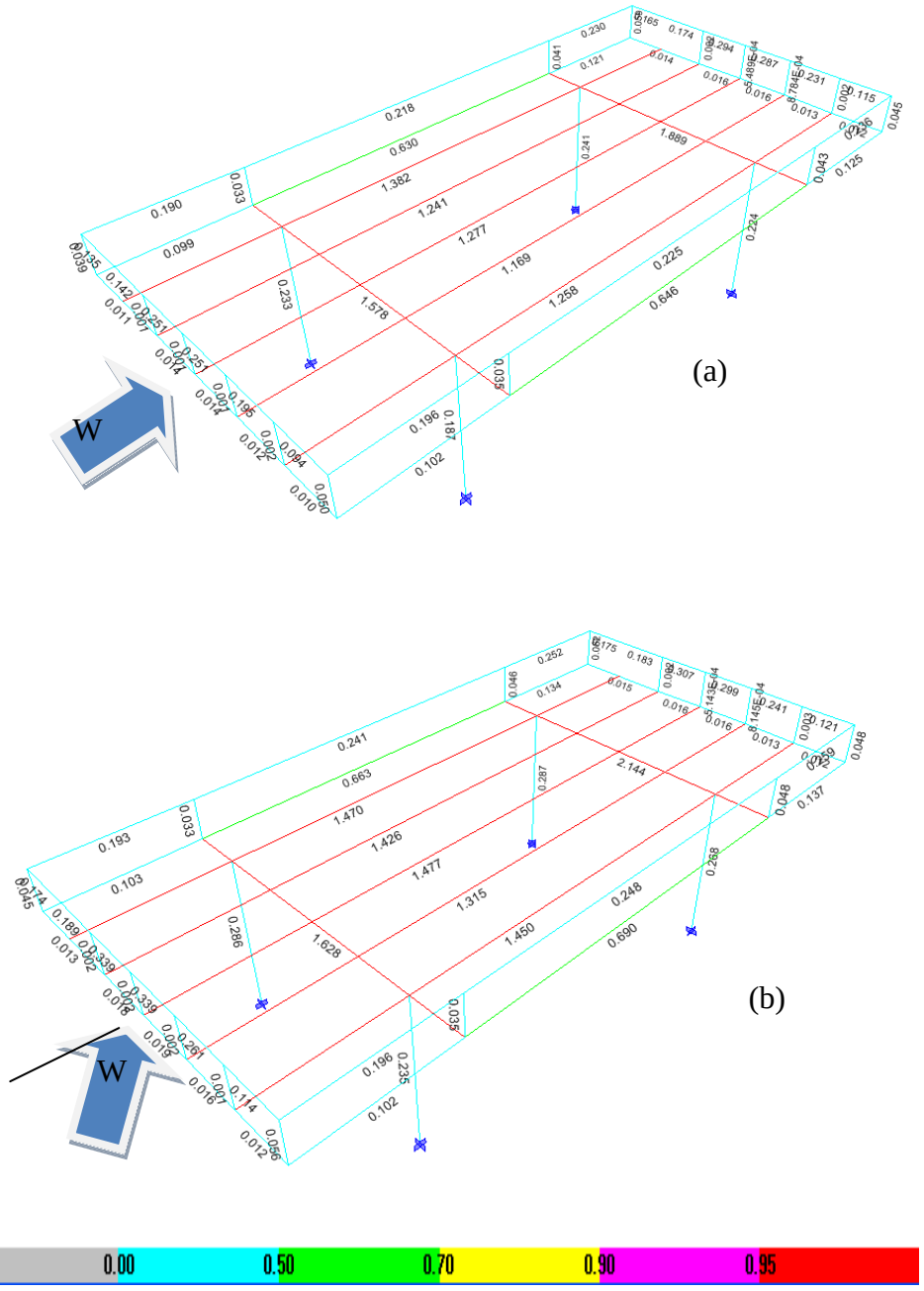

Figure 8.11: Structural steel results from ETABS showing members stress ratios using Method #2 for (a) wind at 0 degrees (b) wind at 30 degrees.

8.4 Case study #1, Shell Gas Station in Pt. Arthur, Texas, Method #3

For the current case study, calculations following Method #3 were based on the guidelines provided by ASCE 7-05. From the current results, the extreme Cn values from Chapter 7 were selected. The calculated wind pressures and the resulting Cn values used are shown in Figure 8.12. The mathematical procedure was performed with Maple, version 11 (Maplesoft, 2008), a symbolic manipulator program. The results of Figure 8.12 show values that vary from +33.1 psf (+1.61 kPa) (downward pressure, zone 1), as well as -16.5 psf (-0.79 kPa) (uplift pressure, zone 2) to +22 psf (1.05 kPa) (downward pressure, zone 3).

Parapet wind pressure values used for structural analysis are indicated in the computer output shown in Figure 8.13. As previously described on Chapter 6, Cn values from the wind tunnel and CFD simulation generally are in agreement. Wind pressure values were applied to the structural model on the parapets. Wind pressures of 43.88 psf (2.1 kPa) in the windward direction and 31.3 psf (1.5 kPa) in the leeward direction were applied to the structural model. Wind direction was applied on both horizontal axis and wind pressures on the parapets are applied at each wind direction. The proposed Method #3 combines the extreme values of the wind loading of 0 and 30 degrees on the roof surface. It includes different parapet heights calculated on Chapter 7.

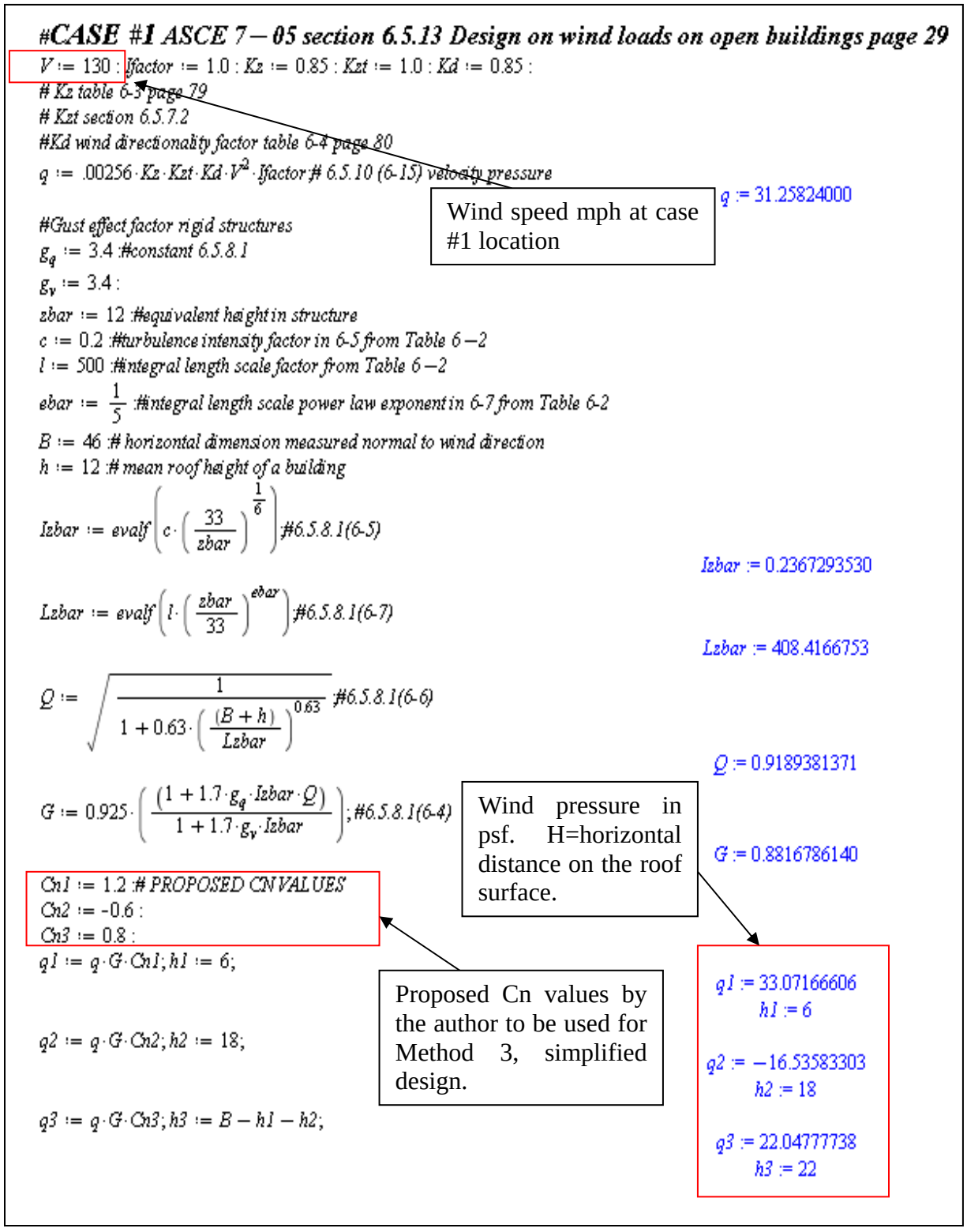

Figure 8.12: Maple layout of Wind pressure calculations for Method #3, using proposed Cn values and ASCE 7-05 procedure, Case# 1.

#Parapet pressure calculation ASCE 7 − 05, section 6.15.2.4 page 28

$V := 130 : Ifactor := 1.0 : Kz := 0.85 : Kzt := 1.0 : Kd := 0.85 :$

Kz table 6-3 page 79

Kzt section 6.5.7.2

#Kd wind directionality factor table 6-4 page 80

$q := .00256 \cdot Kz \cdot Kzt \cdot Kd \cdot V^2 \cdot Ifactor$;# 6.5.10 (6-15) velocity pressure

$q := 31.25824000$

#Combined net pressure coefficient

#GCpn1=1.5 for windward parapet

#GCpn2=-1.0 for leeward parapet

$GCpn1 := 1.5;$

$GCpn1 := 1.5$

$GCpn2 := -1.0;$

$GCpn2 := -1.0$

$q1 := q \cdot GCpn1$;#formula 6-20

$q1 := 46.88736000$

$q2 := q \cdot GCpn2;$

$q2 := -31.25824000$

Figure 8.13: Maple output of Wind pressure results on parapets using ASCE 7-05 Cn values.

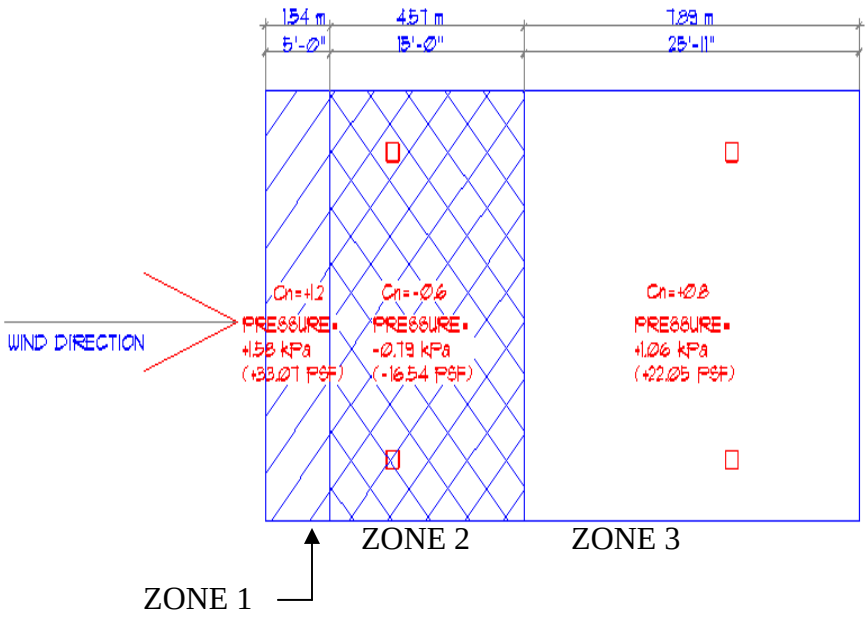

Figure 8.14: Roof canopy pressure Cn and wind pressures for case #1, + means downward pressure, - means uplift pressure.

Table 8.1: Table of wind pressures for Case #1, Method #3 to be used in structural analysis.

Case Study #	1				Zone Length	
Zone #	Cn	Pressure	psf	kPa	h(ft)	h(m)
1	1.2	q1=	33.04	1.58	5	1.5
2	-0.6	q2=	-16.54	-0.79	15	4.6
3	0.8	q3=	22.05	1.06	26	7.9

The wind pressures obtained on Table 8.1 using the ASCE 7-05 method with the proposed Cn values, or Method #3, were imposed on the structural model for the analysis on Case #1. The 3D model used for the structural analysis is shown on Figure 8.15. The plan geometry, height, column and beam sizes of the open canopy were included in the structural model. Wind pressures from Table 8.1 were included and applied to the model. Structural plans for each case were not available, beam spacing and structural layout was approximated from field observations and photographs.

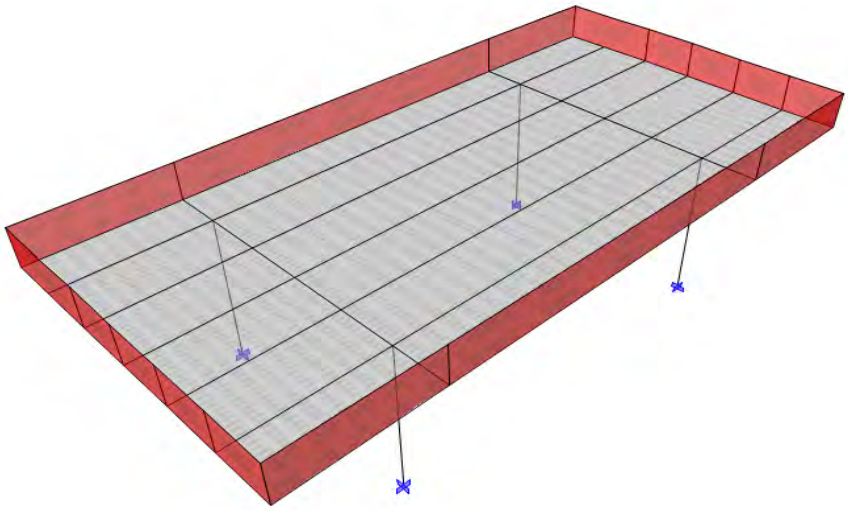

Figure 8.15: Structural model for Case #1 on ETABS.

Figure 8.16 show the deflected shape of the open canopy for Case #1 using Method #3. The actual deflection on the roof edge is about 2.5” in the downward direction. Results from the stress analysis are shown on Figure 8.17. Notice that only one wind case is considered here, since the method combines the extreme values of 0° and 30° incident winds. The differences between using Method #2 and #3 are small. For the leeward beam considered previously, Method #2 leads to 1.889 (stress ratio at 0 degrees) and to 2.144 (stress ratio at 30 degrees), whereas Method #3 (which combines both orientations) yields 2.131. The long beams on the roof reach values of 1.5. Notice that Method #3 does not represent a lower bound in terms of stress ratios, but is very close to that.

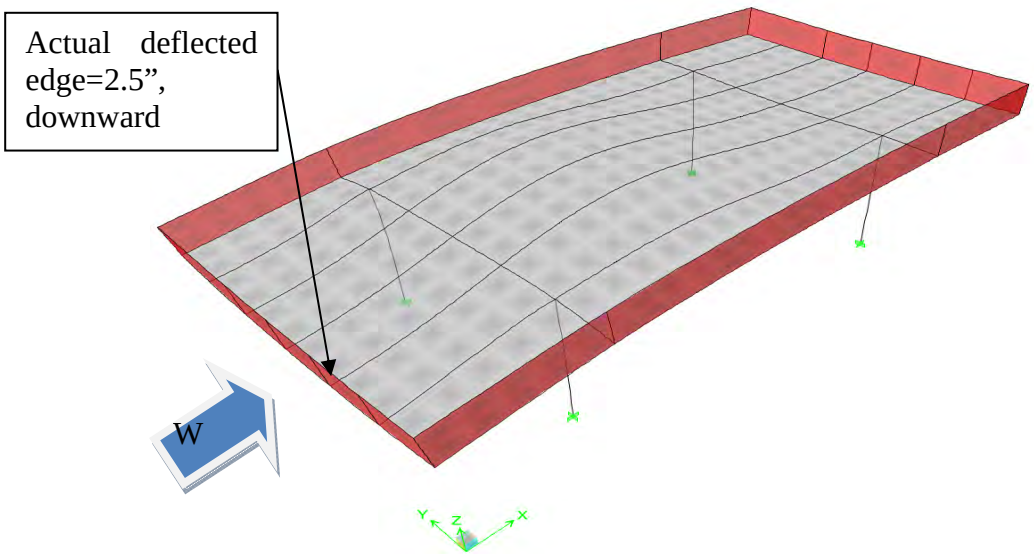

Figure 8.16: Structural model on ETABS showing deflected shape due to wind pressures.

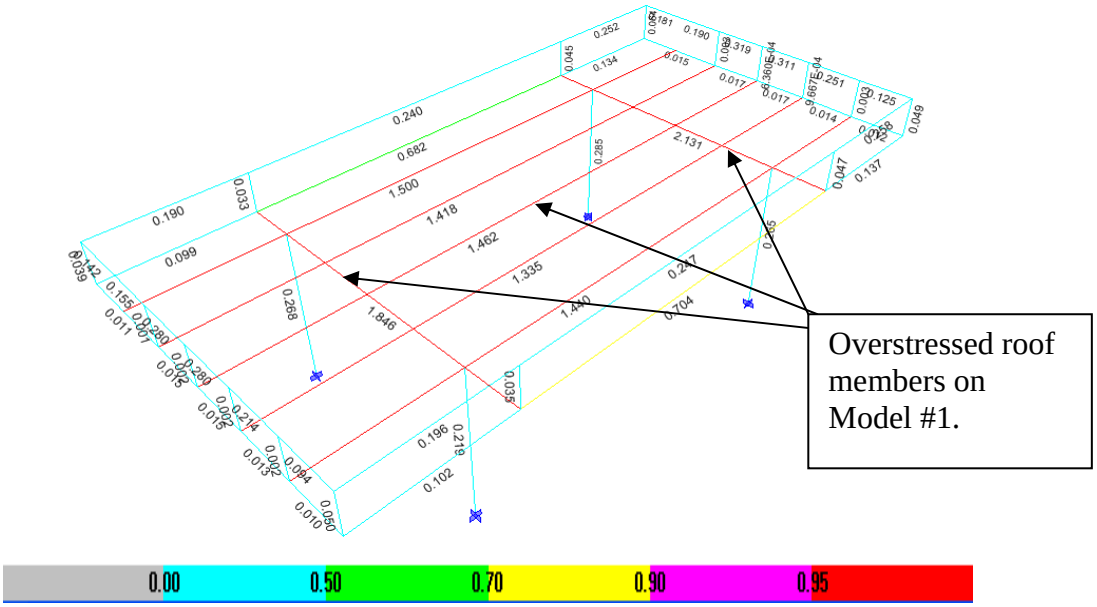

Figure 8.17: Structural model on ETABS showing overstress ratios on roof steel members.

Stress ratios on this structural model show overstressed ratios on the majority of the roof beams. The graphical result shown is an envelope of all possible load combinations generated by wind load cases, gravity loads and wind loads. The overstressed members in this case study coincide with the failed steel elements shown in Figures 8.18 to 8.22. The failed elements coincides with the analysis using a wind velocity as specified by the code, using the proposed Cn values as suggested. All predictions need to be compared with evidence collected during site visits, which are available in the form of photographs. If the Cn values proposed in this work had been applied to carry out the original design, then, the main wind force resisting system (MWFRS) should have been able to withstand the imposed wind pressures and to perform satisfactory during hurricane Rita.

Therefore, Method #3 is simpler to use. It covers the extreme conditions from the wind direction at 0 degrees and 30 degrees, and it includes the influence of different parapets heights.

Because of the simplicity of data entry of the load in Method #3 as compared with Methods 1 and 2, Method #3 will be used for the rest of the cases investigated in this chapter.

Figure 8.18: Case #1 collapsed roof layout showing some of the roof beams damages. Permanent deformation is clearly shown on some of the roof members.

Figure 8.19: Case #1 partial collapsed roof from below. Bottom of roof cladding has been taken away due to high wind pressures.

Figure 8.20: Case #1 roof cladding and beam structural layout. Photograph showing permanent deformation on roof members.

Figure 8.21: Case #1 transversal view of the deformed and collapsed roof.

Figure 8.22: Case #1, close up photograph of roof beams showing buckling and extreme corrosion damage.

8.5 Case study #2, Texaco Gas Station, Port Arthur, Texas

The case study number 2 is a Texaco gas station located in 39th Ave., Pt. Arthur, Texas. Figure 8.23 shows the roof plan and elevations for Case #2. Measurements were taken directly from the field. The floor plan dimensions are 6.1 m (20 ft) in width by 8.8 m (29 ft) in length and 4.3 m (14 ft) in heigth. The open canopy has a system of four steel columns of 0.3 m (1 ft) diameter with steel beams and channels for the gravity system of the structure. Smallest thickness of steel columns and beams were used for the analysis. A steel deck was used for the roof cladding. A parapet of 0.91 m (3 ft) is on the roof perimeter. There is no data available for the foundation size and depth.

For the current case study, calculations were based on Method #3, which uses the guidelines provided by ASCE 7-05. From the current results, the Cn values from Chapter 7 were selected. Refer to Figure 8.24 for calculated wind pressure results and Cn values used. As in other cases, the calculations were done with Maple, and show values that vary from +33.1 psf (+1.61 kPa) (downward pressure, zone 1), -16.5 psf (-0.79 kPa) (uplift pressure, zone 2) to +22 psf (1.05 kPa) (downward pressure, zone 3).

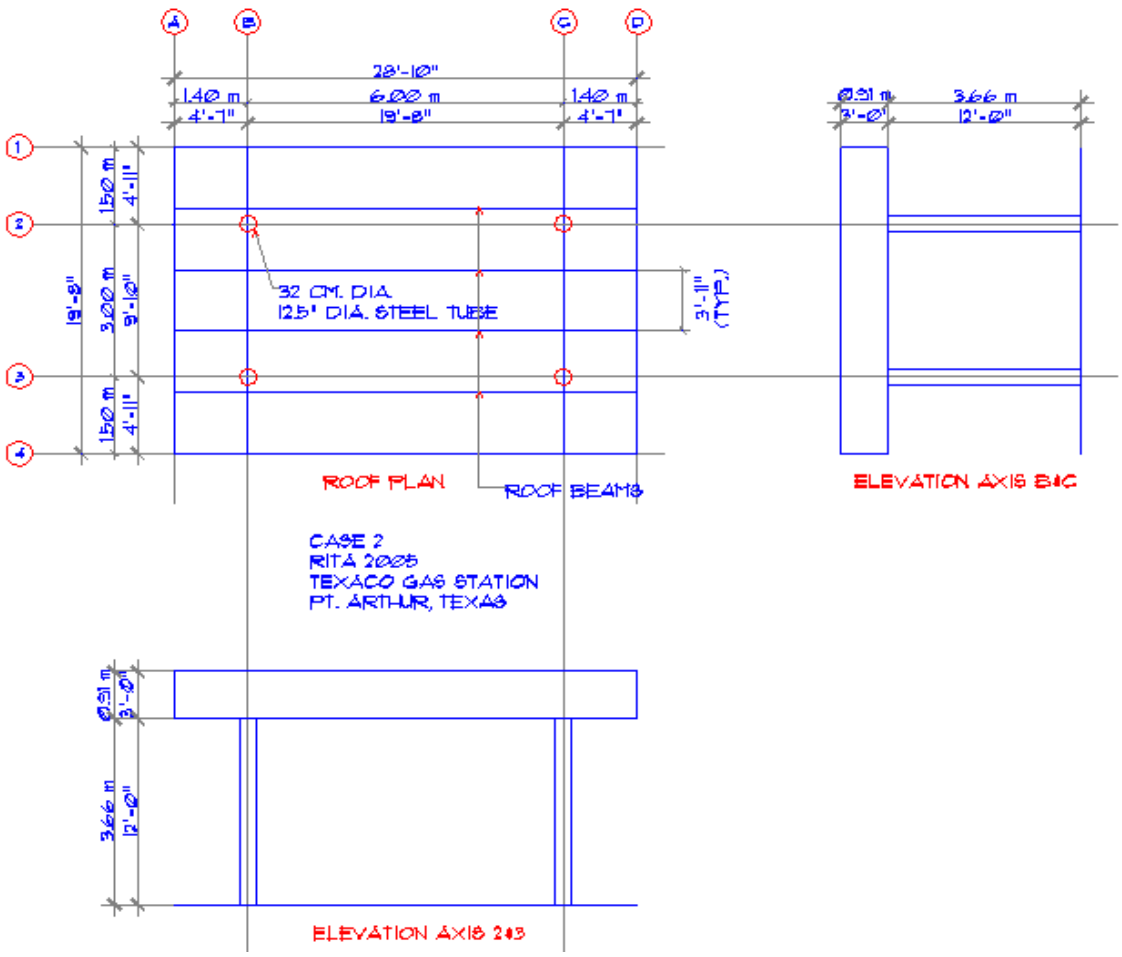

Figure 8.23: Canopy floor plan and elevations for Case study #2.

Parapet wind pressure values used for structural analysis are shown on Figure 8.13. Wind pressures of 43.88 psf (2.1 kPa) on the windward direction and 31.3 psf (1.5 kPa) on the leeward direction were applied to the structural model. Wind direction was applied on both horizontal axis and wind pressures on the parapets are applied at each wind direction.

The obtained wind pressures obtained and shown on Table 8.2 using the ASCE 7-05 method and the proposed Cn values from this thesis were imposed on the structural model for the analysis on Case #2. Refer to Figure 8.26 for the 3D model used for the structural analysis of the

structure on Case #2. Open canopy plan geometry, height, column and beam sizes, were included in the structural model. Wind pressures from Table 8.2 were included and applied to the model.

Stress ratios computed for the structural model show stress ratios values larger than one on all steel columns (Figure 8.26). The graphical result shown in this figure is an envelope of all possible load combinations generated by wind load cases, gravity loads and wind loads, and evaluated using the steel design code (AISC 1989). Unlike what was obtained in our Case study #1, in which the roof beams reached failure, the columns are the weak elements in Case study #2, whereas all roof elements are in safe state. The overstressed members in this case study are the same as the failed steel elements shown on Figure 8.28 to 8.32. The columns used on this open canopy are very slender, and just by looking at the dimensions, only six inches in diameter. Therefore, it does not surprise the author, that they failed so drastically under imposed wind pressures. Plastic hinges are observed in all four columns, and because of the advanced state of deterioration is seems that failure occur for loads (and wind velocities) lower than those considered in the analysis.

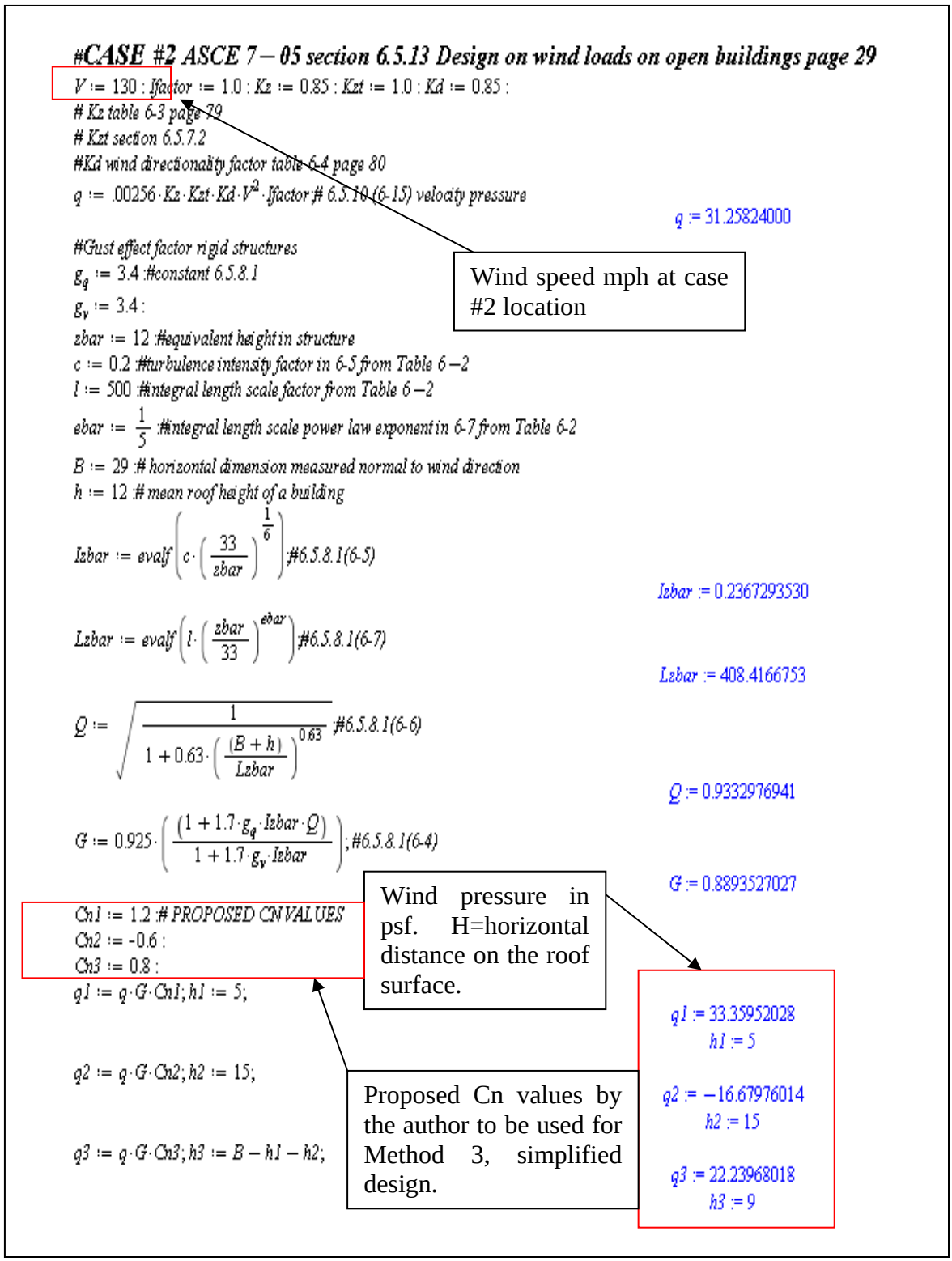

Figure 8.24: Maple output of wind pressure calculations using proposed Cn values with ASCE 7-05 procedure, Case# 2.

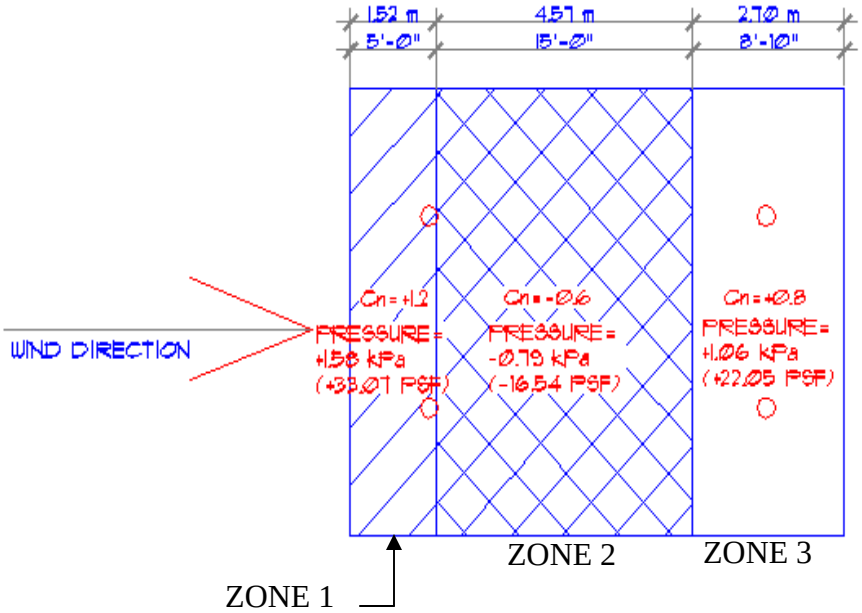

Figure 8.25: Roof canopy pressure Cn and wind pressures for case #2, + means downward pressure, - means uplift pressure.

Table 8.2: Table of wind pressures for Case #2 to be used in structural analysis.

Case Study #	2				Zone Length	
Zone #	Cn	Pressure	psf	kPa	h(ft)	h(m)
1	1.2	q1=	33.04	1.58	5	1.5
2	-0.6	q2=	-16.54	-0.79	15	4.6
3	0.8	q3=	22.05	1.06	9	2.7

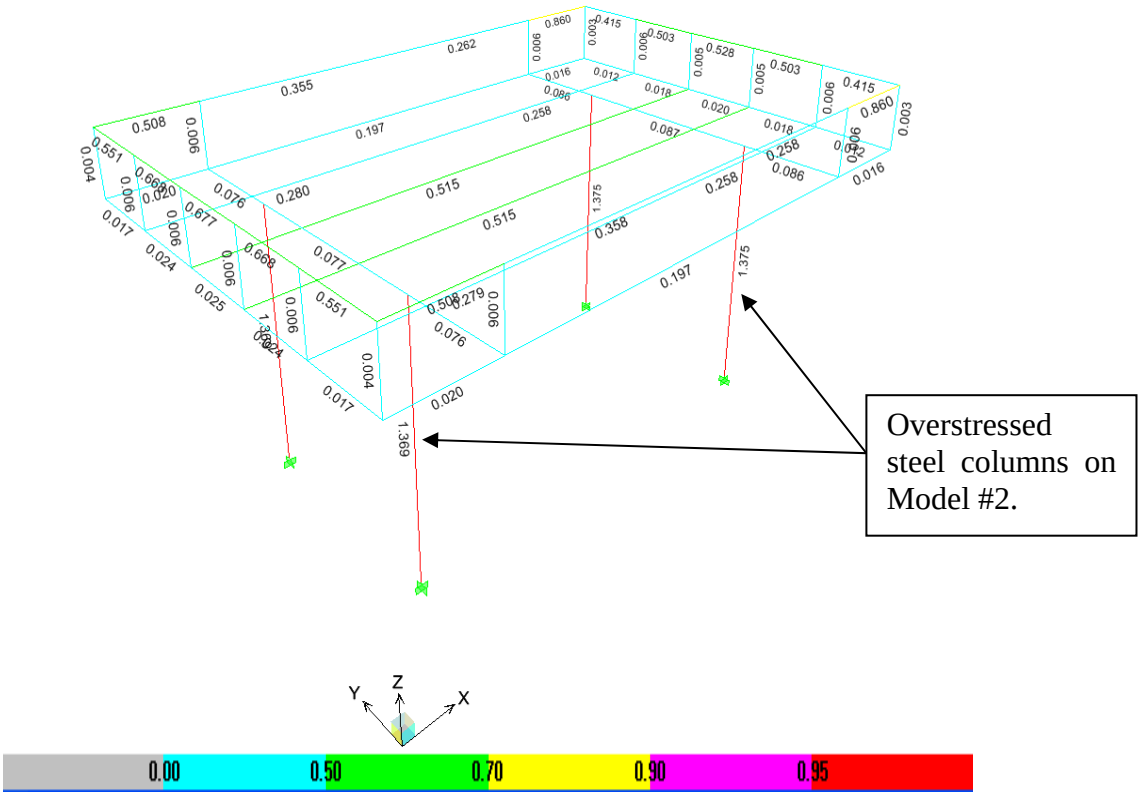

Figure 8.26: Structural model on ETABS showing overstress ratios on steel columns.

Figure 8.27: Case #2, open canopy structure completely collapsed.

Figure 8.28: Case #2, photograph showing a buckled round steel column.

Figure 8.29: Case #2, closer photograph of the round steel column base.

Figure 8.30: Case #2, photograph showing the open canopy structure on top of the gas pumps.

Figure 8.31: Case #2, photograph showing the roof beam layout.

8.6 Case study #3, Chevron Gas station, Vidor, Texas

The case study number 3 is a Chevron gas station located in Road 105 and HW 10, Vidor, Texas. A roof plan and elevations are illustrated in Figure 8.32 and were taken from measurements in the field. The floor plan dimensions are approximately 8.0 m (26 ft) in width by

12.2 m (40 ft) in length and 4.3 m (14 ft) in height. It has a system of two steel columns of 0.3 m (1 ft) x 0.3 m (1 ft) with steel beams and channels for the gravity system of the structure. Smallest thickness of steel columns and beams were used for the analysis. A steel deck was used for the roof cladding. A parapet of 0.91 m (3 ft) is on the roof perimeter. There is no data available concerning the foundation size and depth.

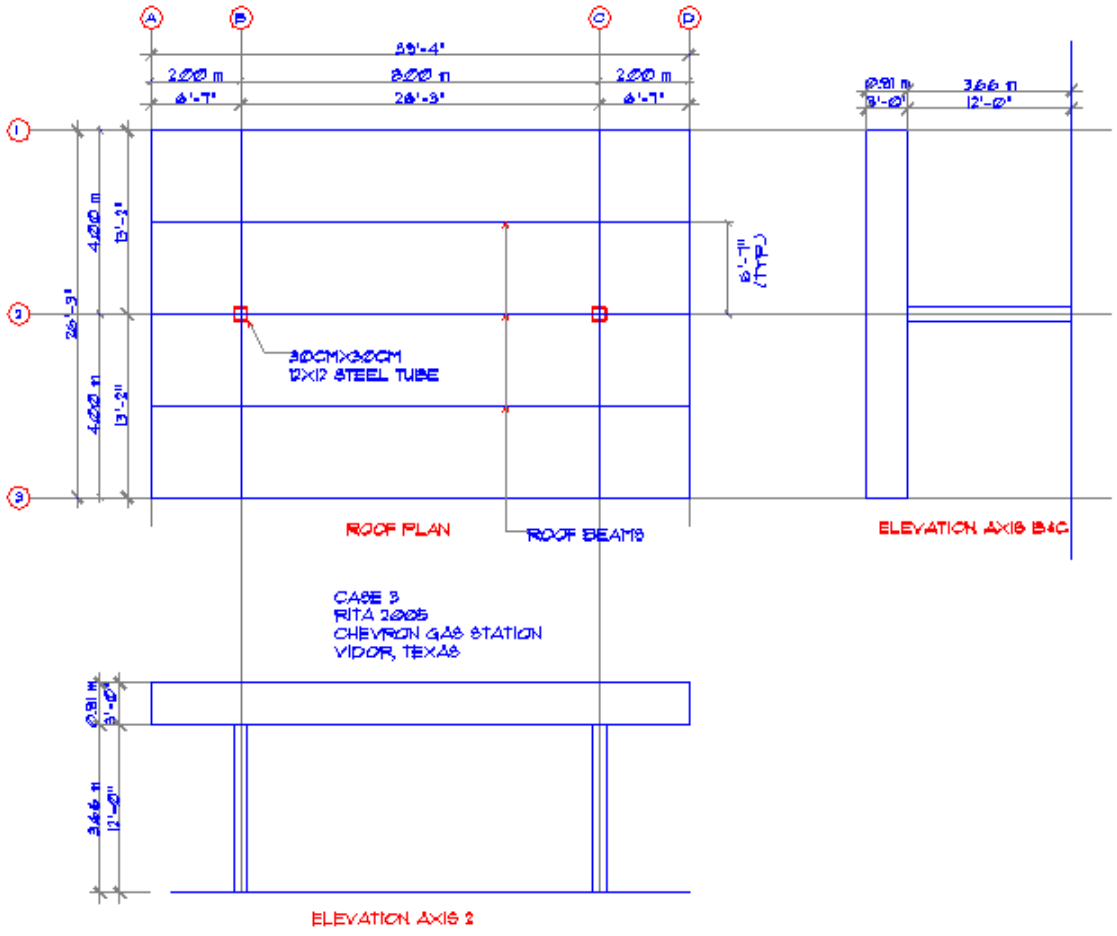

Figure 8.32: Canopy floor plan and elevations for Case study #3.

For the current case study, calculations are based on Method #3, which follows the guidelines provided by ASCE 7-05. The calculated wind pressure results and used Cn values are

shown in Figure 8.33. The values vary from +23.8 psf (+1.14 kPa) (downward pressure, zone 1), -11.9 psf (-.57 kPa) (uplift pressure, zone 2) to +15.8 psf (0.76 kPa) (downward pressure, zone 3).

Parapet wind pressure values used for structural analysis are shown in Figure 8.34. Wind pressure values were applied to the structural model on the parapets. Wind pressures of 33.6 psf (1.6 kPa) on the windward direction and 22.4 psf (1.1 kPa) on the leeward direction are applied to the structural model. Wind direction is applied on both horizontal axis and wind pressures on the parapets are applied at each wind direction.

On Figure 8.36 the structural analysis of the open canopy does not indicate overstress ratios on the roof members. This specific case was characterized by extensive corrosion at the base of the columns, associated with the drainage system of the roof. Thus, the steel columns were modeled to represent the loss of material due to corrosion. Because the actual extent of corrosion was difficult to evaluate, an initial value of the columns thickness was used as ¼" (6.4 mm), and the value was parametrically reduced to almost half of the wall thickness. For the case of 1/8" (3.2 mm), the stress ratios computed are plotted in Figure 8.36. Both columns have values higher than one, whereas the roof members reach half of their capacity at most.

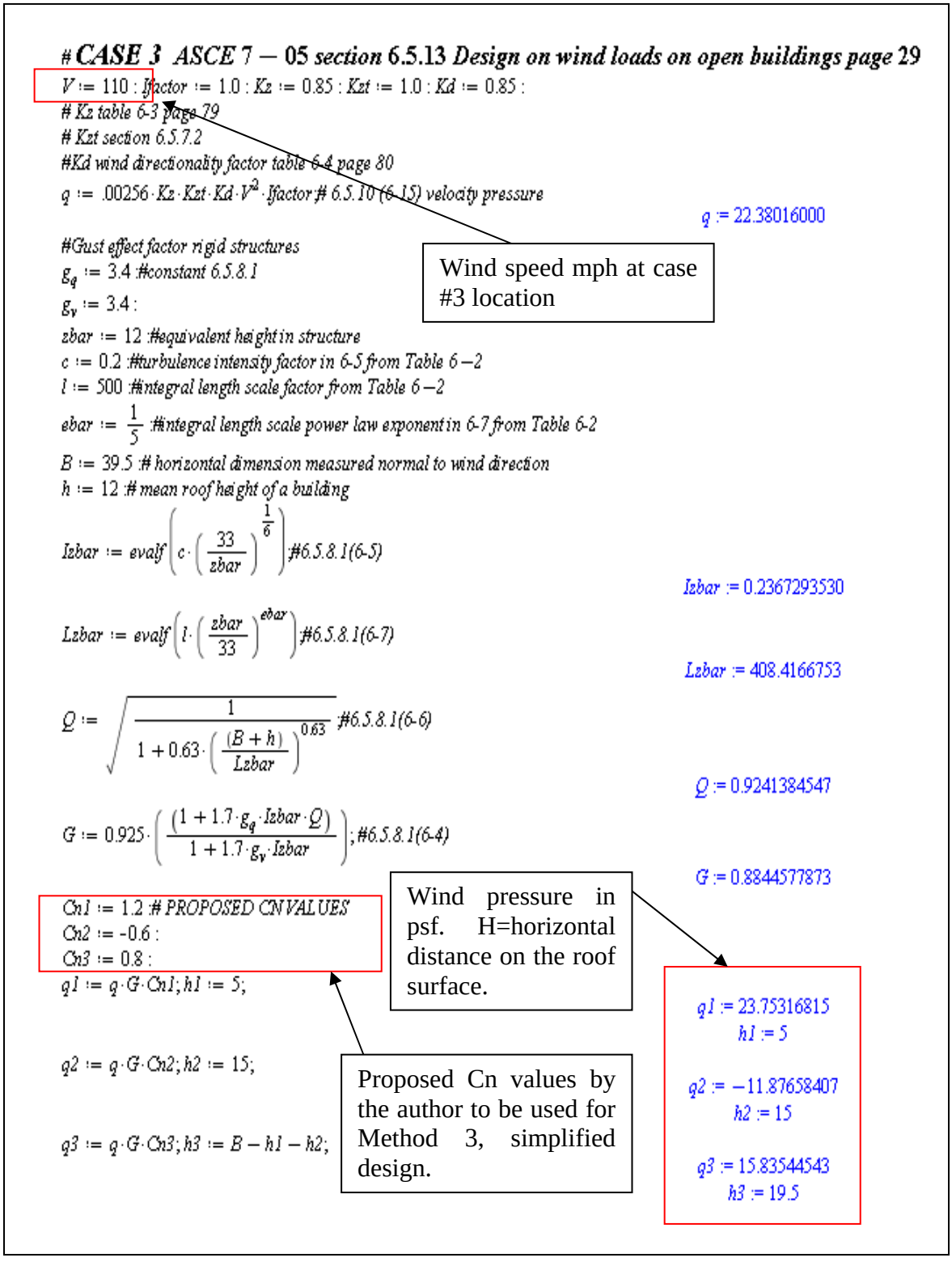

Figure 8.33: Maple output of wind pressure calculations using proposed Cn values with ASCE 7-05 procedure, Case# 3.

#Parapet pressure calculation ASCE 7 − 05, section 6.15.2.4 page 28

$V := 110 : Ifactor := 1.0 : Kz := 0.85 : Kzt := 1.0 : Kd := 0.85 :$

Kz table 6-3 page 79

Kzt section 6.5.7.2

#Kd wind directionality factor table 6-4 page 80

$q := .00256 \cdot Kz \cdot Kzt \cdot Kd \cdot V^2 \cdot Ifactor$;# 6.5.10 (6-15) velocity pressure

$q := 22.38016000$

#Combined net pressure coefficient

#GCpn1=1.5 for windward parapet

#GCpn2=-1.0 for leeward parapet

$GCpn1 := 1.5;$

$GCpn1 := 1.5$

$GCpn2 := -1.0;$

$GCpn2 := -1.0$

$q1 := q \cdot GCpn1$;#formula 6-20

$q1 := 33.57024000$

$q2 := q \cdot GCpn2;$

$q2 := -22.38016000$

Figure 8.34: Maple output of wind pressure results on parapets using ASCE 7-05 Cn values

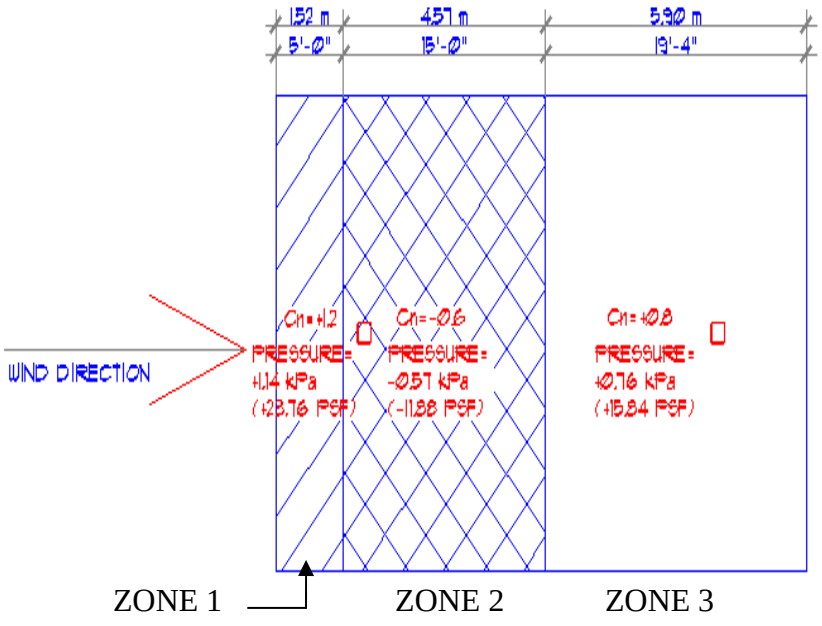

Figure 8.35: Roof canopy pressure Cn and wind pressures for case #3, + means downward pressure, - means uplift pressure.

Table 8.3: Table of wind pressures for Case #3 to be used in structural analysis.

Case Study #	3				Zone Length	
Zone #	Cn	Pressure	psf	kPa	h(ft)	h(m)
1	1.2	q1=	23.75	1.14	5	1.5
2	-0.6	q2=	-11.87	-0.57	15	4.6
3	0.8	q3=	15.83	0.76	19.5	5.9

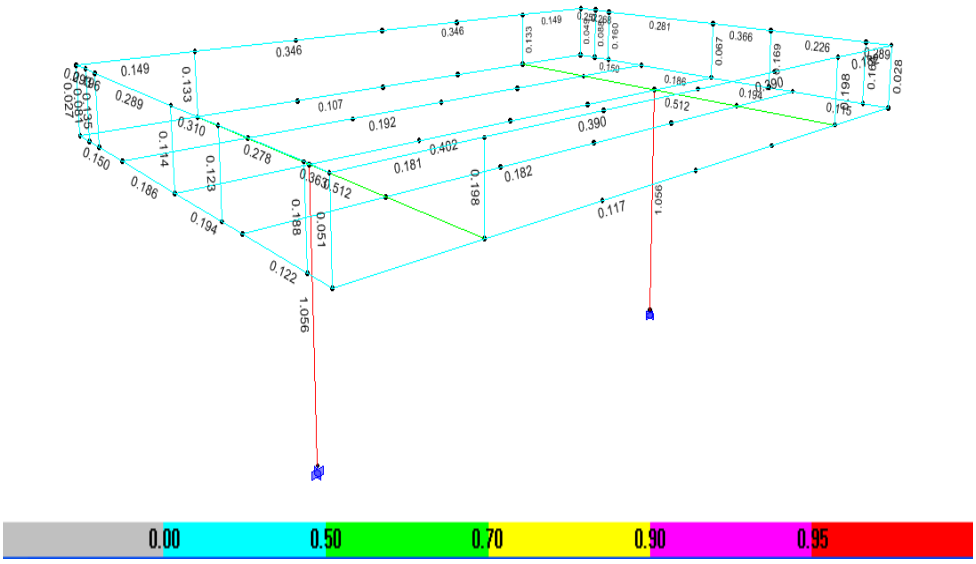

Figure 8.36: Structural model on ETABS showing overstress ratios on roof steel members for Case #3.

Figures 8.38 to 8.40 show the corrosion damage at the base of the steel columns, which is believed to have triggered the collapse of the structure. The steel columns failed below their stress capacity and even the complete structural layout remained intact after the failure of the steel columns. It is remarkable that the whole superstructure, the MWFRS and the secondary members, remained intact after the structure became upside down after the failure. Without the

corrosion damage on the existing structure, only the roof secondary beams would have suffered damage for the applied wind pressures.

Figure 8.37: Case #3, open canopy photograph of the inverted steel structure after the steel columns failed due to corrosion and wind pressures.

Figure 8.38: Case #3, photograph of the existing corrosion condition at the column base.

The deterioration of the column at its base illustrated in Figure 8.38 indicated that the drainage system of the roof, which conducts water through the columns, did not function properly and produced severe metal corrosion. This case calls for improvements in the drainage system (to avoid such drastic corrosion) and an effective maintenance schedule. Although just

one case involving corrosion was analyzed in this chapter, this pattern of deterioration was observed in many cases during site visits.

Figure 8.39: Case #3, additional photograph of the inverted steel structure.

8.7 Case study #4, Exxon Gas station, Hillerbrandt, Texas

The case study number 4 is an Exxon gas station located in Road 365, Hillerbrandt, Texas. A roof plan and elevations as illustrated in Figure 8.40 and were taken from field measurements. The floor plan dimensions are approximately 9.8 m (32 ft) x 25.0 m (85 ft) x 4.3 m (14 ft). It has a system of four steel columns of 0.3 m (1 ft) x 0.3 m (1 ft) with steel beams and channels for the gravity system of the structure. Smallest thickness of steel columns and beams were used for the analysis. A steel deck was used for roof cladding. A parapet of 0.91 m (3 ft) is on the roof perimeter. There is no data available for the foundation size and depth.

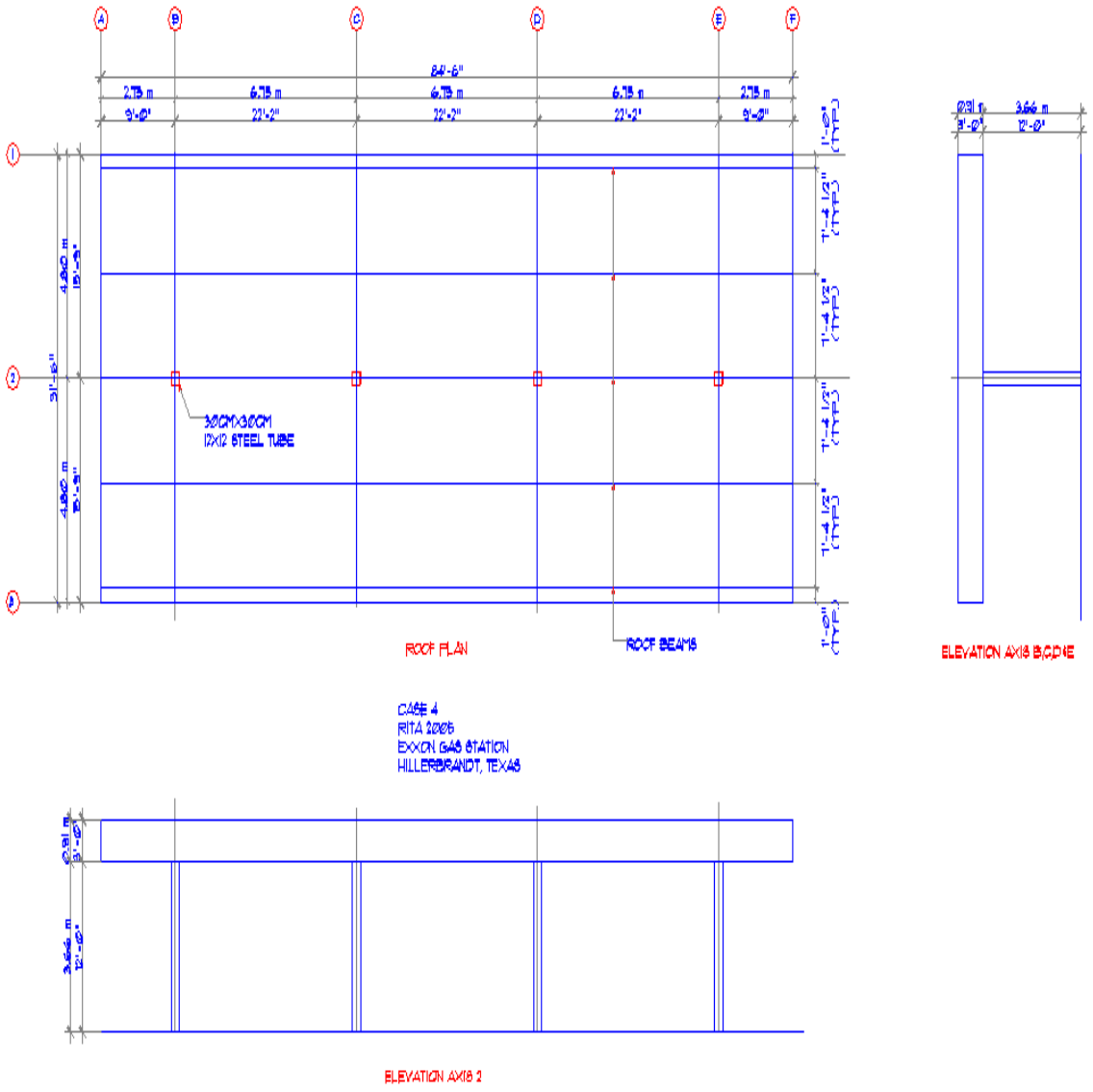

Figure 8.40: Canopy floor plan and elevations for Case study #4.

For the current case study, calculations are based on the guidelines provided by ASCE 7-05, Method #3. Figure 8.41 shows the calculated wind pressures from the proposed Cn, with values that varied from +33.1 psf (+1.61 kPa) (downward pressure, zone 1), -16.5 psf (-.79 kPa) (uplift pressure, zone 2) to +22 psf (1.05 kPa) (downward pressure, zone 3).

Parapet wind pressure values used for structural analysis are shown on Figure 8.13. Wind pressure values were applied to the structural model on the parapets. Wind pressures of 43.88 psf (2.1 kPa) on the windward direction and 31.3 psf (1.5 kPa) on the leeward direction are applied to the structural model. Wind direction is applied on both horizontal axis and wind pressures on the parapets are applied at each wind direction.

Stress ratios larger than one on this structural model show overstressed ratios on all steel columns. The values displayed in Figure 8.43 is an envelope of all possible load combinations generated by wind load cases, gravity loads and wind loads, using steel design code (AISC 1989). As reference values, the maximum service of the column axial load is 17.1 kips and the maximum service moment in the strong axis is 119 k-ft. The maximum ultimate column axial load is 28.2 kips and the maximum ultimate moment in the strong axis is 154.5 k-ft.

In this particular case is very interesting to identify from the photographs the buckling of the column flanges. The maximum capacity of the flanges before the local flange goes into plastic deformation is 138.9 kips. From the computations, it seems that plastic hinge in one of the local flanges has initially formed, causing the rotation and failure of all steel columns. The actual computational model results using Method #3 produce results that are comparable to the failure mechanism and loads that the actual structure suffered from wind forces. The overstressed members in this case coincide with the failed steel column elements shown on Figure 8.45 to 8.48.

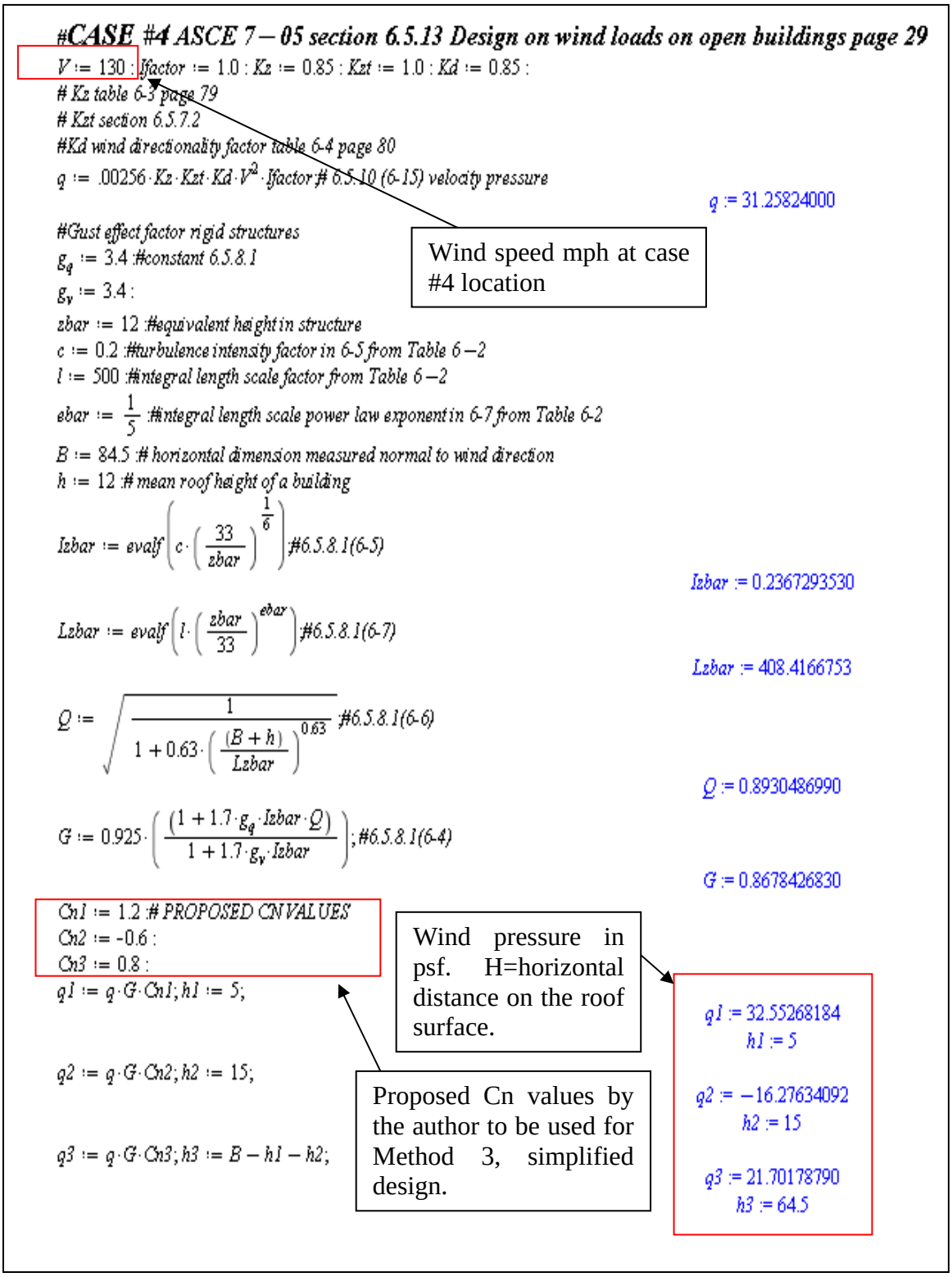

Figure 8.41: Maple output of wind pressure calculations using proposed Cn values with ASCE 7-05 procedure, Case# 4.

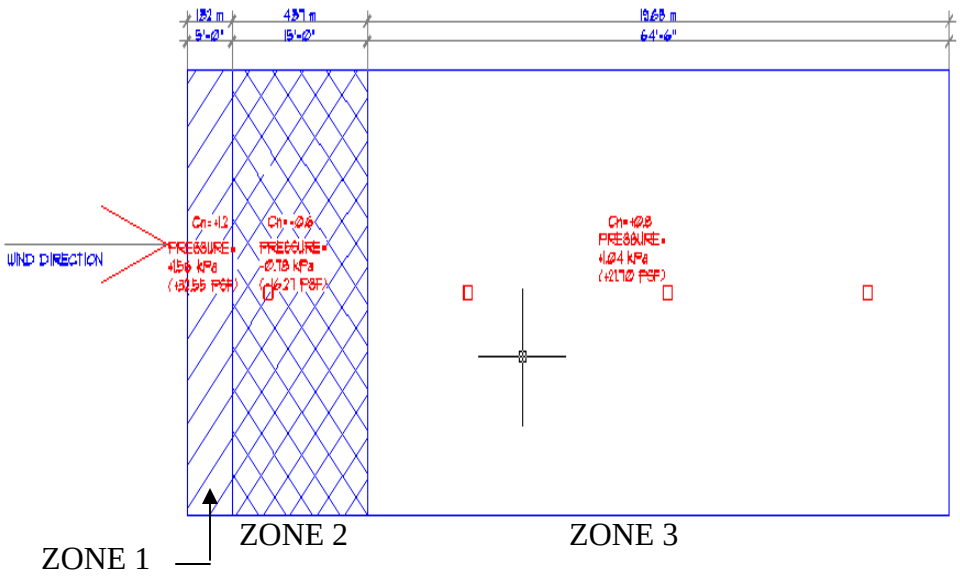

Figure 8.42: Roof canopy pressure Cn and wind pressures for case #4, + means downward pressure, - means uplift pressure.

Table 8.4: Table of wind pressures for Case #4 to be used in structural analysis.

Case Study #	4				Zone Length	
Zone #	Cn	Pressure	psf	kPa	h(ft)	h(m)
1	1.2	q1=	32.53	1.56	5	1.5
2	-0.6	q2=	-16.27	-0.78	15	4.6
3	0.8	q3=	21.7	1.04	64.5	19.7

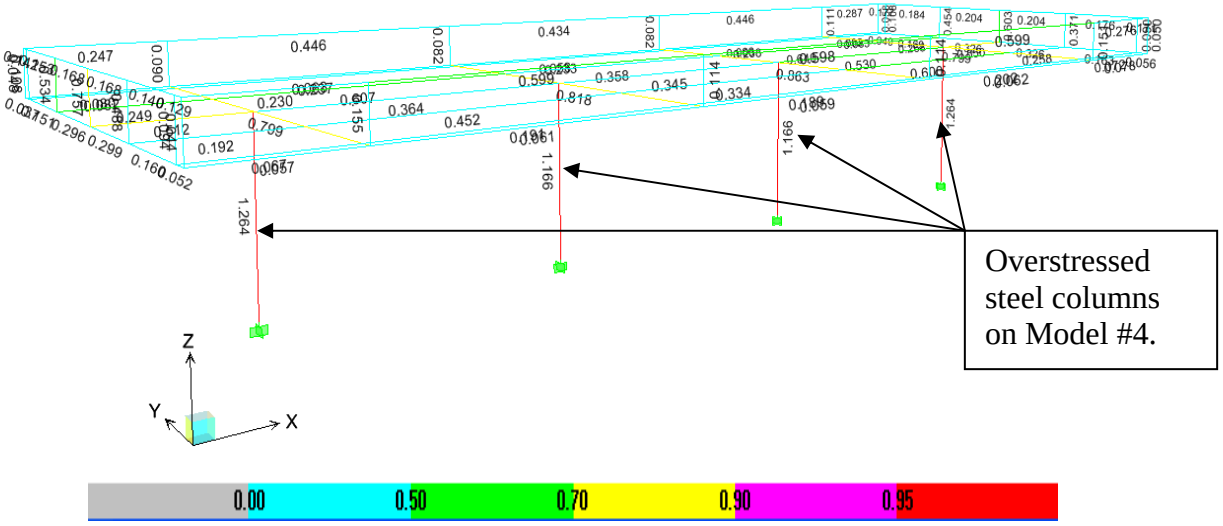

Figure 8.43: Structural model generated with ETABS showing overstress ratios on all steel columns.

Figure 8.44: Case #4, photograph showing closer detail of the buckled steel columns.

Figure 8.45: Case #4, photograph showing the collapsed steel columns.

Figure 8.46: Case #4, additional photograph of buckled steel columns. The photograph shows the internal column flange.

Figure 8.47: Case #4, upper roof beam layout on the collapsed open canopy roof.

8.8 Conclusions drawn from the Case Studies

The Cn values obtained from wind tunnel experiments and CFD simulation were obtained on Chapter 6. CFD simulations could provide Cn values for different geometric configurations and were investigated in Chapter 7. In Chapter 8, three methods of performing structural analysis have been investigated. Method #1, with the actual wind pressures, requires large computer time and effort. Method #2, a simplified version of Method #1, investigates the wind effects at 0 and 30 degrees but using bands of pressures rather than detailed local pressures. The suggested Method #3, using the ASCE 7-05 procedure with the modified Cn factors, combines the wind pressure coefficients in both directions. It has been possible to predict overstressed members and possible failures on open canopy structures using all three methods. In all cases calculated with wind pressures based on Method #3, the suggested Cn values could confirm the expected overstressed members that lead to the catastrophic collapse of the presented cases.

With the use of the suggested Method #3, the safe design of open canopy structures could be made. The design is conservative only by 18 percent, making the simplified Method #3, a very easy and accessible design method for the structural engineering community.

CHAPTER 9. CONCLUSIONS, ORIGINAL RESULTS, FUTURE RESEARCH AND RECOMMENDATIONS

9.1 Conclusions

There is conclusive evidence that a large number of open canopy structures suffered catastrophic damage due to hurricanes in the US during the last decade. This calls for an urgent reassessment of current design methods and provisions used for this class of structures. The most recent version of the ASCE 7 includes considerations for open structures; however, the recommendations do not account for cases of open structures with parapets. For the specific geometries used in this investigation, the calculated Cn values for an open structure without parapets using ASCE 7 are negative on the complete surface and range from -0.8 to -0.3 for the Main Wind Force Resisting System (MWFRS) (ASCE 6.5.13,Table 3.5.7).

Based on the evidence presented in this thesis, the following conclusions can be made:

1) Current ASCE-7 wind provisions are not adequate to estimate wind pressures on open canopies with parapets. The Cn results from wind tunnel and computational simulations show that there is a strong influence of the parapets on the pressure coefficients of a canopy structure; this influence was observed in both, wind tunnel testing and Computational Fluid Dynamics (CFD) simulations, and good agreement has been obtained between the two independent methodologies. For the cases studied, using numerical and wind tunnel simulations, the Cn values obtained in this investigation have a clear pattern of downward pressure, followed by suction, followed by downward pressure along the center line in the direction of the wind. The specific values varies from +1.2 (zone 1), -0.6 (zone 2) and +0.8 (zone 3). The mean roof pressures vary from pressure downward to upward

pressure, depending on the specific locations considered in the roof along the long axis. These values significantly differ from the recommended code values, which predict that only suction or only downward pressure acts in the roof. Further, the resultant forces caused by these Cn values are 40% higher than the recommended values suggested by the current ASCE 7-05. We conclude that ASCE recommendations for this type of structures are not sufficient to carry out safe designs of canopy structures with parapets. It is suggested that current code recommendations for the MWFRS should be modified for open structures and should include new coefficients for open structures with parapets, such as those presented in this research.

2) Parapets have a significant influence on the resultant wind pressures. Wind pressures were first compared on open canopies without parapets with current available data. Cn results derived from wind tunnel and computational simulations show that there is a strong influence of the parapets on the pressure coefficients of a canopy structure. This influence was observed in both, wind tunnel testing and CFD simulations and good agreement has been obtained between the two independent methodologies. CFD simulations of different plan geometries with different parapet heights verify such conclusion.

3) CFD simulations are an adequate tool for the investigation of open canopies with parapets. With the use of the data from the wind tunnel of UNNE, for an open canopy small scale model, a CFD simulation was developed. The Cn values obtained from the CFD simulation are in good agreement with the wind tunnel model results. Because of the similarity of results and the comparative cost of the

two methods, the present studies conclude that CFD is an adequate tool to perform further parametric studies and investigation of failure cases.

4) The present sequential methodology (in which pressures are first determined on a rigid model and subsequently applied to a deformable structure) can represent the failure of real structures occurred during hurricanes. Four cases of real structural collapses were investigated in Chapter 8, showing that the sequential analysis was capable of detecting the specific members that failed in the field.

9.2 Original Results

The investigation reported in this thesis has provided original results in various topics. This is the first time that studies for an open canopy with parapets have been reported in the open literature. Open canopies are frequently used in the construction of civil engineering facilities, either as components of larger structures or as self-supported structures, so that the present results should be taken as a basis for establishing new recommendations in this field. An example of canopies used as self supported structures may be found in most gas stations throughout the nation, in which the roof covers gas pumps and vehicles.

In order to investigate the open canopy with parapets, a wind tunnel study was conducted on a boundary layer wind tunnel at the UNNE. Detailed Cp and mean pressure Cn values were obtained from those tests. In the case investigated, wind was applied at 0 and 30 degrees from the principal axis, because they lead to the most severe wind pressure coefficients. No other wind tunnel studies were available for canopies with parapets, so that the present set of results may serve as reference values for research conducted by other investigators.

Concurrent with the wind tunnel tests, a CFD investigation was made. Similar wind conditions, in comparison to the wind tunnel tests, were used in the computational study, considering the same wind directions. Similar Cp and Cn results were obtained from the two methods, thus confirming and validating the CFD results. This was an important result for the rest of the research, since parametric studies were further conducted using CFD rather than wind tunnel testing. Thus, the obtained CFD results provided the opportunity to investigate additional cases of this type of structures, including additional geometries and configurations. Three planar geometries were investigated, each of the geometries with four different parapet heights. Each parapet height was considered with two different wind directions. The total number of models obtained was twenty-four. With this investigation, graphical output, in 2D and 3D were obtained and extreme Cn values were used for investigating actual open canopy collapses.

Four case studies of collapsed open canopy structures were investigated using structural analysis software. With the obtained Cn values from the wind tunnel investigation and the CFD models, wind pressures from the suggested Cn values were obtained. The method used for obtaining the wind pressures, was that suggested by the ASCE 7-05. We used the Cn values obtained on this investigation for the final wind pressure definition. With the obtained wind pressures, structural analysis was performed using structural engineering software. For all the cases studied, the overstressed members coincide with the actual photos of the collapsed structure. This closes the research circle stating from experimental evidence which is used to build computational models that are in turn validated with field observations. The consistency of the research is given by two independent sets of evidence (experimental measures and field observations) used to validate a complete new methodology.

9.3 Future Research

Because this is the first time an open canopy with parapets is investigated, further research is considered necessary. We have investigated in this research the Main Wind Force Resisting System. Under severe winds, the collapse of open canopies cause a major disaster in terms of providing gas at the time of an emergency and damaging important facilities. That is why further research is necessary and suggested:

1) Investigation of the structure's cladding is very important for this type of construction. Depending on the structural layout, the cladding is a key point, where the structural integrity of the whole structure could be compromised, if not designed correctly. Cp coefficients for the roof cladding need to be included in future design codes.

2) CFD investigation of this type of structures using different simulation programs is suggested in order to compare various ways of representing what is essentially a boundary layer problem. Further calibration of wind energy and dissipation in order to replicate wind turbulence has been obtained in recent investigations and adopting those findings on further research is suggested.

3) Further investigation and development of structural details and standard construction practices is recommended. During this research we noticed that there is no uniformity in the construction practices for this type of structures. It is suggested to involve the gas industries to obtain structural drawings and the standards they are using, to help them improving current design practices for this type of structures. This would be necessary in order to investigate if the supplied structural plans need revision and further retrofit of existing gas stations is necessary.

4) Open canopies with parapets, depending on the structural design, have several collapse mechanisms. Some of those mechanisms have been identified after hurricanes, including lack of maintenance of the structure, lack of structural redundancy, lack of uniformity of structural details in terms of steel connections and foundation design. Further investigation of those collapse mechanisms would be beneficial in terms of evaluating existing open canopies with parapets and developing retrofitting techniques whenever necessary.

9.4 Final Recommendations

Open canopy structures with parapets are not a trivial type of structure. When a catastrophic event, like a hurricane happens, a large number of those structures collapsed as previously illustrated. At present, it is necessary that those types of structures should be designed, with higher safety margins to withstand the applied forces of nature. Open canopy structures should be designed as an essential facility, due to their importance in terms of human risks and security at the time of an emergency.

Providing structural redundancy and adequate maintenance are some of the suggested recommendations for the design and construction of those types of structures. Redundancy is necessary for a robust structural frame system in order to resist the imposed wind forces. With the frame system, a foundation is necessary in order to counter act the effects of uplift and overturning imposed by the structure. That is why with proper code recommendations and further research, adequate and safe design of those structures will be able to be achieved.

Structural maintenance of open canopies is very important, requiring periodic inspection and repair as necessary. Corrosion of steel and deterioration on exposed surfaces, such as those

illustrated by photographs in Chapter 8, are clear indications of poor maintenance. Future inspections of existing open canopy structures could indicate the need for retrofit and reinforcement of such structures.

REFERENCES

ABNT (1988). Associação Brasileira de Normas Técnicas, NBR-6123-87: Forcas Devidas ao Vento em Edificacoes. Brazil.

AISC (1989). *Manual of Steel Construction, Allowable Stress Design*. AISC. Chicago, Illinois, AISC.

Altman, D. R. (2001). Wind uplift forces on roof canopies. M.Sc. Thesis., Clemson University, Clemson , South Carolina.

Anderson, J. D. (1995). Computational Fluid Dynamics, McGraw-Hill. New York, NY.

ASCE 7 (1998). Minimum Design Loads for Buildings and Other Structures. ASCE. Reston, Virginia, American Society of Civil Engineers.

ASCE 7 (2005). Minimum Design Loads for Buildings and Other Structures. ASCE. Reston, Virginia, American Society of Civil Engineers.

Baker, C. J. (2007). "Wind Engineering-Past, present and future." *Journal of Wind Engineering*

and Industrial Aerodynamics 95: 843-870.

Blocken, B., Stathopoulos, T. and Carmeliet J. (2007). "CFD simulation of the atmospheric boundary layer: wall function problems." Atmospheric Environment 41: 238-252.

Cermak, J. E. (2003). "Wind tunnel development and trends in applications to civil engineering." *Journal of Wind Engineering and Industrial Aerodynamics* 91: 355-370.

Cermak, J. E., Cochran, L.S and Leffler RD (1995). "Wind Tunnel Modeling of the Atmospheric Surface Layer." *Journal of Wind Engineering and Industrial Aerodynamics* 54: 505-513.

Cochran, L.S. (2006). "State of the Art Review of Wind Tunnels." Architectural Science Review 49: 7-16.

Cook, N. (1985). The designer's guide to wind loading of building structures, Building Research Establishment, London, England.

CSI (2009). Computers and Structures, Inc. ETABS v9.5. Berkeley, California.

Davenport, A. G. (2002). "Past, present and future of wind engineering." *Journal of Wind Engineering and Industrial Aerodynamics* 90: 1371-1380.

De Bortoli, M.E., Natalini, B., Paluch, M.J. and Natalini, M.B. (2002). "Part depth wind tunnel

simulations of the atmospheric boundary layer." *Journal of Wind Engineering and Industrial Aerodynamics* 90: 281-291.

Eurocode 1 (2002-2006 Draft). Actions on Structures, Part 1-4, General Actions-Wind Actions, CEN TC 250.

Flomerics (2009). Engineering Fluid Dynamics, EFD.Lab v.9. Marlsborough, Massachusetts, USA.

Ginger, J. D. and Letchford, C.W. (1994). "Wind loads on planar canopy roofs, part 2 fluctuating pressure distribution and correlations." *Journal of Wind Engineering and Industrial Aerodynamics* 51: 353-370.

Godoy, L. and Poitevin, A. (2006). “Damage of Canopies in Gas Stations due to Hurricanes Katrina and Rita. *Proceedings of the Fourth International Latin American and Caribbean Conference for Engineering and Technology*. Mayaguez, Puerto Rico, LACCEI.

Godoy, L.A. (2006), “Identification of structural damage in tanks and industrial facilities due to hurricane Katrina”, Final Report to NSF, Award Number 0553986, University of Puerto Rico, Mayaguez.

Gumley, S. J. (1984). "A parametric study of extreme pressures for the static design of canopy structures." *Journal of Wind Engineering and Industrial Aerodynamics* 16: 43-56.

Hargreaves, D.M. and Wright, N.G. (2007), “On the use of the k-epsilon model in commercial CFD software to model the neutral atmospheric boundary layer”, *Journal of Wind Engineering and Industrial Aerodynamics*, 95, p. 355-369.

Holmes, J. (2001). Wind Loading of Structures, London Press. London, England.

ICBO (1997). Uniform Building Code. ICBO. California, ICBO.

Iizumi, E. (2005). *Wind loads on free-standing canopy roofs*. M. Eng. Thesis. Tohoku University. Tohoku, Japan.

International Building Code (2006), *Structural Engineering Design Provisions*, Chapter 16, International Code Council Inc., Country Club Hills, Illinois.

Irwin, H. P. (1981). "The design of spires for wind simulation." *Journal of Wind Engineering and Industrial Aerodynamics* **7**: 361-366.

Japanese Standard (1987). Building Standard law of Japan, Building Center of Japan. Japan.

Koop, G. A., Surry, D. and Mans, C. (2005). "Wind effect of parapets on low buildings: Part 4. Mitigation of corner loads with alternative geometries." *Journal of Wind Engineering and Industrial Aerodynamics* 93: 873-888.

Koop, G. A., Surry, D. and Mans, C. (2005). "Wind effects on parapets on low buildings: Part 2. Structural loads." *Journal of Wind Engineering and Industrial Aerodynamics* 93: 843-855.

Koop, G. A., Surry, D. and Mans, C. (2005). "Wind effects on parapets on low buildings: Part 1. Basic aerodynamics and local loads." *Journal of Wind Engineering and Industrial Aerodynamics* 93: 817-841.

Lam, K. M. and J. G. Zhao (2002). "Occurence of peak lifting actions on a large horizontal cantilevered roof." *Journal of Wind Engineering and Industrial Aerodynamics* 90: 897-940.

Letchford, C. W., Row, A., Vitale, A. and Wolbers, J. (2000). "Mean wind loads on porous canopy roofs." *Journal of Wind Engineering and Industrial Aerodynamics* 84: 197-213.

Letchford, C. W. and Ginger, J.D. (1992). "Wind loads on planar canopy roofs, part 1 mean pressure distributions." *Journal of Wind Engineering and Industrial Aerodynamics* 45: 25-45.

Liu, H. (1991). *Wind Engineering: A Handbook for Structural Engineers*, Prentice Hall. New Jersey, USA.

Lomax, H. and H. T. Pulliam (1999). Fundamentals of Computational Fluid Dynamics, NASA Ames Research Center. Florida, USA.

Mans, C., Koop A.G. and Surry D. (2005). "Wind effects of parapets on low buildings: Part 3. Parapet loads." *Journal of Wind Engineering and Industrial Aerodynamics* 93: 857-872.

Maplesoft (2008). Maple v11. Ontario, Canada

Natalini, B., Marighetti J. and Natalini M.B. (2002). "Wind tunnel modeling of mean pressures on planar canopy roof." *Journal of Wind Engineering and Industrial Aerodynamics* 90: 427-439.

Natalini B., De Bortoli and Natalini M.B. (1998). Full-depth simulation of a neutrally stable atmospheric boundary layer in a wind tunnel. Proceedings of the Second East European Conference on Wind Engineering, (EECWE'98), Prague, Czech Republic.

Natalini M. B., Canavesio O. and Natalini B. (2002). Pressure distribution on Curved Canopy Roofs. *Second Symposium on Wind and Structures*. Bussan, Korea.

NIST (2006). Performance of Physical Structures in Hurricane Katrina and Hurricane Rita: A Reconnaissance Report. Technical Note 1476. National Institute of Standards and Technologies. Gaithersburg, Maryland.

Paluch, M.J., Loredo-Souza A.M. and Blessmann J. (2003). "Wind loads on attached canopies and their effect on the pressure distribution over arch-roof industrial buildings." *Journal of Wind Engineering and Industrial Aerodynamics* 91: 975-994.

Pindado, S. and J. Meseguer (2003). "Wind tunnel study on the influence of different parapets on the roof pressure distribution of low-rise buildings." *Journal of Wind Engineering and Industrial Aerodynamics* 91: 1133-1139.

Portela, G. (2004). *Wind Pressures and Buckling of Metal Cantilever Tanks*. PhD. Dissertation. Recinto Universitario de Mayaguez. Mayaguez, Puerto Rico.

Robertson, A. P. and Hoxey R. (1985). "A full-scale study of wind loads on agricultural ridged canopy roof structures and proposals for design." *Journal of Wind Engineering and Industrial Aerodynamics* 21: 167-205.

SA (1989b) Minimum Design Loads on Structures – SAA. Loading Code Part 2 - Wind loads AS 1170.2 - 1989 Standards. Australia.

SDGS (2005). Wind Loads on Structures. Standard Design Group Inc. Lubbock, Texas, USA.

Simiu, E. and Miyata, T. (2006). *Design of Buildings and Bridges for Wind*, John Wiley & Sons. New Jersey, USA.

SolidWorks, C. (2009). 3D Cad Software, Concord, Massachusetts, USA.

Stathopoulos, T. and Baskaran, A. (1987). "Wind pressures on flat roofs with parapets." *American Journal of Structural Engineering,* Vol. 113, No. 11: 2166-2180.

Stathopoulos, T. and Saathoff, P. (1991). "Wind pressures on roofs of various geometries." *Journal of Wind Engineering and Industrial Aerodynamics* 38: 273-284.

Stathopoulus, T., Saathoff, P. and Du, X. (2002). "Wind loads on parapets." *Journal of Wind Engineering and Industrial Aerodynamics* 90: 503-514.

Tieleman, H. (2003). "Wind tunnel simulation of wind loading on low-rise structures: a review." *Journal of Wind Engineering and Industrial Aerodynamics* 91: 1627-1649.

Uematsu, Y., Izumi E. and Stathopoulos T. (2007). "Wind Force Coefficients for Designing Free-Standing Canopy Roofs." *Journal of Wind Engineering and Industrial Aerodynamics* 95: 1486-1510.

Uematsu, Y. and Stathopoulos T. (2003). "Wind Loads on Free Standing Canopy Roofs: A Review." *Journal of Wind Engineering and Industrial Aerodynamics* 95: 245-256.

Uematsu Y., Izumi E. and Stathopoulos T. (2008). "Wind loads on free-standing canopy roofs: Part 1 local wind pressures." *Journal of Wind Engineering and Industrial Aerodynamics* 96: (2008): 1015-1028.

Uniform Building Code (1997), *Structural Engineering Design Provisions*. Vol. 2, International Conference of Building Officials, California.

Wittwer A. and Moller, S. (2000). "Characteristics of the low speed wind tunnel of the UNNE." *Journal of Wind Engineering and Industrial Aerodynamics* 84: 307-320.

Zingg, D. (1999). Fundamentals of Computational Fluid Dynamics Studies, NASA Ames Research Center, University of Toronto Institute for Aerospace Studies, Toronto, Canada.

APPENDIX A

EFD.Lab modeling procedure

Several steps are required in order to create an EFD.Lab project, although the specific steps can differ from one project to another. For the cases investigated in this particular research, a step by step description of the procedure for creating an open canopy is as follows;

1) File, New, New document-At this step, it is possible to create a 3D component of an arrangement of components previously created. First we create the roof component as shown in Figure A. .

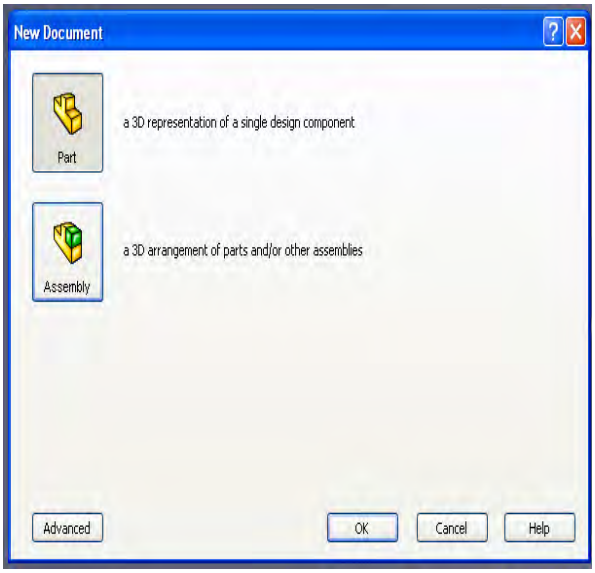

Figure A.1: New document option on EFD.Lab

2) Using the sketch feature, we define an object to be used as the roof of our open canopy. In this particular case, a flat roof surface of 7.6 m (25 ft) x 7.6m (25ft) with 0.15 m (6 in) thickness is defined as shown in Figure A.2. EFD.Lab has built in a program named

Solidworks (SolidWorks 2009). It is used in the program for creating 3D objects that can have properties, like dimensions, thickness and materials, in order to create parts that can be assembled later for the final CFD analysis.

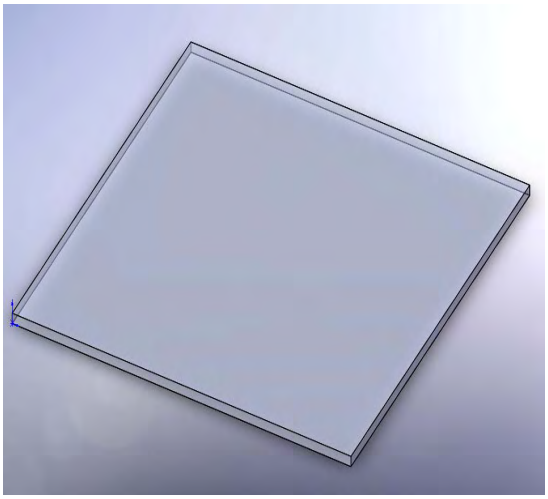

Figure A.2: Roof surface created using EFD.Lab

3) A new component, created with SolidWorks, to be used as the parapet of the open canopy is modeled with the same dimensions of the roof surface. The thickness of the parapet walls is 6 inches. Refer to Figure A.3.

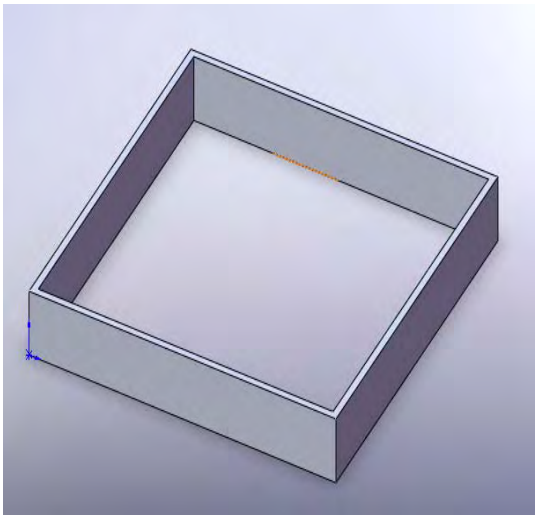

Figure A.3: Parapet element created using EFD.Lab

4) A third component, called an assembly was created using the previously created single parts, that combines the roof surface and the parapet created on the previous steps. This final component to be used in the analysis is shown in Figure A.4.

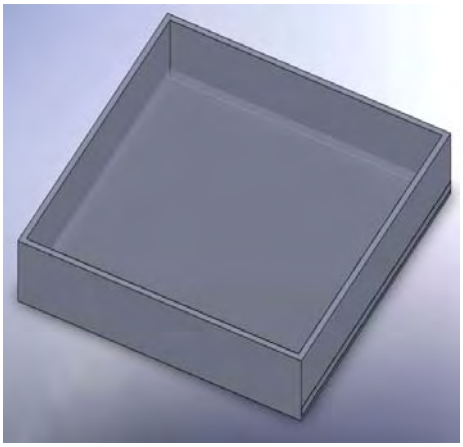

Figure A.4: Canopy model combining roof element and parapet element using EFD.Lab

5) Using the wizard project configuration, the user should specify the Units to used in the analysis, the analysis type (choosing between internal and external flow), default fluid to be used (in this case air), wall conditions, and initial and ambient conditions. With

reference to Figure A.5 through Figure A.8, the parameters for pressure, temperature, wind velocity and turbulence parameters can be included.

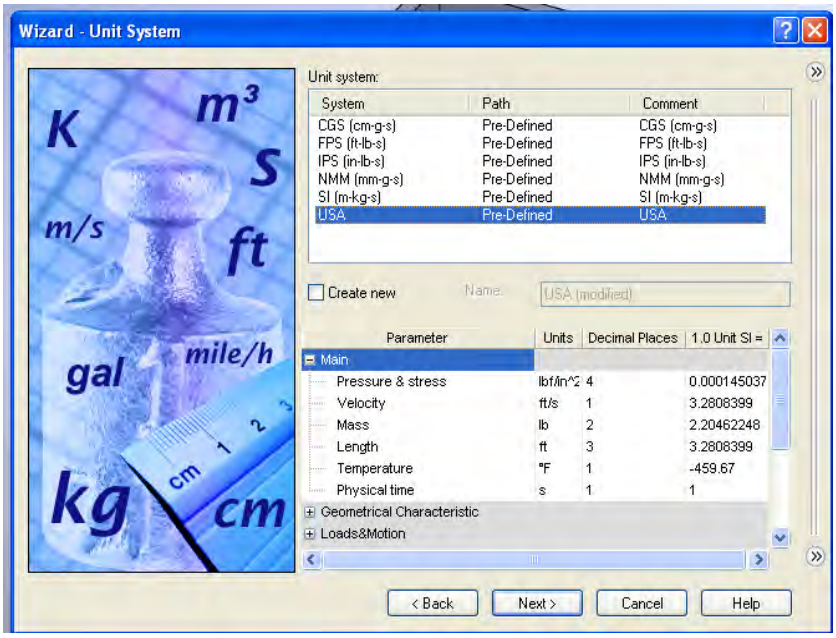

Figure A.5: EFD.Lab unit selection wizard screen.

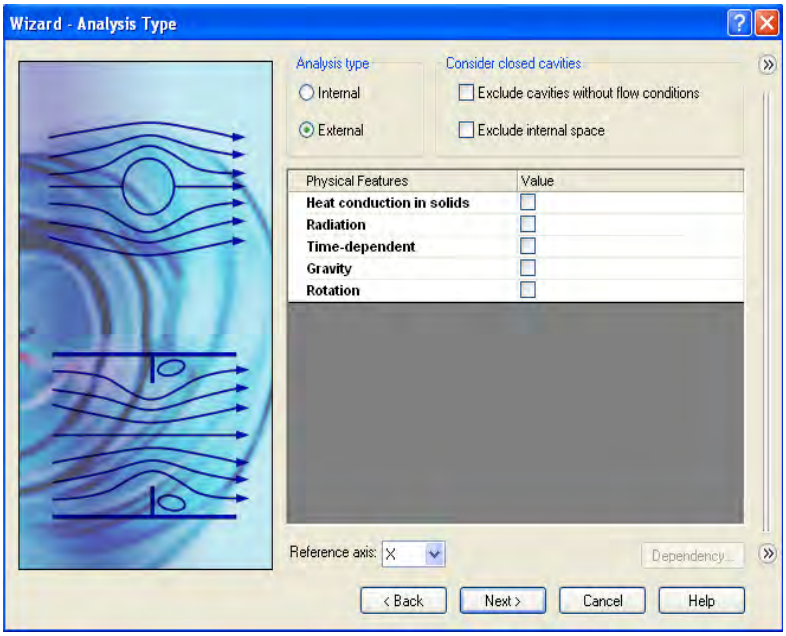

Figure A.6: EFD.Lab screen for input of internal or external analysis.

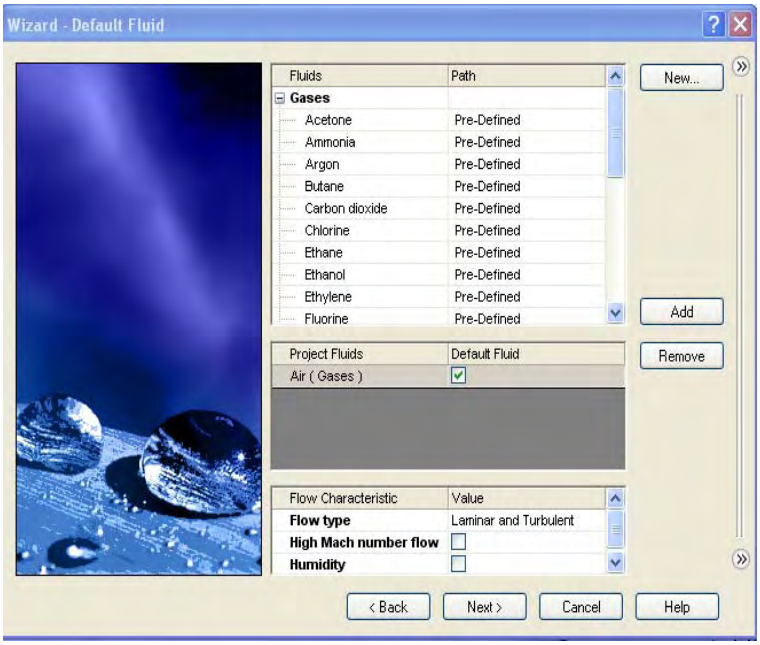

Figure A.7: Fluid type and analysis type on EFD.Lab wizard.

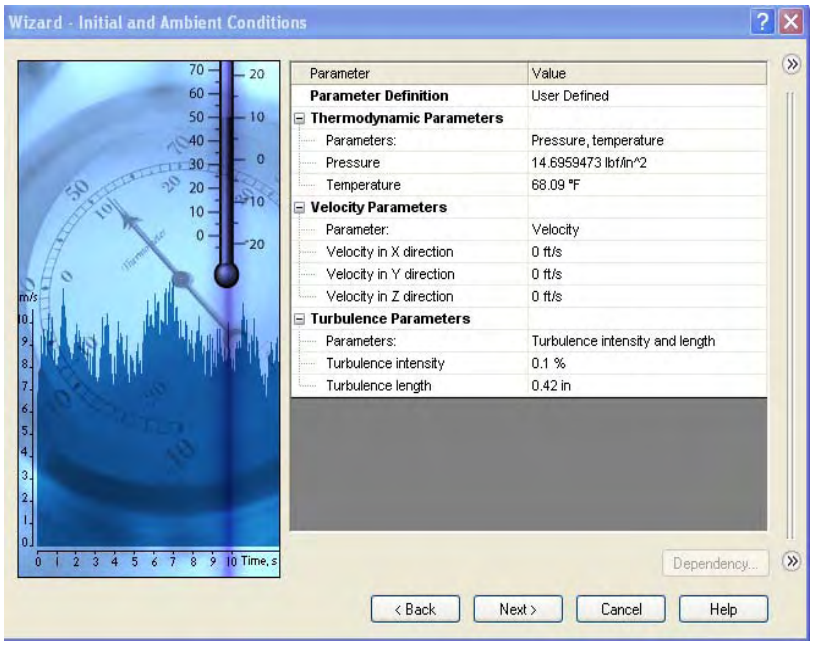

Figure A.8: Initial and ambient conditions in EFD.Lab

6) Results and geometry resolution is the default option that the program uses to mesh the domain. In this option, it is possible to specify the mesh density to be used in the

numerical solution. The program default allows for a quick response of a coarse solution. Further meshing and finer resolutions are changed in the final model for this investigation. Refer to Figure A.9.

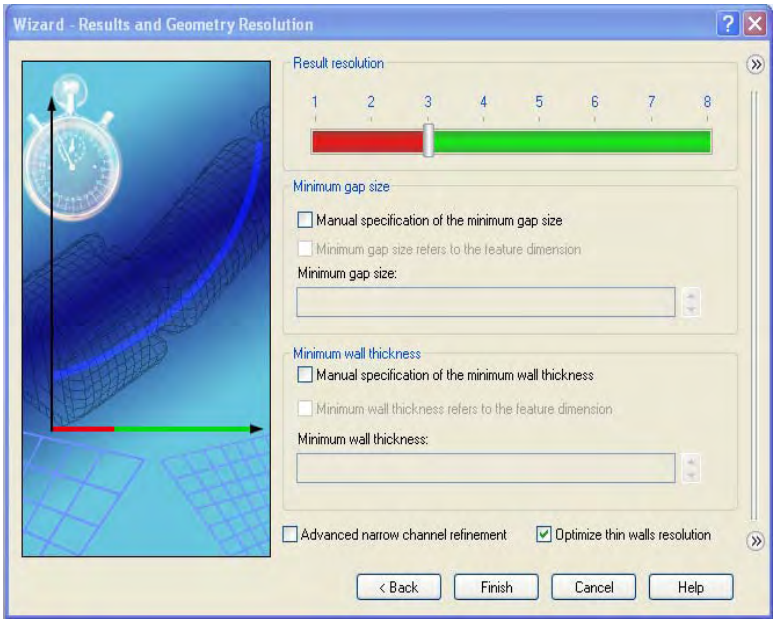

Figure A.9: Default meshing based on the geometry on EFD.Lab.

7) An automatic domain region is created by the program. The program default can be modified to obtain a different sized region. For the current research, the modified simple boundary dimensions in the x, y and z directions respectively, 45.7 m (150 ft), 24.4 m (80 ft) and 25.9 m (85 ft). Refer to Figure A.10.

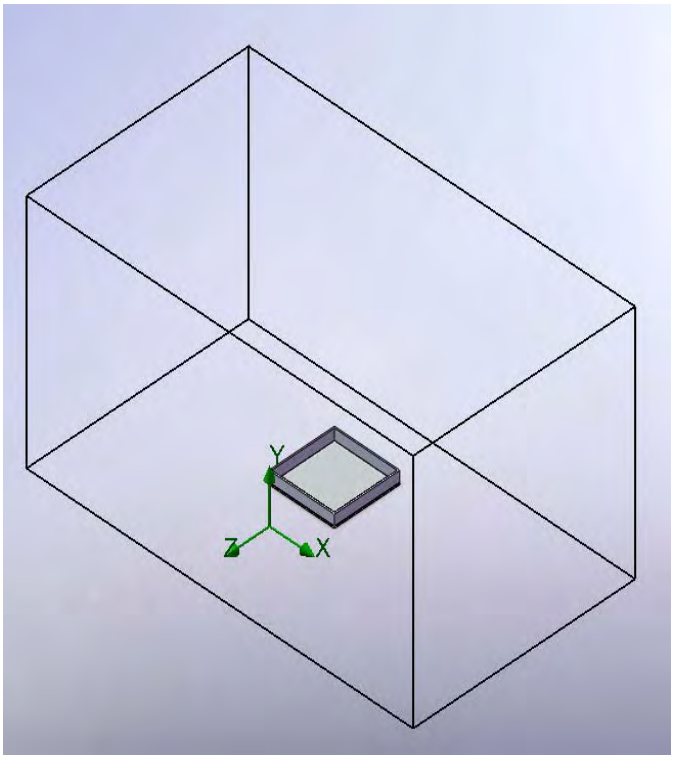

Figure A.10: Model and computational domain in EFD.Lab.

8) At this stage, the model is ready to be analyzed. The required time to solve the mathematical model depends on the size of the domain and the meshing on the cells.

APPENDIX B

Wind tunnel data: Transducer voltage data obtained at the wind tunnel at UNNE for the open canopy with parapets scale model.

Facultad de Ingeniería – UNNE
Túnel de viento "J. P. Gorecki"

PRESIONES MEDIAS EXTERIORES EN TECHO DE MODELO 1 CON PARAPETOS

Fecha 18/02/09 Hora de inicio 9:12

α = 330° Hora de finalización

	Voltaje medio	Temp	Presión atm.	q_{ref}
0		28°	759	
1	3.440			
2	3.424			
3	3.390			
4	3.369			
5	3.349			
6	3.414			
7	3.399			
8	3.365			
9	3.389			
10	3.356			
11	3.337			
12	3.401			
13	3.382			
14	3.433			
15	3.384			
16	3.369			

1

2

α = 30°

	Voltaje medio	Temp	Presión atm.	q_{ref}
0			759	
1	3.340			
2	3.331			
3	3.322			
4	3.324			
5	3.339			
6	3.333			
7	3.326			
8	3.327			
9	3.331			
10	3.326			
11	3.326			
12	3.327			
13	3.330			
14	3.337			
15	3.352			
16	3.325			

3

Facultad de Ingeniería – UNNE
Túnel de viento "J. P. Gorecki"

PRESIONES MEDIAS EXTERIORES EN TECHO DE MODELO 1 CON PARAPETOS

Fecha

Hora de inicio

Hora de finalización 10:59

$\alpha = 210°$

	Voltaje medio	Temp	Presión atm.	q_{ref}
~~0~~				
1	3.552			
2	3.535			
3	3.618			
4	3.523			
5	3.534			
6	3.530			
7	3.509			
8	3.484			
9	3.489			
10	3.459			
11	3.462			
12	3.463			
13	3.448			
14	3.417			
15	3.422			
16	3.415			

4

5

$\alpha = 150$

	Voltaje medio	Temp	Presión atm.	q_{ref}
~~0~~		30°		
1	3.459			
2	3.427			
3	3.423			
4	3.479			
5	3.530			
6	3.491			
7	3.402			
8	3.452			
9	3.383			
10	3.380			
11	3.461			
12	3.358			
13	3.332			
14	3.336			
15	3.370			
16	3.429			

6

Facultad de Ingeniería – UNNE
Túnel de viento "J. P. Gorecki"

Fecha: 18/2/09

Temp. inicial: 28°
Temp. final: 31°

CALIBRACION DE TRANSDUCTOR

PRESION [Pa]	Lecturas [voltios]	
	Inicio	Fin
0	3.459	3.394
20	3.499	3.450
40	3.538	3.488
60	3.577	3.527
-10	3.440	3.392
-20	3.421	3.372
-30	3.401	3.353
-40	3.381	3.333
-50	3.361	3.315

9:00 11:03

Facultad de Ingeniería – UNNE
Túnel de viento "J. P. Gorecki"

Presión dinámica de referencia

Lectura 1	Lectura 2	Lectura 3	Lectura 4	Lectura 5
112	115	113	117	112
109	109	112	105	116
108	112	115	110	114
114	119	112	112	115
112	117	116	110	111
113	114	112	111	113
110	118	115	114	115
109	113	115	116	112
108	112	116	115	115
113	113	117	110	115
116	118	119	113	117
113	122	116	112	118
110	121	117	118	115

- 114 -
- 113 -
- 115 -
- 117 -
- 114 -
- 109 -
- 110 -
- 104 -
- 107 -
- 112 -
- 115 -
- 112 -
- 107 -

PRESIONES MEDIAS INTERIORES SOBRE PARAPETOS DE MODELO I

Fecha 3|25|04 Hora de inicio 10:15

$\alpha = 210°$ Hora de finalización

Temp: $\alpha = 330°$ Pres. atm.: 760.5 mmHg

1	3.641	1	3.409
2	3.653		3.407
3	3.633		3.403
4	3.638		3.397
5	3.636		3.390
6	3.632		3.405
7	3.606		3.403
8	3.663		3.398
9	3.651		3.406
10	3.617		3.408
11	3.673		3.405
12	3.662		3.415
13	3.632		3.413
14	3.656		3.416
15	3.650		3.414
16	3.605		3.415
17	3.592		3.410
18	3.584		3.411 ←3
19	3.533	2	3.405
20	3.534		3.403

T = 30°C

Facultad de Ingeniería – UNNE
Túnel de viento "J. P. Gorecki"

$\alpha = 330°$

1	3.422	
2	3.416	
3	3.438	
4	3.444	
5	3.503	
6	3.511	
7	3.500	
8	3.515	
9	3.526	
10	3.516	
11	3.504	
12	3.506	
13	3.485	
14	3.489	
15	3.481	
16	3.455	
17	3.456	
18	3.447	
19	3.504	← 4
20	3.500	

T = 31°C

Facultad de Ingeniería – UNNE
Túnel de viento "J. P. Gorecki"

Fecha: 3/25/09

Temp. inicial: 25°C
Temp. final: 32°C

CALIBRACION DE TRANSDUCTOR

PRESION [Pa]	Lecturas [voltios]	
	Inicio	Fin
0	3.506	3.511
20	3.546	3.551
40	3.586	3.591
60	3.625	3.631
-10	3.486	3.491
-20	3.466	3.472
-30	3.447	3.452
-40	3.426	3.482
-50	3.406	3.411
	10:15	12:25

Presión dinámica de referencia

Lectura 1	Lectura 2	Lectura 3	Lectura 4	Lectura 5
117	110	105	114	
115	111	109	116	
111	109	107	113	
112	109	112	111	
107	108	114	110	
109	110	113	108	
108	111	110	107	
107	112	108	110	
108	114	115	112	
111	115	108	111	
110	114	112	111	
112	112	114	114	
114	112	107	113	

Facultad de Ingeniería – UNNE
Túnel de viento "J. P. Gorecki"

PRESIONES MEDIAS INTERIORES SOBRE PARAPETOS DE MODELO 1

Fecha 3/23/09 Hora de inicio 16:20

$\alpha = 0°$ Hora de finalización 18:15

Temp: $\alpha = 180°$ Pres. atm.: 757½ mmHg

1	3.431	1	3.556	1
2	3.431		3.546	
3	3.427		3.573	
4	3.434		3.573	
5	3.436		3.563	
6	3.437		3.543	
7	3.439		3.541	
8	3.438		3.567	
9	3.445		3.547	
10	3.443		3.517	
11	3.443		3.583	
12	3.440		3.570	
13	3.436		3.525	
14	3.435		3.556	
15	3.430		3.535	
16	3.425		3.515	
17	3.415		3.491	
18	3.409		3.475	
19	3.426	2	3.455	③
20	3.416		3.445	

$T_2 = 34°C$

Facultad de Ingeniería – UNNE
Túnel de viento "J. P. Gorecki"

$\alpha = 150°$

1	3.655		
2	3.670		
3	3.588		
4	3.596		
5	3.540		
6	3.531		
7	3.491		
8	3.572		
9	3.558		
10	3.524		
11	3.601		
12	3.581		
13	3.543		
14	3.571		
15	3.554		
16	3.533		
17	3482		
18	3.466		
19	3.451	④	
20	3.434		

$T = 32.5°C$

Facultad de Ingeniería – UNNE
Túnel de viento "J. P. Gorecki"

Fecha: 3|23|09

Temp. inicial: 36°C
Temp. final: 32°C

CALIBRACION DE TRANSDUCTOR

PRESION [Pa]	Lecturas [voltios]	
	Inicio	Fin
0	3.516	3.513
20	3.555	3.553
40	3.595	3.593
60	3.635	3.632
-10	3.496	3.493
-20	3.475	3.473
-30	3.455	3.454
-40	3.436	3.433
-50	3.416	3.413

16:10

Presión dinámica de referencia 9 ~~23~~

Lectura 1	Lectura 2	Lectura 3	Lectura 4	Lectura 5
109	109	108	110	
109	110	109	108	
107	108	107	111	
104	110	109	110	
98	113	102	107	
103	112	106	112	
104	111	105	114	
106	111	105	108	
107	106	110	112	
104	105	109	111	
103	108	108	111	
105	104	103	108	
105	102	102	113	

Facultad de Ingeniería – UNNE
Túnel de viento "J. P. Gorecki"

PRESIONES MEDIAS EXTERIORES SOBRE PARAPETOS DE MODELO 1

Fecha 19/03/09

Hora de inicio 18:10

Hora de finalización 19:13

Temp: 31°

Pres. atm.: 761,5

	α=30		α=330°	
0				
1	3.695	1	3.690	
2	3.713		3.702	
3	3.705		3.693	
4	3.724		3.703	
5	3.688		3.639	
6	3.731		3.670	
7	3.725		3.666	
8	3.696		3.604	
9	3.747		3.624	
10	3.753		3.627	
11	3.563		3.368	
12	3.578		3.370	
13	3.577		3.368	
14	3.569		3.360	
15	3.592		3.360	
16	3.581		3.356	
17	3.578		3.392	
18	3.582		3.393	
19	3.586		3.417	
20	3.587	2	3.416	3

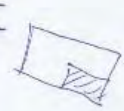

761,5 mm Hg

Facultad de Ingeniería – UNNE
Túnel de viento "J. P. Gorecki"

Fecha: 19/03/09

Temp. inicial: 31°
Temp. final: 28°

CALIBRACION DE TRANSDUCTOR

PRESION [Pa]	Lecturas [voltios]	
	Inicio	Fin
0	3.513	3.512
20	3.554	3.552
40	3.593	3.592
60	3.633	3.632
-10	3.494	3.492
-20	3.474	3.472
-30	3.454	3.452
-40	3.434	3.433
-50	3.415	3.413
	18:00	19:20

Presión dinámica de referencia

Lectura 1	Lectura 2	Lectura 3	Lectura 4	Lectura 5
108	116	111		
108	111	111		
111	105	116		
113	109	110		
116	110	114		
110	108	110		
107	105	113		
105	107	114		
102	110	115		
107	111	113		
105	109	113		
104	109	108		
108	113	112		

Facultad de Ingeniería – UNNE
Túnel de viento "J. P. Gorecki"

PRESIONES MEDIAS EXTERIORES SOBRE PARAPETOS DE MODELO 1

Fecha 19/03/09

Hora de inicio : 9:10

Hora de finalización

Temp: 23°

Pres. atm.: 763,5

	α = 0°		α = 180°	
0				
1	3.743	1	3.449	
2	3.760		3.450	
3	3.748		3.455	
4	3.751		3.448	
5	3.699		3.445	
6	3.745		3.444	
7	3.730		3.445	
8	3.678		3.440	
9	3.722		3.438	
10	3.723		3.431	
11	3.303		3.485	
12	3.295		3.487	
13	3.307		3.481	
14	3.365		3.494	
15	3.350		3.499	
16	3.351		3.493	
17	3.466		3.500	
18	3.455		3.505	
19	3.486		3.499	
20	3.482	2	3.499	3

Facultad de Ingeniería – UNNE
Túnel de viento "J. P. Gorecki"

	$\alpha = 150°$		$\alpha = 210°$
0			
1	3.407		3.435
2	3.403		3.435
3	3.401		3.444
4	3.399		3.444
5	3.383		3.461
6	3.377		3.462
7	3.369		3.456
8	3.381		3.457
9	3.371		3.457
10	3.372		3.452
11	3.515		3.456
12	3.526		3.459
13	3.526		3.456
14	3.543		3.454
15	3.562		3.456
16	3.549		3.452
17	3.576		3.445
18	3.591		3.441
19	3.580		3.437
20	3.588	4	3.437 5

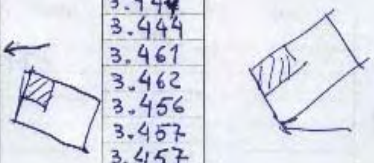

764 mm Hg

Facultad de Ingeniería – UNNE
Túnel de viento "J. P. Gorecki"

ANALISIS DE ERROR EN LECTURAS DE PRESIÓN

TOMA N°: 16 $\alpha = 210°$

~~Inicio~~ Fin

	Voltaje medio	Temp	Presión atm.	q_{ref}
1	3.453			
2	3.451			
3	3.449			
4	3.451			
5	3.447			
6	3.450			
7	3.453			
8	3.448			
9	3.449			
10	3.446			

5

TOMA N°: 2 $\alpha = 0°$

~~Inicio~~ Fin

	Voltaje medio	Temp	Presión atm.	q_{ref}
1	3.759			
2	3.749			
3	3.764			
4	3.790			
5	3.759			
6	3.761			
7	3.780			
8	3.772			
9	3.770			
10	3.758			

5

Facultad de Ingeniería – UNNE
Túnel de viento "J. P. Gorecki"

Fecha: 19/03/09

Temp. inicial: 23°
Temp. final: 27°

CALIBRACION DE TRANSDUCTOR

PRESION [Pa]	Lecturas [voltios]	
	Inicio	Fin
0	3.507	3.507
20	3.548	3.547
40	3.588	3.587
60	3.627	3.627
-10	3.488	3.487
-20	3.468	3.467
-30	3.448	3.447
-40	3.428	3.427
-50	3.408	3.407
	8:50	11:15

Presión dinámica de referencia

Lectura 1	Lectura 2	Lectura 3	Lectura 4	Lectura 5
106	112	110	109	112
108	108	107	111	107
111	111	109	112	111
112	109	113	116	110
108	112	115	113	107
111	116	115	114	105
114	115	112	116	111
117	119	114	112	108
115	114	112	110	109
108	113	108	109	109
110	116	109	107	108
112	115	116	106	105
116	113	111	109	105

Facultad de Ingeniería – UNNE
Túnel de viento "J. P. Gorecki"

PRESIONES MEDIAS INTERIORES MODELO 1 SIN PARAPETOS

Fecha 05/03/09

Hora de inicio 10:17

Hora de finalización 11:25

Temp: 26°

Pres. atm.: 762

	α = 30		α = 330	
0				
1	3.503	1	3.427	2
2	3.419		3.411	
3	3.419		3.414	
4	3.426		3.389	
5	3.451		3.385	
6	3.514		3.476	
7	3.515		3.477	
8	3.500		3.483	
9	3.475		3.493	
10	3.521		3.506	
11	3.518		3.510	
12	3.480		3.497	
13	3.518		3.505	
14	3.498		3.503	
15	3.514		3.514	
16	3.517		3.506	

	α = 210	
0		
1	3.503	3
2	3.504	
3	3.502	
4	3.502	
5	3.500	
6	3.504	
7	3.507	
8	3.507	
9	3.506	
10	3.507	
11	3.506	
12	3.503	
13	3.509	
14	3.511	
15	3.511	
16	3.519	4

Facultad de Ingeniería – UNNE
Túnel de viento "J. P. Gorecki"

Fecha: 05/03/09

Temp. inicial: 26°
Temp. final: 27°

CALIBRACION DE TRANSDUCTOR

PRESION [Pa]	Lecturas [voltios]	
	Inicio	Fin
0	3.506	3.507
20	3.546	3.547
40	3.586	3.587
60	3.626	3.626
-10	3.486	3.487
-20	3.466	3.467
-30	3.447	3.447
-40	3.426	3.427
-50	3.406	3.408
	10:08	11:26

Presión dinámica de referencia

Lectura 1	Lectura 2	Lectura 3	Lectura 4	Lectura 5
106	108	106	111	
108	109	105	112	
113	113	107	110	
112	112	110	112	
110	113	109	108	
108	114	110	112	
112	111	111	116	
116	106	113	112	
112	107	110	115	
113	111	109	111	
109	111	108	109	
106	114	111	108	
107	109	110	106	

Facultad de Ingeniería – UNNE
Túnel de viento "J. P. Gorecki"

PRESIONES MEDIAS INTERIORES MODELO 1 SIN PARAPETOS

Fecha 04/03/09

Hora de inicio 10:41
Hora de finalización 11:50

Temp: 32°

Pres. atm.: 757

	α = 0°		α = 0	
0				
1	4.508	1	3.438	1
2	4.506		3.409	
3	4.5		3.428	←
4			3.408	
5			3.403	←
6			3.514	
7			3.506	
8			3.496	
9			3.509	
10			3.517	
11			3.519	
12			3.510	
13			3.518	
14			3.520	
15			3.518	
16			3.515	

	α = 180°		α = 180°	
0				
1	3.497	2	3.456	
2	3.498		3.480	
3	3.500		3.495	
4	3.501		3.498	
5	3.493		3.498	
6	3.506		3.455	
7	3.506		3.482	
8	3.511		3.511	
9	3.506		3.465	
10	3.513		3.507	
11	3.519		3.516	
12	3.507		3.446	←
13	3.515		3.496	
14	3.506		3.452	←
15	3.517		3.519	
16	3.519	3	3.513	4

35°

Facultad de Ingeniería – UNNE
Túnel de viento "J. P. Gorecki"

Fecha: 04/03/09

Temp. inicial: 32°
Temp. final: 35°

CALIBRACION DE TRANSDUCTOR

PRESION [Pa]	Lecturas [voltios]	
	Inicio	Fin
0	3.510	3.516
20	3.551	3.556
40	3.590	3.596
60	3.630	3.636
-10	3.490	3.497
-20	3.471	3.477
-30	3.451	3.457
-40	3.431	3.437
-50	3.411	3.416
	10:30	12:00

Presión dinámica de referencia

Lectura 1	Lectura 2	Lectura 3	Lectura 4	Lectura 5
102	105	106	107	
100	103	104	106	
108	101	108	104	
105	102	108	107	
100	109	107	108	
104	106	104	100	
103	102	105	100	
106	99	100	105	
102	104	103	102	
108	105	107	108	
101	107	104	104	
107	106	102	105	
103	101	106	103	

Facultad de Ingeniería – UNNE
Túnel de viento "J. P. Gorecki"

PRESIONES MEDIAS INTERIORES EN TECHO DE MODELO 1 CON PARAPETOS

Fecha 02/03/09 Hora de inicio 17:20

Hora de finalización

Temp: 34° Pres. atm.: 759

	α=330		α=30
0			
1	3.361	1	3.460
2	3.357		3.249
3	3.341		3.185
4	3.332		3.239
5	3.297		3.301
6	3.381		3.481
7	3.368		3.478
8	3.344		3.342
9	3.396		3.411
10	3.406		3.501
11	3.399		3.483
12	3.439		3.377
13	3.448		3.496
14	3.472		3.400
15	3.470		3.492
16	3.491	2	3.504 3

	α=210
0	
1	3.483
2	3.483
3	3.480
4	3.473
5	3.465
6	3.485
7	3.489
8	3.484
9	3.484
10	3.495
11	3.487
12	3.482
13	3.494
14	3.482
15	3.495
16	3.505 4

Facultad de Ingeniería – UNNE
Túnel de viento "J. P. Gorecki"

Fecha: 02/03/09

Temp. inicial: 34°
Temp. final: 34°

CALIBRACION DE TRANSDUCTOR

PRESION [Pa]	Lecturas [voltios]	
	Inicio	Fin
0	3.513	3.514
20	3.553	3.553
40	3.592	3.594
60	3.632	3.633
-10	3.493	3.494
-20	3.472	3.474
-30	3.453	3.454
-40	3.433	3.435
-50	3.413	3.415
	17:15	18:42

Presión dinámica de referencia

Lectura 1	Lectura 2	Lectura 3	Lectura 4	Lectura 5
104	106	108	109	
107	108	109	115	
103	109	107	113	
107	105	110	116	
109	109	111	114	
106	111	108	114	
101	109	112	113	
108	107	113	107	
108	111	107	105	
106	109	112	103	
108	110	112	106	
105	106	113	105	
106	108	113	107	

Facultad de Ingeniería – UNNE
Túnel de viento "J. P. Gorecki"

PRESIONES MEDIAS INTERIORES EN TECHO DE MODELO 1 CON PARAPETOS

Fecha 2/03/09 Hora de inicio 10:25
Hora de finalización 11:33
Temp: 29° Pres. atm.: ~~7~~60,5

	α=0		α=180°	
~~0~~				
1	3.278	1	3.475	
2	3.280		3.473	
3	3.290		3.474	
4	3.298		3.474	
5	3.311		3.475	
6	3.350		3.475	
7	3.324		3.482	
8	3.312		3.487	
9	3.340		3.487	
10	3.397		3.487	
11	3.370		3.493	
12	3.476		3.491	
13	3.466		3.497	
14	3.496		3.486	
15	3.472		3.501	
16	3.464	2	3.497	3

STBL

Wind

	α=150°	
0		
1	3.393	
2	3.397	
3	3.438	
4	3.449	
5	3.455	
6	3.386	
7	3.389	
8	3.475	
9	3.391	
10	3.472	
11	3.490	
12	3.385	
13	3.426	
14	3.377	
15	3.493	
16	3.486	4

760,5

Facultad de Ingeniería – UNNE
Túnel de viento "J. P. Gorecki"

Fecha: 02/03/09

Temp. inicial: 29°
Temp. final: 29°

CALIBRACION DE TRANSDUCTOR

PRESION [Pa]	Lecturas [voltios]	
	Inicio	Fin
0	3.508	3.508
20	3.548	3.549
40	3.588	3.588
60	3.628	3.629
-10	3.488	3.488
-20	3.469	3.469
-30	3.449	3.449
-40	3.429	3.429
-50	3.409	3.409
	10:15	11:38

Presión dinámica de referencia

Lectura 1	Lectura 2	Lectura 3	Lectura 4	Lectura 5
107	106	104	109	
105	110	106	106	
103	105	103	105	
106	105	108	104	
105	107	106	102	
104	107	110	101	
108	109	108	103	
105	107	103	111	
101	108	101	109	
109	106	106	106	
108	105	105	104	
104	105	105	104	
107	104	108	105	

Facultad de Ingeniería – UNNE
Túnel de viento "J. P. Gorecki"

PRESIONES MEDIAS EXTERIORES EN TECHO DE MODELO 1 CON PARAPETOS

Fecha 26/02/09

Hora de inicio

Hora de finalización 19:15

Temp: 32

Pres. atm.: 758,5

	$\alpha = 150°$		$\alpha = 210°$	
0				
1	3.575	1	3.650	
2	3.537		3.630	
3	3.538		3.624	
4	3.588		3.620	
5	3.637		3.638	
6	3.546		3.636	
7	3.511		3.598	
8	3.565		3.588	
9	3.498		3.597	
10	3.500		3.562	
11	3.574		3.564	
12	3.476		3.559	
13	3.461		3.556	
14	3.445		3.521	
15	3.480		3.523	
16	3.548	2	3.510	3

Inestable

$P_{atm} = 758,5$

Facultad de Ingeniería – UNNE
Túnel de viento "J. P. Gorecki"

Fecha: 26/02/09

Temp. inicial: 32°
Temp. final: 31°

CALIBRACION DE TRANSDUCTOR

PRESION [Pa]	Lecturas [voltios]	
	Inicio	Fin
0	3.510	3.511
20	3.550	3.551
40	3.590	3.590
60	3.630	3.631
-10	3.490	3.491
-20	3.471	3.471
-30	3.451	3.452
-40	3.431	3.432
-50	3.411	3.412
	18:22	19:17

Presión dinámica de referencia

Lectura 1	Lectura 2	Lectura 3	Lectura 4	Lectura 5
110	109	109		
107	108	109		
112	106	111		
107	107	112		
109	111	111		
105	111	110		
108	108	114		
109	113	110		
107	114	110		
111	100	115		
113	115	116		
117	113	115		
114	112	112		

Facultad de Ingeniería – UNNE
Túnel de viento "J. P. Gorecki"

PRESIONES MEDIAS EXTERIORES EN TECHO DE MODELO 1 CON PARAPETOS

Fecha 26/02/09
Hora de inicio: 9:40
Hora de finalización 11:11
Temp: 25°
Pres. atm.: 760.5

	α = 0		α = 180	
0				
1	3.428	1	3.575	
2	3.419		3.563	
3	3.414		3.590	
4	3.411		3.586	
5	3.409		3.562	
6	3.417		3.538	
7	3.409		3.521	
8	3.408		3.531	
9	3.408		3.508	
10	3.402		3.512	
11	3.393		3.490	
12	3.403		3.479	
13	3.394		3.480	
14	3.409		3.440	
15	3.401		3.465	
16	3.391	2	3.443	3

	α = 30°		α = 330	
0				
1	3.398		3.495	
2	3.389		3.478	
3	3.387		3.442	
4	3.389		3.431	
5	3.400		3.405	
6	3.390		3.472	
7	3.382		3.455	
8	3.389		3.450	
9	3.390		3.419	
10	3.384		3.443	
11	3.384		3.417	
12	3.389		3.443	
13	3.390		3.429	
14	3.409		3.490	
15	3.416		3.431	
16	3.429	4	3.424	5

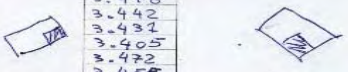

761 mm Hg

Facultad de Ingeniería – UNNE
Túnel de viento "J. P. Gorecki"

Fecha: 26/02/09

Temp. inicial: 25°
Temp. final: 28°

CALIBRACION DE TRANSDUCTOR

PRESION [Pa]	Lecturas [voltios]	
	Inicio	Fin
0	3.505	3.507
20	3.545	3.546
40	3.585	3.586
60	3.625	3.627
-10	3.486	3.487
-20	3.466	3.467
-30	3.446	3.447
-40	3.427	3.427
-50	3.407	3.407

9:29

Presión dinámica de referencia

Lectura 1	Lectura 2	Lectura 3	Lectura 4	Lectura 5
115	112	117	118	114
113	111	116	118	110
114	112	119	115	111
113	117	118	118	115
124	116	120	114	116
115	118	114	121	114
118	118	118	120	109
116	116	108	116	112
121	110	113	113	119
120	119	120	114	116
118	117	121	111	112
120	119	119	110	114
117	116	115	112	112

Facultad de Ingeniería – UNNE
Túnel de viento "J. P. Gorecki"

PRESIONES MEDIAS EXTERIORES EN MODELO 1 SIN PARAPETOS

Fecha 25/02/09 Hora de inicio 17:12
Hora de finalización 18:56
Temp: 31 Pres. atm.: 760,5

	α = 30°		α = 330	
0				
1	3.509	1	3.445	
2	3.476		3.441	
3	3.477		3.444	
4	3.463		3.430	
5	3.458		3.424	
6	3.505		3.489	
7	3.512		3.486	
8	3.507		3.489	
9	3.494		3.493	
10	3.516		3.501	
11	3.514		3.504	
12	3.487		3.497	
13	3.516		3.505	
14	3.492		3.497	
15	3.517		3.507	
16	3.515	2	3.506	3

	α = 150		α = 210	
0				
1	3.465		3.505	
2	3.479		3.502	
3	3.490		3.506	
4	3.491		3.507	
5	3.496		3.506	
6	3.470		3.508	
7	3.989		3.507	
8	3.500		3.510	
9	3.475		3.508	
10	3.502		3.511	
11	3.505		3.512	
12	3.474		3.508	
13	3.495		3.508	
14	3.465		3.506	
15	3.508		3.512	
16	3.507	4	3.511	5

Patm = 760

Facultad de Ingeniería – UNNE
Túnel de viento "J. P. Gorecki"

Fecha: 25/02/09

Temp. inicial: 31°
Temp. final: 31°

CALIBRACION DE TRANSDUCTOR

PRESION [Pa]	Lecturas [voltios]	
	Inicio	Fin
0	3.509	3.510
20	3.548	3.550
40	3.588	3.590
60	3.628	3.630
-10	3.488	3.490
-20	3.468	3.470
-30	3.449	3.451
-40	3.429	3.431
-50	3.409	3.410
	16:44	18:57

Presión dinámica de referencia

Lectura 1	Lectura 2	Lectura 3	Lectura 4	Lectura 5
108	107	110	111	111
107	105	108	112	108
112	107	112	114	115
108	109	112	109	116
106	105	110	110	114
107	111	107	117	114
109	107	106	112	117
107	112	110	105	115
110	107	108	106	114
111	111	107	109	112
110	104	103	111	119
111	106	103	112	117
107	103	105	111	112

Facultad de Ingeniería – UNNE
Túnel de viento "J. P. Gorecki"

PRESIONES MEDIAS EXTERIORES EN MODELO 1 SIN PARAPETOS

Fecha 25/02/09

Hora de inicio 10:30

Hora de finalización 11:35

Temp: 25° 27

Pres. atm.: 763 mm Hg 763

	α=0		α=180	
0			3.487	
1	3.452	1	3.487	
2	3.432		3.491	
3	3.444		3.492	
4	3.428			
5	3.411		3.496	
6	3.492		3.496	
7	3.487		3.496	
8	3.486		3.500	
9	3.495		3.497	
10	3.502		3.504	
11	3.501		3.503	
12	3.498		3.500	
13	3.503		3.505	
14	3.493		3.499	
15	3.505		3.507	
16	3.503	2	3.506	3

Facultad de Ingeniería – UNNE
Túnel de viento "J. P. Gorecki"

Fecha: 25/02/09

Temp. inicial: 25°
Temp. final: 27°

CALIBRACION DE TRANSDUCTOR

PRESION [Pa]	Lecturas [voltios]	
	Inicio	Fin
0	3.506	3.506
20	3.546	3.546
40	3.586	3.586
60	3.625	3.626
-10	3.486	3.486
-20	3.466	3.466
-30	3.446	3.446
-40	3.425	3.426
-50	3.406	3.406

10:28 11:35

Facultad de Ingeniería – UNNE
Túnel de viento "J. P. Gorecki"

Presión dinámica de referencia

Lectura 1	Lectura 2	Lectura 3	Lectura 4	Lectura 5
116	116	112		
114	116	111		
111	114	115		
117	116	113		
114	117	115		
110	115	114		
112	118	114		
111	115	115		
114	111	116		
113	116	114		
119	117	117		
117	118	119		
116	114	115		

APPENDIX C

Open canopy without parapets: spreadsheet calculations.

Presiones exteriores, interiores y totales en Modelo1

Sin parapetos

$\alpha = 0$

Presiones exteriores					Presiones interiores					Presiones netas
Toma	Potencial [V]	Pres.Dif.[Pa]	q_{ref} [Pa]	c_e	Toma	Potencial [V]	Pres.Dif.[Pa]	q_{ref} [Pa]	c_i	c
1	3.452	-27	114.2	-0.2	1	3.438	-38	103.8	-0.4	0.1
2	3.432	-37	114.3	-0.3	2	3.409	-52	103.8	-0.5	0.2
3	3.444	-31	114.3	-0.3	3	3.428	-43	103.8	-0.4	0.1
4	3.428	-39	114.4	-0.3	4	3.408	-53	103.8	-0.5	0.2
5	3.411	-47	114.5	-0.4	5	3.407	-53	103.8	-0.5	0.1
6	3.492	-7	114.6	-0.1	6	3.514	0	103.8	0.0	-0.1
7	3.487	-9	114.7	-0.1	7	3.506	-4	103.8	0.0	0.0
8	3.486	-10	114.8	-0.1	8	3.496	-9	103.8	-0.1	0.0
9	3.495	-5	114.9	0.0	9	3.509	-2	103.8	0.0	0.0
10	3.502	-2	115.0	0.0	10	3.517	2	103.8	0.0	0.0
11	3.501	-2	115.1	0.0	11	3.519	3	103.8	0.0	0.0
12	3.498	-4	115.2	0.0	12	3.51	-2	103.8	0.0	0.0
13	3.503	-1	115.3	0.0	13	3.518	2	103.8	0.0	0.0
14	3.493	-6	115.4	-0.1	14	3.52	3	103.8	0.0	-0.1
15	3.505	0	115.5	0.0	15	3.518	2	103.8	0.0	0.0
16	3.505	0	115.6	0.0	16	3.515	1	103.8	0.0	0.0

Presiones exteriores, interiores y totales en Modelo1

Sin parapetos

$\alpha = 180$

Presiones exteriores					Presiones interiores					Presiones netas
Toma	Potencial [ ]	Pres.Dif.[Pa]	q_{ref} [Pa]	c_e	Toma	Potencial [ ]	Pres.Dif.[Pa]	q_{ref} [Pa]	c_i	c
1	3.487	-9	115.6	-0.1	1	3.497	-8	103.8	-0.1	0.0
2	3.487	-9	115.5	-0.1	2	3.498	-8	103.9	-0.1	0.0
3	3.491	-7	115.5	-0.1	3	3.5	-7	104.0	-0.1	0.0
4	3.492	-7	115.4	-0.1	4	3.501	-6	104.1	-0.1	0.0
5	3.496	-5	115.3	0.0	5	3.493	-10	104.1	-0.1	0.1
6	3.496	-5	115.3	0.0	6	3.506	-4	104.2	0.0	0.0
7	3.496	-5	115.2	0.0	7	3.506	-4	104.3	0.0	0.0
8	3.5	-3	115.1	0.0	8	3.511	-1	104.3	0.0	0.0
9	3.497	-4	115.1	0.0	9	3.506	-4	104.4	0.0	0.0
10	3.504	-1	115.0	0.0	10	3.513	0	104.5	0.0	0.0
11	3.503	-1	114.9	0.0	11	3.514	0	104.6	0.0	0.0
12	3.5	-3	114.9	0.0	12	3.507	-3	104.6	0.0	0.0
13	3.505	0	114.8	0.0	13	3.515	1	104.7	0.0	0.0
14	3.499	-3	114.7	0.0	14	3.506	-4	104.8	0.0	0.0
15	3.507	1	114.7	0.0	15	3.517	2	104.9	0.0	0.0
16	3.506	0	114.6	0.0	16	3.519	3	104.9	0.0	0.0

Presiones exteriores, interiores y totales en Modelo1

Sin parapetos

$\alpha = 30$

Presiones exteriores					Presiones interiores					Presiones netas
Toma	Potencial [ ]	Pres.Dif.[Pa]	q_{ref} [Pa]	c_e	Toma	Potencial [ ]	Pres.Dif.[Pa]	q_{ref} [Pa]	c_i	c
1	3.504	-3	108.7	0.0	1	3.503	-2	110.2	0.0	0.0
2	3.476	-17	108.6	-0.2	2	3.419	-44	110.2	-0.4	0.2
3	3.477	-16	108.5	-0.1	3	3.419	-44	110.2	-0.4	0.2
4	3.463	-23	108.4	-0.2	4	3.426	-40	110.2	-0.4	0.2
5	3.458	-26	108.3	-0.2	5	3.451	-28	110.3	-0.3	0.0
6	3.505	-2	108.2	0.0	6	3.514	4	110.3	0.0	-0.1
7	3.512	1	108.1	0.0	7	3.515	4	110.3	0.0	0.0
8	3.507	-1	108.0	0.0	8	3.5	-3	110.4	0.0	0.0
9	3.494	-8	107.9	-0.1	9	3.475	-16	110.4	-0.1	0.1
10	3.516	3	107.8	0.0	10	3.521	7	110.4	0.1	0.0
11	3.514	2	107.7	0.0	11	3.518	6	110.5	0.1	0.0
12	3.487	-11	107.6	-0.1	12	3.48	-13	110.5	-0.1	0.0
13	3.516	3	107.5	0.0	13	3.518	6	110.5	0.1	0.0
14	3.492	-9	107.4	-0.1	14	3.498	-4	110.6	0.0	0.0
15	3.517	4	107.3	0.0	15	3.514	4	110.6	0.0	0.0
16	3.515	3	107.2	0.0	16	3.517	5	110.6	0.0	0.0

Sin parapetos

α = 330

Presiones exteriores					Presiones interiores					Presiones netas
Toma	Potencial [ ]	Pres.Dif.[Pa]	q_{ref} [Pa]	c_e	Toma	Potencial [ ]	Pres.Dif.[Pa]	q_{ref} [Pa]	c_i	c
1	3.445	-32	107.2	-0.3	1	3.427	-40	110.6	-0.4	0.1
2	3.441	-34	107.3	-0.3	2	3.411	-48	110.5	-0.4	0.1
3	3.444	-33	107.3	-0.3	3	3.414	-46	110.4	-0.4	0.1
4	3.43	-40	107.3	-0.4	4	3.389	-59	110.3	-0.5	0.2
5	3.424	-43	107.4	-0.4	5	3.385	-61	110.2	-0.6	0.2
6	3.484	-13	107.4	-0.1	6	3.476	-15	110.1	-0.1	0.0
7	3.486	-12	107.4	-0.1	7	3.477	-15	110.0	-0.1	0.0
8	3.489	-10	107.5	-0.1	8	3.483	-12	109.9	-0.1	0.0
9	3.493	-8	107.5	-0.1	9	3.493	-7	109.8	-0.1	0.0
10	3.501	-4	107.6	0.0	10	3.506	0	109.7	0.0	0.0
11	3.504	-3	107.6	0.0	11	3.51	2	109.6	0.0	0.0
12	3.497	-6	107.6	-0.1	12	3.497	-5	109.5	0.0	0.0
13	3.505	-2	107.7	0.0	13	3.505	-1	109.4	0.0	0.0
14	3.497	-6	107.7	-0.1	14	3.503	-2	109.3	0.0	0.0
15	3.507	-1	107.7	0.0	15	3.514	4	109.3	0.0	0.0
16	3.506	-2	107.8	0.0	16	3.506	0	109.2	0.0	0.0

Sin parapetos

α = 210

Presiones exteriores					Presiones interiores					Presiones netas
Toma	Potencial [ ]	Pres.Dif.[Pa]	q_{ref} [Pa]	c_e	Toma	Potencial [ ]	Pres.Dif.[Pa]	q_{ref} [Pa]	c_i	c
1	3.505	-2	110.7	0.0	1	3.503	-2	109.2	0.0	0.0
2	3.502	-4	110.9	0.0	2	3.504	-1	109.3	0.0	0.0
3	3.506	-2	111.2	0.0	3	3.502	-2	109.4	0.0	0.0
4	3.507	-1	111.4	0.0	4	3.502	-2	109.5	0.0	0.0
5	3.506	-2	111.6	0.0	5	3.5	-3	109.6	0.0	0.0
6	3.508	-1	111.8	0.0	6	3.504	-1	109.7	0.0	0.0
7	3.507	-1	112.1	0.0	7	3.507	0	109.9	0.0	0.0
8	3.51	0	112.3	0.0	8	3.507	0	110.0	0.0	0.0
9	3.508	-1	112.5	0.0	9	3.506	0	110.1	0.0	0.0
10	3.511	1	112.8	0.0	10	3.507	0	110.2	0.0	0.0
11	3.512	1	113.0	0.0	11	3.506	0	110.3	0.0	0.0
12	3.508	-1	113.2	0.0	12	3.503	-2	110.5	0.0	0.0
13	3.508	-1	113.5	0.0	13	3.509	1	110.6	0.0	0.0
14	3.506	-2	113.7	0.0	14	3.511	2	110.7	0.0	0.0
15	3.512	1	113.9	0.0	15	3.511	2	110.8	0.0	0.0
16	3.511	1	114.2	0.0	16	3.519	6	110.9	0.1	0.0

Presiones exteriores, interiores y totales en Modelo1

Sin parapetos

$\alpha = 150$

Presiones exteriores					Presiones interiores					Presiones netas
Toma	Potencial [ ]	Pres.Dif.[Pa]	q_{ref} [Pa]	c_e	Toma	Potencial [ ]	Pres.Dif.[Pa]	q_{ref} [Pa]	c_i	c
1	3.465	-22	107.8	-0.2	1	3.456	-29	104.9	-0.3	0.1
2	3.479	-15	108.0	-0.1	2	3.48	-17	104.9	-0.2	0.0
3	3.49	-10	108.2	-0.1	3	3.495	-9	104.9	-0.1	0.0
4	3.491	-9	108.4	-0.1	4	3.498	-8	104.8	-0.1	0.0
5	3.496	-7	108.5	-0.1	5	3.498	-8	104.8	-0.1	0.0
6	3.47	-20	108.7	-0.2	6	3.455	-29	104.8	-0.3	0.1
7	3.489	-10	108.9	-0.1	7	3.482	-16	104.8	-0.2	0.1
8	3.5	-5	109.1	0.0	8	3.511	-1	104.7	0.0	0.0
9	3.475	-17	109.3	-0.2	9	3.465	-24	104.7	-0.2	0.1
10	3.502	-4	109.5	0.0	10	3.507	-3	104.7	0.0	0.0
11	3.505	-2	109.7	0.0	11	3.516	1	104.7	0.0	0.0
12	3.474	-18	109.9	-0.2	12	3.446	-34	104.6	-0.3	0.2
13	3.495	-7	110.1	-0.1	13	3.496	-9	104.6	-0.1	0.0
14	3.465	-22	110.3	-0.2	14	3.452	-31	104.6	-0.3	0.1
15	3.508	-1	110.5	0.0	15	3.519	3	104.6	0.0	0.0
16	3.507	-1	110.7	0.0	16	3.513	0	104.5	0.0	0.0

APPENDIX D

Open canopy with parapets: spreadsheet calculations.

Presiones exteriores, interiores y totales en Modelo1

Sin parapetos

$\alpha = 0$

Presiones exteriores					Presiones interiores					Presiones netas
Toma	Potencial [V]	Pres.Dif.[Pa]	q_{ref} [Pa]	c_e	Toma	Potencial [ ]	Pres.Dif.[Pa]	q_{ref} [Pa]	c_i	c
1	3.428	-39	117.6	-0.3	1	3.278	-116	105.5	-1.1	0.8
2	3.419	-44	117.5	-0.4	2	3.28	-115	105.6	-1.1	0.7
3	3.414	-46	117.3	-0.4	3	3.29	-110	105.7	-1.0	0.6
4	3.411	-48	117.2	-0.4	4	3.298	-106	105.7	-1.0	0.6
5	3.409	-49	117.0	-0.4	5	3.311	-99	105.8	-0.9	0.5
6	3.417	-45	116.9	-0.4	6	3.35	-80	105.8	-0.8	0.4
7	3.409	-49	116.8	-0.4	7	3.324	-93	105.9	-0.9	0.5
8	3.408	-49	116.6	-0.4	8	3.312	-99	106.0	-0.9	0.5
9	3.408	-49	116.5	-0.4	9	3.44	-34	106.0	-0.3	-0.1
10	3.402	-52	116.3	-0.5	10	3.397	-56	106.1	-0.5	0.1
11	3.393	-57	116.2	-0.5	11	3.37	-70	106.2	-0.7	0.2
12	3.403	-52	116.0	-0.4	12	3.476	-16	106.2	-0.2	-0.3
13	3.394	-56	115.9	-0.5	13	3.466	-21	106.3	-0.2	-0.3
14	3.409	-49	115.7	-0.4	14	3.496	-6	106.3	-0.1	-0.4
15	3.401	-53	115.6	-0.5	15	3.472	-18	106.4	-0.2	-0.3
16	3.391	-58	115.5	-0.5	16	3.464	-22	106.5	-0.2	-0.3

Presiones exteriores, interiores y totales en Modelo1

Sin parapetos

$\alpha = 180$

Presiones exteriores					Presiones interiores					Presiones netas
Toma	Potencial [ ]	Pres.Dif.[Pa]	q_{ref} [Pa]	c_e	Toma	Potencial [ ]	Pres.Dif.[Pa]	q_{ref} [Pa]	c_i	c
1	3.575	35	115.5	0.3	1	3.475	-17	106.5	-0.2	0.5
2	3.563	29	115.5	0.2	2	3.473	-18	106.4	-0.2	0.4
3	3.59	42	115.6	0.4	3	3.474	-17	106.3	-0.2	0.5
4	3.586	40	115.7	0.3	4	3.474	-17	106.3	-0.2	0.5
5	3.562	28	115.8	0.2	5	3.475	-17	106.2	-0.2	0.4
6	3.538	16	115.9	0.1	6	3.475	-17	106.2	-0.2	0.3
7	3.521	7	116.0	0.1	7	3.482	-13	106.1	-0.1	0.2
8	3.531	12	116.1	0.1	8	3.487	-11	106.1	-0.1	0.2
9	3.508	1	116.2	0.0	9	3.487	-11	106.0	-0.1	0.1
10	3.512	3	116.2	0.0	10	3.487	-11	106.0	-0.1	0.1
11	3.49	-8	116.3	-0.1	11	3.493	-8	105.9	-0.1	0.0
12	3.479	-14	116.4	-0.1	12	3.491	-9	105.8	-0.1	0.0
13	3.48	-13	116.5	-0.1	13	3.497	-6	105.8	-0.1	-0.1
14	3.44	-33	116.6	-0.3	14	3.486	-11	105.7	-0.1	-0.2
15	3.465	-21	116.7	-0.2	15	3.501	-4	105.7	0.0	-0.1
16	3.443	-32	116.8	-0.3	16	3.497	-6	105.6	-0.1	-0.2

Presiones exteriores, interiores y totales en Modelo1

Sin parapetos

$\alpha = 30$

Presiones exteriores					Presiones interiores					Presiones netas
Toma	Potencial [ ]	Pres.Dif.[Pa]	q_{ref} [Pa]	c_e	Toma	Potencial [ ]	Pres.Dif.[Pa]	q_{ref} [Pa]	c_i	c
1	3.398	-54	116.8	-0.5	1	3.46	-27	108.3	-0.2	-0.2
2	3.389	-59	116.7	-0.5	2	3.249	-133	108.4	-1.2	0.7
3	3.387	-60	116.6	-0.5	3	3.185	-165	108.6	-1.5	1.0
4	3.389	-59	116.5	-0.5	4	3.239	-138	108.7	-1.3	0.8
5	3.4	-53	116.4	-0.5	5	3.301	-107	108.9	-1.0	0.5
6	3.39	-58	116.3	-0.5	6	3.481	-16	109.0	-0.1	-0.4
7	3.382	-63	116.2	-0.5	7	3.478	-18	109.1	-0.2	-0.4
8	3.389	-59	116.1	-0.5	8	3.342	-86	109.3	-0.8	0.3
9	3.39	-58	116.0	-0.5	9	3.411	-51	109.4	-0.5	0.0
10	3.384	-62	115.9	-0.5	10	3.501	-6	109.6	-0.1	-0.5
11	3.384	-62	115.8	-0.5	11	3.483	-15	109.7	-0.1	-0.4
12	3.389	-59	115.8	-0.5	12	3.377	-69	109.8	-0.6	0.1
13	3.39	-58	115.7	-0.5	13	3.496	-9	110.0	-0.1	-0.4
14	3.409	-49	115.6	-0.4	14	3.4	-57	110.1	-0.5	0.1
15	3.416	-45	115.5	-0.4	15	3.492	-11	110.2	-0.1	-0.3
16	3.429	-39	115.4	-0.3	16	3.504	-5	110.4	0.0	-0.3

Presiones exteriores, interiores y totales en Modelo1

Sin parapetos

α = 330

Presiones exteriores					Presiones interiores					Presiones netas
Toma	Potencial [ ]	Pres.Dif.[Pa]	q_{ref} [Pa]	c_e	Toma	Potencial [ ]	Pres.Dif.[Pa]	q_{ref} [Pa]	c_i	c
1	3.495	-6	115.4	0.0	1	3.361	-77	106.0	-0.7	0.7
2	3.478	-14	115.2	-0.1	2	3.357	-79	106.2	-0.7	0.6
3	3.442	-32	115.1	-0.3	3	3.341	-87	106.3	-0.8	0.5
4	3.431	-38	114.9	-0.3	4	3.332	-91	106.5	-0.9	0.5
5	3.405	-51	114.7	-0.4	5	3.297	-109	106.6	-1.0	0.6
6	3.472	-17	114.6	-0.2	6	3.381	-67	106.8	-0.6	0.5
7	3.455	-26	114.4	-0.2	7	3.368	-73	106.9	-0.7	0.5
8	3.45	-28	114.3	-0.2	8	3.344	-85	107.1	-0.8	0.5
9	3.419	-44	114.1	-0.4	9	3.396	-59	107.2	-0.6	0.2
10	3.443	-32	114.0	-0.3	10	3.406	-54	107.4	-0.5	0.2
11	3.417	-45	113.8	-0.4	11	3.399	-57	107.5	-0.5	0.1
12	3.443	-32	113.6	-0.3	12	3.439	-37	107.7	-0.3	0.1
13	3.429	-39	113.5	-0.3	13	3.448	-33	107.8	-0.3	0.0
14	3.49	-8	113.3	-0.1	14	3.472	-21	108.0	-0.2	0.1
15	3.431	-38	113.2	-0.3	15	3.47	-22	108.2	-0.2	-0.1
16	3.424	-41	113.0	-0.4	16	3.491	-11	108.3	-0.1	-0.3

Presiones exteriores, interiores y totales en Modelo1

Sin parapetos

α = 210

106.0 108.3 110.4 109.8

Presiones exteriores					Presiones interiores					Presiones netas
Toma	Potencial [ ]	Pres.Dif.[Pa]	q_{ref} [Pa]	c_e	Toma	Potencial [ ]	Pres.Dif.[Pa]	q_{ref} [Pa]	c_i	c
1	3.65	70	109.8	0.6	1	3.483	-15	110.4	-0.1	0.8
2	3.63	60	109.9	0.5	2	3.483	-15	110.3	-0.1	0.7
3	3.624	57	110.0	0.5	3	3.48	-17	110.3	-0.2	0.7
4	3.62	55	110.1	0.5	4	3.473	-20	110.3	-0.2	0.7
5	3.638	64	110.2	0.6	5	3.465	-24	110.2	-0.2	0.8
6	3.636	63	110.3	0.6	6	3.485	-14	110.2	-0.1	0.7
7	3.598	44	110.4	0.4	7	3.489	-12	110.1	-0.1	0.5
8	3.588	39	110.6	0.4	8	3.484	-15	110.1	-0.1	0.5
9	3.597	43	110.7	0.4	9	3.484	-15	110.1	-0.1	0.5
10	3.562	26	110.8	0.2	10	3.495	-9	110.0	-0.1	0.3
11	3.564	27	110.9	0.2	11	3.487	-13	110.0	-0.1	0.4
12	3.559	24	111.0	0.2	12	3.482	-16	109.9	-0.1	0.4
13	3.556	23	111.1	0.2	13	3.494	-10	109.9	-0.1	0.3
14	3.521	5	111.2	0.0	14	3.482	-16	109.9	-0.1	0.2
15	3.523	6	111.3	0.1	15	3.495	-9	109.8	-0.1	0.1
16	3.51	0	111.5	0.0	16	3.505	-4	109.8	0.0	0.0

Presiones exteriores, interiores y totales en Modelo1

Sin parapetos

α = 150

Presiones exteriores					Presiones interiores					Presiones netas
Toma	Potencial [ ]	Pres.Dif.[Pa]	q_{ref} [Pa]	c_e	Toma	Potencial [ ]	Pres.Dif.[Pa]	q_{ref} [Pa]	c_i	c
1	3.575	32	109.8	0.3	1	3.393	-58	105.6	-0.5	0.8
2	3.537	13	109.9	0.1	2	3.397	-56	105.6	-0.5	0.7
3	3.538	14	110.0	0.1	3	3.438	-35	105.6	-0.3	0.5
4	3.588	39	110.1	0.4	4	3.449	-30	105.6	-0.3	0.6
5	3.637	64	110.2	0.6	5	3.455	-27	105.5	-0.3	0.8
6	3.546	18	110.3	0.2	6	3.386	-61	105.5	-0.6	0.7
7	3.511	0	110.4	0.0	7	3.389	-60	105.5	-0.6	0.6
8	3.565	27	110.6	0.2	8	3.475	-17	105.5	-0.2	0.4
9	3.498	-6	110.7	-0.1	9	3.391	-59	105.5	-0.6	0.5
10	3.5	-5	110.8	0.0	10	3.472	-18	105.4	-0.2	0.1
11	3.574	32	110.9	0.3	11	3.49	-9	105.4	-0.1	0.4
12	3.476	-18	111.0	-0.2	12	3.385	-62	105.4	-0.6	0.4
13	3.461	-25	111.1	-0.2	13	3.426	-41	105.4	-0.4	0.2
14	3.445	-33	111.2	-0.3	14	3.377	-66	105.3	-0.6	0.3
15	3.48	-15	111.3	-0.1	15	3.493	-8	105.3	-0.1	-0.1
16	3.548	19	111.5	0.2	16	3.486	-11	105.3	-0.1	0.3

APPENDIX E

Parapets: spreadsheet calculations.

Presiones exteriores, interiores y totales en Modelo1

Sin parapetos

$\alpha = 0$

Presiones exteriores					Presiones interiores					Presiones netas
Toma	Potencial [V]	Pres.Dif.[Pa]	q_{ref} [Pa]	c_e	Toma	Potencial [ ]	Pres.Dif.[Pa]	q_{ref} [Pa]	c_i	c
1	3.743	118	111.4	1.1	1	3.431	-42	104.9	-0.40	1.5
2	3.76	126	111.5	1.1	2	3.431	-42	105.1	-0.40	1.5
3	3.748	120	111.6	1.1	3	3.427	-44	105.3	-0.42	1.5
4	3.751	122	111.7	1.1	4	3.434	-40	105.5	-0.38	1.5
5	3.699	96	111.8	0.9	5	3.436	-39	105.7	-0.37	1.2
6	3.745	119	111.9	1.1	6	3.437	-39	105.8	-0.37	1.4
7	3.73	111	112.0	1.0	7	3.439	-38	106.0	-0.36	1.4
8	3.678	85	112.1	0.8	8	3.438	-38	106.2	-0.36	1.1
9	3.722	107	112.2	1.0	9	3.445	-35	106.4	-0.33	1.3
10	3.723	108	112.3	1.0	10	3.443	-36	106.6	-0.34	1.3
11	3.303	-102	112.4	-0.9	11	3.443	-36	106.7	-0.3	-0.6
12	3.295	-106	112.5	-0.9	12	3.44	-37	106.9	-0.3	-0.6
13	3.307	-100	112.6	-0.9	13	3.436	-39	107.1	-0.4	-0.5
14	3.365	-71	112.7	-0.6	14	3.438	-38	107.3	-0.4	-0.3
15	3.35	-79	112.8	-0.7	15	3.43	-42	107.5	-0.4	-0.3
16	3.351	-78	112.9	-0.7	16	3.425	-45	107.7	-0.4	-0.3
17	3.466	-21	113.0	-0.2	17	3.415	-50	107.8	-0.5	0.3
18	3.455	-26	113.1	-0.2	18	3.409	-53	108.0	-0.5	0.3
19	3.486	-11	113.2	-0.1	19	3.426	-44	108.2	-0.4	0.3
20	3.482	-13	113.3	-0.1	20	3.416	-49	108.4	-0.5	0.3

Presiones exteriores, interiores y totales en Modelo1

Sin parapetos

$\alpha = 180$

Presiones exteriores					Presiones interiores					Presiones netas
Toma	Potencial [ ]	Pres.Dif.[Pa]	q_{ref} [Pa]	c_e	Toma	Potencial [ ]	Pres.Dif.[Pa]	q_{ref} [Pa]	c_i	c
1	3.449	-29	113.3	-0.3	1	3.556	21	108.4	0.2	-0.5
2	3.45	-29	113.2	-0.3	2	3.546	16	108.3	0.1	-0.4
3	3.455	-26	113.2	-0.2	3	3.573	30	108.2	0.3	-0.5
4	3.448	-30	113.1	-0.3	4	3.573	30	108.1	0.3	-0.5
5	3.445	-31	113.0	-0.3	5	3.563	24	108.0	0.2	-0.5
6	3.444	-32	112.9	-0.3	6	3.543	14	107.9	0.1	-0.4
7	3.445	-31	112.8	-0.3	7	3.541	13	107.8	0.1	-0.4
8	3.44	-34	112.8	-0.3	8	3.567	26	107.6	0.2	-0.5
9	3.438	-35	112.7	-0.3	9	3.547	16	107.5	0.2	-0.5
10	3.431	-38	112.6	-0.3	10	3.517	1	107.4	0.0	-0.4
11	3.485	-11	112.5	-0.1	11	3.583	35	107.3	0.3	-0.4
12	3.487	-10	112.5	-0.1	12	3.57	28	107.2	0.3	-0.4
13	3.481	-13	112.4	-0.1	13	3.525	5	107.1	0.1	-0.2
14	3.494	-7	112.3	-0.1	14	3.556	21	107.0	0.2	-0.3
15	3.499	-4	112.2	0.0	15	3.535	10	106.9	0.1	-0.1
16	3.493	-7	112.2	-0.1	16	3.515	0	106.8	0.0	-0.1
17	3.5	-4	112.1	0.0	17	3.491	-12	106.7	-0.1	0.1
18	3.505	-1	112.0	0.0	18	3.475	-20	106.6	-0.2	0.2
19	3.499	-4	111.9	0.0	19	3.455	-30	106.5	-0.3	0.2
20	3.499	-4	111.8	0.0	20	3.445	-35	106.4	-0.3	0.3

Presiones exteriores, interiores y totales en Modelo1

Sin parapetos

$\alpha = 30$

Presiones exteriores					Presiones interiores					Presiones netas
Toma	Potencial [ ]	Pres.Dif.[Pa]	q_{ref} [Pa]	c_e	Toma	Potencial [ ]	Pres.Dif.[Pa]	q_{ref} [Pa]	c_i	c
1	3.695	92	108.2	0.8	1	3.409	-50	111.3	-0.4	1.3
2	3.713	101	108.2	0.9	2	3.407	-51	111.3	-0.5	1.4
3	3.705	97	108.3	0.9	3	3.403	-53	111.2	-0.5	1.4
4	3.724	106	108.4	1.0	4	3.397	-56	111.1	-0.5	1.5
5	3.688	88	108.4	0.8	5	3.39	-59	111.1	-0.5	1.3
6	3.731	110	108.5	1.0	6	3.405	-52	111.0	-0.5	1.5
7	3.725	107	108.6	1.0	7	3.403	-53	111.0	-0.5	1.5
8	3.696	92	108.6	0.8	8	3.398	-55	110.9	-0.5	1.3
9	3.747	118	108.7	1.1	9	3.408	-50	110.9	-0.5	1.5
10	3.753	121	108.8	1.1	10	3.408	-50	110.8	-0.5	1.6
11	3.563	25	108.8	0.2	11	3.405	-52	110.8	-0.5	0.7
12	3.578	33	108.9	0.3	12	3.415	-47	110.7	-0.4	0.7
13	3.577	32	109.0	0.3	13	3.413	-48	110.7	-0.4	0.7
14	3.569	28	109.0	0.3	14	3.416	-46	110.6	-0.4	0.7
15	3.592	40	109.1	0.4	15	3.414	-47	110.6	-0.4	0.8
16	3.581	34	109.2	0.3	16	3.415	-47	110.5	-0.4	0.7
17	3.578	33	109.3	0.3	17	3.41	-49	110.5	-0.4	0.7
18	3.582	35	109.3	0.3	18	3.411	-49	110.4	-0.4	0.8
19	3.586	37	109.4	0.3	19	3.405	-52	110.4	-0.5	0.8
20	3.587	37	109.5	0.3	20	3.403	-53	110.3	-0.5	0.8

Presiones exteriores, interiores y totales en Modelo1

Sin parapetos

α = 330

110.846154 111.307692 110.307692 111.538462

Presiones exteriores					Presiones interiores					Presiones netas
Toma	Potencial [ ]	Pres.Dif.[Pa]	q_{ref} [Pa]	c_e	Toma	Potencial [ ]	Pres.Dif.[Pa]	q_{ref} [Pa]	c_i	c
1	3.69	89	109.5	0.8	1	3.422	-43	110.3	-0.4	1.2
2	3.702	95	109.6	0.9	2	3.416	-46	110.4	-0.4	1.3
3	3.693	90	109.8	0.8	3	3.438	-35	110.4	-0.3	1.1
4	3.703	96	110.0	0.9	4	3.444	-32	110.5	-0.3	1.2
5	3.639	63	110.2	0.6	5	3.503	-3	110.6	0.0	0.6
6	3.67	79	110.4	0.7	6	3.511	1	110.6	0.0	0.7
7	3.666	77	110.6	0.7	7	3.5	-4	110.7	0.0	0.7
8	3.604	46	110.8	0.4	8	3.515	3	110.8	0.0	0.4
9	3.624	56	111.0	0.5	9	3.526	9	110.8	0.1	0.4
10	3.627	57	111.1	0.5	10	3.516	4	110.9	0.0	0.5
11	3.368	-73	111.3	-0.7	11	3.504	-2	111.0	0.0	-0.6
12	3.37	-72	111.5	-0.6	12	3.506	-1	111.0	0.0	-0.6
13	3.368	-73	111.7	-0.7	13	3.485	-12	111.1	-0.1	-0.5
14	3.36	-77	111.9	-0.7	14	3.489	-10	111.1	-0.1	-0.6
15	3.36	-77	112.1	-0.7	15	3.481	-14	111.2	-0.1	-0.6
16	3.356	-79	112.3	-0.7	16	3.455	-27	111.3	-0.2	-0.5
17	3.392	-61	112.4	-0.5	17	3.456	-26	111.3	-0.2	-0.3
18	3.393	-60	112.6	-0.5	18	3.447	-31	111.4	-0.3	-0.3
19	3.417	-48	112.8	-0.4	19	3.504	-2	111.5	0.0	-0.4
20	3.416	-49	113	-0.4	20	3.5	-4	111.5	0.0	-0.4

Presiones exteriores, interiores y totales en Modelo1

Sin parapetos

α = 210

Presiones exteriores					Presiones interiores					Presiones netas
Toma	Potencial [ ]	Pres.Dif.[Pa]	q_{ref} [Pa]	c_e	Toma	Potencial [ ]	Pres.Dif.[Pa]	q_{ref} [Pa]	c_i	c
1	3.435	-36	111.1	-0.3	1	3.641	66	110.8	0.6	-0.9
2	3.435	-36	110.9	-0.3	2	3.653	72	110.9	0.7	-1.0
3	3.444	-32	110.8	-0.3	3	3.633	62	110.9	0.6	-0.8
4	3.444	-32	110.6	-0.3	4	3.638	65	110.9	0.6	-0.9
5	3.461	-23	110.5	-0.2	5	3.636	64	110.9	0.6	-0.8
6	3.462	-23	110.3	-0.2	6	3.632	62	111.0	0.6	-0.8
7	3.456	-26	110.2	-0.2	7	3.606	49	111.0	0.4	-0.7
8	3.457	-25	110.0	-0.2	8	3.663	77	111.0	0.7	-0.9
9	3.457	-25	109.9	-0.2	9	3.651	71	111.0	0.6	-0.9
10	3.452	-28	109.7	-0.3	10	3.617	54	111.1	0.5	-0.7
11	3.456	-26	109.6	-0.2	11	3.673	82	111.1	0.7	-1.0
12	3.459	-24	109.4	-0.2	12	3.662	77	111.1	0.7	-0.9
13	3.456	-26	109.3	-0.2	13	3.632	62	111.1	0.6	-0.8
14	3.454	-27	109.1	-0.2	14	3.656	74	111.2	0.7	-0.9
15	3.456	-26	109.0	-0.2	15	3.65	71	111.2	0.6	-0.9
16	3.452	-28	108.8	-0.3	16	3.605	48	111.2	0.4	-0.7
17	3.445	-31	108.7	-0.3	17	3.592	42	111.2	0.4	-0.7
18	3.441	-33	108.5	-0.3	18	3.584	38	111.3	0.3	-0.6
19	3.437	-35	108.4	-0.3	19	3.533	12	111.3	0.1	-0.4
20	3.437	-35	108.2	-0.3	20	3.534	13	111.3	0.1	-0.4

Presiones exteriores, interiores y totales en Modelo1												
Sin parapetos												
α = 150				104.923077	108.384615	106.384615	110.384615					
Presiones exteriores						**Presiones interiores**					**Presiones netas**	
Toma	Potencial [ ]	Pres.Dif.[Pa]	q_{ref} [Pa]	c_e		Toma	Potencial [ ]	Pres.Dif.[Pa]	q_{ref} [Pa]	c_i	c	
1	3.407	-50	111.8	-0.4		1	3.655	71	106.4	0.7	-1.1	
2	3.403	-52	111.8	-0.5		2	3.67	78	106.6	0.7	-1.2	
3	3.401	-53	111.8	-0.5		3	3.588	37	106.8	0.3	-0.8	
4	3.399	-54	111.7	-0.5		4	3.596	41	107.0	0.4	-0.9	
5	3.383	-62	111.7	-0.6		5	3.54	13	107.2	0.1	-0.7	
6	3.377	-65	111.6	-0.6		6	3.531	8	107.4	0.1	-0.7	
7	3.369	-69	111.6	-0.6		7	3.491	-12	107.6	-0.1	-0.5	
8	3.381	-63	111.6	-0.6		8	3.572	29	107.9	0.3	-0.8	
9	3.371	-68	111.5	-0.6		9	3.558	22	108.1	0.2	-0.8	
10	3.372	-68	111.5	-0.6		10	3.524	5	108.3	0.0	-0.7	
11	3.515	4	111.4	0.0		11	3.601	44	108.5	0.4	-0.4	
12	3.526	9	111.4	0.1		12	3.581	34	108.7	0.3	-0.2	
13	3.526	9	111.4	0.1		13	3.543	14	108.9	0.1	0.0	
14	3.543	18	111.3	0.2		14	3.571	29	109.1	0.3	-0.1	
15	3.562	27	111.3	0.2		15	3.554	20	109.3	0.2	0.1	
16	3.549	21	111.2	0.2		16	3.533	9	109.5	0.1	0.1	
17	3.576	34	111.2	0.3		17	3.482	-16	109.8	-0.1	0.5	
18	3.591	42	111.2	0.4		18	3.466	-24	110.0	-0.2	0.6	
19	3.58	36	111.1	0.3		19	3.451	-32	110.2	-0.3	0.6	
20	3.588	40	111.1	0.4		20	3.434	-40	110.4	-0.4	0.7	

APPENDIX F

CFD test of different wind angles on open canopy to verify assumption of wind at 0° and 30°.

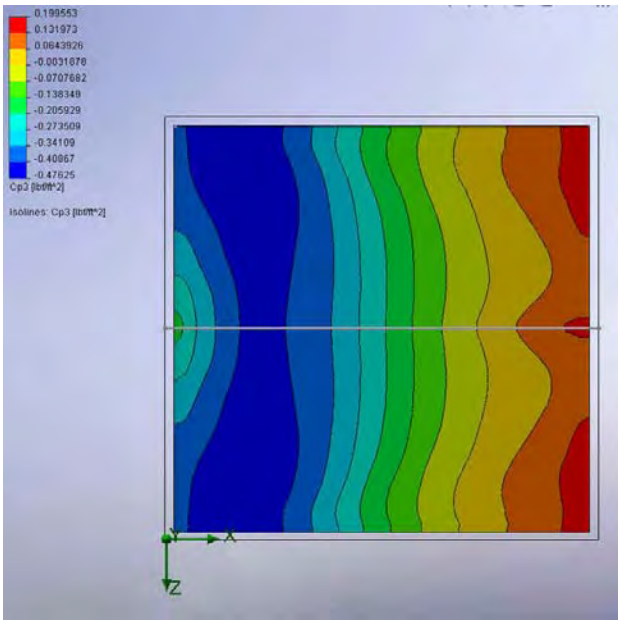

Wind at 0°.

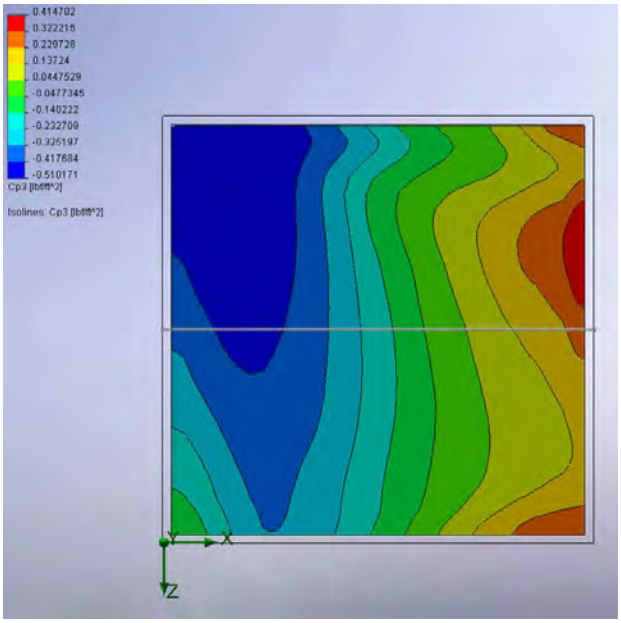

Wind at 15°.

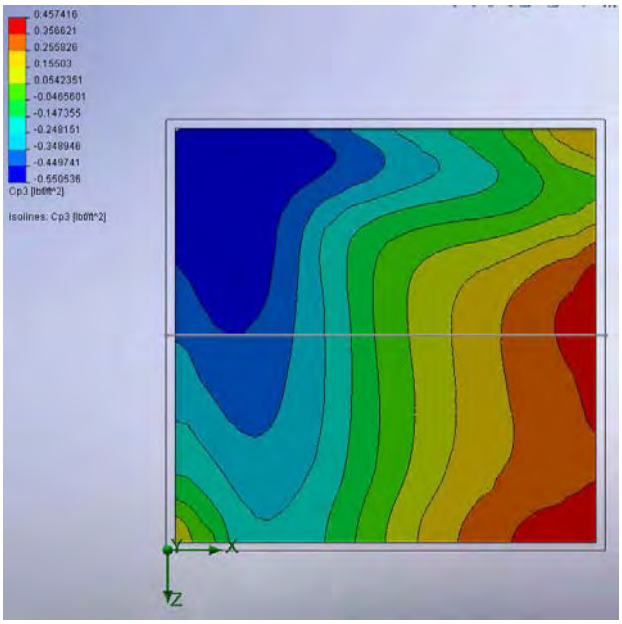

Wind at 30°.

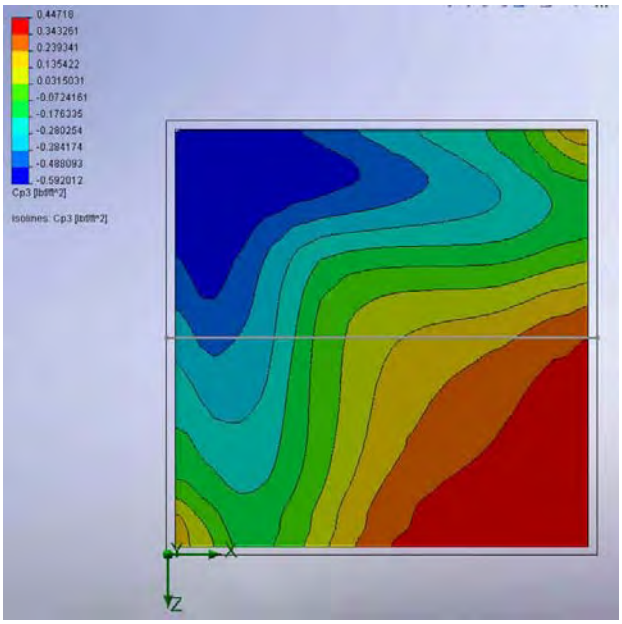

Wind at 45°.

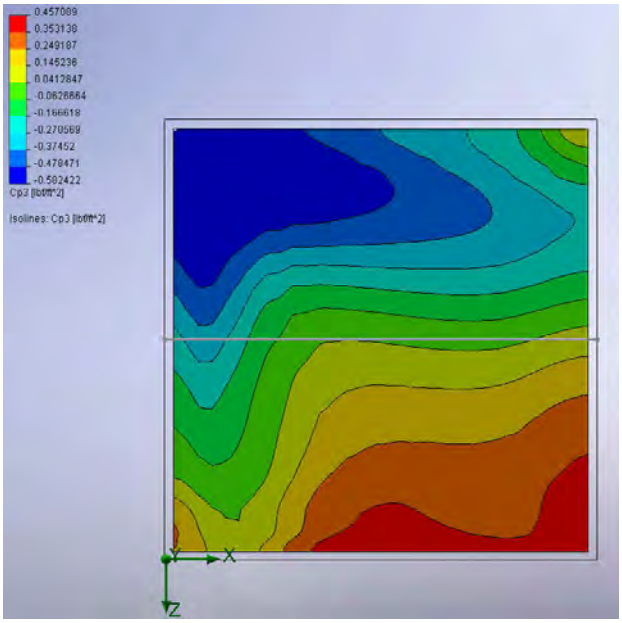

Wind at 60°.

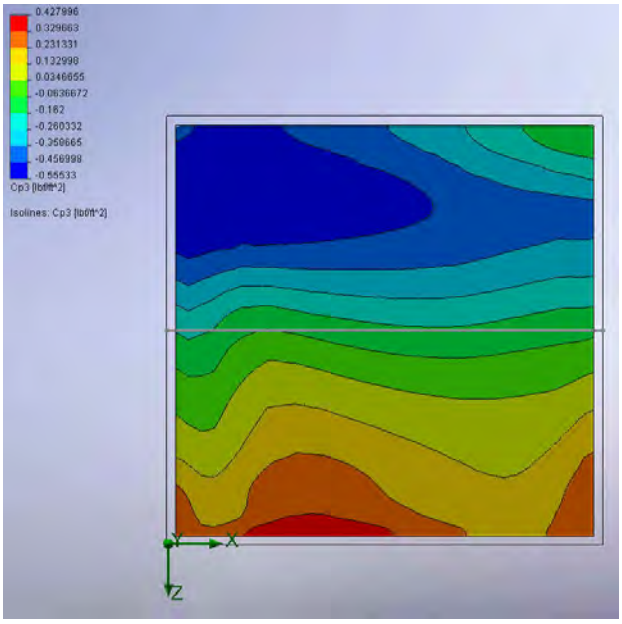

Wind at 75°.

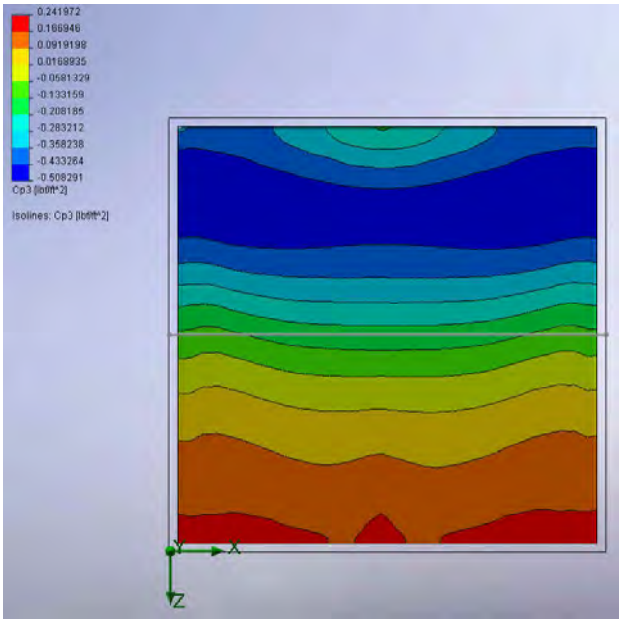
0.241972
0.166946
0.0919198
0.0168935
-0.0581329
-0.133159
-0.208185
-0.283212
-0.358238
-0.433264
-0.508291
Cp3 [lbf/ft^2]
Isolines: Cp3 [lbf/ft^2]
Y
X
Z

Wind at 90°.

APPENDIX G

T-test statistical analysis example. Used for determination of sample variation.

	t-Test: Two-Sample Assuming Equal Variances		
	CFD values		**UNNE values**
1	0.3867	1	0.7616
2	-0.0752	2	0.7616
3	-0.2290	3	0.7125
4	-0.2367	4	0.6424
5	-0.1391	5	0.5905
6	-0.0254	6	0.5191
7	0.0709	7	0.3676
8	0.1355	8	0.4554
9	0.2192	9	0.5069
10	0.3489	10	-0.1000
11	0.4938	11	0.0767
12	0.0230	12	0.1645
13	-0.2308	13	-0.2940
14	0.0840	14	-0.2865
15	0.2286	15	-0.3636
16	0.3610	16	-0.2857
17	0.5852	17	-0.2923
18	-0.1559	18	0.7616
19	-0.2048	19	0.7125
20	0.0193	20	0.6424
21	0.1365	21	0.5905
22	0.3430	22	0.5191
23	0.6572	23	0.3676
24	0.1803	24	0.4554
25	0.1881	25	0.5069
26	0.2812	26	-0.1000
27	-0.0961	27	0.0767
28	-0.1968	28	0.1645
29	-0.0011	29	-0.2940
30	0.1084	30	-0.2865
31	0.7633	31	-0.3636
32	0.2665	32	-0.2857
33	0.7561	33	-0.2923
34	0.2667	34	0.4578
35	-0.0975	35	0.4148
36	-0.1978	36	0.5275
37	-0.0021	37	0.5099
38	0.1071	38	0.4007
39	0.6543	39	0.2964
40	0.1801	40	0.1895
41	0.1875	41	0.2092
42	0.2816	42	0.1096
43	0.5841	43	0.1269
44	-0.1571	44	0.0034
45	-0.2064	45	-0.0346
46	0.0187	46	-0.0586
47	0.1356	47	-0.1789
48	0.3443	48	-0.1421
49	0.4855	49	-0.2177
50	0.0194	50	0.4578
51	-0.2313	51	0.4148
52	0.0837	52	0.5275
53	0.2267	53	0.5099
54	0.3621	54	0.4007
55	0.3567	55	0.2964
56	-0.0821	56	0.1895
57	-0.2336	57	0.2092
58	-0.2397	58	0.1096
59	-0.1392	59	0.1269
60	-0.0263	60	0.0034
61	0.0709	61	-0.0346
62	0.1341	62	-0.0586
63	0.2158	63	-0.1789
64	0.3437	64	-0.1421
Na	64	Nb	64
Ma	0.1327	Mb	0.1962
Ssa	4.4317	SSb	7.2865
Ma-Mb=	-0.0635		
Variance=	0.0930		
tandard deviatior	0.0539		
t=	**-1.1782**		
df=	126		

Figure G.1: Excel spreadsheet calculating t-test for a Cn sample. Wind at 0°, Figure 6.10, page 81

Two-Sample T-Test and CI: C1, C2

```
Two-sample T for C1 vs C2

     N   Mean  StDev  SE Mean
C1  64  0.133  0.265    0.033
C2  64  0.196  0.340    0.043


Difference = mu (C1) - mu (C2)
Estimate for difference:  -0.0635
95% CI for difference:  (-0.1702, 0.0432)
T-Test of difference = 0 (vs not =): T-Value = -1.18  P-Value = 0.241  DF = 126
Both use Pooled StDev = 0.3050
```

Figure G-2: Minitab statistical software calculating t-test for a Cn sample. Used for verification.